Towards improved drug action : target binding kinetics and functional efficacy at the mGlu2 receptor

Doornbos, M.L.J.

Towards improved drug action

Target binding kinetics and functional efficacy
at the $mGlu_2$ receptor

Maarten Doornbos

The research described in this thesis was performed at the division of Drug Discovery and Safety of the Leiden Academic Centre for Drug Research (LACDR), Leiden University, The Netherlands. The research was financially supported by the Vlaams Agentschap Innoveren & Ondernemen, project number 120491.
Printing of the thesis was financially supported by PerkinElmer Nederland B.V. and the LACDR, Leiden University.

Cover design and thesis layout: Maarten Doornbos

Printed by ProefschriftMaken ‖ www.proefschriftmaken.nl

ISBN: 978-94-93019-54-6

Towards improved drug action

Target binding kinetics and functional efficacy at the $mGlu_2$ receptor

PROEFSCHRIFT

ter verkrijging van
de graad van Doctor aan de Universiteit Leiden,
op gezag van Rector Magnificus prof.mr. C.J.J.M. Stolker,
volgens besluit van het College voor Promoties
te verdedigen op woensdag 12 september 2018
klokke 15.00 uur

door

Maarten Lieuwe Jacobus Doornbos
geboren te Leiden
in 1989

Promotor:	Prof. dr. Ad IJzerman
Co-promotor:	Dr. Laura Heitman
Promotiecommissie:	Prof. dr. Hubertus Irth - Voorzitter
	Prof. dr. Joke Bouwstra - Secretaris
	Prof. dr. Hans Bräuner-Osborne (Universiteit Kopenhagen)
	Prof. dr. Jean-Philippe Pin (Universiteit Montpellier)
	Prof. dr. Mario van der Stelt (Universiteit Leiden)

TABLE OF CONTENTS

CHAPTER 1

General Introduction

ABOUT THIS THESIS

During the course of our lives we all come across the use of medicines at many points in time. Given the enormous number of medicines taken today it is hard to imagine a world with only a small number of medicines available. Yet back around a century in time this was actually the case. The number of medicines available was much smaller and those available were mostly derived from plants. Many diagnoses that were grim or even life threatening at that time, are nowadays handled with relative ease using available medicines.

Drug research as we know it today, evolved from the maturation of chemistry and pharmacology to a point where molecules could be designed and the effect on the human body could be described and understood.[1] In 1905 John Newport Langley introduced the concept of a drug receptor[2] and around the same time Paul Ehrlich aimed to understand the selectivity of molecules and came up with the famous expression *"corpora non agunt nisi fixata"* (drugs do not act unless they are bound).[3] Over the 20th and 21st century the art of drug discovery progressed enormously to a point where large compound libraries are screened towards a specific drug target in order to find a hit molecule. Subsequently, this hit compound can be altered and improved through rational design to obtain a lead candidate which can be further evaluated and may eventually become a new medicine.

Cell-cell communication in the central nervous system (CNS) occurs through secretion of signaling molecules, so-called neurotransmitters. These neurotransmitters exert their action via binding to different receptors, including the metabotropic glutamate receptor 2 ($mGlu_2$). For multiple CNS diseases involving a distorted glutamatergic signaling this receptor may be a potential drug target. Therefore, pharmaceutical industry has embarked on the design and synthesis of potential medicines acting via this receptor. Unfortunately this has not resulted in a marketed drug so far. For a better understanding of the receptor, this thesis zooms in at a molecular level to study the mechanism of action of the $mGlu_2$ receptor from different perspectives with a focus on binding kinetics. This chapter provides a background for the research presented followed by the aim and outline of this thesis.

GPCRs

G protein-coupled receptors (GPCRs) are critical signal transduction gatekeepers and represent the largest protein family in the human genome with more than 800 members.[4] Structurally, these receptors share a common architecture of seven transmembrane helices connected by three intracellular and three extracellular loops, and are classified into five subgroups: class A (rhodopsin), class B (secretin), class C (glutamate), adhesion and frizzled/taste2.[5,6] Located in the cell membrane, GPCRs recognize a variety of extracellular stimuli including photons, ions, small molecules, peptides and proteins. Upon receptor activation by its endogenous agonist, a conformational change in receptor structure occurs inducing downstream signalling events via different intracellular proteins including heterotrimeric G proteins (hence the name GPCR), arrestins and kinases.[7] These signal-transduction pathways are very diverse between individual GPCRs as different downstream signalling pathways can be activated and multiple of these pathways can be activated at the same time. The pathways that are being activated can even differ between receptor ligands, so-called biased signalling.[8] Signalling events via GPCRs are vital for a good functioning of the human body, but may be distorted in diseases. Therefore, many drugs have been successfully developed that target these receptors and currently more than 30% of drugs on the market act via these receptors.[9]

Allosteric modulation

For decades, the development of drug substances for GPCRs was focused on the orthosteric binding site, which is the site where the endogenous receptor ligand binds. However, like many proteins most GPCRs provide one or more other, so-called allosteric, binding sites that are topographically distinct from the orthosteric binding site. Ligands that bind such a secondary binding site are called "allosteric modulators" and in the case of GPCRs they may alter the protein conformation of the receptor such that the affinity and/or signalling efficacy of the endogenous orthosteric agonist is modulated as depicted in figure 1. The concept of allosteric modulation was first described and formalized in the 1960s by Monod, Wyman and Changeux when they observed enzyme inhibition by a compound that bound a secondary binding site remote from the substrate binding site.[10] Ligands that potentiate the affinity and/or efficacy of the endogenous agonist are referred to as positive allosteric modulators (PAMs), ligands that inhibit these parameters are referred to as negative allosteric modulators (NAMs) and ligands that bind the allosteric binding site without altering the action of any orthosteric ligands are known as neutral or silent allosteric ligands (NALs/SALs).[11] Across the five major classes of GPCRs allosteric modulators have been described and at present there are two marketed drugs that allosterically modulate GPCR function: Cinacalcet, a calcium sensing receptor (CaSR) PAM and Maraviroc, a C-C chemokine receptor 5 (CCR5) NAM.[12]

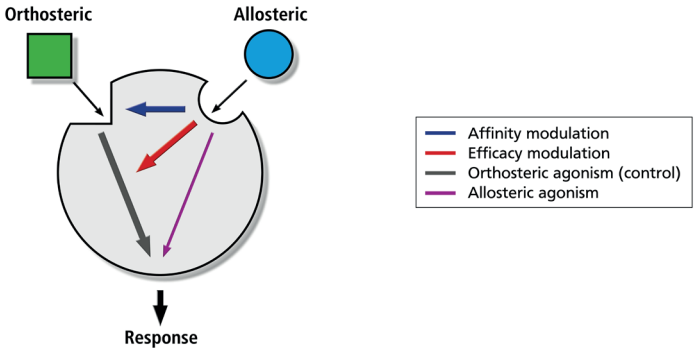

Figure 1. Schematic representation of modes of action of allosteric modulators.
Allosteric ligands (blue) bind to a binding site topographically distinct from the orthosteric binding site to modulate affinity (dark blue) and/or efficacy (red). Some allosteric modulators can directly activate the receptor (purple). Figure was adapted from Conn *et al.* (2009).[13]

Metabotropic glutamate receptors

In contrast to the electrical signalling within neurons, communication between neurons is performed by neurotransmitters, which are exchanged via synapses. Glutamate serves as neurotransmitter at the majority of excitatory synapses in the central nervous system (CNS): around 60% of neurons in the human brain use glutamate as their primary neurotransmitter.[14] Glutamate is the major mediator of sensory information, motor coordination, emotions and cognition.[15] Upon neuronal repolarization, glutamate stored in specific vesicles is released into the synapse where it exerts its fast action via ionotropic glutamate (iGlu) receptors and modulates synaptic activity via metabotropic glutamate (mGlu) receptors.[16]

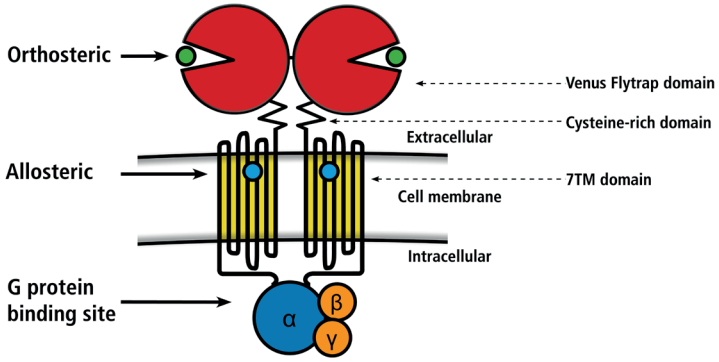

Figure 2. Schematic representation of an mGlu receptor dimer embedded in the cell membrane.
The large extracellular VFT domain is connected to the 7TM domain via a cysteine-rich domain. The 7TM domain contains seven alpha-helices that cross the cell membrane and are connected by three intracellular and three extracellular loops. Orthosteric ligands (green) bind in the glutamate binding site which is located in the VFT domain. Allosteric modulators (blue) bind in an allosteric binding pocket found in the 7TM domain. Upon receptor activation a single G protein is activated and released from the receptor initiating subsequent downstream signalling events.

mGlu receptors are class C GPCRs and were first described in the 1980s as phospholipase C-coupled receptors.[17–19] Structurally, class C GPCRs are characterized by a large extracellular orthosteric ligand binding domain, the so-called Venus Flytrap domain (VFT), which is connected to the typical seven transmembrane (7TM) domain via a cysteine-rich domain (CRD),[20,21] as shown schematically in figure 2. They are obligatory dimers that are predominantly expressed as homodimers linked by a disulfide bond in the VFT.[22,23] Eight mGlu receptors have been found that are divided into three subgroups, group I ($mGlu_{1, 5}$), group II ($mGlu_{2, 3}$) and group III ($mGlu_{4, 6-8}$), based on sequence homology, second messenger coupling and pharmacology.[24,25] In contrast to group I mGlu receptors that are mainly expressed on post-synaptic neurons, groups II & III mGlu receptors are mainly presynaptic receptors that inhibit neurotransmitter release at various types of synapses.[15]

The $mGlu_2$ receptor

Activation of the $mGlu_2$ receptor, which is expressed throughout the central nervous system, reduces glutamate release into the synapse. Hence, it has emerged as a therapeutic target for psychiatric diseases characterized by glutamatergic dysfunction.[21,26] $mGlu_2$ receptor activation can reduce glutamate hyperfunction in diseases like schizophrenia and anxiety,[27,28] whereas $mGlu_2$ receptor blockade can decrease glutamate hypofunction in depression and cognition.[29,30] Although the structure of the $mGlu_2$ VFT domain is known,[31] the current structural understanding of the 7TM domain is based on NAM-bound crystal structures of the $mGlu_1$ and $mGlu_5$ receptors.[32–35] A variety of glutamate-like agonists has been developed, of which LY2140023, a prodrug of LY404039 showed improvement in positive and negative symptoms in schizophrenic patients, which unfortunately could not be confirmed in later clinical studies.[28,36] Inhibition of the $mGlu_2$ receptor can be achieved by (orthosteric) antagonists of which LY341495 is the most studied.[37]

Development of orthosteric ligands presents challenges for selectivity and brain penetration and therefore discovery efforts have largely shifted to the development of allosteric modulators that bind in a less conserved pocket in the 7TM domain.[13] Many $mGlu_2$ PAMs showed activity in *in vivo* experimentation[12] and two PAMs have advanced into clinical trials: AZD8529[38] and JNJ-40411813/ADX71149.[39,40] Reported negative allosteric modulators (NAMs) include RO4491533[41] and decoglurant of which the latter has advanced into clinical trials as well.[30]

Binding Kinetics

The idea that binding kinetics of the drug-receptor complex are important for drug efficacy in addition to the occupied receptor binding sites was first described in 1961 by William Paton in his 'rate theory'.[42] However, since then the majority of new models describing drug

efficacy, such as the 'two-state receptor model', considered efficacy in terms of the ability to stabilize an active receptor conformation under equilibrium conditions.[43] Typically, affinity and efficacy are measured under equilibrium conditions, whereas in open systems like the human body both drug and target have fluctuating concentrations. Over the last decade it has become increasingly apparent that not only a ligand's affinity is crucial for a good efficacy, but that also the ligand's binding kinetics – described by the second order association rate constant k_{on} and the first order dissociation rate constant k_{off} – are important parameters to be optimized to improve efficacy.[44,45] In addition to classical equilibrium assays, affinity (K_D) can be determined by k_{off} / k_{on}. Based on the k_{off} the so-called drug-target residence time (RT) can be calculated. This parameter is indicative for the lifetime of the drug-target complex and is defined as the reciprocal of the dissociation rate constant, $1/k_{off}$ (Fig. 3).[46]

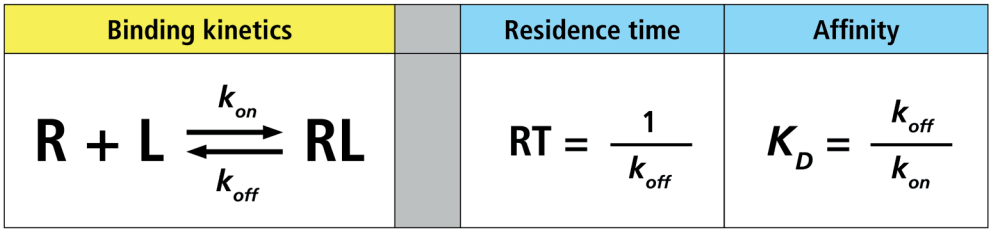

Figure 3. Binding of a ligand (L) to a receptor (R) is described by the association rate constant (k_{on}) and dissociation of the ligand-receptor complex (LR) is described by the dissociation rate constant (k_{off}). From these rate constants, residence time (RT) and affinity (K_D) can be derived.

The relevance of RT was retrospectively shown for multiple marketed GPCR drugs.[47] For example the successful anti-asthma drug tiotropium – the drug that was spent the most money on in The Netherlands in 2016[48] – is a long RT muscarinic acetylcholine M_3 receptor antagonist, which results in longer duration of action and subsequently a lower side-effect burden.[49] Although RT and k_{off} have been the focus of most kinetic studies, k_{on} has also been described to be important for fast drug action, a high receptor occupancy and even a longer duration of action.[50–52] Recently, the importance of k_{on} was further emphasized when it was shown that extrapyramidal side effects induced by D_2 receptor antagonists are linked to k_{on} rather than k_{off} as was the general consensus so far.[53,54]

Covalent probes

A special kinetic profile can be obtained by changing a ligand such that it binds its target covalently, resulting in 'ultimate' RT and continuous target occupancy. Such covalent ligands have proven to be successful medicines for various indications, exemplified by well-known drugs such as aspirin, penicillin and omeprazole. However, covalent molecules are generally avoided in drug discovery due to safety concerns. The development of covalent ligands was inspired by the rhodopsin receptor that forms a covalent bond with its native ligand 11-*cis*-retinal.[55] As such, this covalent interaction is involved in our vision via rod cells in the eye.

Introduction of covalent 'warheads' into ligands that were optimised for non-covalent affinity may result in highly targeted, selective lead molecules that thereby overcome some of the difficulties of off-target binding.[56] Generally, covalent GPCR ligands consist of a high affinity pharmacophore and a reactive electrophilic warhead that is able to form a covalent bond with a specific nucleophilic amino acid residue in the receptor binding pocket. Commonly used warheads include reactive thiols, Michael acceptors, isothiocyanates and the fluorosulfonyl moiety.[57] Over the last decade the structural understanding of GPCRs has vastly increased by the great number of receptor crystal structures obtained. To facilitate this receptor crystallization, covalent ligands can be used to stabilize the receptor in a specific conformation. This approach was successfully used to obtain the crystal structures of the Adenosine A1 and multiple β2 adrenergic receptors amongst others and could be of special interest for crystallization of active state receptors as these are notoriously difficult to crystallize.[58,59] Further functionalisation of covalent ligands for affinity-based protein profiling (AfBPP) can be achieved by photoaffinity labelling. As direct substitution of a photoreactive tag likely decreases affinity, this is commonly accomplished via a 'clickable' handle on the covalent ligand which can be used to attach a photoreactive tag following receptor binding and covalent bond formation,[60] as was recently shown for an $mGlu_5$ NAM.[61] In summary, over the last years covalent GPCR ligands have emerged as valuable tool compounds for characterization of receptor structure, mechanism of action, expression patterns in native tissues and binding kinetics.[57] Additionally, covalent allosteric modulators are more likely to be used as therapeutics due to their preferential safety profile as they only exert their effect whilst the endogenous agonist is bound.[62]

Label-free assays

Within the field of *in vitro* pharmacology a wide variety of different assays for GPCRs is used to characterize novel molecules. These assays can be divided into two groups: binding assays that evaluate how well (affinity) and fast (binding kinetics) ligands bind the receptor and functional assays that evaluate how well ligands exert their functional effect(s) (potency and efficacy). The majority of these methods are dependent on labels that are attached to ligands or the receptor itself. Radioligand binding is a robust and well-characterized method within the field and is used in this thesis to evaluate ligand binding and functional responses mediated by the G protein.[63] These assays however require expensive and specialized laboratories and careful handling regarding safety and waste disposal. Therefore, other methods have been developed which often use fluorescent labels, such as BRET and FRET assays.[64] Labelling of compounds or receptors with bulky fluorescent groups may alter the properties of these molecules thereby potentially leading to false positive or false negative results. Furthermore classical functional assays are mostly pathway-biased as they often focus on a single signalling pathway.

New assays are emerging that lack the need for any kind of label. These so-called label-free assays can be used to assess ligand binding and functional responses in real-time. To measure binding kinetics and affinity, surface plasmon resonance (SPR) and surface acoustic wave (SAW) biosensors have been developed, which were followed more recently by ligand binding assays using mass spectrometry (MS).[65] Whereas these assays use isolated protein or membrane preparations, other biosensor-based label-free assays assess functional responses of GPCR ligands on whole cells by via ligand-induced morphological changes.[66] These biosensors measure changes in cell morphology either optically, such as EPIC,[67] or by changes in impedance, such as xCELLigence.[68] Cell types used include recombinant cell lines, cell lines endogenously expressing the receptor of interest and even cells derived from patients.[69] By eliminating the need for labels, these whole cell biosensor-based assays have the capability of assessing endogenous receptor function in real-time under more physiologically relevant conditions.[70] Hence, label-free assays may provide more translational insights into the *in vitro* – *in vivo* translation.

OBJECTIVES AND OVERVIEW OF THIS THESIS

Aim

During the drug development process many potential medicines are withdrawn as they are unsafe or lack efficacy. The translational step between *in vitro* and *in vivo* experiments is not as predictive as one would desire. Therefore, many promising compounds fail during *in vivo* experiments or even in later stages of the drug development process, thereby spilling lab animals, time and money. This is not different for the $mGlu_2$ receptor for which no marketed drug is available so far, despite huge discovery efforts. Taken together, there is a need to improve the understanding of key *in vitro* parameters that drive *in vivo* efficacy. Hence, the aim of this thesis was to provide detailed insights into binding kinetics of PAMs at the $mGlu_2$ receptor and to evaluate the potential of kinetic profiling of an established $mGlu_2$ PAM library for prediction of *in vivo* efficacy. This required in depth understanding of the mechanism of allosteric modulation from a functional and a kinetics perspective. An additional aim was to develop a label-free assay which allows evaluation of functional kinetics, constitutive receptor activity and inverse agonism. The last aim was to design, synthesize and characterize a novel covalent $mGlu_2$ PAM.

Outline of this thesis

Chapter 2 focuses on the characterization of the PAM JNJ-46281222 that is used throughout this thesis as pharmacological tool compound. Additionally, the molecular mechanism of allosteric modulation of the $mGlu_2$ receptor is evaluated. In **Chapter 3** this mechanism

is further evaluated from a binding kinetics perspective. Kinetic parameters for orthosteric $mGlu_2$ ligands including endogenous glutamate are determined in the absence and presence of allosteric modulators and functional assays are performed to study the interplay between the orthosteric and allosteric binding sites. **Chapter 4** describes the synthesis and biological evaluation of a novel series of novel $mGlu_2$ PAMs. Affinity, potency and binding kinetics are determined followed by extensive structure-kinetics relationships (SKR) in addition to the more classical structure-activity relationships (SAR). The kinetic profiles of the PAMs are evaluated by comparison of kinetic parameters with *in vitro* equilibrium parameters and ultimately with *in vivo* efficacy data. **Chapter 5** describes the design, synthesis and pharmacological evaluation of the first covalent PAM probe within the family of class C GPCRs, which presents a novel pharmacological tool with 'ultimate' binding kinetics and a wide range of applications in the $mGlu_2$ receptor field. Additionally, the binding mode of this pharmacological tool compound is studied using computational and receptor mutagenesis approaches. In **Chapter 6** an impedance-based label-free biosensor assay is developed in order to study $mGlu_2$ pharmacology and in particular constitutive receptor activity and inverse agonism. The results and forthcoming future opportunities are summarized in **chapter 7**. Hopefully, the results obtained in this thesis will contribute to an increased understanding of the key *in vitro* parameters necessary for *in vivo* and *in patient* efficacy, ultimately resulting in novel safe and efficacious drugs.

REFERENCES

1. Drews J. *Science*. **2000**; 287: 1960–4.
2. Langley JN. *J Physiol*. **1905**; 33: 374–413.
3. Ehrlich P. *Lancet*. **1913**; 182: 445–451.
4. Bjarnadóttir TK, Gloriam DE, Hellstrand SH, Kristiansson H, Fredriksson R, Schiöth HB. *Genomics*. **2006**; 88: 263–273.
5. Fredriksson R, Lagerström MC, Lundin L, Schiöth HB. *Mol Pharmacol*. **2003**; 63: 1256–72.
6. Rosenbaum DM, Rasmussen SGF, Kobilka BK. *Nature*. **2009**; 459: 356–63.
7. Rajagopal S, Shenoy SK. *Cell Signal*. **2018**; 41: 9–16.
8. Smith JS, Lefkowitz RJ, Rajagopal S. *Nat Rev Drug Discov*. **2018**.
9. Hauser AS, Attwood MM, Rask-Andersen M, Schiöth HB, Gloriam DE. *Nat Rev Drug Discov*. **2017**; 16: 829–842.
10. Monod J, Wyman J, Changeux JP. *J Mol Biol*. **1965**; 12: 88–118.
11. Christopoulos A, Changeux J-P, Catterall WA, Fabbro D, Burris TP, Cidlowski JA, Olsen RW, Peters JA, Neubig RR, Pin J-P, Sexton PM, Kenakin TP, Ehlert FJ, Spedding M, Langmead CJ. *Pharmacol Rev*. **2014**; 66: 918–947.
12. Lindsley CW, Emmitte KA, Hopkins CR, Bridges TM, Gregory KJ, Niswender CM, Conn PJ. *Chem Rev*. **2016**; 116: 6707–6741.
13. Conn PJ, Christopoulos A, Lindsley CW. *Nat Rev Drug Discov*. **2009**; 8: 41–54.
14. Javitt DC. *Mol Psychiatry*. **2004**; 9: 984–997.

15. Nicoletti F, Bockaert J, Collingridge GL, Conn PJ, Ferraguti F, Schoepp DD, Wroblewski JT, Pin JP. *Neuropharmacology*. **2011**; 60: 1017–41.

16. Kew JNC, Kemp JA. *Psychopharmacology (Berl)*. **2005**; 179: 4–29.

17. Nicoletti F, Wroblewski JT, Novelli A, Alho H, Guidotti A, Costa E. *J Neurosci*. **1986**; 6: 1905–11.

18. Sladeczek F, Pin JP, Récasens M, Bockaert J, Weiss S. *Nature*. **1985**; 317: 717–9.

19. Sugiyama H, Ito I, Hirono C. *Nature*. **1987**; 325: 531–533.

20. Muto T, Tsuchiya D, Morikawa K, Jingami H. *Proc Natl Acad Sci U S A*. **2007**; 104: 3759–64.

21. Niswender CM, Conn PJ. *Annu Rev Pharmacol Toxicol*. **2010**; 50: 295–322.

22. Romano C, Yang W-L, O'Malley KL. *J Biol Chem*. **1996**; 271: 28612–28616.

23. Kniazeff J, Prézeau L, Rondard P, Pin J-P, Goudet C. *Pharmacol Ther*. **2011**; 130: 9–25.

24. Pin J-P, Duvoisin R. *Neuropharmacology*. **1995**; 34: 1–26.

25. Alexander SPH, Benson HE, Faccenda E, Pawson AJ, Sharman JL, Spedding M, Peters JA, Harmar AJ. *Br J Pharmacol*. **2013**; 170: 1459–581.

26. Marek GJ. *Eur J Pharmacol*. **2010**; 639: 81–90.

27. Dunayevich E, Erickson J, Levine L, Landbloom R, Schoepp DD, Tollefson GD. *Neuropsychopharmacology*. **2008**; 33: 1603–10.

28. Patil ST, Zhang L, Martenyi F, Lowe SL, Jackson KA, Andreev B V, Avedisova AS, Bardenstein LM, Gurovich IY, Morozova MA, Mosolov SN, Neznanov NG, Reznik AM, Smulevich AB, Tochilov VA, Johnson BG, Monn JA, Schoepp DD. *Nat Med*. **2007**; 13: 1102–7.

29. Feyissa AM, Woolverton WL, Miguel-Hidalgo JJ, Wang Z, Kyle PB, Hasler G, Stockmeier CA, Iyo AH, Karolewicz B. *Prog Neuropsychopharmacol Biol Psychiatry*. **2010**; 34: 279–83.

30. Goeldner C, Ballard TM, Knoflach F, Wichmann J, Gatti S, Umbricht D. *Neuropharmacology*. **2013**; 64: 337–46.

31. Monn JA, Prieto L, Taboada L, Pedregal C, Hao J, Reinhard MR, Henry SS, Goldsmith PJ, Beadle CD, Walton L, Man T, Rudyk H, Clark B, Tupper D, Baker SR, Lamas C, Montero C, Marcos A, Blanco J, Bures M, Clawson DK, Atwell S, Lu F, Wang J, Russell M, Heinz BA, Wang X, Carter JH, Xiang C, Catlow JT, Swanson S, Sanger H, Broad LM, Johnson MP, Knopp KL, Simmons RM a, Johnson BG, Shaw DB, McKinzie DL. *J Med Chem*. **2015**; 58: 1776–1794.

32. Doré AS, Okrasa K, Patel JC, Serrano-Vega M, Bennett K, Cooke RM, Errey JC, Jazayeri A, Khan S, Tehan B, Weir M, Wiggin GR, Marshall FH. *Nature*. **2014**; 511: 557–62.

33. Wu H, Wang C, Gregory KJ, Han GW, Cho HP, Xia Y, Niswender CM, Katritch V, Meiler J, Cherezov V, Conn PJ, Stevens RC. *Science*. **2014**; 344: 58–64.

34. Christopher JA, Aves SJ, Bennett KA, Doré AS, Errey JC, Jazayeri A, Marshall FH, Okrasa K, Serrano-Vega MJ, Tehan BG, Wiggin GR, Congreve M. *J Med Chem*. **2015**; 58: 6653–6664.

35. Christopher J, Orgován Z, Congreve M, Dore AS, Errey JC, Marshall FH, Mason JS, Okrasa K, Rucktooa P, Serrano-Vega MJ, Ferenczy GG, Keseru GM. *J Med Chem*. **2018**: acs.jmedchem.7b01722.

36. Adams DH, Kinon BJ, Baygani S, Millen BA, Velona I, Kollack-Walker S, Walling DP. *BMC Psychiatry*. **2013**; 13: 143.

37. Kingston A., Ornstein P., Wright R., Johnson B., Mayne N., Burnett J., Belagaje R, Wu S, Schoepp D. *Neuropharmacology*. **1998**; 37: 1–12.

38. Litman RE, Smith MA, Doherty JJ, Cross A, Raines S, Gertsik L, Zukin SR. *Schizophr Res*. **2016**; 172: 152–157.

39. Cid JM, Tresadern G, Duvey G, Lütjens R, Finn T, Rocher J, Poli S, Vega JA, de Lucas AI, Matesanz E, Linares ML, Andrés JI, Alcazar J, Alonso JM, Macdonald GJ, Oehlrich D, Lavreysen H, Ahnaou A, Drinkenburg W, Mackie C, Pype S, Gallacher D,

Trabanco AA. *J Med Chem*. **2014**; 57: 6495–512.

40. Kent JM, Daly E, Kezic I, Lane R, Lim P, De Smedt H, De Boer P, Van Nueten L, Drevets WC, Ceusters M. *Prog Neuro-Psychopharmacology Biol Psychiatry*. **2016**; 67: 66–73.

41. Woltering TJ, Wichmann J, Goetschi E, Knoflach F, Ballard TM, Huwyler J, Gatti S. *Bioorg Med Chem Lett*. **2010**; 20: 6969–74.

42. Paton WDM. *Proc R Soc B Biol Sci*. **1961**; 154: 21–69.

43. Leff P. *Trends Pharmacol Sci*. **1995**; 16: 89–97.

44. Copeland RA. *Nat Rev Drug Discov*. **2016**; 15: 87–95.

45. Guo D, Heitman LH, IJzerman AP. *Chem Rev*. **2017**; 117: 38–66.

46. Copeland RA, Pompliano DL, Meek TD. *Nat Rev Drug Discov*. **2006**; 5: 730–739.

47. Tummino PJ, Copeland RA. *Biochemistry*. **2008**; 47: 5481–5492.

48. Stichting Farmaceutische Kengetallen. Data en feiten 2017 - Het jaar 2016 in cijfers, **2017**.

49. Sykes DA, Dowling MR, Charlton SJ. *Mol Pharmacol*. **2009**; 76: 543–51.

50. Vauquelin G. *Br J Pharmacol*. **2016**; 173: 2319–2334.

51. de Witte WEA, Danhof M, van der Graaf PH, de Lange ECM. *Trends Pharmacol Sci*. **2016**; 37: 831–842.

52. Schoop A, Dey F. *Drug Discov Today Technol*. **2015**; 17: 9–15.

53. Sykes DA, Moore H, Stott L, Holliday N, Javitch JA, Lane JR, Charlton SJ. *Nat Commun*. **2017**; 8: 763.

54. Kapur S, Seeman P. *Am J Psychiatry*. **2001**; 158: 360–369.

55. Bownds D, Wald G. *Nature*. **1965**; 205: 254–257.

56. Baillie TA. *Angew Chemie - Int Ed*. **2016**; 55: 13408–13421.

57. Weichert D, Gmeiner P. *ACS Chem Biol*. **2015**; 10: 1376–1386.

58. Glukhova A, Thal DM, Nguyen AT, Vecchio EA, Jörg M, Scammells PJ, May LT, Sexton PM, Christopoulos A. *Cell*. **2017**; 168: 867–877.e13.

59. Weichert D, Kruse AC, Manglik A, Hiller C, Zhang C, Hubner H, Kobilka BK, Gmeiner P. *Proc Natl Acad Sci*. **2014**; 111: 10744–10748.

60. Lapinsky DJ. *Bioorganic Med Chem*. **2012**; 20: 6237–6247.

61. Gregory KJ, Velagaleti R, Thal DM, Brady RM, Christopoulos A, Conn PJ, Lapinsky DJ. *ACS Chem Biol*. **2016**; 11: 1870–1879.

62. Lu S, Zhang J. *Drug Discov Today*. **2017**; 22: 447–453.

63. Flanagan CA. *Methods Cell Biol*. **2016**; 132: 1–25.

64. Lohse MJ, Nuber S, Hoffmann C. *Pharmacol Rev*. **2012**; 64: 299–336.

65. Massink A, Holzheimer M, Hölscher A, Louvel J, Guo D, Spijksma G, Hankemeier T, IJzerman AP. *Purinergic Signal*. **2015**; 11: 581–594.

66. Yu N, Atienza JM, Bernard J, Blanc S, Zhu J, Wang X, Xu X, Abassi Y. *Anal Chem*. **2006**; 78: 35–43.

67. Scott CW, Peters MF. *Drug Discov Today*. **2010**; 15: 704–716.

68. Lundstrom K. *Expert Opin Drug Discov*. **2017**; 12: 335–343.

69. Hillger JM, Lieuw W-L, Heitman LH, IJzerman AP. *Drug Discov Today*. **2017**; 22: 1808-1815

70. Fang Y. *Expert Opin Drug Discov*. **2015**; 10: 331–343.

CHAPTER 2

Molecular mechanism of positive allosteric modulation of the metabotropic glutamate receptor 2 by JNJ-46281222

Maarten L J Doornbos, Laura Pérez-Benito, Gary Tresadern, Thea Mulder-Krieger, Ilse Biesmans, Andrés A Trabanco, Jose María Cid, Hilde Lavreysen, Adriaan P IJzerman & Laura H Heitman

British Journal of Pharmacology 173 (2016) 588–600. doi:10.1111/bph.13390

2

ABSTRACT

Background and purpose:

Allosteric modulation of the $mGlu_2$ receptor is a potential strategy for treatment of various neurological and psychiatric disorders. Here we describe the *in vitro* characterization of the $mGlu_2$ PAM JNJ-46281222 and its radiolabelled counterpart [^{3}H]JNJ-46281222. Using this novel tool, we also describe the allosteric effect of orthosteric glutamate binding and the presence of a bound G protein on PAM binding and use computational approaches to further investigate the binding mode.

Experimental approach:

We have used radioligand binding studies, functional assays, site-directed mutagenesis, homology modelling and molecular dynamics to study the binding of JNJ-46281222.

Key results:

JNJ-46281222 is an $mGlu_2$-selective, highly potent PAM with nanomolar affinity (K_D = 1.7 nM). Binding of [^{3}H]JNJ-46281222 was increased by the presence of glutamate and greatly reduced by the presence of GTP, indicating the preference for a G protein bound state of the receptor for PAM binding. Its allosteric binding site was visualized and analysed by a computational docking and molecular dynamics study. The simulations revealed amino acid movements in regions expected to be important for activation. The binding mode was supported by [^{3}H]JNJ-46281222 binding experiments on mutant receptors.

Conclusion and implications:

Our results obtained with JNJ-46281222 in unlabelled and tritiated form further contribute to our understanding of $mGlu_2$ allosteric modulation. The computational simulations and mutagenesis provide a plausible binding mode with indications of how the ligand permits allosteric activation. This study is therefore of interest for $mGlu_2$ and class C receptor drug discovery.

INTRODUCTION

The metabotropic glutamate (mGlu) receptors modulate cell excitability and synaptic transmission when activated by endogenous glutamate. They belong to the glutamate-like subfamily (class C) of G protein-coupled receptors (GPCRs) and are divided into three subgroups, Group I ($mGlu_{1, 5}$), Group II ($mGlu_{2, 3}$) and Group III ($mGlu_{4, 6-8}$), based on their sequence homology, second messenger coupling and pharmacology.[1,2]

Structurally, class C GPCRs are characterized by a large extracellular orthosteric binding domain, the so called Venus Flytrap Domain (VFT), which is connected to the seven transmembrane (7TM) domain by a cysteine-rich domain (CRD).[3,4] They are obligatory dimers and mainly exist as homodimers linked by a disulfide bond in the VFT.[5,6]

Activation of the $mGlu_2$ receptor is a potential strategy for the treatment of psychiatric disorders such as schizophrenia, anxiety and depression.[7] Interestingly, $mGlu_2$ receptor activation can be enhanced by positive allosteric modulators (PAMs), which have little or no intrinsic efficacy and enlarge the effect exerted by endogenously released glutamate.[8] The orthosteric binding site is highly conserved between mGlu receptors and it is thus hard to develop selective orthosteric ligands. Next to that, allosteric ligands are more capable of crossing the blood brain barrier as they are less polar, due to their binding in the more hydrophobic 7TM domain.[9] For these reasons the number of PAMs described has increased tremendously over the last decade.[10] These include compounds such as LY487379[11], BINA[12], THIIC (also known as LY2607540)[13] and JNJ-40068782[14], which have been extensively characterized both *in vitro* and *in vivo*. Importantly, two $mGlu_2$ PAMs have reached clinical trials so far. Development of AZD8529 (described in patent WO2008150233)[15] from AstraZeneca was discontinued after a Phase 2a study in schizophrenic patients due to a lack of efficacy.[16] JNJ-40411813 (also known as ADX71149) from Janssen Pharmaceuticals and Addex Therapeutics failed to meet the criterion for efficacy signal in patients with major depressive disorder with significant anxiety symptoms. In contrast, in an exploratory Phase 2a study in schizophrenia, not powered to determine statistical significance of effects rather a signal generation study, JNJ-40411813 met the primary objectives of safety and tolerability and also demonstrated an effect in patients with residual negative symptoms.[17]

The $mGlu_2$ allosteric binding pocket has been elucidated by mutagenesis studies, which revealed an overlap between PAM and negative allosteric modulator (NAM) binding sites.[18–22] The recent crystallization of the first Class C GPCRs $mGlu_1$ and $mGlu_5$ 7TM in complex with NAM molecules enables accurate mGlu homology modelling.[23,24]

Here, the *in vitro* properties of JNJ-46281222 are described and we characterize [^{3}H]JNJ-46281222 as a high affinity $mGlu_2$ PAM. Its binding was studied in order to gain a better understanding of the relation between orthosteric and allosteric binding sites at the $mGlu_2$ receptor. In addition, molecular dynamics simulations based on an active state 7TM $mGlu_2$ receptor model were performed to analyse the binding mode of JNJ-46281222, which was validated experimentally in subsequent mutagenesis experiments. Altogether this work offers new insights into the functioning of the $mGlu_2$ receptor, which might contribute to development of new and improved PAMs.

METHODS

Chemicals and reagents

BINA, THIIC (a.k.a. LY2607540), RO4491533[25], AZD8529, JNJ-40068782, JNJ-46281222 (Fig. 1)[26] and [^{3}H]JNJ-46281222 were synthesized at Janssen Research and Development. DCG-IV was purchased at R&D systems Europe (Abingdon, United Kingdom). [^{3}H]DCG-IV and [^{3}H]LY341495 were obtained from American Radiolabeled Companies (St. Louis, MO, USA). GTP and glutamate were purchased from Sigma-Aldrich (St. Louis, MO, USA). Chinese hamster ovary cells (CHO-K1, ATCC: CCL-61) were from ATCC (Rockville, MD, USA). Other chemicals were from standard commercial sources.

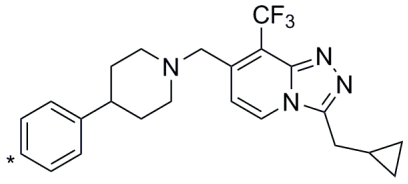

Figure 1. Chemical structure of JNJ-46281222. The position of the tritium label in [^{3}H]JNJ-46281222 is denoted by *.

Tritiation of JNJ-46281222

A solution of triethylamine (110μL) in ethanol (5 mL) was prepared. From this solution 0.2 mL was added to a tritiation reaction vial which contained the brominated precursor 7-((4-(4-bromophenyl)piperidin-1-yl)methyl)-3-(cyclopropylmethyl)-8-(trifluoromethyl)-[1,2,4]triazolo[4,3-a]pyridine (1.9 mg) and palladium on carbon (10%, 1.9 mg). The reaction mixture was attached to a tritium manifold (RC Tritec, Teufen, Switzerland) and degassed. Next tritium gas was placed on top of the reaction mixture (approximately 180 mbar) and was stirred for 8 minutes at room temperature. The remaining tritium gas was trapped on a uranium bed and all volatile compounds were lyophilized to a waste ampoule. The crude reaction mixture was rinsed with methanol (3x150 μL), dissolved in ethanol

(4x1mL), and filtered over an Acrodisc filter, yielding 2.04 GBq crude material. A portion (0.5 GBq) of this material was further purified and analyzed by high-performance liquid chromatography to obtain 0.36 GBq tritiated compound 7-((4-(4-tritiumphenyl)piperidin-1-yl)methyl)-3-(cyclopropylmethyl)-8-(trifluoromethyl)-[1,2,4]triazolo[4,3-a]pyridine (radiochemical purity of 97.4%; specific activity of 25 Ci/mmol).

Cell Culture

CHO-K1 cells stably expressing the wildtype (WT) $hmGlu_2$ receptor (CHO-K1_$hmGlu_2$) were grown in Dulbecco's modified Eagle's medium (DMEM) supplemented with 10% (v/v) fetal calf serum, 88 IU·mL^{-1} penicillin, 88 μg·mL^{-1} streptomycin, 30.5 μg·mL^{-1} L-proline and 400 μg·mL^{-1} G418 at 37°C and 5% CO_2. CHO-K1 cells were cultured in the same medium without G418. Cells were subcultured at a ratio of 1:10 twice every week.

Cell Membrane Preparation

CHO-K1_$hmGlu_2$ cells were plated into 15 cm Ø plates in DMEM without G418. When cells were grown to 70% confluency sodium butyrate (final concentration 5 mM) was added to the plates.[27] After 24 hours cells were detached from the plates by scraping them into 5 ml of PBS and subsequently centrifuged for 5 min at 1500 rpm. The pellets were resuspended into ice-cold Tris buffer (50 mM Tris-HCl pH 7.4) and homogenized using an Ultra Turrax homogenizer (IKA-Werke GmbH & Co.KG, Staufen, Germany). Membranes and the cytosolic fraction were separated by centrifugation at 31,000 rpm in an Optima LE-80 K ultracentrifuge (Beckman Coulter, Fullerton, CA) at 4°C for 20 min. Pellets were resuspended in 10 ml Tris buffer and the centrifugation and homogenization steps were repeated. The remaining pellets were suspended into assay buffer (50 mM Tris-HCl pH 7.4, 2 mM $CaCl_2$, 10 mM $MgCl_2$) and the homogenization step was repeated. Aliquots of membrane suspension were stored at -80°C. Membrane protein concentrations were determined using a BCA protein determination.[28]

Transient Transfection

Transient transfections were performed as previously described.[22]

Western blot analysis

$hmGlu_2$ receptor membrane samples were thawed and homogenized using an Ultra Turrax homogenizer at 24,000 rpm. For each membrane suspension sample 200 μl was transferred to an eppendorf tube and 400 μl of RIPA buffer (150 mM NaCl, 1.0% IGEPAL® CA-630, 0.5% sodium deoxycholate, 0.1% SDS, 50 mM Tris, pH 8.0, Sigma-Aldrich) complemented with phosphatase and protease inhibitors (Roche, Basel, Switzerland) was added. Homogenates were incubated for 30 min on ice and centrifuged at 14,000 rpm (20 min, 4°C). The supernatants were collected and protein concentrations were determined using the BCA method

(Smith et al., 1985). Samples were diluted with RIPA buffer (0.15 μg/ml) and denatured by LDS sample buffer and reducing agent (Life Technologies, Invitrogen, Carlsbad, CA, USA) (final concentration 0.1 μg/ml). The membrane protein samples were electrophoresed (3 μg), using an 18-well 4-12% polyacrylamide gel (Bio-Rad, Hercules, CA, USA) at 90-160V. The proteins on the gels were then electroblotted onto a Trans blot turbo 0.2 μm nitrocellulose membrane (Bio-Rad), by using a Trans-blot Turbo transfer system (Bio-Rad). Membranes were blocked for 1 hour at room temperature in Tween-20 Tris-buffered Saline (TBS-T: 10 mM Tris-HCl pH 8.0, 150 mM NaCl, 0.05% Tween-20) containing 5% non-fat dry milk (Santa Cruz Biotechnology, Dallas, TX, USA), and incubated with the primary antibody overnight at 4 °C allowing gentle shaking at a final concentration of 0.75 μg/ml (specific monoclonal mouse anti-hmGlu2 antibody, Abcam ab15672, Cambride, United Kingdom). Blots were washed five times with TBS-T buffer and incubated with the secondary antibody for 1h at room temperature (polyclonal HRP-linked sheep anti-mouse IgG whole antibody, GE healthcare, little Chalfont Buckinghamshire, United Kingdom). Immunostaining was revealed after washing with TBST buffer via SuperSignal West Dura Extended Duration Substrate (Thermo scientific, Cramlington, United Kingdom). Signals were captured and quantified by chemiluminescence (G-box Syngene, Syngene, Cambridge, United Kingdom). For reprobing, membranes were stripped of using Restore™ Western Blot Stripping Buffer (Thermo scientific) for 15 min with agitation at room temperature. Before incubation with anti actin antibody (Millipore, Billerica, CA, USA, MAB1501, dilution 1:10000), the membranes were washed 3 times (5 min) in TBS-T and blocked 1h in 5% non-fat dry milk.

Radioligand binding assays

[^{3}H]JNJ-46281222 Binding

After thawing, membranes were homogenized using an Ultra Turrax homogenizer at 24,000 rpm. Samples were diluted in ice-cold assay buffer (50 mM Tris-HCl pH 7.4, 2 mM $CaCl_2$, 10 mM $MgCl_2$) to a total reaction volume of 100 μl and incubated at 15°C. Nonspecific binding was determined using 10 μM JNJ-40068782, DMSO concentrations were ≤0.25%.

For saturation experiments CHO-K1_hmGlu$_2$ membrane aliquots, containing 30 μg protein, and nine increasing concentrations of radioligand, ranging from 0.4 to 20 nM, were incubated for 60 minutes to allow equilibrium to be reached for all concentrations of radioligand. Nonspecific binding was determined at three concentrations of radioligand.

Association experiments were carried out by incubation of 6 nM of radioligand and membrane aliquots, containing 20 or 30 μg of protein for assays in presence or absence of 1 mM glutamate, respectively. The amount of receptor-bound radioligand was determined at different time points up to 180 minutes.

Dissociation experiments were performed by a 60 minute pre-incubation of 6 nM radioligand and membrane aliquots containing 30 μg protein or for assays in the presence of 1 mM glutamate or GTP, 20 or 50 μg respectively. Dissociation was initiated by addition of 10 μM

JNJ-40068782 (final concentration) in 5 µl. and the amount of remaining receptor-bound radioligand was determined at different time points up to 120 minutes.

Displacement experiments were performed using 6 nM of radioligand and 10 concentrations of competing ligand, diluted by an HP D300 digital dispenser (Tecan, Giessen, The Netherlands) and incubated for 60 minutes. Membrane protein aliquots containing 30 or 40 µg were used for membranes stably expressing the $hmGlu_2$ receptor or for transiently transfected $hmGlu_2$ receptor constructs, respectively.

For all assays, incubation was terminated by rapid filtration over GF/C filters through a Brandel harvester 24 (Brandel, Gaithersburg, MD, USA) or over GF/C filterplates (PerkinElmer, Groningen, The Netherlands) on a PerkinElmer filtermate harvester. Filters were subsequently washed at least three times using ice-cold wash buffer (50 mM TRIS-HCl pH 7.4). Filter-bound radioactivity was determined using liquid scintillation spectrometry on a TRI-Carb 2810 TR counter (PerkinElmer) or a P-E 1450 Microbeta Wallac Trilux scintillation counter (PerkinElmer). [^{3}H]JNJ-46281222 did not bind to CHO-K1 membranes without $hmGlu_2$ receptor expression (data not shown). For all radioligand binding experiments, radioligand concentrations were chosen such that <10% of the amount added was receptor-bound.

[^{3}H]LY341495 Binding

For saturation experiments, various concentrations of [^{3}H]LY341495 from 0.5 to 30 nM were incubated with 10 µg membrane protein from the same batch of membranes as used for [^{3}H]JNJ-46281222 saturation binding experiments at 15°C for 60 minutes in a total volume of 100 µl. Nonspecific binding was determined at three concentrations of radioligand in the presence of 1 mM glutamate. Incubations were terminated and samples obtained and analysed as described under '*[^{3}H]JNJ-46281222 Binding*'.

[^{3}H]DCG-IV Binding

For saturation experiments, unlabelled DCG-IV was spiked with 20% [^{3}H]DCG-IV, resulting in final concentrations from 50 to 1500 nM. DCG-IV was incubated with 75 µg membrane protein from the same batch of membranes as used for [^{3}H]JNJ-46281222 saturation binding experiments at 15°C for 60 minutes in a total volume of 100 µl. Nonspecific binding was determined at three concentrations of radioligand in presence of 10 µM LY341495. Incubations were terminated and samples obtained and analysed as described under '*[^{3}H]JNJ-46281222 Binding*'.

[^{35}S]GTPγS Binding

[^{35}S]GTPγS binding experiments were performed as previously described.[14]

Data analysis

Data analyses were performed using Prism 5.00 (GraphPad software, San Diego, CA, USA). K_D and B_{max} were determined by a saturation binding analysis, using the equation $Y = B_{max} \times K_D / (K_D + X)$. pIC_{50} values were obtained using non-linear regression curve fitting into a sigmoidal concentration-response curve using the equation: Y=Bottom + (Top-Bottom)/(1+10$^{(X-LogIC50)}$). pK_i values were obtained from pIC_{50} values using the Cheng-Prusoff equation.[29] Dissociation rate constants k_{off} were determined by using an exponential decay analysis of radioligand binding. Association rate constants k_{on} were determined using the equation $k_{on} = (k_{obs} - k_{off})/[L]$, in which L is the concentration of radioligand used for association experiments and k_{obs} is determined using exponential association analysis. Data shown are the mean ± SEM of at least three individual experiments performed in duplicate, unless stated otherwise. Statistical analysis was performed if indicated, using a two-tailed unpaired Student's t-test or one-way ANOVA with Dunnett's post-test. Observed differences were considered statistically significant if p-values were below 0.05.

Building an $mGlu_2$ receptor homology model

An active state model of the 7TM domain of human $mGlu_2$ receptor (Uniprot code Q14416) bound to G protein was built using a combination of structural templates. The crystal structure of the human $mGlu_5$ (PDB 4OO9)[24] was used to model all 7TM helices except TM6. Extracellular loop 2 (ECL2) is not refined in the $mGlu_5$ X-ray structure therefore this important loop was modelled based on the $mGlu_1$ receptor crystal structure (PDB 4OR2).[23] Finally, the β_2AR (PDB ID 3SN6)[30] active structure was used to model both TM6 in its distinct open conformation as well as the corresponding G protein. This monomer 7TM has been shown experimentally to be activated upon PAM binding[31] The sequence identity between $mGlu_2$ and $mGlu_5$ 7TM's was 51%. The initial model was constructed in MOE v2014.9 (Chemical computing group Inc., Montreal, QC, Canada) and then Maestro (Schrodinger LLC, New York, NY, USA) was used for structure preparation. The Protein Preparation tool was used to fix any missing sidechains/atoms, PROPKA assigned protonation states, the hydrogen bonding network was optimized, and brief minimisation to RMSD 0.5 Å was applied to remove any structural clashes. Amino acid numbering is based on recent recommendations.[32]

Docking of JNJ-46281222

The ligand was prepared for docking using Maestro. Its basic pK_a value was measured experimentally as 6.6. The structure activity relationship (SAR) of molecules from this series does not require a charged centre for $mGlu_2$ PAM activity.[33] Hence, JNJ-46281222 was modelled in an unionised state. Conformational sampling was performed with ConfGen and multiple conformers were docked into the $mGlu_2$ active state model using Glide XP. The docking grid was centered on the ligand position in the $mGlu_1$ receptor structure. Sampling was increased

in the Glide docking by turning on expanded sampling and passing 100 initial poses to post-docking minimisation. All other docking parameters were set to the defaults.

Molecular Dynamics Simulations

Molecular dynamics (MD) simulations were performed with GROMACS v4.6.5.[34] Ligand-receptor complexes were embedded in a pre-equilibrated box (10x10x19 nm) containing a lipid bilayer (297 POPC molecules) with explicit solvent (~47000 waters) and 0.15 M concentration of Na^+ and Cl^- (~490 ions). The total size of the system was 174000 atoms. Each system was energy minimized and subjected to a 5 step MD equilibration of 10, 5, 2, 2 and 2 ns respectively. In the first step the whole system was fixed except for the hydrogens. In the second, the protein loops were released from restraints. In the final three steps the restraints on the ligand and proteins were relaxed from 100, 50 and 10 $kJ.mol^{-1}nm^{-2}$ respectively. Production simulations were performed for time periods between 200 and 500 ns without restraints using a 2 fs time step. Constant temperature of 300K using separate v-rescale thermostats for Protein-Ligand, lipids, and water plus ions was used. The LINCS algorithm was applied to freeze bond lengths. Lennard-Jones interactions were computed using a 10 Å cut-off, and the electrostatic interactions were treated using PME also with a 10 Å cut-off. The AMBER99SD-ILDN force field[35] was used for the protein, the parameters described by Berger *et al.* (1997)[36] for lipids, and the general Amber force field (GAFF) and HF/6-31G*-derived RESP atomic charges for the ligand. This combination of protein and lipid parameters has recently been validated.[37]

RESULTS

Characterization of [^{3}H]JNJ-46281222

Firstly, the affinity of [^{3}H]JNJ-46281222 for the $mGlu_2$ receptor was determined by performing saturation binding experiments on membranes of CHO-K1 cells stably expressing the $hmGlu_2$ receptor (Fig. 2A). Receptor binding was saturable and defined by a K_D of 1.7 nM with a B_{max} of 1.1 pmol/mg protein. Homologous displacement experiments with [^{3}H]JNJ-46281222 resulted in a pK_i value of 8.33 for JNJ-46281222. In addition, a series of reference PAMs and a NAM based on various chemical scaffolds fully displaced [^{3}H]JNJ-46281222 binding, resulting in pK_i values ranging from 6.43 to 8.09 (Table 1), while pseudo-Hill coefficients were all close to unity. Secondly, kinetic association and dissociation experiments were performed to determine the association (k_{on}) and dissociation (k_{off}) rate constants (Fig. 2B; Table 2). Equilibrium binding of [^{3}H]JNJ-46281222 was reached within 30 minutes as assessed by kinetic association experiments and best fit with a one-phase model, whereas the dissociation curve was best fit with a two-phase model. This resulted in a k_{obs} value of 0.24 min^{-1} describing the association

and two values describing the dissociation, i.e. a $k_{off,1}$ value of 0.040 min^{-1} and a $k_{off,2}$ value of 0.77 min^{-1}.

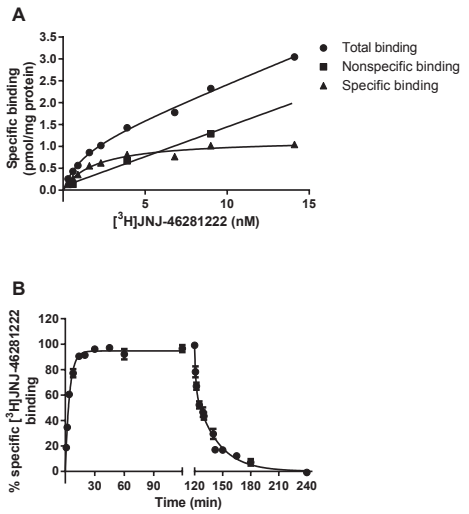

Figure 2. Characterization of [^{3}H]JNJ-46281222 binding to $mGlu_2$ receptors stably expressed at CHO-K1 membranes.
(A) Saturation analysis of [^{3}H]JNJ-46281222 binding. A representative experiment is shown with similar data being obtained in two additional experiments.
(B) Association and dissociation kinetics of 6 nM [^{3}H]JNJ-46281222 at the $mGlu_2$ receptor at 15°C. Association data was best fitted using a one-phase exponential association model, whereas data for dissociation curves were best fitted using a two-phase exponential decay model. Data are expressed as percentage of specific [^{3}H]JNJ-46281222 binding and are shown as mean ± SEM of at least four individual experiments. Where bars are not shown SEM values are within the symbol.

Table 1. Receptor affinity of $mGlu_2$ allosteric modulators determined by [^{3}H]JNJ-46281222 displacement experiments.

Compound	pK_i
JNJ-46281222	8.33 ± 0.14
JNJ-40068782	7.58 ± 0.08
BINA	7.22 ± 0.15
THIIC	7.10 ± 0.04
AZD8529	6.43 ± 0.03
RO4491533	8.09 ± 0.09

Data are shown as mean ± SEM of at least three individual experiments performed in duplicate.

Table 2. Kinetic binding parameters for [^{3}H]JNJ-46281222 binding to human $mGlu_2$ receptors in absence or presence of 1 mM glutamate.

	k_{obs} (min^{-1})	k_{on} ($nM^{-1}.min^{-1}$)[a]	k_{off} (min^{-1})[b]		K_D (nM)[c]
			$k_{off,1}$	$k_{off,2}$	
[^{3}H]JNJ-46281222	0.24 ± 0.019	-	0.040 ± 0.0061	0.77 ± 0.18	-
[^{3}H]JNJ-46281222 + 1 mM glutamate	0.19 ± 0.031	0.019 ± 0.0051	0.070 ± 0.0056	-	3.6 ± 0.99

Data are shown as mean ± SEM of at least three individual experiments performed in duplicate. [a] k_{on} was determined using the formula $k_{on} = (k_{obs} - k_{off})/[L]$. [b] All parameters were determined by computer analysis using a one-phase model, except for dissociation of [^{3}H]JNJ-46281222 in absence of glutamate which was best described by a two-phase model. [c] K_D was determined as the ratio k_{off} / k_{on}.

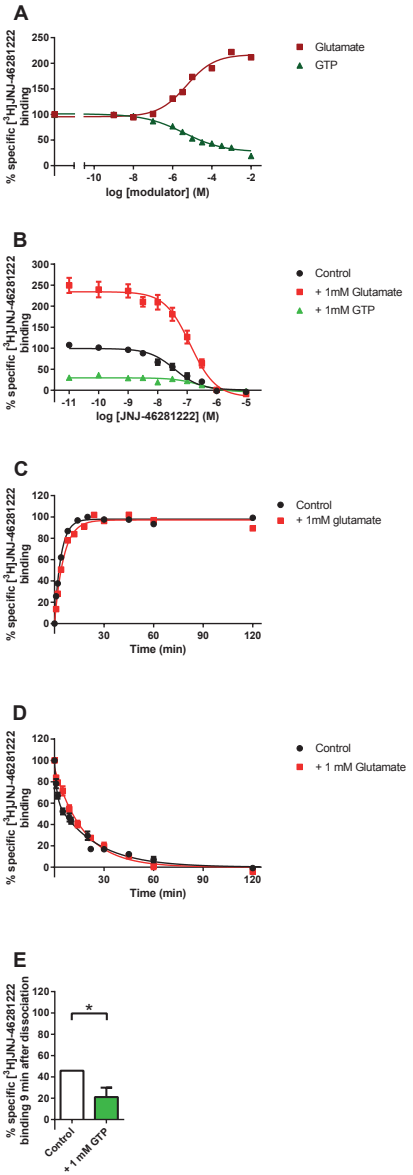

The effect of glutamate on [^{3}H]JNJ-46281222 binding to the mGlu$_2$ receptor

Increasing concentrations of glutamate enhanced [^{3}H]JNJ-46281222 binding by more than 2-fold (Fig. 3A; Table 3) with a modulatory potency (pEC_{50}) for glutamate of 5.27. [^{3}H]JNJ-46281222 displacement assays in the absence or presence of glutamate were performed with JNJ-46281222 and JNJ-40068782, which did not result in a significant change in affinity for both compounds (Fig. 3B; Table 4).

In addition, saturation binding of [^{3}H]JNJ-46281222 in the absence or presence of glutamate was performed (Fig. 4A), showing that the number of mGlu$_2$ PAM binding sites (B_{max}) was increased more than 2-fold in the presence of 1 mM glutamate, whereas the affinity (K_D) was not significantly affected (Table 5).

Next, the effect of glutamate on the kinetic association and dissociation rates of [^{3}H]JNJ-46281222 was examined. Glutamate decreased both rate constants to a small non-significant extent (Fig. 3C and 3D, Table 2). Moreover, whereas dissociation in the absence of glutamate was best described using a two-phase model, dissociation in the presence of 1 mM glutamate was best described with a one-phase model, with a k_{off} value of 0.070 min^{-1}. This presence of glutamate enabled further determination of the association rate constant k_{on}, which was 0.019 nM^{-1} min^{-1}. Based on these

Figure 3. The effects of glutamate and GTP on [^{3}H]JNJ-46281222 binding. (A) Increasing concentrations of glutamate enhance the specific binding of 6 nM [^{3}H]JNJ-46281222 to mGlu$_2$ receptors expressed at CHO-K1 cell membranes, whereas GTP inhibits specific [^{3}H]JNJ-46281222 binding. (B) Effects of glutamate and GTP on homologous displacement of [^{3}H]JNJ-46281222 from mGlu$_2$ receptors expressed at CHO-K1 membranes. Data are normalized to specific binding in absence of glutamate or GTP (set at 100%). (C, D) The effect of glutamate on mGlu$_2$ receptor association and dissociation of [^{3}H]JNJ-46281222. Data are expressed as specific binding of the respective curve, association plateaus are fixed at 100% specific [^{3}H]JNJ-46281222 binding, dissociation plateau fixed at 0% specific [^{3}H]JNJ-46281222 binding. (E) Specific [^{3}H]JNJ-46281222 binding after nine minutes of dissociation in absence or presence of GTP. * p-value <0.05 versus control, determined using a two-tailed unpaired Student's t-test. All graphs are shown as mean ± SEM of three to six individual experiments performed in duplicate. Where bars are not shown SEM values are within the symbol.

kinetic parameters, the kinetic K_D was determined according to the equation $K_D = k_{off} / k_{on}$, resulting in a K_D value of 3.6 nM for [^{3}H]JNJ-46281222 in the presence of glutamate (Table 2), which was in good agreement with the K_D value obtained from saturation experiments.

Table 3. Pharmacological characterization of the effects of glutamate or GTP on specific [^{3}H]JNJ-46281222 binding to mGlu$_2$ receptors.

	pEC_{50} / pIC_{50}	E_{max} (%)[a]	Hill slope
Glutamate	5.27 ± 0.08	125 ± 9.0	0.49 ± 0.04
GTP	5.95 ± 0.21	-65 ± 8.0	-0.58 ± 0.03

Data are shown as mean ± SEM of three individual experiments performed in duplicate. [a] E_{max} was determined as difference in total specific binding compared to binding in absence of glutamate or GTP (set at 100%).

The effect of GTP on [^{3}H]JNJ-46281222 binding to the mGlu$_2$ receptor

Radioligand displacement assays in the presence of increasing GTP concentrations were performed to evaluate the importance of the presence of a bound G protein for [^{3}H]JNJ-46281222 binding. As depicted in Figure 3A, GTP inhibits [^{3}H]JNJ-46281222 binding by 65% with a pIC_{50} value of 5.95. The affinity of JNJ-46281222 was significantly decreased in the presence of 1 mM GTP, whereas this was not the case for JNJ-40068782 (Table 4). Subsequently, the effect of 1 mM GTP on the dissociation rate of [^{3}H]JNJ-46281222 was examined. Since it was impossible to obtain reliable full curves with the vastly decreased [^{3}H]JNJ-46281222 window under these conditions, [^{3}H]JNJ-46281222 dissociation in the presence of 1 mM GTP was only determined at a single time point (i.e. after nine minutes) and compared to the extent of dissocation in the absence of GTP at that same time point (Fig. 3E). In the presence of 1 mM GTP the relative amount of [^{3}H]JNJ-46281222 still bound to the receptor after nine minutes was significantly lower than in its absence, indicating an increased dissociation rate.

Table 4. Displacement of [^{3}H]JNJ-46281222 by mGlu$_2$ PAMs JNJ-46281222 and JNJ-40068782 from human mGlu$_2$ receptors in absence (control) or presence of 1 mM glutamate or GTP.

	pIC_{50}			E_{max} (%)[a]	
	Control	+ 1mM Glu	+ 1mM GTP	+ 1mM Glu	+ 1mM GTP
JNJ-46281222	7.71 ± 0.17	7.63 ± 0.14	7.00 ± 0.16*	150 ± 24	-71 ± 4.4
JNJ-40068782	6.89 ± 0.06	7.15 ± 0.10	6.85 ± 0.06	127 ± 20	-77 ± 4.5

Data are shown as mean ± SEM of at least three individual experiments performed in duplicate. [a] Emax was determined as difference in total specific binding compared to binding in absence of glutamate or GTP (set at 100%). * p-value < 0.05 compared to pIC_{50} control, determined using one-way ANOVA with Dunnett's post-test.

Saturation binding of orthosteric radioligands to the mGlu$_2$ receptor

For comparison of the number of accesible orthosteric and allosteric binding sites, saturation experiments were performed using the orthosteric radioligands [^{3}H]DCG-IV and [^{3}H]LY341495 (Fig. 4B and 4C, Table 5). The mGlu$_2$ agonist [^{3}H]DCG-IV had a low affinity of 365 nM and a B_{max} value of 1.2 pmol/mg that corresponded to the B_{max} value of 1.1 pmol/mg

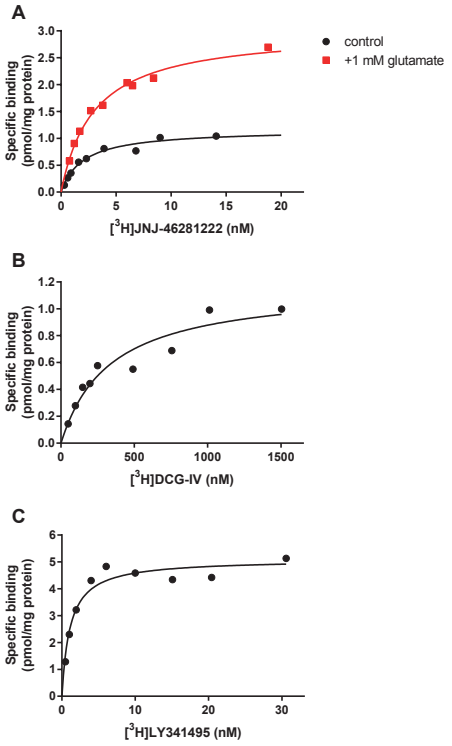

Figure 4. Saturation binding of radioligands to $mGlu_2$ receptors expressed at CHO-K1 membranes. (A) Saturation binding of [^{3}H]JNJ-46281222 to the $mGlu_2$ allosteric binding site in absence or presence of glutamate. (B) Saturation binding of [^{3}H]DCG-IV to the $mGlu_2$ orthosteric binding site, determined by "spiked" saturation (see text). (C) Saturation binding of [^{3}H]LY341495 to the orthosteric binding site. Graphs shown are from a representative experiment performed in duplicate in each case.

obtained for [^{3}H]JNJ-46281222. The high affinity antagonist [^{3}H]LY341495 had a K_D value of 2.4 nM and a B_{max} value of 5.1 pmol/mg, approximately 5-fold higher than for the PAM and for the agonist.

Quantification of potency of JNJ-46281222 at the $mGlu_2$ receptor

Figure 5A shows data from a representative determination of the concentration-effect curve of the glutamate-induced binding of [^{35}S]GTPγS in the absence and presence of various concentrations of JNJ-46281222; similar data were obtained in a second experiment. A 100 nM concentration of JNJ-46281222 enhanced the maximum glutamate-induced [^{35}S]GTPγS binding, i.e. glutamate's efficacy, by approximately 2-fold, shifting the curve upward, and increased the glutamate potency 5-fold, shifting the curve leftward. The potency of JNJ-46281222 was determined by quantifying the increase in response to a fixed EC_{20} glutamate concentration (4 μM), as depicted in Figure 5B. A pEC_{50} of 7.71 ± 0.02 was calculated while the maximal response, 193 ± 5%, was almost 2-fold higher compared to the maximal glutamate response exerted by 1 mM glutamate alone. In the absence of glutamate JNJ-46281222 shows a submaximal receptor activation of 42 ± 3% with a 10-fold lower pEC_{50} value of 6.75 ± 0.08.

Table 5. Characteristics of saturation binding of [^{3}H]JNJ-46281222 in absence or presence of glutamate, and the orthosteric radioligands [^{3}H]DCG-IV and [^{3}H]LY341495

Radioligand	K_D (nM)	B_{max} (pmol/mg protein)
[^{3}H]JNJ-46281222	1.7 ± 0.17	1.1 ± 0.12
+ 1 mM glutamate	2.5 ± 0.26	2.7 ± 0.25
[^{3}H]DCG-IV	330 / 400	1.1 / 1.2
[^{3}H]LY341495	2.4 ± 0.71	5.1 ± 0.39

Data for [^{3}H]JNJ-46281222 and [^{3}H]LY341495 are shown as mean ± SEM of at least three individual experiments performed in duplicate. The same parameters measured for [^{3}H]DCG-IV are from two independent experiments (values of both experiments are given).

Docking of JNJ-46281222 into the $mGlu_2$ 7TM Model

JNJ-46281222 was docked into the active state $mGlu_2$ homology model (Fig. 6A and 6B). The most energetically favourable binding pose is shown. The triazopyridine scaffold and lipophilic side chain substituent interact with the hydrophobic cluster formed between amino acids L639$^{3.32a.36c}$, F643$^{3.36a.40c}$, L732$^{5.43a.44c}$, W773$^{6.48a.50c}$ and F776$^{6.51a.53c}$. The cyclopropylmethyl substituent goes deepest into the receptor and interacts closely with F776$^{6.51a.53c}$. The hydrophobic residues cluster tightly around the triazopyridine scaffold with L639$^{3.32a.36c}$ and F643$^{3.36a.40c}$ interacting on one face of the scaffold and L732$^{5.43a.44c}$ and W773$^{6.48a.50c}$ on the other. Amino acid N735$^{5.47a.47c}$ acts as an H-bond donor to the nitrogen acceptor (2.0 Å) in the triazo ring of the scaffold. The sidechain of tryptophan W773$^{6.48a.50c}$, which is conserved in the mGlu receptors, points into the membrane in the same orientation as in the $mGlu_5$ inactive state 7TM crystal structure. The cyclopropyl group makes a steric interaction at 2.3 Å distance. The CF_3 group of the scaffold enters between TM3 and TM5 above N735$^{5.47a.47c}$, and interacts with S731$^{5.42a.43c}$. The 4-phenylpiperidine substituent is directed towards the extracellular side of the binding site and the distal phenyl sits between F623$^{2.61a.56c}$ and H723^{ECL2}. The predicted binding mode overlaps with the allosteric site in $mGlu_1$ whereas the $mGlu_5$ modulator goes deeper into the receptor (Fig. S1).

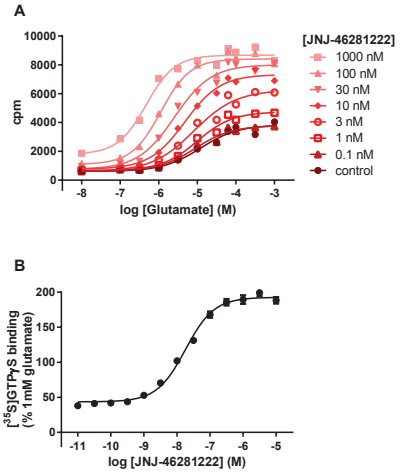

Figure 5. Characterization of potency of JNJ-46281222. (A) Stimulation of [^{35}S]GTPγS binding to $mGlu_2$ receptors induced by increasing concentrations of JNJ-46281222. A representative experiment is shown, with similar data obtained in a second experiment. Data are expressed as the percentage of maximal response induced by 1 mM glutamate. (B) Dose-response curve of JNJ-46281222 in presence of glutamate (EC_{20}, 4 μM) on the binding of [^{35}S]GTPγS binding. Data are expressed as the percentage of maximal response induced by 1 mM glutamate and are shown as mean ± SEM of thirteen individual experiments performed in triplicate. Where bars are not shown SEM values are within the symbol.

The location of the allosteric binding pocket of JNJ-46281222 at the $mGlu_2$ receptor

In order to validate the suggested location of the JNJ-46281222 binding site, radioligand binding assays were performed on transiently transfected $mGlu_2$ wild-type and mutant receptors. For the latter, mutations F643A$^{3.36a.40c}$ and N735D$^{5.47a.47c}$ were selected, since molecular docking studies indicated that these amino acids (amongst others) had important interactions with JNJ-46281222. Receptor expression was confirmed by Western blot analysis (Fig.7B). [^{3}H]JNJ-46281222 binding to the selected $mGlu_2$ receptor mutants, was significantly decreased by approximately 10-fold compared to WT, as shown in Figure 7A.

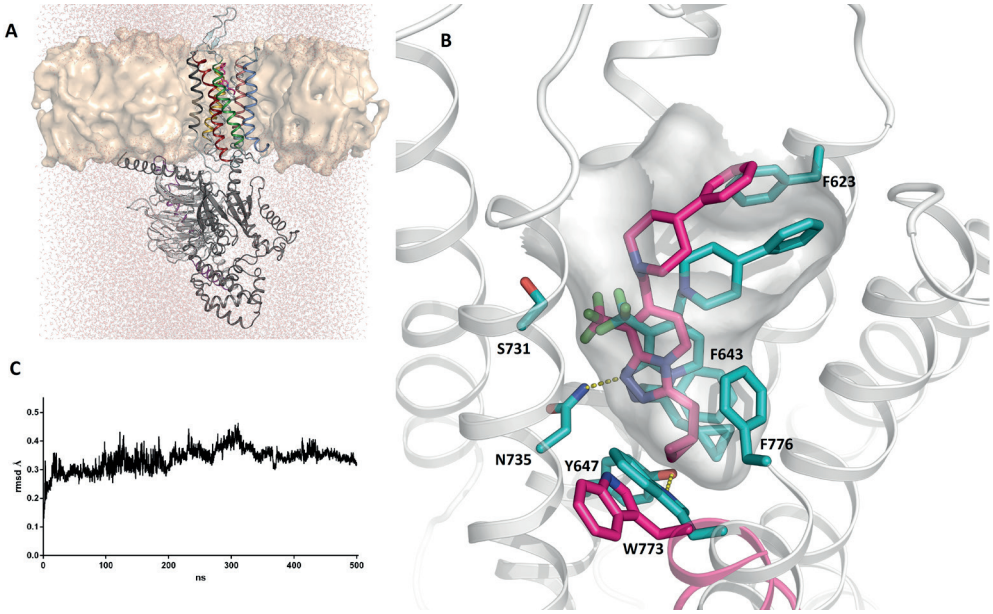

Figure 6. Molecular dynamics (MD) simulations of the binding of JNJ-46281222 to the $mGlu_2$ receptor. (A) The complete system used for MD simulations, including $mGlu_2$ receptor 7TM monomer, G protein, ligand (JNJ-46281222, magenta), lipids and solvent. (B) Close up of 7TM binding site showing interaction with a subset of important amino acids. MD starting position for ligand is coloured magenta; snapshot after 200 ns is turquoise. Movement of $W773^{6.48a.50c}$ from outwards orientation (magenta) at start of simulation to inwards orientation (turquoise) is highlighted. (C) RMSD of $mGlu_2$ receptor monomer during the simulation.

Molecular dynamics simulations of JNJ-46281222 and $mGlu_2$ 7TM Model

MD simulations of JNJ-46281222 docked in the WT active state $mGlu_2$ receptor model together with the G protein were performed for 500 ns. The overall structure was stable throughout the simulation with little fluctuation in RMSD of the 7TM (Fig. 6C). The G protein also showed little structural fluctuation and remained bound to the intracellular side of the receptor keeping TM6 in an open conformation. The ligand maintained key interactions with amino acids such as $L639^{3.32a.36c}$, $F643^{3.36a.40c}$ and $N735^{5.47a.47c}$ (Fig. 6B). Amino acids in the vicinity of JNJ-46281222 moved, and adopted alternative orientations which remained stable throughout the rest of the simulation. For instance, $W773^{6.48a.50c}$ made a large rotational movement inwards after 20 ns which was permitted by adjustment of the cyclopropylmethyl away from TM5 and towards $F643^{3.36a.40c}$. The tryptophan $W773^{6.48a.50c}$ then rotated into the 7TM binding site to maintain interaction with the ligand whilst forming a new H-bond interaction via its indole NH donor to the phenolic oxygen of $Y647^{3.39a.43c}$. Three additional replica simulations were performed for 200 ns using the same input but different starting velocities. Two of these showed consistent behaviour of $W773^{6.48a.50c}$. Additional MD simulations performed on the same system but without ligand did not display the inward rotation of $W773^{6.48a.50c}$. Likewise, the sidechain remained outwards during a separate simulation with ligand but

without G protein. Regarding the distal tail of JNJ-46281222, the phenyl moiety moved deeper into the 7TM binding site during the 500 ns simulation and continued to interact with F623$^{2.61a.56c}$ but no longer had contacts with H723 (mutation of which had previously shown no effect on JNJ-46281222 functional activity.)[22] Simulations performed on F643A$^{3.36a.40c}$ and N735D$^{5.47a.47c}$ mutant receptors were also stable with respect to the overall 7TM. However, for the N735D$^{5.47a.47c}$ mutant, the ligand made a significant departure from its starting orientation. In summary, the MD simulations revealed the predicted binding mode to be stable and consistent with amino acids making key interactions.

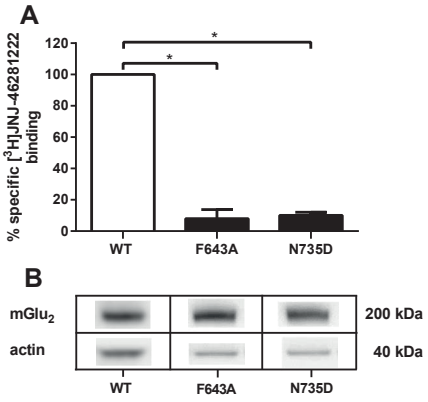

Figure 7. (A) Radioligand binding to $mGlu_2$ receptor mutants F643$^{3.36a.40c}$ and N735$^{5.47a.47c}$. Specific [^{3}H]JNJ-46281222 binding to WT or mutant $mGlu_2$ receptors, transiently transfected in CHO-K1 cells. Data were normalized to % specific binding compared to binding to WT $mGlu_2$ receptors and are expressed as mean ± SEM of three individual experiments performed in duplicate. (B) Representative immunoblot of WT (left panel) and mutant $mGlu_2$ receptors (middle, F643, and right, N735, panel) and actin. * p-value < 0.05 compared to WT, analysis was done using unnormalized data and determined using one-way repeated-measures ANOVA with Dunnett's post-test.

DISCUSSION

We describe JNJ-46281222 as a high affinity $mGlu_2$ PAM (K_D = 1.7 nM) with a high modulatory potency (pEC_{50} = 7.71 ± 0.02) on the effect of the endogenous agonist glutamate in a [^{35}S]GTPγS binding assay, where it increased glutamate's maximum effect by approximately 2-fold to its 'ceiling' allosteric effect.[38] These data are in line with previously reported affinity data for JNJ-46281222.[22] JNJ-46281222 on its own displayed a submaximal receptor activation of 43 ± 3% in the [^{35}S]GTPγS binding assay, with a potency (pEC_{50} = 6.75 ± 0.08) that is 10-fold lower compared to its potency to modulate glutamate activity. However, we prefer to refer to JNJ-46281222 as a PAM and not as a PAM-agonist for at least two reasons. First, we cannot fully rule out the presence of endogenous receptor-bound glutamate. Secondly, the cell line used has a high receptor density, potentially amplifying receptor responses. The potency and affinity of this PAM are higher than any other extensively reported $mGlu_2$ PAMs including JNJ-40068782 (Table 1).[10,14] In addition to its valuable properties for *in vitro* experiments,

[^{3}H]JNJ-46281222 can also be used for *ex vivo* $mGlu_2$ receptor occupancy studies, whereas this cannot be done with [^{3}H]JNJ-40068782.[39]

To investigate the relation between the orthosteric, allosteric and G protein binding sites, we performed [^{3}H]JNJ-46281222 binding experiments in the absence and presence of either glutamate or GTP. The observation by Lavreysen *et al.* (2013)[14] and Lundström *et al.* (2011)[21] - binding of an $mGlu_2$ PAM is enhanced in the presence of a high concentration of the orthosteric agonist glutamate - was taken as a starting point for our work. In our case, the total amount of sites accesible for JNJ-46281222 binding was significantly enlarged by approximately 2.5-fold by the addition of glutamate (Fig. 3B and 4A). This indicates a conformational change in receptor structure that increases the population of receptors in a more favourable state for PAM binding and recognition. In addition, we performed [^{3}H]JNJ-46281222 binding experiments in the presence of increasing concentrations of glutamate, confirming the increase in specific binding with a micromolar potency for glutamate (pEC_{50} = 5.27) and a pseudo-Hill slope of less than unity (n_H = 0.49), indicative of allosteric enhancement of JNJ-46281222 binding by the agonist. Thereby, this experiment clearly revealed two-way allosterism between orthosteric and allosteric binding sites.[40]

We showed that the presence of glutamate does not significantly change the affinity of $mGlu_2$ PAMs, as was observed previously for $mGlu_5$ PAMs.[41] Specifically, the affinity of JNJ-46281222 was not affected by the presence of glutamate, as both K_D values were similar (1.7 and 2.4 nM, Table 5), just like the pIC_{50} values of 7.71 and 7.63 (Table 4). For JNJ-40068782 we did not find a significant increase in affinity, as shown by the pIC_{50} values, whereas Lavreysen *et al.* (2013)[14] showed an increase in K_D values. This could be indicative for between membrane pool or between lab variations. The presence of glutamate decreased the rate of both association and dissociation of [^{3}H]JNJ-46281222 to a small non-significant extent. Most striking was the ability of glutamate to change the two-phasic character of dissociation towards a one-phase dissociation. In general, a two-phasic character can be explained by the presence of two binding sites, known as the high- and low affinity binding sites within a receptor population.[38] In this case, one could postulate that glutamate increases the number of PAM binding sites and fixes the receptor into a single conformational state resulting in a single dissociation rate.

Previous studies showed that binding of only one PAM per dimer is sufficient for enhancement of receptor activity.[42] It was hypothesized that upon receptor activation only one of the 7TM domains is turned on and activates a G protein.[43] Whereas these studies came to their conclusions using changes in the receptor structure, we evaluated the number of orthosteric and allosteric binding sites using radioligand saturation binding assays on the WT $mGlu_2$ receptor. Interestingly, saturation binding of the orthosteric agonist [^{3}H]DCG-IV revealed a B_{max} similar to [^{3}H]JNJ-46281222 (Table 5), indicating the same number of binding sites for

both orthosteric agonists and PAMs. So, whereas only one PAM per receptor dimer is necessary for efficacy,[43] it seems that two PAMs actually bind the receptor in the absence of glutamate. On the other hand, presence of glutamate increases the number of allosteric binding sites, as shown by the increased B_{max} of [^{3}H]JNJ-46281222 (Table 5). This indicates that addition of glutamate might lead to [^{3}H]JNJ-46281222 binding to both glutamate-bound and -unbound receptors. Interestingly, the increase in accesible PAM binding sites induced by the presence of glutamate was not seen the other way around. Both $mGlu_2$ PAMs JNJ-40068782 and JNJ-40411813 increased the affinity of [^{3}H]DCG-IV but not its B_{max} value.[14,39]

The presence of GTP decreased [^{3}H]JNJ-46281222 binding by 65%, indicating that PAM binding is dependent on the availability of receptors that are coupled to a G protein. Moreover, the pseudo-Hill coefficient of less than unity (n_H = -0.58), confirms an allosteric rather than competitive effect of GTP on JNJ-46281222 binding. The necessity of a coupled G protein for PAM binding was further confirmed by saturation binding experiments with [^{3}H]JNJ-46281222, the orthosteric agonist [^{3}H]DCG-IV and antagonist [^{3}H]LY341495, showing that approximately 5-fold more receptors are labeled by an antagonist than an agonist or PAM radioligand (Fig. 4, Table 5). Decades ago, the presence of GTP has already been shown to decrease agonist but not antagonist binding in class A GPCRs (e.g., Williams and Lefkowitz, 1977).[44] For the $mGlu_2$ receptor this was also shown for the orthosteric agonists DCG-IV and LY354740, where GTPγS decreased their binding up to 80% with nanomolar potency.[45,46] In our hands, in addition to a reduction of the total binding level, GTP also induced a significant decrease in binding affinity of JNJ-46281222, whereas it did not change the affinity of JNJ-40068782 (Table 4). These findings contribute to the idea that different PAMs can have different effects on the interplay between receptor binding sites. To our knowledge we are the first to describe the necessity for a G protein bound state of the receptor for PAM binding, as shown by the effects of GTP on the binding of [^{3}H]JNJ-46281222 to the $mGlu_2$ receptor.

Previous mutagenesis studies revealed the molecular determinants vital for $mGlu_2$ PAM functional activity.[18,19,22] However, PAM binding on mutant receptors has not been previously examined. Docking of JNJ-46281222 into the 7TM $mGlu_2$ receptor model revealed direct interactions with, amongst others, F643$^{3.36a.40c}$ and N735$^{5.47a.47c}$. In order to confirm the proposed binding pose of JNJ-46281222 within the $mGlu_2$ 7TM domain, we performed [^{3}H]JNJ-46281222 binding experiments to transiently transfected $mGlu_2$ receptor mutants F643A$^{3.36a.40c}$ and N735D$^{5.47a.47c}$. Their binding was reduced evenly and significantly compared to the transiently transfected WT $mGlu_2$ receptor, showing that these amino acid residues are vital for $mGlu_2$ PAM binding. Together, these results indicate that the loss in $mGlu_2$ PAM functional efficacy, exerted by $mGlu_2$ receptor mutants F643A$^{3.36a.40c}$ and N735D$^{5.47a.47c}$, is caused by a loss of receptor binding.

We have presented hypotheses for the overlap and possible binding mode of $mGlu_2$ PAMs.[22,47] Here we used MD simulations of JNJ-46281222 in an active state 7TM $mGlu_2$ model which confirmed the binding mode was stable throughout the simulation. We observed movement of $W773^{6.48a.50c}$ which is part of a WLAFxPI sequence on TM6 that is conserved across mGlu receptors. The sidechain rotated inwards and interacted with the ligand and $Y647^{3.39a.43c}$. The 6.48a.50c position is located on TM6 in the transmission switch for class A GPCRs.[48] Rotamer movements of this tryptophan in rhodopsin along with the kink induced by the neighbouring proline, contribute to the outward movement of TM6 to permit activation. Also, the movement of $W773^{6.48a.50c}$ to disturb H-bonding in the cluster of amino acids involving $Y647^{3.39a.43c}$ and the conserved water molecule may play a role in the functional activity of class C allosteric modulators.[24] This is just above the important region for Na^+ ion modulation of $A_{2A}AR$ receptors.[49] Finally, a recent report suggests activation of $mGlu_2$ dimers proceeds from inactive TM4/5-TM4/5 interaction to TM6-TM6 interaction in the active state.[50] It seems plausible that inward movement of large sidechains on TM6 will enable the rotation of the monomers to the active state. Further work is needed to provide a deeper understanding of the allosteric modulator action on this $mGlu_2$ monomer and the full length dimeric receptor.

In conclusion, we have characterized the selective and highly potent $mGlu_2$ PAM JNJ-46281222 and its corresponding radioligand [^{3}H]JNJ-46281222. Its characteristics make it the preferred PAM radioligand for studying the $mGlu_2$ receptor. The orthosteric agonist glutamate was shown to increase the number of PAM binding sites without affecting the affinity of JNJ-46281222. The necessity of a coupled G protein was shown by the fact that GTP induced a large decrease of PAM binding and that the number of PAM binding sites, like the orthosteric agonist, was much lower than the number of G protein independent antagonist binding sites. Both mutations $F643A^{3.36a.40c}$ and $N735D^{5.47a.47c}$ caused a large decrease in PAM binding, thereby experimentally confirming the binding site as determined from the modelling and molecular dynamics studies. Together, these results contribute to the understanding of the mechanism of PAM binding and effect, which will hopefully contribute to current and future $mGlu_2$ PAM drug discovery programs.

Supporting figure S1

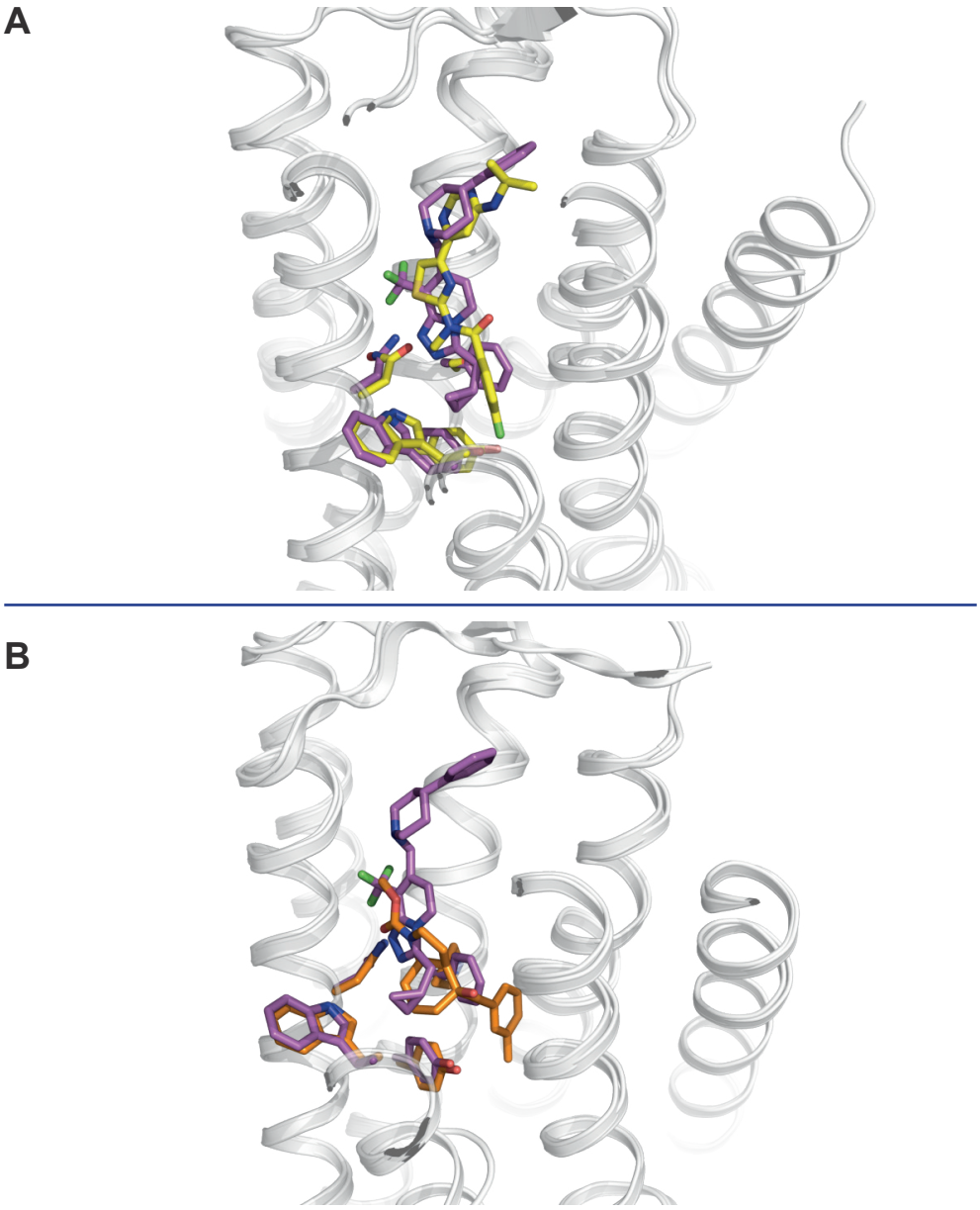

Figure S1. Comparison of the predicted JNJ-46281222 binding mode (purple) with that of NAMs in the $mGlu_1$ (A, yellow) and $mGlu_5$ (B, orange) receptor X-ray structures. A) $mGlu_1$ (yellow) compared to $mGlu_2$ model (purple). Position of allosteric ligand and selected amino acid side chains can be seen. mGlu1 X-ray structure is from PDB code 4OR2. B) $mGlu_5$ (orange) compared to $mGlu_2$ model (purple). Position of allosteric ligand and selected amino acid side chains can be seen. $mGlu_5$ X-ray structure is from PDB code 4OO9.

REFERENCES

1. Pin J-P, Duvoisin R. *Neuropharmacology*. **1995**; 34: 1–26.

2. Alexander SPH, Benson HE, Faccenda E, Pawson AJ, Sharman JL, Spedding M, Peters JA, Harmar AJ. *Br J Pharmacol*. **2013**; 170: 1459–581.

3. Muto T, Tsuchiya D, Morikawa K, Jingami H. *Proc Natl Acad Sci U S A*. **2007**; 104: 3759–64.

4. Niswender CM, Conn PJ. *Annu Rev Pharmacol Toxicol*. **2010**; 50: 295–322.

5. Romano C, Yang W-L, O'Malley KL. *J Biol Chem*. **1996**; 271: 28612–28616.

6. Kniazeff J, Prézeau L, Rondard P, Pin J-P, Goudet C. *Pharmacol Ther*. **2011**; 130: 9–25.

7. Nicoletti F, Bockaert J, Collingridge GL, Conn PJ, Ferraguti F, Schoepp DD, Wroblewski JT, Pin JP. *Neuropharmacology*. **2011**; 60: 1017–41.

8. Conn PJ, Christopoulos A, Lindsley CW. *Nat Rev Drug Discov*. **2009**; 8: 41–54.

9. Gregory KJ, Dong EN, Meiler J, Conn PJ. *Neuropharmacology*. **2011**; 60: 66–81.

10. Trabanco AA, Cid JM. *Expert Opin Ther Pat*. **2013**; 23: 629–47.

11. Johnson MP, Baez M, Jagdmann GE, Britton TC, Large TH, Callagaro DO, Tizzano JP, Monn JA, Schoepp DD. *J Med Chem*. **2003**; 46: 3189–92.

12. Galici R, Jones CK, Hemstapat K, Nong Y, Echemendia NG, Williams LC, de Paulis T, Conn PJ. *J Pharmacol Exp Ther*. **2006**; 318: 173–85.

13. Fell MJ, Witkin JM, Falcone JF, Katner JS, Perry KW, Hart J, Rorick-Kehn L, Overshiner CD, Rasmussen K, Chaney SF, Benvenga MJ, Li X, Marlow DL, Thompson LK, Luecke SK, Wafford KA, Seidel WF, Edgar DM, Quets AT, Felder CC, Wang X, Heinz BA, Nikolayev A, Kuo M-S, Mayhugh D, Khilevich A, Zhang D, Ebert PJ, Eckstein JA, Ackermann BL, Swanson SP, Catlow JT, Dean RA, Jackson K, Tauscher-Wisniewski S, Marek GJ, Schkeryantz JM, Svensson KA. *J Pharmacol Exp Ther*. **2011**; 336: 165–177.

14. Lavreysen H, Langlois X, Ahnaou A, Drinkenburg W, te Riele P, Biesmans I, Van der Linden I, Peeters L, Megens A, Wintmolders C, Cid JM, Trabanco AA, Andrés JI, Dautzenberg FM, Lütjens R, Macdonald G, Atack JR. *J Pharmacol Exp Ther*. **2013**; 346: 514–27.

15. Ball M, Boyd A, Churchill G, Cuthbert M, Drew M, Fielding M, Ford G, Frodsham L, Golden M, Leslie K, Lyons S, McKeever-Abbas B, Stark A, Tomlin P, Gottschling S, Hajar A, Jiang J, Lo J, Suchozak B. *Org Process Res Dev*. **2012**; 16: 741–747.

16. Cook D, Brown D, Alexander R, March R, Morgan P, Satterthwaite G, Pangalos MN. *Nat Rev Drug Discov*. **2014**; 13: 419–31.

17. Cid JM, Tresadern G, Duvey G, Lütjens R, Finn T, Rocher J, Poli S, Vega JA, de Lucas AI, Matesanz E, Linares ML, Andrés JI, Alcazar J, Alonso JM, Macdonald GJ, Oehlrich D, Lavreysen H, Ahnaou A, Drinkenburg W, Mackie C, Pype S, Gallacher D, Trabanco AA. *J Med Chem*. **2014**; 57: 6495–512.

18. Schaffhauser H, Rowe BA, Morales S, Chavez-Noriega LE, Yin R, Jachec C, Rao SP, Bain G, Pinkerton AB, Vernier J, Bristow LJ, Varney MA, Daggett LP. *Mol Pharmacol*. **2003**; 64: 798–810.

19. Rowe BA, Schaffhauser H, Morales S, Lubbers LS, Bonnefous C, Kamenecka TM, McQuiston J, Daggett LP. *J Pharmacol Exp Ther*. **2008**; 326: 240–51.

20. Hemstapat K, Da Costa H, Nong Y, Brady AE, Luo Q, Niswender CM, Tamagnan GD, Conn PJ. *J Pharmacol Exp Ther*. **2007**; 322: 254–64.

21. Lundström L, Bissantz C, Beck J, Wettstein JG, Woltering TJ, Wichmann J, Gatti S. *Br J Pharmacol*. **2011**; 164: 521–37.

22. Farinha A, Lavreysen H, Peeters L, Russo B, Masure S, Trabanco AA, Cid J, Tresadern G. *Br J Pharmacol*. **2015**; 172: 2383–96.

23. Wu H, Wang C, Gregory KJ, Han GW, Cho HP, Xia Y, Niswender CM, Katritch V, Meiler J, Cherezov V, Conn PJ, Stevens RC. *Science*. **2014**; 344: 58–64.

24. Doré AS, Okrasa K, Patel JC, Serrano-Vega M, Bennett K, Cooke RM, Errey JC, Jazayeri A, Khan S, Tehan B, Weir M, Wiggin GR, Marshall FH. *Nature*. **2014**; 511: 557–62.

25. Woltering TJ, Wichmann J, Goetschi E, Knoflach F, Ballard TM, Huwyler J, Gatti S. *Bioorg Med Chem Lett*. **2010**; 20: 6969–74.

26. Cid-Nuñez, J. M., Oehlrich, D., Trabanco-Suárez, A. A., Tresadern, G. J., Vega Ramiro, J. A., MacDonald, G. J.WO 2010/130424 A1 **2010**.

27. Cuisset L, Tichonicky L, Jaffray P, Delpech M. *J Biol Chem*. **1997**; 272: 24148–24153.

28. Smith PK, Krohn RI, Hermanson GT, Mallia AK, Gartner FH, Provenzano MD, Fujimoto EK, Goeke NM, Olson BJ, Klenk DC. *Anal Biochem*. **1985**; 150: 76–85.

29. Cheng Y, Prusoff WH. *Biochem Pharmacol*. **1973**; 22: 3099–108.

30. Rasmussen SGF, DeVree BT, Zou Y, Kruse AC, Chung KY, Kobilka TS, Thian FS, Chae PS, Pardon E, Calinski D, Mathiesen JM, Shah ST a, Lyons J a, Caffrey M, Gellman SH, Steyaert J, Skiniotis G, Weis WI, Sunahara RK, Kobilka BK. *Nature*. **2011**; 477: 549–55.

31. El Moustaine D, Granier S, Doumazane E, Scholler P, Rahmeh R, Bron P, Mouillac B, Banères J-L, Rondard P, Pin J-P. *Proc Natl Acad Sci U S A*. **2012**; 109: 16342–7.

32. Isberg V, de Graaf C, Bortolato A, Cherezov V, Katritch V, Marshall FH, Mordalski S, Pin J-P, Stevens RC, Vriend G, Gloriam DE. *Trends Pharmacol Sci*. **2015**; 36: 22–31.

33. Cid JM, Tresadern G, Vega JA, de Lucas AI, Matesanz E, Iturrino L, Linares ML, Garcia A, Andrés JI, Macdonald GJ, Oehlrich D, Lavreysen H, Megens A, Ahnaou A, Drinkenburg W, Mackie C, Pype S, Gallacher D, Trabanco AA. *J Med Chem*. **2012**; 55: 8770–89.

34. Hess B, Kutzner C, van der Spoel D, Lindahl E. *J Chem Theory Comput*. **2008**; 4: 435–447.

35. Lindorff-Larsen K, Piana S, Palmo K, Maragakis P, Klepeis JL, Dror RO, Shaw DE. *Proteins*. **2010**; 78: 1950–8.

36. Berger O, Edholm O, Jähnig F. *Biophys J*. **1997**; 72: 2002–13.

37. Cordomí A, Caltabiano G, Pardo L. *J Chem Theory Comput*. **2012**; 8: 948–958.

38. Christopoulos A, Kenakin T. *Pharmacol Rev*. **2002**; 54: 323–74.

39. Lavreysen H, Ahnaou A, Drinkenburg W, Langlois X, Mackie C, Pype S, Lütjens R, Le Poul E, Trabanco AA, Nuñez JMC. *Pharmacol Res Perspect*. **2015**; 3: e00096.

40. Keov P, Sexton PM, Christopoulos A. *Neuropharmacology*. **2011**; 60: 24–35.

41. Gregory KJ, Noetzel MJ, Rook JM, Vinson PN, Stauffer SR, Rodriguez AL, Emmitte K a, Zhou Y, Chun AC, Felts AS, Chauder B a, Lindsley CW, Niswender CM, Conn PJ. *Mol Pharmacol*. **2012**; 82: 860–75.

42. Goudet C, Kniazeff J, Hlavackova V, Malhaire F, Maurel D, Acher F, Blahos J, Prézeau L, Pin J-P. *J Biol Chem*. **2005**; 280: 24380–5.

43. Hlavackova V, Goudet C, Kniazeff J, Zikova A, Maurel D, Vol C, Trojanova J, Prézeau L, Pin J-P, Blahos J. *EMBO J*. **2005**; 24: 499–509.

44. Williams LT, Lefkowitz RJ. *J Biol Chem*. **1977**; 252: 7207–13.

45. Schaffhauser H, Richards JG, Cartmell J, Chaboz S, Kemp JA, Klingelschmidt A, Messer J, Stadler H, Woltering T, Mutel V. *Mol Pharmacol*. **1998**; 53: 228–33.

46. Cartmell J, Adam G, Chaboz S, Henningsen R, Kemp JA, Klingelschmidt A, Metzler V, Monsma F, Schaffhauser H, Wichmann J, Mutel V. *Br J Pharmacol*. **1998**; 123: 497–504.

47. Tresadern G, Cid JM, Macdonald GJ, Vega JA, de Lucas AI, García A, Matesanz E, Linares ML, Oehlrich D, Lavreysen H, Biesmans I, Trabanco AA. *Bioorg Med Chem Lett*. **2010**; 20: 175–9.

48. Deupi X, Standfuss J. *Curr Opin Struct Biol*. **2011**; 21: 541–551.

49. Liu W, Chun E, Thompson A a, Chubukov P, Xu F, Katritch V, Han GW, Roth CB, Heitman LH, IJzerman AP, Cherezov V, Stevens RC. *Science*. **2012**; 337: 232–6.

50. Xue L, Rovira X, Scholler P, Zhao H, Liu J, Pin J-P, Rondard P. *Nat Chem Biol*. **2015**; 11: 134–40.

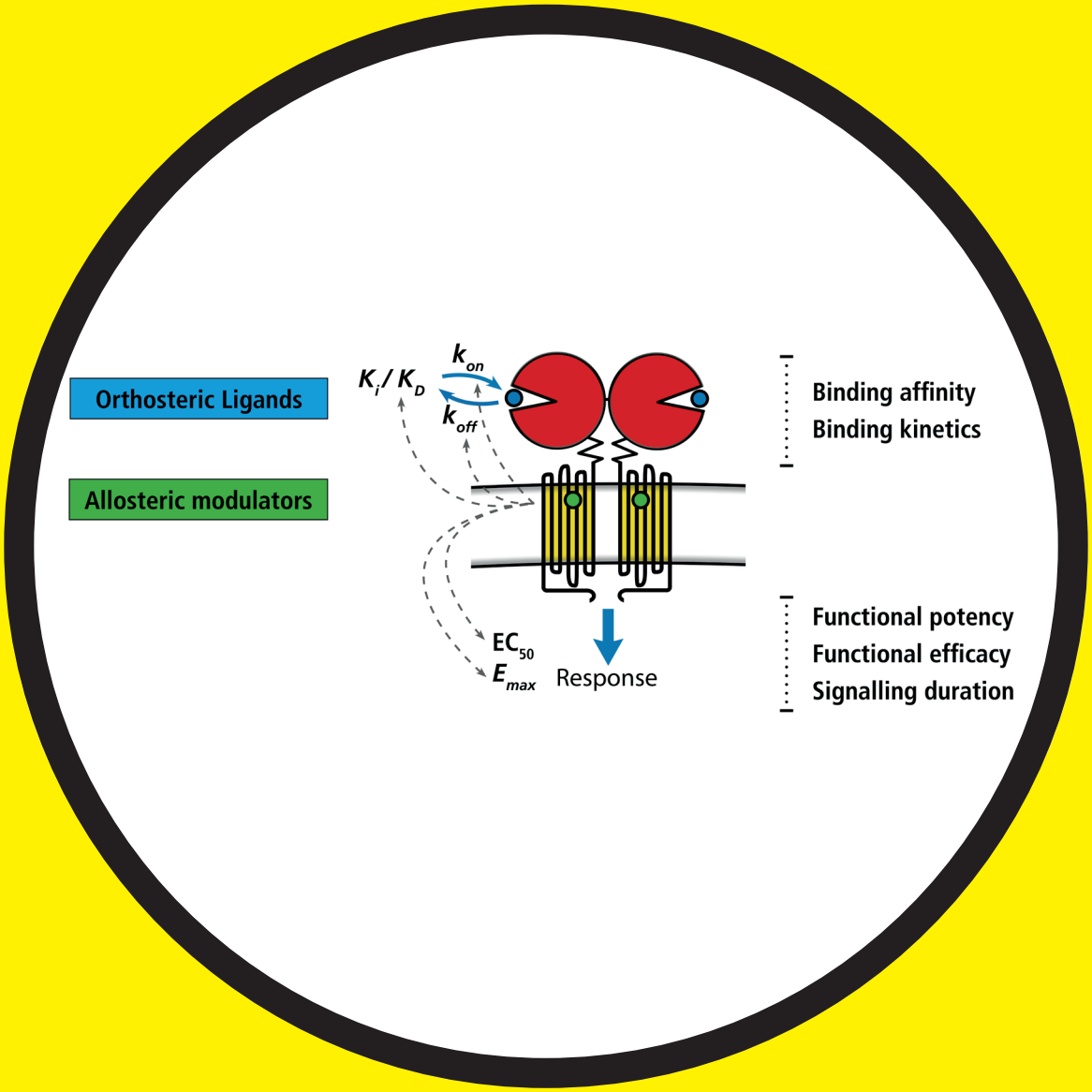
Orthosteric Ligands
Allosteric modulators
K_i / K_D
k_{on}
k_{off}
EC_{50}
E_{max}
Response
Binding affinity
Binding kinetics
Functional potency
Functional efficacy
Signalling duration

CHAPTER 3

Impact of allosteric modulation: Exploring the binding kinetics of glutamate and other orthosteric ligands of the metabotropic glutamate receptor 2

Maarten L J Doornbos, Sophie C Vermond, Hilde Lavreysen, Gary Tresadern, Adriaan P IJzerman & Laura H Heitman

Biochemical Pharmacology 155 (2018) 356–365. doi:10.1016/j.bcp.2018.07.014

3

ABSTRACT

While many orthosteric ligands have been developed for the $mGlu_2$ receptor, little is known about their target binding kinetics and how these relate to those of the endogenous agonist glutamate. Here, the kinetic rate constants, i.e. k_{on} and k_{off}, of glutamate were determined for the first time followed by those of the synthetic agonist LY354740 and antagonist LY341495. To increase the understanding of the binding mechanism and impact of allosteric modulation thereon, kinetic experiments were repeated in the presence of allosteric modulators. Functional assays were performed to further study the interplay between the orthosteric and allosteric binding sites, including an impedance-based morphology assay.

We found that dissociation rate constants of orthosteric $mGlu_2$ ligands were all within a small 6-fold range, whereas association rate constants were ranging over more than three orders of magnitude and correlated to both affinity and potency. The latter showed that target engagement of orthosteric $mGlu_2$ ligands is k_{on}-driven *in vitro*. Moreover, only the off-rates of the two agonists were decreased by a positive allosteric modulator (PAM), thereby increasing their affinity. Interestingly, a PAM increased the duration of a glutamate-induced cellular response. A negative allosteric modulator (NAM) increased both on- and off-rate of glutamate without changing its affinity, while it did not affect these parameters for LY354740, indicating probe-dependency.

In conclusion, we found that affinity- or potency-based orthosteric ligand optimization primarily results in ligands with high k_{on} values. Moreover, positive allosteric modulators alter the binding kinetics of orthosteric agonists mainly by decreasing k_{off}, which we were able to correlate to a lengthened cellular response. Together, this study shows the importance of studying binding kinetics in early drug discovery, as this may provide important insights towards improved efficacy *in vivo*.

INTRODUCTION

Glutamate is the most important excitatory neurotransmitter in the central nervous system where it modulates synaptic responses via activation of ionotropic glutamate receptors and metabotropic glutamate (mGlu) receptors.[1] mGlu receptors are class C G protein-coupled receptors (GPCRs) that structurally consist of a large extracellular glutamate binding domain, the so-called Venus Flytrap (VFT) domain, which is connected via a cysteine-rich domain to the typical seven-transmembrane (7TM) domain.[2] The $mGlu_2$ receptor, which is expressed presynaptically in the periphery of the synapse, is of interest in drug discovery as it negatively modulates the release of glutamate into the synapse.[3] Hence, $mGlu_2$ receptor activation can reduce glutamate hyperfunction in diseases like schizophrenia and anxiety,[4,5] whereas $mGlu_2$ receptor blockade can be beneficial for glutamate hypofunction in depression and impaired cognition.[6,7]

A variety of glutamate-like ligands targeting the orthosteric binding site in the VFT domain was developed including the reference agonist LY354740 and antagonist LY341495.[8,9] Until the recent disclosure of the $mGlu_2$ selective agonist LY2812223,[10] development of orthosteric ligands presented challenges for receptor subtype selectivity and therefore discovery efforts shifted to allosteric modulators that bind in a less conserved pocket in the 7TM domain.[11] Allosteric modulators enhance or inhibit the potency and/or efficacy of the endogenous/orthosteric agonist with little or no intrinsic activity.[12] . Two positive allosteric modulators (PAMs) have advanced into clinical trials: AZD8529[13,14] and JNJ-40411813/ADX71149.[15,16] Reference PAMs in the field include BINA[17], JNJ-40068782[18] and JNJ-46281222.[19] A number of negative allosteric modulators (NAMs) have been characterized *in vivo*, including a recent series of Janssen, RO4491533 and decoglurant of which the latter has advanced into clinical trials.[7,20–22]

Over the last decade it has become increasingly clear that *in vivo* efficacy is not only depending on optimized *in vitro* affinity and efficacy parameters, but also on optimized kinetics of both receptor binding and activation.[23] The dissociation rate constant k_{off} and its derived parameter residence time (RT = $1/k_{off}$) have received increasing attention since the *in vivo* efficacy of multiple marketed GPCR drugs was shown to be related to long RT at the target, such as the long-acting M_3 receptor antagonist tiotropium.[24,25] Although most kinetic studies have emphasized dissociation rate constants, association rate constants have also been described to be important for fast onset of drug action, a high receptor occupancy and even a longer duration of action.[26,27] The importance of k_{on} was further underscored for its potential in drug safety by Sykes *et al.* (2017) who showed that extrapyramidal side effects induced by dopamine D_2 receptor antagonists are linked to k_{on} rather than k_{off} as had been the general hypothesis so far.[28]

We have recently shown the importance of k_{on} and k_{off} for $mGlu_2$ PAMs, where their affinity was k_{on}-driven and their k_{off} was linked to *in vivo* efficacy, as shown in **Chapter 4**.[29] Except for this study, no previous studies have extensively focused on binding kinetics of $mGlu_2$ ligands. Understanding of binding kinetics may also be helpful in drug discovery of novel orthosteric $mGlu_2$ ligands. Moreover, appreciating the kinetic binding parameters of the endogenous agonist is important when designing orthosteric ligands as they have to compete for the same binding site.[30] Furthermore, determination of alterations of the kinetic parameters of the endogenous ligand induced by an allosteric modulator will provide valuable mechanistic insights. Since kinetic binding parameters of the endogenous $mGlu_2$ agonist glutamate have not been quantified before we set up a kinetic radioligand binding assay to enable quantification of kinetic parameters for orthosteric ligands. The major mechanism of action of many allosteric modulators is to modulate endogenous agonist affinity by affecting its kinetic binding parameters, as affinity is determined by $K_D = k_{off} / k_{on}$. Therefore, kinetic binding experiments with orthosteric ligands were also performed in the presence of a PAM or NAM. Additionally, we performed functional assays, i.e. [^{35}S]GTPγS binding assays measuring G protein activation and a label-free biosensor assay that measures changes in cell morphology representing a more integral cellular response. These functional assays were used to further study the interplay between the orthosteric and allosteric binding sites, and its effect on the level of functional efficacy. Importantly, the cell morphology assay enabled recording in real-time, thereby providing the opportunity to evaluate functional receptor-induced responses over time in addition to the time-dependent binding kinetics assays.

This work provides insights on the binding kinetics of orthosteric ligands at the $mGlu_2$ receptor and modulation thereof by PAMs or NAMs. As such, it contributes to increased molecular understanding which may strengthen future drug discovery projects focusing on the development of both orthosteric ligands or allosteric modulators for the $mGlu_2$ receptor as well as for other GPCRs.

MATERIALS AND METHODS

Chemicals and Reagents

LY354740, JNJ-46281222, JNJ-40068782, BINA, RO4491533, and [^{3}H]JNJ-46281222 were synthesized at Janssen Research and Development. LY341495 was from Tocris BioScience (Bristol, UK). [^{3}H]LY341495 was obtained from American Radiolabeled Companies (St. Louis, MO, USA) and [^{35}S]GTPγS from PerkinElmer (Groningen, The Netherlands). Dulbecco's modified Eagle's medium (DMEM), glutamate, GDP and Glutamate-pyruvate transaminase (GPT) were from Sigma Aldrich (St. Louis, MO, USA). Penicillin, streptomycin, L-Proline and

G418 were obtained from Duchefa Biochemie (Haarlem, The Netherlands). Fetal calf serum (FCS) was from Biowest (Nuaillé, France). CHO-K1 cells stably expressing the wildtype (WT) $hmGlu_2$ receptor (CHO-K1_$hmGlu_2$) were from Janssen Research and Development. Other chemicals were from standard commercial sources.

Cell culture

CHO-K1_$hmGlu_2$ cells were cultured in Dulbecco's modified Eagle's medium (DMEM) supplemented with 10% (v/v) fetal calf serum, 200 IU·mL^{-1} penicillin, 200 μg·mL^{-1} streptomycin, 30.5 μg·mL^{-1} L-proline and 400 μg·mL^{-1} G418 at 37°C and 5% CO_2. Cells were subcultured twice every week at a ratio of 1:10.

Membrane preparation

Membrane preparation was performed as in **Chapter 2**.

Radioligand binding assays

[^{3}H]LY341495 binding assays

Membranes were thawed and subsequently homogenized using an Ultra Turrax homogenizer at 24,000 rpm (IKA-Werke GmbH & Co.KG, Staufen, Germany). Assay buffer (50 mM Tris-HCl pH 7.4, 2 mM $CaCl_2$, 10 mM $MgCl_2$) was used to dilute the samples to a total reaction volume of 100 μl containing 5 μg membrane protein and 4 nM [^{3}H]LY341495. Incubations were performed at 0°C. Nonspecific binding was determined using 1 mM glutamate and DMSO concentrations were ≤0.25%.

Displacement experiments were carried out using radioligand and a competing ligand at multiple concentrations. Samples were incubated for 60 minutes, after which receptor-bound radioactivity was determined.

Association experiments were performed by incubation of radioligand in the absence or presence of allosteric modulator at 1 μM with membrane aliquots. The amount of receptor-bound radioligand was determined at different time points up to 60 minutes.

Dissociation experiments were carried out by a 60 minute pre-incubation of radioligand and membrane aliquots in the absence or presence of allosteric modulator at 1 μM. The amount of receptor-bound radioligand was determined after dissociation at different time points up to 60 minutes which was initiated by addition of 5 μl assay buffer containing LY341495 (final concentration 10 μM).

Competition association experiments were performed by incubation of radioligand, competing ligand at its IC_{50} concentration in the absence or presence of allosteric modulator at 1 μM with membrane aliquots. The amount of receptor-bound radioligand was determined at different time points up to 60 minutes.

For all assays, incubations were terminated by rapid filtration over GF/C filter plates (PerkinElmer) using a PerkinElmer 96w Filtermate harvester. Subsequently filters were

washed five times using ice-cold wash buffer (50 mM Tris-HCl pH 7.4). Filter-bound reactivity was determined using liquid scintillation spectrometry on a Microbeta 2450[2] microplate counter (PerkinElmer).

[^{3}H]JNJ-46281222 binding assays

Experiments were performed as described under '[^{3}H]LY341495 binding assays' with the following alterations: [^{3}H]JNJ-46281222 was used at 6 nM, membrane aliquots contained 30 μg, incubations were performed at 15°C and non-specific binding was determined using 10 μM JNJ-40068782. Incubations were terminated by rapid filtration over Whatman GF/C filters (GE Healthcare Life Sciences, Buckinghamshire, UK) on a Brandel harvester 24 (Brandel, Gaithersburg, MD, USA). Filters were washed three times with ice-cold wash buffer (50 mM Tris-HCl pH 7.4). Filter-bound reactivity was determined using a TriCarb 2810 TR counter (PerkinElmer).

[^{35}S]GTPγS binding assays

Membrane homogenates (10 μg) were diluted in assay buffer (50 mM Tris-HCl pH 7.4, 100 mM NaCl, 3 mM $MgCl_2$) supplemented with 5 μg saponin and 10 μM GDP to a total volume of 80 μl containing increasing concentrations of ligand of interest in the absence or presence of a glutamate concentration equivalent to its EC_{80} value (60 μM), if indicated. Basal and maximal receptor activity was determined in the presence of only assay buffer or 1 mM glutamate, respectively. After a 30 minute pre-incubation at 25°C, 20 μl [^{35}S]GTPγS (final concentration 0.3 nM) was added. Reactions were stopped after 90 minutes incubation at 25°C. Filtration was performed and filter-bound radioactivity determined as described under '[^{3}H]LY341495 binding assays' except that GF/B filter plates were used and the wash-buffer consisted of 50 mM TRIS-HCl and 5 mM $MgCl_2$.

Impedance-based morphology assays

Impedance-based morphology assays were performed using the real-time cell analyser (RTCA) xCELLigence SP system (ACEA Biosciences, San Diego, CA, USA),[31,32] as previously described.[33] The system measures electrical impedance generated by adherence of cells to gold-coated electrodes at the bottom of 96 wells PET E-plates (obtained from Bioké, Leiden, the Netherlands). Changes in impedance (Z) are measured continuously and are displayed as Cell Index (CI), which is defined as $(Z_i - Z_0)\ \Omega / 15\Omega$. Z_i is the impedance at a given time and Z_0 is the baseline impedance measured at the start of the experiment in the absence of cells. Baseline impedance was determined using 45 μl culture medium (as described under 'cell culture') per well in a 96 well E-plate. 40,000 CHO-K1_hmGlu$_2$ cells were added in a volume of 50 μl per well. After resting at room temperature for 30 minutes, the plate was mounted in the recording station within a humidified 37°C, 5% CO_2 incubator. Impedance was measured every 15 minutes overnight. 18 hours after cell seeding, wells were stimulated with increasing concentrations of glutamate in the absence or presence of 1 μM PAM JNJ-46281222, resulting in final well volumes of 100 μl. DMSO concentrations were 0.025% and constant between wells.

Data analysis

Data analyses were performed using Prism 7.00 (GraphPad software, San Diego, CA, USA). pIC_{50} values in radioligand displacement assays were obtained by non-linear regression curve fitting into a sigmoidal concentration-response curve using the equation: Y=Bottom + (Top-Bottom)/(1+10$^{(X-LogIC50)}$). pK_i values were obtained from pIC_{50} values using the Cheng-Prusoff equation.[34] Dissociation rate constant k_{off} was obtained using an exponential decay analysis of radioligand binding. Association rate constant k_{on} was determined using the equation $k_{on} = (k_{obs} - k_{off})/[L]$, in which L is the concentration of radioligand and k_{obs} was determined using an exponential association analysis of radioligand binding.

Association and dissociation rate constants for unlabelled $mGlu_2$ PAMs were determined by nonlinear regression analysis of competition association data as described by Motulsky and Mahan.[35]

$$K_A = k_1[L]\cdot 10^{-9} + k_2$$
$$K_B = k_3[I]\cdot 10^{-9} + k_4$$
$$S = \sqrt{(K_A - K_B)^2 + 4\cdot k_1 \cdot k_3 \cdot L \cdot I \cdot 10^{-18}}$$
$$K_F = 0.5(K_A + K_B + S)$$
$$K_S = 0.5(K_A + K_B - S)$$
$$Q = \frac{B_{\max}\cdot k_1 \cdot L \cdot 10^{-9}}{K_F - K_S}$$
$$Y = Q\cdot\left(\frac{k_4\cdot(K_F - K_S)}{K_F \cdot K_S} + \frac{k_4 - K_F}{K_F}e^{(-K_F\cdot X)} - \frac{k_4 - K_S}{K_S}e^{(-K_S\cdot X)}\right)$$

pEC_{50} and pIC_{50} values in the [^{35}S]GTPγS binding assays were determined using non-linear regression curve fitting into a sigmoidal concentration-response curve using the equation: Y=Bottom + (Top-Bottom)/(1+10^($LogEC_{50}$-X)*Hill Slope)). The same equation was used to determine pEC_{50} values from the impedance-based morphology assay. Baseline-corrected ΔCI levels at indicated time points were used to obtain these concentration-response curves. Data are shown as mean ± SEM of at least three individual experiments performed in duplicate. Statistical analyses were performed as indicated. If p-values were below 0.05, observed differences were considered statistically significant.

RESULTS

Affinity of orthosteric compounds in the absence or presence of allosteric modulators

The affinities of orthosteric agonists glutamate and LY354740 and antagonist LY341495 were determined by [^{3}H]LY341495 displacement assays in the absence and presence of PAMs JNJ-46281222 (1 μM), BINA (10 μM) and JNJ-40068782 (1 μM) or NAM RO4491533 (1 μM)

(Fig. 1A-C, Table 1). The affinity of both the endogenous agonist glutamate and the synthetic agonist LY354740 was significantly increased in the presence of all PAMs. Specifically, in presence of JNJ-46281222, glutamate affinity was increased by 7-fold (pK_i 4.52 ± 0.04 to 5.40 ± 0.08 in the absence and presence of JNJ-46281222, respectively), while the affinity of LY354740 was increased by 5-fold (pK_i 6.79 ± 0.01 to 7.51 ± 0.15 in the absence and presence of JNJ-46281222, respectively). The affinity of antagonist LY341495 (pK_i 8.39 ± 0.09) was not affected by any of the PAMs. The presence of 1 μM NAM RO4491533 did not affect the affinity of glutamate, LY354740 or LY341495, which shows that the presence of the NAM does not inhibit the orthosteric agonists and antagonist from binding to the receptor. Since JNJ-46281222 induced the highest shift in agonist affinity it was used as representative PAM for further experimentation, along with RO4491533 as a representative NAM. Of note, both JNJ-46281222 and RO4491533 were not able to displace the radiolabelled orthosteric antagonist [^{3}H]LY341495 by themselves (Fig. 1D), which indicates that they bind to an allosteric site at the $mGlu_2$ receptor.

Figure 1. Effect of allosteric modulators on the affinity of orthosteric ligands. [^{3}H]LY341495 displacement by orthosteric agonists A) glutamate and B) LY354740 and antagonist C) LY341495 in

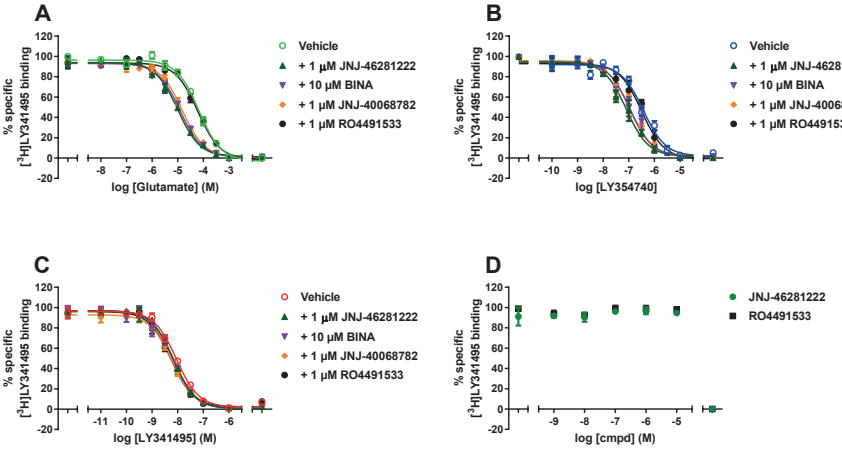

the absence or presence of PAMs or NAM. D) [^{3}H]LY341495 binding in the presence of increasing concentrations of the PAM JNJ-46281222 or NAM RO4491533. Data represent the mean ± SEM of three individual experiments performed in duplicate. If not shown, error bars are within the symbol.

Table 1. Affinity (pK_i) of orthosteric ligands in the absence and presence of allosteric modulators determined in [^{3}H]LY341495 displacement assays.

	Glutamate	LY354740	LY341495
Vehicle	4.52 ± 0.04	6.79 ± 0.01	8.39 ± 0.09
+ *1 μM JNJ-46281222*	5.40 ± 0.08***	7.51 ± 0.15*	8.54 ± 0.02
+ *10 μM BINA*	5.30 ± 0.09***	7.38 ± 0.03*	8.57 ± 0.08
+ *1 μM JNJ-40068782*	5.23 ± 0.04***	7.43 ± 0.19*	8.59 ± 0.05
+ *1 μM RO4491533*	4.56 ± 0.03	6.93 ± 0.15	8.65 ± 0.10

Values represent the mean ± SEM of three individual experiments performed in duplicate. Statistical analyses were performed using a one-way ANOVA with Dunnett's post-test. * < 0.05, *** < 0.001.

Binding kinetics of orthosteric compounds

We set-up radioligand binding assays allowing the determination of binding kinetics of orthosteric compounds in the absence or presence of allosteric modulators. The kinetic binding parameters k_{on} and k_{off} of [^{3}H]LY341495 were determined using classical (direct) association and dissociation assays (Fig. 2A, Table 2). [^{3}H]LY341495 associated rapidly to the mGlu$_2$ receptor, where complete association was reached within 5 minutes, resulting in a k_{obs} value of 0.015 ± 0.0007 s^{-1}. Dissociation induced by 10 µM unlabelled LY341495 yielded a k_{off} value of 0.0066 ± 0.0001 s^{-1}. Based on these k_{obs} and k_{off} values and the concentration of the radioligand used, k_{on} was calculated as 2.2 ± 0.17 x 10^6 M^{-1} s^{-1}. To obtain kinetic binding parameters for unlabelled orthosteric compounds, a competition association assay was performed (Fig. 2B-D). The assay was first validated using unlabelled LY341495, for which k_{on} and k_{off} values were comparable to those obtained in the classical association and dissociation assays (Table 2). Subsequently, the kinetic binding parameters of glutamate and LY354740 were assessed (Fig. 2C,D; Table 3). Compared to LY341495, glutamate had a significantly lower k_{on} value of 1.6 ± 0.3 x 10^3 M^{-1}s^{-1} and a faster dissociation rate (k_{off} 0.036 ± 0.008 s^{-1}). Interestingly, LY354740 had a k_{off} value similar to that of glutamate, but a 40-fold higher k_{on} value (k_{off} 0.045 ± 0.010 min^{-1} and k_{on} 7.1 ± 2.9 x 10^4 M^{-1}s^{-1}, respectively). Of note, the K_D values, i.e. calculated based on their k_{on} and k_{off} values, for glutamate, LY35470 and LY341495, were in good agreement with the K_i values obtained from equilibrium displacement assays (compare Tables 1 and 3).

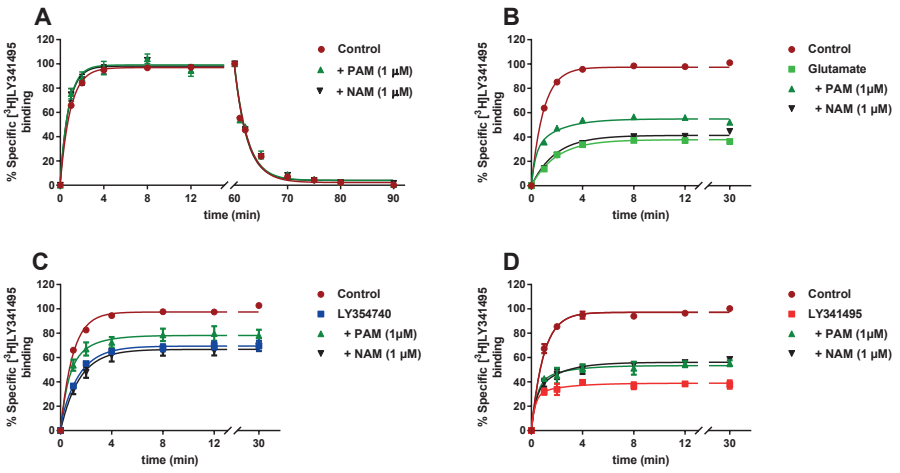

Figure 2. Binding kinetics of orthosteric ligands and the effects of allosteric modulators thereon. A) Association and dissociation kinetics of 4 nM [^{3}H]LY341495 at the mGlu$_2$ receptor at 0°C in the absence or presence of PAM JNJ-46281222 or NAM RO4491533 at 1 µM. Competition association of the agonists B) glutamate and C) LY354740 and D) antagonist LY341495 in the absence or presence of PAM JNJ-46281222 or NAM RO4491533 at 1 µM. Data represent the mean ± SEM of at least three individual experiments performed in duplicate.

Table 2. Comparison of kinetic binding parameters (k_{on}, k_{off}) antagonist LY341495 in the absence or presence of JNJ-46281222 (PAM) or RO4491533 (NAM), determined by direct [3H]LY341495 association and dissociation assays.

	K_D (nM)[a]	k_{on} (M^{-1} s^{-1})	k_{off} (s^{-1})
LY341495	2.9 ± 0.23	(2.2 ± 0.17) x 10^6	0.0066 ± 0.0001
+ *1 μM PAM*	2.9 ± 0.24	(2.2 ± 0.67) x 10^6	0.0063 ± 0.0003
+ *1 μM NAM*	3.2 ± 0.17	(2.1 ± 0.65) x 10^6	0.0068 ± 0.0002

[a] Kinetic K_D values, defined by $K_D = k_{off} / k_{on}$. Values represent the mean ± SEM of three individual experiments performed in duplicate.

Table 3. Kinetic binding parameters (k_{on}, k_{off}) for agonists glutamate and LY354740 and antagonist LY341495 in the absence or presence of JNJ-46281222 (PAM) or RO4491533 (NAM) obtained from competition association assays using [^{3}H]LY341495.

	K_D (nM)[a] (pK_D)	k_{on} (M^{-1} s^{-1})	k_{off} (s^{-1})
Glutamate	23000 ± 6900 (4.65)	(1.6 ± 0.3) x 10^3	0.036 ± 0.008
+ *1 μM PAM*	4700 ± 600* (5.33)	(2.4 ± 0.18) x 10^3	0.012 ± 0.001*
+ *1 μM NAM*	23500 ± 2400 (4.63)	(5.2 ± 0.37) x 10^3***	0.12 ± 0.009***
LY354740	630 ± 290 (6.20)	(7.1 ± 2.9) x 10^4	0.045 ± 0.010
+ *1 μM PAM*	180 ± 20 (6.74)	(7.3 ± 0.56) x 10^4	0.013 ± 0.001*
+ *1 μM NAM*	550 ± 200 (6.26)	(8.5 ± 2.1) x 10^4	0.047 ± 0.013
LY341495	3.5 ± 0.46 (8.45)	(2.4 ± 0.18) x 10^6	0.0087 ± 0.0009
+ *1 μM PAM*	2.8 ± 0.40 (8.56)	(3.5 ± 0.46) x 10^6	0.0096 ± 0.0006
+ *1 μM NAM*	3.4 ± 1.2 (8.46)	(3.9 ± 0.93) x 10^6	0.013 ± 0.003

[a] Kinetic K_D values, defined by $K_D = k_{off} / k_{on}$. Values represent the mean ± SEM of three individual experiments performed in duplicate. Statistical analyses were performed using a one-way ANOVA with Dunnett's post-test. * < 0.05, ** < 0.01, *** < 0.001.

The effect of allosteric modulators on the binding kinetics of orthosteric compounds

The kinetic binding parameters k_{on} and k_{off} of glutamate, LY354740 and LY341495 were determined in the presence of PAM JNJ-46281222 or NAM RO4491533 at 1 μM (Fig. 2B-D; Table 3). The k_{on} value for glutamate in the presence of 1 μM JNJ-46281222 was slightly but not significantly increased to 2.4 ± 0.18 x 10^3 $M^{-1}s^{-1}$ compared to its value obtained in the absence of PAM. The k_{off} value on the other hand was significantly decreased by 3-fold to 0.012 ± 0.001 min^{-1}. Together, this resulted in an approximately 5-fold increased 'kinetic' affinity (K_D) for glutamate from 23 ± 6.9 to 4.7 ± 0.6 μM, which was also observed in the equilibrium displacement assays (K_i values, compare Tables 1 and 3). In the presence of 1 μM RO4491533, the k_{on} value of glutamate was significantly increased by 3-fold to 5.2 ± 0.37 x 10^3 $M^{-1}s^{-1}$, while the k_{off} value was also significantly increased by 3-fold to 0.12 ± 0.009 s^{-1}. As a result, the kinetic K_D value did not change compared to glutamate in the absence of NAM (24 ± 2.4 μM and 23 ± 6.9 μM in absence or presence of NAM, respectively).

The k_{on} value of LY354740 was left unchanged in the presence of 1 μM JNJ-46281222 (7.3 ± 0.56 x 10^4 $M^{-1}s^{-1}$), whereas the k_{off} value was decreased by 3-fold to 0.013 ± 0.001 s^{-1}. Together

this led to an increased kinetic K_D value of 180 ± 20 nM of the agonist LY354740 in the presence of PAM JNJ-46281222. Interestingly, in contrast to glutamate, no significant shifts in k_{on} or k_{off} values were seen for the agonist LY354740 in the presence of 1 μM RO4491533, and therefore the kinetic K_D was also unaffected (630 ± 290 and 550 ± 200 nM in absence or presence of NAM, respectively). Lastly, both k_{on} and k_{off} values of the antagonist LY341495 were not significantly altered by the presence of PAM or NAM. This was the case for both the direct [^{3}H]LY341495 association and dissociation assays (Fig. 2A, Table 2), as well as for the competition association assays (Fig. 2D, Table 3). Hence, K_D values were similar to those obtained in the absence of allosteric modulator.

Potency and efficacy of orthosteric ligands, effects of allosteric modulators on LY354740 potency and efficacy

To evaluate the effects of JNJ-46281222 and RO4491533 on the functional responses induced by orthosteric compounds, a functional [^{35}S]GTPγS binding assay was used that measures compound-induced G protein activation. Firstly, concentration-response curves of the agonists glutamate and LY354740 were made (Fig. 3A), which led to pEC_{50} values of 4.95 ± 0.01 and 6.94 ± 0.04, respectively. The maximum level of [^{35}S]GTPγS binding induced by the synthetic agonist LY354740 was 83.5 ± 1.2% compared to the maximum response induced by the endogenous agonist glutamate (100% at 1 mM) (Table 4). The potency of the antagonist LY341495 was determined in the presence of an EC_{80} concentration of glutamate (60 μM). LY341495 inhibited glutamate-induced [^{35}S]GTPγS binding with a pIC_{50} value of 7.40 ± 0.04 (Fig. 3A). Secondly, the effects of increasing concentrations of JNJ-46281222 or RO4491533 on the concentration-response curves of LY354740 were assessed (Fig. 3B, Table 4). Increasing concentrations of the PAM JNJ-46281222 induced a concentration-dependent increase in E_{max} up to approximately 220% at a concentration of 30 nM or higher. Moreover, the potency of LY354740 was increased significantly from 6.94 ± 0.04 in the absence of PAM to 7.69 ± 0.07 in the presence of 100 nM JNJ-46281222. In contrast, when LY35470 was treated with increasing concentrations of the NAM RO4491533, the E_{max} values of the concentration-response curves were reduced concentration-dependently. At a concentration of 30 nM RO4491533 or higher, LY354740-induced [^{35}S]GTPγS binding was completely abolished (Fig. 3C, Table 4). Interestingly, the potency of LY354740 did not change significantly in the presence of increasing NAM concentrations.

Effect of PAM JNJ-46281222 on duration of glutamate-induced cellular response using an impedance-based morphology assay

To gain further insights in the functional impact of allosteric modulation, receptor activation by glutamate was evaluated using an impedance-based morphology assay (i.e. xCELLigence). This method can record receptor-specific cellular responses in real-time, and thus compound-induced changes in cellular dynamics can be measured over time.

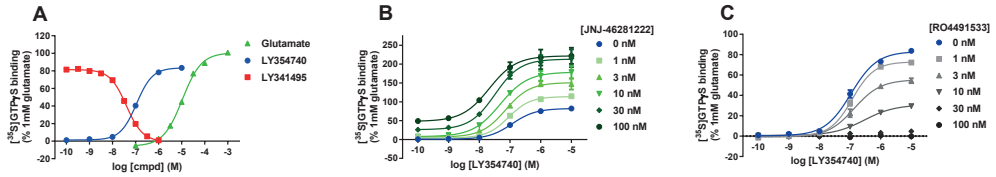

Figure 3. Effect of allosteric modulators on intrinsic agonist potency and efficacy. A) Concentration-response curves of glutamate- and LY354740-induced [^{35}S]GTP**γ**S binding and concentration-response curve of inhibition of glutamate induced (EC_{80}: 60μM) [^{35}S]GTP**γ**S binding by LY341495. Effects of increasing concentrations of B) JNJ-46281222 and C) RO4491533 on concentration-response curves of LY354740 in the [^{35}S]GTP**γ**S binding assay. Data are expressed as the percentage of maximal response induced by 1 mM glutamate (100%) and represent the mean ± SEM of three individual experiments performed in duplicate. If not shown, error bars are within the symbol.

Table 4. Effect of allosteric modulators JNJ-46281222 (PAM) and RO4491533 (NAM) on LY354740-induced [^{35}S]GTPγS binding.

	pEC_{50}	E_{max} (%)[a]
LY354740	6.94 ± 0.04	83.5 ± 1.2
+ *1 nM JNJ-46281222*	7.04 ± 0.10	117 ± 4.2
+ *3 nM JNJ-46281222*	7.14 ± 0.08	154 ± 11**
+ *10 nM JNJ-46281222*	7.35 ± 0.10**	178 ± 16***
+ *30 nM JNJ-46281222*	7.50 ± 0.07****	215 ± 22****
+ *100 nM JNJ-46281222*	7.69 ± 0.07****	222 ± 22****
+ *1 nM RO4491533*	6.91 ± 0.07	74.5 ± 1.3**
+ *3 nM RO4491533*	6.87 ± 0.11	55.5 ± 2.5****
+ *10 nM RO4491533*	6.69 ± 0.05	30.0 ± 1.6****

[a] Expressed as percentage of [^{35}S]GTPγS binding induced by 1 mM glutamate (set at 100%). Values represent the mean ± SEM of three individual experiments performed in duplicate. Statistical analyses were performed using a one-way ANOVA with Dunnett's post-test. ** < 0.01, *** < 0.001, **** < 0.0001.

Glutamate-induced responses were recorded at increasing concentrations in the absence and presence of 1 μM PAM JNJ-46281222 resulting in a concentration-dependent increase in impedance, depicted as Cell Index (Fig.4A,B). Similar to the [^{35}S]GTPγS assay, the glutamate potency was significantly ($p < 0.05$, student's t-test) increased from pEC_{50} 5.27 ± 0.19 to 5.99 ± 0.12 in the absence and presence of PAM, respectively. Furthermore, the PAM-induced shift in potency for glutamate in the morphology assay was comparable to the shift for LY354740 in the [^{35}S]GTPγS assay (Table 4). Interestingly, the duration of the glutamate-induced response in the presence of PAM was also increased from approximately 45 to over 60 minutes. To further evaluate this effect, concentration-response curves of glutamate in the absence and presence of the PAM were obtained at two different time points after stimulation, i.e. 15 and 45 minutes (Fig. 4C,D). Comparison of these concentration-response curves yielded a 2-fold decrease in efficacy for the curve from the later time point (Fig. 4C), congruent with the almost loss of glutamate signal in the absence of PAM at 45 minutes (Fig. 4A). In contrast, the

glutamate efficacy in the presence of PAM did not change significantly, when comparing the concentration-response curves of 15 and 45 minutes after stimulation. This is in line with the observation that the duration of the glutamate-induced response is prolonged by the PAM to approximately 60 minutes, and thus a decrease in cellular impedance was not yet observed at 45 minutes (Fig. 4B). Of note, when comparing the potencies for each condition, i.e. glutamate in the absence or presence of PAM, these were not significantly different at the two time points selected (Fig. 4C,D).

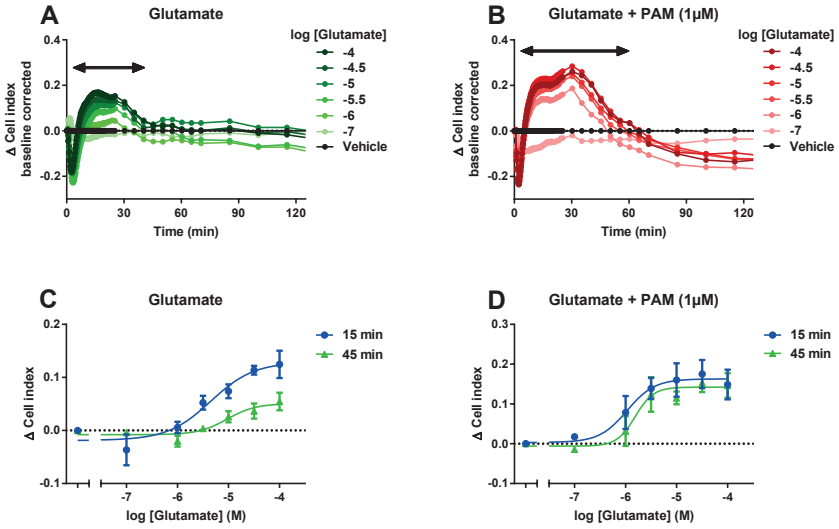

Figure 4. Effect of PAM JNJ-46281222 on the duration of glutamate-induced signalling, as determined by an impedance-based morphology assay. A,B) 18 hours after seeding, CHO-K1_hmGlu$_2$ cells (40,000 cells/well) were stimulated by increasing concentrations of the agonist glutamate in absence (A) or presence of 1 μM of the PAM JNJ-46281222 (B). Medium with 0.025% DMSO was used as vehicle control. DMSO concentrations were 0.025% in all cases. A representative example is shown of a baseline-corrected response, the so-called Δ cell index (ΔCI), which was repeated at least three times in duplicate. C,D) Concentration-response curves were obtained from the ΔCI values at 15 or 45 minutes after stimulation. pEC$_{50}$ values are mentioned in the results section. xCELLigence traces (A, B) are from a representative experiment. Curves (C, D) represent mean ± SEM of at least three individual experiments performed in duplicate.

Correlations and kinetic map

To compare the parameters obtained from the different radioligand binding assays, correlation plots were made (Fig. 5A-C). As mentioned above, the affinity values obtained from [^{3}H]LY341495 equilibrium displacement assays (K_i) and [^{3}H]LY341495 competition association assays (K_D) were in very good agreement, as exemplified by a high linear correlation (Fig. 5A, R^2 = 0.95), further corroborating the robustness of the latter assay. A significant correlation was also found between affinity (K_i) and association rate constants (k_{on}) (Fig. 5B, R^2 = 0.99). Such a correlation, however, was not found between affinity (K_i) and dissociation rate

constants (k_{off}) (Fig. 5C, $R^2 = 0.29$), indicating that affinities of these orthosteric compounds are predominantly k_{on}-driven.

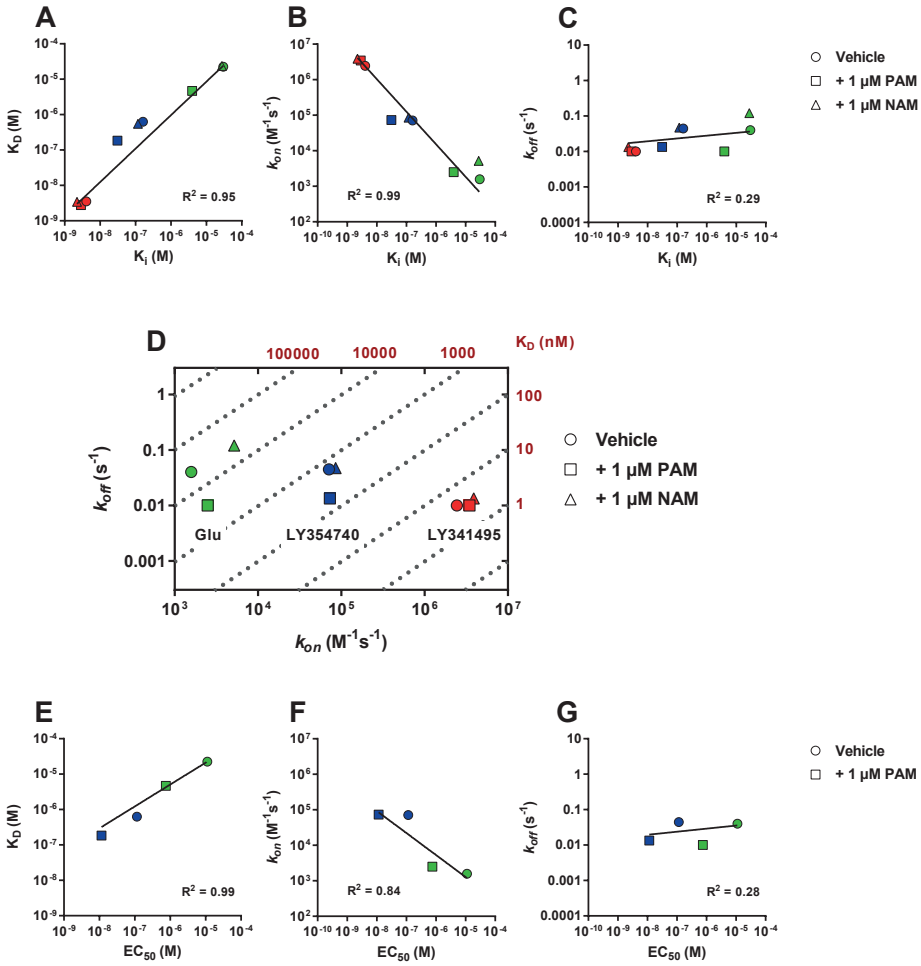

Figure 5. Correlations between affinity, potency and kinetic parameters. A,B,C) Correlation between affinity of glutamate (green), LY354740 (blue) and LY341495 (red) determined in [^{3}H]LY341495 equilibrium displacement assays (K_i) and affinity determined based on kinetic parameters k_{on} and k_{off} obtained from [^{3}H]LY341495 competition association assays (K_D) (A); affinity (K_i) and association rate constant (k_{on}) (B); affinity (K_i) and dissociation rate constant (k_{off}) (C). D) Kinetic map with the association rate constant (k_{on}) plotted on the x-axis and the dissociation rate constant (k_{off}) on the y-axis. Identical affinity (K_D) values may result from different combinations of k_{on} and k_{off} ($K_D = k_{off} / k_{on}$, diagonal dashed lines). E,F,G) Correlation between potency of glutamate and LY354740 determined in [^{35}S]GPTγS assays (EC_{50}) and affinity determined based on kinetic parameters k_{on} and k_{off} obtained from [^{3}H]LY341495 competition association assays (K_D) (E). The EC_{50} of glutamate in the presence of 1 µM PAM is from [19]; potency (EC_{50}) and association rate constant (k_{on}) (F); potency (EC_{50}) and dissociation rate constant (k_{off}) (G).

A kinetic map was made, to further compare the kinetic and affinity parameters (Fig. 5D). In this map k_{on} (x-axis), k_{off} (y-axis) and K_D (diagonal lines) values were plotted. k_{on} and K_D values ranged over more than three orders of magnitude, whereas k_{off} values were only spread within a single order of magnitude and therefore appeared at a similar horizontal level in the kinetic map (Fig. 5D).

As shown in Table 3, k_{on} and k_{off} values of glutamate were affected by both PAM and NAM, which was exemplified in the kinetic map by a spread in symbols. Specifically, in the presence of PAM, the k_{off} of glutamate was decreased by 3-fold. In the presence of NAM both k_{on} and k_{off} were increased 3-fold resulting in the same affinity as illustrated by a diagonal shift of the NAM symbol, i.e. a shift along the line of similar K_D. In the presence of PAM, the k_{off} of LY354740 was similarly affected compared to glutamate, i.e. in both cases this resulted in a downward shift on the kinetic map, whereas in the presence of NAM no significant shifts were observed, resulting in nearly overlapping symbols. Since the k_{on} and k_{off} values of LY34195 were not affected by PAM or NAM all three symbols are overlapping in the kinetic map.

To compare the functional potency of agonists in the absence or presence of PAM to the kinetic parameters k_{on} and k_{off} further correlation plots were made (Fig. 5E-G). Firstly, the potencies (EC_{50}) obtained in [^{35}S]GTPγS assays of agonists glutamate and LY354740 were shown to be strongly correlated (Fig. 5E, $R^2 = 0.99$) to the affinity obtained from competition association assays (K_D), showing that potencies are driven by the agonist binding affinities although the absolute values differed by approximately one log unit. As the affinities were shown to be correlated to on-rates, a correlation was also found between agonist potencies and k_{on} values (Fig. 5F, $R^2 = 0.84$), showing that a high agonist potency is obtained from a high on-rate. No correlation was found between agonist potency and dissociation rate constant (k_{off}) (Fig. 5G, $R^2 = 0.28$). However, in the presence of PAM the agonist k_{off} was decreased for both glutamate and LY354740, which then was the driver for an increased agonist potency, as was also observed for agonist affinity in the presence of PAM.

DISCUSSION

Traditionally, affinity and potency are the main parameters studied in *in vitro* drug discovery. In addition, a ligand's target binding kinetic parameters are nowadays commonly appreciated as valuable information for the early phases of drug discovery.[25] For the development of novel and effective orthosteric $mGlu_2$ ligands it is valuable to know their kinetic binding parameters, but also to understand how these relate to the binding kinetics of the endogenous agonist glutamate.[30] Moreover, a variety of high affinity and selective PAMs and

NAMs have been developed that modulate glutamate potency, efficacy and/or affinity. As for orthosteric compounds, it is equally useful to know the allosteric modulator's binding kinetics, as was shown in **Chapter 4**. Likewise it is also relevant to know how a modulator affects the kinetic binding parameters of the endogenous ligand glutamate. Hence, in the present study we aimed to increase the understanding of binding kinetics of orthosteric $mGlu_2$ ligands both on their own and upon modulation by an allosteric ligand.

The orthosteric ligands used in this study were the endogenous agonist glutamate and reference orthostertic ligands LY354740 (agonist) and LY341495 (antagonist). Radioligand displacement experiments (Fig.1, Table 1) showed that these ligands bind the same orthosteric binding site, which is in line with previous observations.[2,4] The kinetic parameters k_{on} and k_{off} of glutamate were quantified for the first time, using competition association experiments. To allow the set-up of this assay kinetic [^{3}H]LY341495 binding experiments were performed which showed that this ligand associates to its binding site within four minutes and dissociates in approximately ten minutes (Fig. 2A). For the set-up of the competition association assay, the association and dissociation of the radioligand should ideally be slower allowing more data points on the steep part of the curves.[36] This is often achieved by a temperature reduction. However, in these assays the temperature could not be lowered, since it had to be set at 0°C already to allow quantification of kinetic measurements using this commercially available radioligand. Still we could produce robust data between the different binding assays indicating their validity. To obtain values for kon and koff of unlabelled ligands in the absence and presence of allosteric modulators, the Motulsky and Mahan model was used [35,38]. This model requires input for the values of k_{on} and k_{off} (k_1 and k_2 in the model) of the labelled radioligand (i.e. [^{3}H]LY341495). Importantly, these values should remain constant throughout the experiments, as was the case here for [^{3}H]LY341495 which provided similar values for k_{on} and k_{off} both in the absence and presence of allosteric modulators (Table 2). Due to the nature of the radioligand (i.e. fast receptor association) there is not much resolution in the association phase of the curves, making it difficult to observe differences in the rates by eye. However, by analysis of the data with the Motulsky and Mahan model we were able to obtain robust binding kinetic parameters between different experiments.[35,36]

We found that glutamate dissociation (0.036 s^{-1}, Table 3) is fast in comparison to the series of $mGlu_2$ PAMs we studied in **Chapter 4**, which dissociate on a minute-range at 28°C (k_{off} values between 0.00033 and 0.0040 s^{-1}), which would be even slower at 0°C. The observation of fast glutamate binding kinetics is in line with studies using FRET sensors that found $mGlu_1$ receptor conformational changes upon glutamate binding within seconds.[37,38] Fast receptor dissociation of glutamate relates to its physiological role as a neurotransmitter, where short bursts of glutamate at high concentrations are released into the synapse where it should evoke its function during that burst only.[3] Similarly, fast off-rates were obtained for other

endogenous neurotransmitters as exemplified by 2-AG and anandamide on the CB_2 receptor (k_{off} = 0.053 s^{-1} and 0.012 s^{-1} at 25°C, respectively)[39] and acetylcholine on the M_3 receptor (k_{off} = 0.093 s^{-1} at 37°C).[40] Comparison of these values is troublesome, since for practical reasons experiments were performed at different temperatures. Still, they all share off-rates on the second to minute scale, indicating fast receptor dissociation particularly when comparing to synthetic ligands at the same receptors.[39,40]

It is generally acknowledged that allosteric modulators may change the affinity and/or potency of agonists by modulating their k_{on} and/or k_{off} values.[41] Generally this has been determined by radioligand dissociation experiments in the presence of allosteric modulators that enable quantification of modulated off-rates.[42] Limitations of such assays are that it is impossible to detect effects on a radioligand's on-rate and that the orthosteric/endogenous ligand of interest needs to be radiolabelled. This is not suitable for most endogenous agonists including glutamate due to a too low target affinity, or too high non-specific binding. Therefore, we used the competition association assay for quantification of both k_{on} and k_{off} values of unlabelled orthosteric ligands in the absence or presence of PAM or NAM, as was recently published for an adenosine A_1 receptor PAM.[36] The presence of PAM JNJ-46281222 at 1 μM significantly reduced the k_{off} of glutamate and LY354740, resulting in an increased affinity for both these agonists. This was in line with the results from the radioligand displacement assay (Table 1) and can be considered a typical PAM effect.[41] A similar effect was also seen in the functional [^{35}S]GTPγS binding assay where the potency of LY354740 was increased by the PAM JNJ-46281222 by almost 6-fold and its efficacy was more than doubled in line with the results obtained using glutamate in **Chapter 2**. Furthermore, a decreased k_{off}, i.e. increased residence time, for glutamate in the presence of 1 μM PAM JNJ-46281222 results in a prolonged receptor occupancy, which correlated to a prolonged cellular response in the morphology assay (Fig. 4). This functional assay is performed on whole cells under physiologically more relevant conditions (i.e. in culture medium, at 37°C, in a CO_2 incubator) and is therefore considered to be more translational than classical functional assays.[31,32]

Furthermore, the assay can be performed in real-time, which enabled translation from kinetic binding parameters towards functional efficacy over time. Previous studies have also used this assay to study the link between receptor binding kinetics, functional activation kinetics and duration of signalling for agonist-induced responses on the dopamine D_2 and neurokinin 1 receptors.[43,44] Of note, we have shown in **Chapter 6** that culture medium contains 100 μM endogenous glutamate,[45] and therefore the enzyme glutamate-pyruvate transaminase (GPT) is often used to reduce this level. In the current study we were interested in the effect of a PAM on glutamate-responses, as this is the endogenous ligand and thus most relevant for PAM drug discovery. Therefore, GPT could not be used as this would deplete exogenous glutamate in addition to endogenous glutamate.

The NAM RO4491533 at 1 μM positively modulated both k_{on} and k_{off} of glutamate (Table 3), resulting in an unchanged affinity. Of note, these effects on glutamate kinetics cannot be observed in the classical radioligand displacement assays at equilibrium conditions, and would therefore be missed (Table 1). On the other hand, RO4491533 was not able to change k_{on} and k_{off} of LY354740, which shows that the effects of this NAM on binding kinetics of agonists were probe-dependent.[12] This finding highlights the importance of using endogenous agonists in studies of allosteric modulation, since results on other (synthetic) agonists may provide different conclusions as a result of probe-dependency. The observation that a high 1 μM concentration of NAM RO4491533 did not modulate the affinity of both agonists indicated that these ligands still bind the orthosteric binding site in the presence of this NAM, which is therefore behaving as a silent or neutral allosteric ligand (NAL) concerning orthosteric ligand binding.[11] On the contrary, RO4491533 displayed a strong negative cooperativity in the functional [^{35}S]GTPγS binding assay as it concentration-dependently decreased the efficacy of the agonist LY354740 without changing its potency, eventually resulting in abolished LY354740 efficacy (Fig. 3; Table 4), similar to its effects on glutamate activity.[22] This mode of negative allosteric modulation, i.e. only affecting efficacy, has been found across the class C GPCR family. NAMs such as CPCCOEt ($mGlu_1$) and MPEP ($mGlu_5$) also abolished agonist efficacy without modulation of binding affinity.[46,47] The absence of cooperativity between LY341495 and both PAM and NAM was further illustrated by the observation that k_{on} and k_{off} of LY341495 were not affected by any allosteric modulator (Table 3).

The kinetic parameters of glutamate, LY354740 and LY341495 were most different in k_{on}, ranging over more than three orders of magnitude (from 1.6 ± 0.3 x 10^3 to 2.4 ± 0.18 x 10^6 $M^{-1}min^{-1}$) as did their affinity values, whereas k_{off} values were all within a 6-fold range (from 0.0087 ± 0.0009 to 0.045 ± 0.010). The correlation plots figure 5 show that k_{on} is strongly correlated to the agonist affinity and potency, which indicates that target engagement of orthosteric $mGlu_2$ ligands is k_{on}-driven. Recent simulation studies have emphasized the role of high k_{on} values for receptor occupancy and drug dosing.[26,27] A mechanism responsible for these effects may be receptor rebinding, which is described as the binding of newly dissociated ligand from the local environment of the receptor.[48] The interstitial localization of the $mGlu_2$ receptor may result in more rebinding due to less diffusion and therefore higher local concentrations. However, rebinding to the $mGlu_2$ receptor seems less likely for glutamate due to its low k_{on} value (both in the absence and presence of a PAM – Table 3) and the active lowering of local glutamate concentrations by glutamate transporters expressed on the neuronal cell membrane and surrounding glial cells.[49] In contrast, rebinding may play a more prominent role in binding of synthetic ligands which have higher k_{on} values and are not actively transported away from their site of action, resulting in higher *in vivo* receptor occupancy.[48] The plots in figure 5 furthermore showed that whereas between different PAMs a higher affinity is obtained from a higher k_{on}, the higher agonist affinity and potency obtained in the presence

of a PAM results from a lowered k_{off} value as has been shown to be a common mechanism of action for many PAMs at different GPCRs.[41] As shown in figure 5, k_{off} is not correlated to both affinity and potency. This is similar to our recent work on $mGlu_2$ PAMs presented in **Chapter 4** and this may therefore be a receptor-specific property. Furthermore, this earlier study provided a first indication that PAM k_{off} values may be correlated to *in vivo* efficacy, as measured by effects on sleep-wake architecture in rats, more specifically suppression of Rapid Eye Movement (REM) sleep.[50] In the light of the current observation that the presence of a PAM prolonged glutamate-induced cellular responses by decreasing its k_{off}, it may be speculated that k_{off} values of both the PAM and the endogenous agonist are important for the duration of action and thus also for *in vivo* efficacy. As such, this information is valuable for the design of novel orthosteric and allosteric ligands in early drug discovery.

CONCLUSION

In conclusion, the set-up of a competition association radioligand binding assay enabled quantification of the parameters of binding kinetics for glutamate for the first time. k_{off} values of the orthosteric compounds were within a single order of magnitude, whereas k_{on} values were spread over more than three orders of magnitude and were strongly correlated to affinity, indicating that $mGlu_2$ target engagement is driven by k_{on} rather than k_{off}. Binding kinetics of agonists were modulated by the PAM, showing a decrease in k_{off} of both agonists and a prolonged functional response for glutamate. The NAM altered k_{on} and k_{off} of glutamate without changing glutamate's affinity, but did not induce such alterations for agonist LY354740, which indicates probe-dependency. These results show that affinity or potency-only optimization of orthosteric ligands will result in a high k_{on} value but not necessarily optimized k_{off} values, which is essential for optimal *in vivo* efficacy, as shown by previous studies. Together, this work contributes to an increased understanding of the molecular processes that underlie the mechanism of GPCR allosteric modulation, specifically how allosteric modulators affect the kinetic parameters of the endogenous agonist. Therefore, this study further emphasizes the need for evaluation of binding kinetics during drug discovery of both orthosteric and allosteric drug candidates for the $mGlu_2$ receptor as well as for other GPCRs.

REFERENCES

1. Kew JNC, Kemp JA. *Psychopharmacology (Berl)*. **2005**; 179: 4–29.

2. Pin J-P, Duvoisin R. *Neuropharmacology*. **1995**; 34: 1–26.

3. Nicoletti F, Bockaert J, Collingridge GL, Conn PJ, Ferraguti F, Schoepp DD, Wroblewski JT, Pin JP. *Neuropharmacology*. **2011**; 60: 1017–41.

4. Dunayevich E, Erickson J, Levine L, Landbloom R, Schoepp DD, Tollefson GD. *Neuropsychopharmacology*. **2008**; 33: 1603–10.

5. Patil ST, Zhang L, Martenyi F, Lowe SL, Jackson KA, Andreev B V, Avedisova AS, Bardenstein LM, Gurovich IY, Morozova MA, Mosolov SN, Neznanov NG, Reznik AM, Smulevich AB, Tochilov VA, Johnson BG, Monn JA, Schoepp DD. *Nat Med*. **2007**; 13: 1102–7.

6. Feyissa AM, Woolverton WL, Miguel-Hidalgo JJ, Wang Z, Kyle PB, Hasler G, Stockmeier CA, Iyo AH, Karolewicz B. *Prog Neuropsychopharmacol Biol Psychiatry*. **2010**; 34: 279–83.

7. Goeldner C, Ballard TM, Knoflach F, Wichmann J, Gatti S, Umbricht D. *Neuropharmacology*. **2013**; 64: 337–46.

8. Kingston A., Ornstein P., Wright R., Johnson B., Mayne N., Burnett J., Belagaje R, Wu S, Schoepp D. *Neuropharmacology*. **1998**; 37: 1–12.

9. Schaffhauser H, Richards JG, Cartmell J, Chaboz S, Kemp JA, Klingelschmidt A, Messer J, Stadler H, Woltering T, Mutel V. *Mol Pharmacol*. **1998**; 53: 228–33.

10. Monn JA, Prieto L, Taboada L, Hao J, Reinhard MR, Henry SS, Beadle CD, Walton L, Man T, Rudyk H, Clark B, Tupper D, Baker SR, Lamas C, Montero C, Marcos A, Blanco J, Bures M, Clawson DK, Atwell S, Lu F, Wang J, Russell M, Heinz BA, Wang X, Carter JH, Getman BG, Catlow JT, Swanson S, Johnson BG, Shaw DB, McKinzie DL. *J Med Chem*. **2015**: 7526–48.

11. Conn PJ, Christopoulos A, Lindsley CW. *Nat Rev Drug Discov*. **2009**; 8: 41–54.

12. Keov P, Sexton PM, Christopoulos A. *Neuropharmacology*. **2011**; 60: 24–35.

13. Homepage: https://clinicaltrials.gov/show/NCT00986531. The Effects AZD8529 on Cognition and Negative Symptoms in Schizophrenics. (accessed April 12, 2018)

14. Homepage: https://clinicaltrials.gov/show/NCT02401022. The Study of AZD8529 for Smoking Cessation in Female Smokers. (accessed April 12, 2018)

15. Salih H, Anghelescu I, Kezic I, Sinha V, Hoeben E, Van Nueten L, De Smedt H, De Boer P. *J Psychopharmacol*. **2015**; 29: 414–425.

16. Kent JM, Daly E, Kezic I, Lane R, Lim P, De Smedt H, De Boer P, Van Nueten L, Drevets WC, Ceusters M. *Prog Neuro-Psychopharmacology Biol Psychiatry*. **2016**; 67: 66–73.

17. Galici R, Echemendia NG, Rodriguez AL, Conn PJ. *J Pharmacol Exp Ther*. **2005**; 315: 1181–7.

18. Lavreysen H, Langlois X, Ahnaou A, Drinkenburg W, te Riele P, Biesmans I, Van der Linden I, Peeters L, Megens A, Wintmolders C, Cid JM, Trabanco AA, Andrés JI, Dautzenberg FM, Lütjens R, Macdonald G, Atack JR. *J Pharmacol Exp Ther*. **2013**; 346: 514–27.

19. Doornbos MLJ, Pérez-Benito L, Tresadern G, Mulder-Krieger T, Biesmans I, Trabanco AA, Cid JM, Lavreysen H, IJzerman AP, Heitman LH. *Br J Pharmacol*. 2016; 173: 588–600.

20. Homepage: https://clinicaltrials.gov/show/NCT01457677. ARTDeCo Study: A study of RO4995819 in patients with major depressive disorder and inadequate response to ongoing antidepressant treatment. (Accessed April 12, 2018)

21. Van Gool M, Alonso De Diego SA, Delgado O, Trabanco AA, Jourdan F, Macdonald GJ, Somers M, Ver Donck L. *ChemMedChem*. **2017**; 12: 905–912.

22. Campo B, Kalinichev M, Lambeng N, El Yacoubi M, Royer-Urios I, Schneider M, Legrand C, Parron D, Girard F, Bessif A,

Poli S, Vaugeois J-M, Le Poul E, Celanire S. *J Neurogenet*. **2011**; 25: 152–66.

23. Swinney DC, Haubrich BA, Liefde I Van, Vauquelin G. *Curr Top Med Chem*. **2015**; 15: 2504–22.

24. Dowling MR, Charlton SJ. *Br J Pharmacol*. **2006**; 148: 927–37.

25. Copeland RA. *Nat Rev Drug Discov*. **2016**; 15: 87–95.

26. Vauquelin G. *Br J Pharmacol*. **2016**; 173: 2319–2334.

27. de Witte WEA, Danhof M, van der Graaf PH, de Lange ECM. *Trends Pharmacol Sci*. **2016**; 37: 831–842.

28. Sykes DA, Moore H, Stott L, Holliday N, Javitch JA, Lane JR, Charlton SJ. *Nat Commun*. **2017**; 8: 763.

29. Doornbos MLJ, Cid JM, Haubrich J, Nunes A, van de Sande JW, Vermond SC, Mulder-Krieger T, Trabanco AA, Ahnaou A, Drinkenburg WH, Lavreysen H, Heitman LH, IJzerman AP, Tresadern G. *J Med Chem*. **2017**; 60: 6704–6720.

30. Nederpelt I, Bleeker D, Tuijt B, IJzerman AP, Heitman LH. *Biochem Pharmacol*. **2016**; 118: 88–95.

31. Xi B, Yu N, Wang X, Xu X, Abassi YA. *Biotechnol J*. **2008**; 3: 484–495.

32. Yu N, Atienza JM, Bernard J, Blanc S, Zhu J, Wang X, Xu X, Abassi Y. *Anal Chem*. **2006**; 78: 35–43.

33. Hillger JM, Schoop J, Boomsma DI, Eline Slagboom P, IJzerman AP, Heitman LH. *Biosens Bioelectron*. **2015**; 74: 233–242.

34. Cheng Y, Prusoff WH. *Biochem Pharmacol*. **1973**; 22: 3099–108.

35. Motulsky HJ, Mahan LC. *Mol Pharmacol*. **1984**; 25: 1–9.

36. Guo D, Venhorst SN, Massink A, van Veldhoven JPD, Vauquelin G, IJzerman AP, Heitman LH. *Br J Pharmacol*. **2014**; 171: 5295–312.

37. Tateyama M, Abe H, Nakata H, Saito O, Kubo Y. *Nat Struct Mol Biol*. **2004**; 11: 637–42.

38. Hlavackova V, Zabel U, Frankova D, Bätz J, Hoffmann C, Prezeau L, Pin J-P, Blahos J, Lohse MJ. *Sci Signal*. **2012**; 5: ra59.

39. Martella A, Sijben H, Rufer A, Fingerle J, Grether U, Ullmer C, Hartung T, IJzerman A, van der Stelt M, Heitman L. *Mol Pharmacol*. **2017**: mol.117.108605.

40. Sykes DA, Dowling MR, Charlton SJ. *Mol Pharmacol*. **2009**; 76: 543–51.

41. Christopoulos A, Kenakin T. *Pharmacol Rev*. **2002**; 54: 323–74.

42. Lane JR, May LT, Parton RG, Sexton PM, Christopoulos A. *Nat Chem Biol*. **2017**; 13: 929–937.

43. Nederpelt I, Kuzikov M, de Witte WEA, Schnider P, Tuijt B, Gul S, IJzerman AP, de Lange ECM, Heitman LH. *Sci Rep*. **2017**; 7: 14169.

44. Klein Herenbrink C, Sykes DA, Donthamsetti P, Canals M, Coudrat T, Shonberg J, Scammells PJ, Capuano B, Sexton PM, Charlton SJ, Javitch JA, Christopoulos A, Lane JR. *Nat Commun*. **2016**; 7: 1–14.

45. Doornbos MLJ, Van der Linden I, Vereyken L, Tresadern G, IJzerman AP, Lavreysen H, Heitman LH. *Biochem Pharmacol*. **2018**; 152: 201–210.

46. Litschig S, Gasparini F, Rueegg D, Stoehr N, Flor PJ, Vranesic I, Prézeau L, Pin JP, Thomsen C, Kuhn R. *Mol Pharmacol*. **1999**; 55: 453–61.

47. Bradley SJ, Langmead CJ, Watson JM, Challiss RAJ. *Mol Pharmacol*. **2011**; 79: 874–85.

48. Vauquelin G, Charlton SJ. *Br J Pharmacol*. **2010**; 161: 488–508.

49. Marcaggi P, Attwell D. *Glia*. **2004**; 47: 217–225.

50. Ahnaou A, Lavreysen H, Tresadern G, Cid JM, Drinkenburg WH. *PLoS One*. **2015**; 10: e0144017.

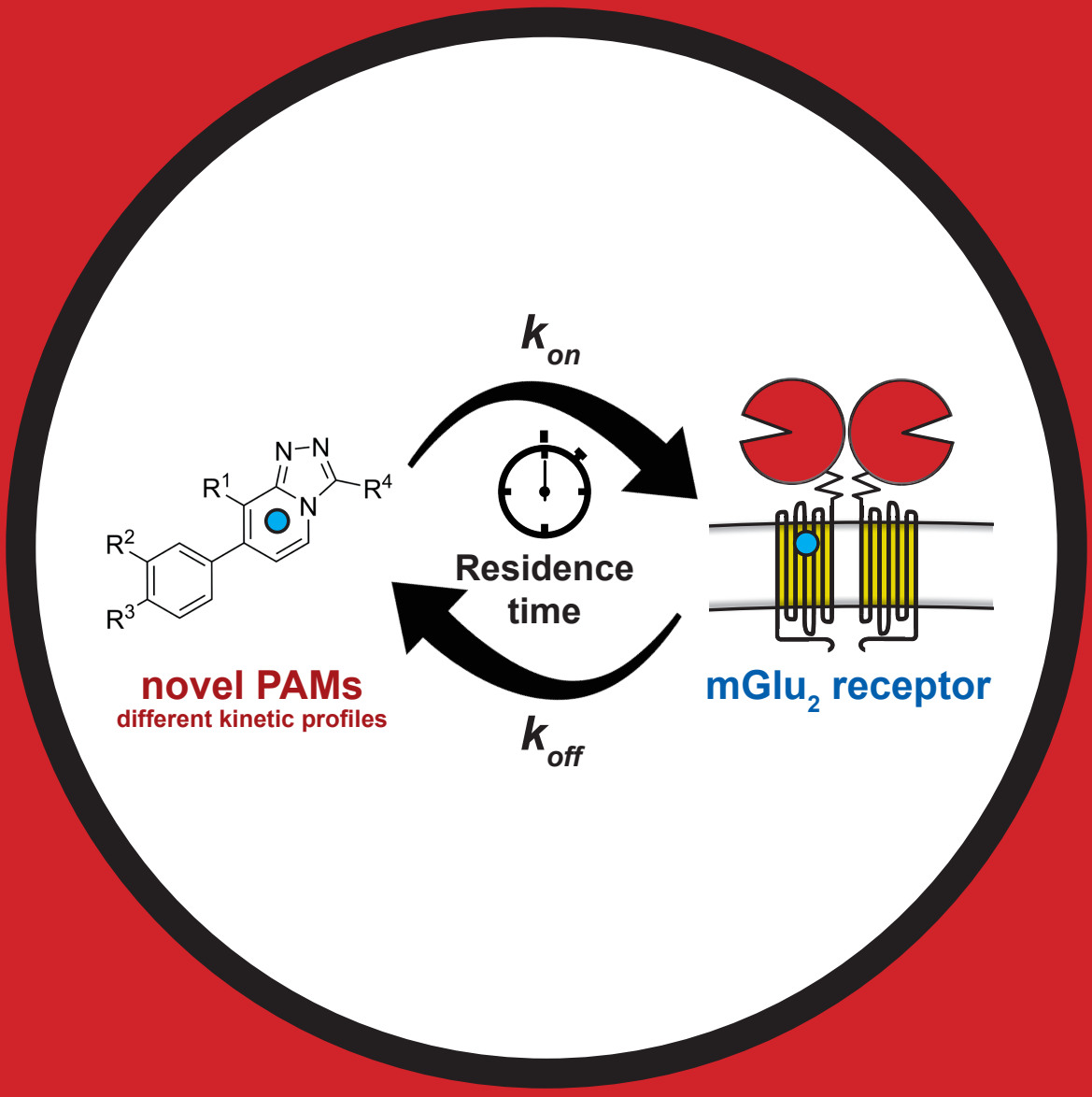
k_{on}
Residence time
k_{off}
novel PAMs
different kinetic profiles
mGlu$_2$ receptor

CHAPTER 4

Discovery and kinetic profiling of 7-aryl-1,2,4-triazolo[4,3-a]pyridines: positive allosteric modulators of the metabotropic glutamate receptor 2.

Maarten L J Doornbos, José María Cid, Jordi Haubrich, Alexandro Nunes, Jasper W van de Sande, Sophie C Vermond, Thea Mulder-Krieger, Andrés A Trabanco, Abdellah Ahnaou, Wilhelmus H Drinkenburg, Hilde Lavreysen, Laura H Heitman, Adriaan P IJzerman & Gary Tresadern

Journal of Medicinal Chemistry 60 (2017) 6704–6720. doi:10.1021/acs.jmedchem.7b00669.

4

ABSTRACT

We report the synthesis and biological evaluation of a series of 7-aryl-1,2,4-triazolo[4,3-a] pyridines with $mGlu_2$ positive allosteric modulator (PAM) activity and affinity. Besides traditional *in vitro* parameters of potency and affinity, kinetic parameters k_{on}, k_{off} and residence time (RT) were determined. The PAMs showed various kinetic profiles; k_{on} values ranged over two orders of magnitude, whereas RT values were within a 10-fold range. Association rate constant k_{on} was linearly correlated to affinity. Evaluation of a short, medium and long RT compound in a label-free assay indicated a correlation between RT and functional effect. The effects of long RT compound **9** on sleep-wake states indicated long RT was translated into sustained inhibition of rapid eye movement (REM) *in vivo*. These results show that affinity-only driven selection would have resulted in $mGlu_2$ PAMs with high values for k_{on}, but not necessarily optimized RT, which is key to predict optimal efficacy *in vivo*.

INTRODUCTION

Glutamate is an important neurotransmitter in the human central nervous system (CNS), where it modulates synaptic responses by activating ionotropic glutamate receptors (iGlu) and metabotropic glutamate receptors (mGlu).[1] The eight known mGlu receptors, which belong to the class C G protein-coupled receptors (GPCRs), have been divided into three subclasses based on sequence homology, signaling pathway and pharmacological profile: group I ($mGlu_{1, 5}$), group II ($mGlu_{2, 3}$) and group III ($mGlu_{4, 6, 7, 8}$).[2] Structurally, class C GPCRs consist of a large extracellular orthosteric binding domain, the so-called venus flytrap (VFT), a cysteine-rich domain connecting the VFT to the seven-transmembrane (7TM) domain.[2,3] Group II mGlu receptors are coupled to the $G\alpha_{i/o}$ protein and are generally expressed presynaptically in the periphery of the synapse where they inhibit the release of glutamate upon activation.[4] The activation of $mGlu_2$ receptors has been shown to be a potential strategy for the treatment of psychiatric diseases involving abnormal glutamatergic neurotransmission, such as schizophrenia and anxiety disorder.[5,6] Drug discovery efforts include the development of positive allosteric modulators (PAMs) for which subtype-selectivity can be more easily obtained as they bind within the less conserved 7TM domain and have little or no intrinsic activity on their own.[7,8] The $mGlu_2$ PAMs *N*-(4-(2-Methoxyphenoxy)phenyl)-*N*-(2,2,2-trifluoroethylsulfonyl) pyrid-3-ylmethylamine (**1**, LY487379)[9], Biphenyl-indanone A (**2**, BINA)[10], *N*-(4-((2-(Trifluoromethyl)-3-Hydroxy-4-(Isobutyryl)phenoxy)methyl)benzyl)-1-Methyl-1*H*-Imidazole-4-Carboxamide (**3**, THIIC, also known as LY2607540)[11] and 3-cyano-1-cyclopropylmethyl-4-(4-phenyl-piperidin-1-yl)-pyridine-2(1*H*)-one (**4**, JNJ-40068782)[12] have been characterized both *in vitro* and *in vivo*. To date, two $mGlu_2$ PAMs have reached clinical trials. The development of 7-methyl-5-[3-(piperazin-1-ylmethyl)-1,2,4-oxadiazol-5-yl]-2-[[4-(trifluoromethoxy)phenyl] methyl]-3H-isoindol-1-one (**5**, AZD8529) by AstraZeneca was discontinued after a phase 2 schizophrenia trial in which it did not show clinical efficacy when tested as monotherapy.[13,14] Compound **5** recently finished a phase II clinical trial to study smoking cessation in female smokers.[15]

Meanwhile, the Janssen/Addex $mGlu_2$ PAM 1-butyl-3-chloro-4-(4-phenyl-1-piperidinyl)-(1*H*)-pyridone (**6**, JNJ-40411813/ADX71149) met the primary objectives of safety and tolerability in an exploratory phase IIa study in schizophrenia. Moreover, patients treated with antipsychotics who experience residual negative symptoms were identified as the subgroup that may potentially benefit from add-on treatment with **6**, although this is yet to be established in a formal proof-of-concept study. In addition, in a second phase IIa study with **6** as adjunctive therapy in patients having major depressive disorder (MDD) with significant anxiety symptoms, **6** did not meet the criterion for efficacy vs placebo. Although **6** showed efficacy signals on several anxiety and depression measures, the primary end point was

not met and overall the results did not suggest efficacy for **6** as an adjunctive treatment for patients with MDD with significant anxious symptoms.[16–22]

To understand more about the key *in vitro* parameters that could drive *in vivo* efficacy, we have focused on the ligand binding kinetics in addition to more classical *in vitro* parameters. It is now becoming increasingly apparent that *in vivo* efficacy can depend on optimized kinetic behavior.[23] Indeed, in the last decade the concept of ligand binding kinetics has received an increasing amount of interest.[24–27] Both the association and dissociation rate constants k_{on} and k_{off} have been studied for various drug targets including GPCRs.[28] The relevance of residence time (RT), defined as the reciprocal of the dissociation rate constant (RT = $1/k_{off}$), for *in vivo* efficacy was retrospectively shown for multiple marketed GPCR drugs, such as the long acting M_3 receptor antagonist tiotropium and fast dissociating D_2 antagonists with lower side-effect burden.[29–31] Whereas dissociation rates have been the focus of most kinetic studies, association rates have also been described to be important for fast drug action and high receptor occupancy.[32–34]

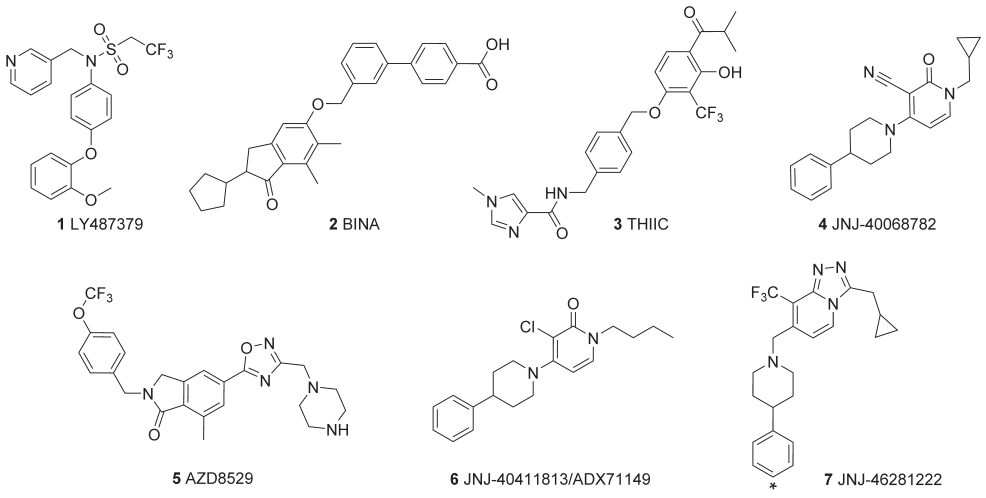

Figure 1. Structures of reference $mGlu_2$ PAMs. The position of the tritium label of [^{3}H]JNJ-46281222 (**7**) is denoted by *.

Here, we report the synthesis and biological evaluation of a novel series of 7-aryl-1,2,4-triazolo[4,3-a]pyridines, which evolved from a pyridone series (**4** and **6**) through a scaffold hopping drug-design strategy previously described.[35,36] These compounds were characterized as $mGlu_2$ PAMs in a functional assay and additionally, radioligand binding experiments were performed to determine their affinity and kinetic binding parameters. We demonstrate that the differentiated binding kinetics result in a varied response in a label-free assay on whole cells. In this way we have been able for the first time to obtain both structure-activity/affinity relationships and structure-kinetic relationships for a class C GPCR.

CHEMISTRY

The target compounds **8**–**48** were prepared via Suzuki cross coupling of the corresponding 7-halotriazolopyridines (**49a,b**; **50a-c** and **51a,b**) with an array of boronic esters (**52a-v**) as shown in Scheme 1. The chemical structures of compounds **8**–**48** are shown in Tables 3-6).

The key 7-halotriazolopyridines (**49a,b**; **50a-c** and **51a,b**) and non-commercially available boronic esters (**52a-v**) were prepared following the procedures previously described.[37,38]

Scheme 1. Synthesis of Final Compounds **8** – **48**[a]

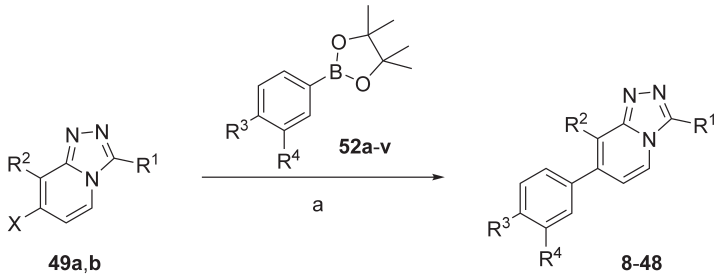

49a: R^1 = ^{c}propylmethyl; R^2 = CF_3; X = Cl
49b: R^1 = ethoxymethyl; R^2 = CF_3; X = Cl
50a: R^1 = ^{c}propylmethyl; R^2 = Cl; X = I
50b: R^1 = ethoxymethyl; R^2 = Cl; X = I
50c: R^1 = trifluoroethyl; R^2 = Cl; X = I
51a: R^1 = ^{c}propylmethyl; R^2 = Me; X = Cl
51b: R^1 = ^{c}propylmethyl; R^2 = ^{c}propyl; X = Cl

52a: R^3 = 2,6-dimethylpyridyl-3-oxy; R^4 = F
52b: R^3 = 2,6-dimethylpyridyl-3-oxy; R^4 = Cl
52c: R^3 = 2-methylpyridyl-4-oxy; R^4 = F
52d: R^3 = 2-ethylpyridyl-4-oxy; R^4 = F
52e: R^3 = 2,6-dimethylpyridyl-4-oxy; R^4 = F
52f: R^3 = 2-^{c}propylpyridyl-4-oxy; R^4 = F
52g: R^3 = ^{i}propylamino; R^4 = F
52h: R^3 = ^{i}propylamino; R^4 = Cl
52i: R^3 = ^{c}propylamino; R^4 = F
52j: R^3 = ^{c}propylamino; R^4 = Cl
52k: R^3 = 2-methoxypyridyl-5-methyloxy; R^4 = F
52l: R^3 = 2-methoxypyridyl-5-methyloxy; R^4 = H
52m: R^3 = 3-methoxypyridyl-5-methylamino; R^4 = F
52n: R^3 = 3-methoxypyridyl-5-methylamino; R^4 = H
52o: R^3 =tetrahydro-pyranyl-4-oxy; R^4 = Cl
52p: R^3 =tetrahydro-pyranyl-4-amino; R^4 = Cl
52q: R^3 =tetrahydro-pyranyl-4-aminomethyl; R^4 = Cl
52r: R^3 =*trans*-4-hydroxy-cyclohexylamino; R^4 = Cl
52s: R^3 =*cis*-4-hydroxy-cyclohexylamino; R^4 = Cl
52t: R^3 =*cis*-4-^{c}propyl-4-hydroxy-cyclohexylamino; R^4 = Cl
52u: R^3 =*trans*-4-hydroxy-cyclohexyloxy; R^4 = Cl
52v: R^3 =*cis*-4-hydroxy-cyclohexyloxy; R^4 = Cl

[a] Reagents and conditions: (a) $Pd(PPh_3)_4$, $NaHCO_3$, H_2O/1,4-dioxane, 150°C, 5-30 min, microwave.

BIOLOGY

The potency of the compounds was determined by quantifying the increase in response of a fixed EC_{20} glutamate concentration (4 μM) observed in a functional [^{35}S]GTPγS binding assay. The affinity of all compounds was determined in a full curve radioligand displacement assay in the presence of 6 nM of the $mGlu_2$ PAM 3-(Cyclopropylmethyl)-7-[(4-phenyl-1-piperidinyl)methyl]-8-(trifluoromethyl)-1,2,4-triazolo[4,3-a]pyridine (**7**, JNJ-46281222), which was radioactively labelled with tritium and extensively characterized in **chapter 2**.[39] In order to determine the kinetic parameters k_{on} and k_{off}, we performed a radioligand competition association assay characterized by the equations of Motulsky and Mahan that describe the binding between two ligands competing for the same receptor binding site.[40] For this purpose, first the association rate constant k_{on} and dissociation rate constant k_{off} of **7** were determined in radioligand association and dissociation experiments using a scintillation proximity assay (SPA).[41] Kinetic parameters were determined at 28°C, presumably these will increase at 37°C. All kinetic assays were performed in the presence of 1 mM glutamate; as was shown in **chapter 2**, this condition induced a monophasic association process of the PAM, which is required for the determination of the kinetic parameters of unlabeled PAMs.[39] **Chapter 2** also showed that the presence of glutamate was shown to not affect affinity and kinetic parameters of **7**.[39] Ultimately, three compounds with representative RT values were selected for comparison in a label-free, impedance based assay (xCELLigence) which measures ligand-induced responses on whole cells. This assay provided further understanding of the influence of RT on the duration of PAM-induced receptor activation.

RESULTS AND DISCUSSION

Kinetic rate constants k_{on} and k_{off} for **7** were similar when obtained in the association and dissociation assays compared to the competition association assay (Table 1), which validated the use of the competition association assay for all other compounds. Kinetic K_D values were comparable to the values reported in **chapter 2**.[39]

Reference $mGlu_2$ PAMs **2**-**5** (Table 2) showed moderate to good potency and affinity at the $mGlu_2$ receptor, in agreement with previous reports including **chapter 2**.[39,42,43] Kinetic parameters k_{on}, k_{off} and RT were also determined. Reference compound **2** was shown to have a RT of 11.6 minutes. The other reference PAMs had RTs in the same range, from 7.8 minutes for **5** to 17.3 minutes for **7** (Table 1).

Table 1. Comparison of kinetic parameters of compound 7 determined by two different methods[a]

Assay	K_D (nM)[b]	k_{on} (M^{-1} min^{-1})	k_{off} (min^{-1})	RT (min)
Association and dissociation[c]	1.1 ± 0.22	(7.1 ± 0.43) x 10^7	0.080 ± 0.015	12.5 ± 2.3
Competition association[d]	2.5 ± 0.71	(2.3 ± 0.60) x 10^7	0.058 ± 0.005	17.3 ± 1.6

[a]Values represent the mean ± SEM of at least three individual experiments performed in duplicate. [b]Kinetic K_D values, defined by $K_D = k_{off} / k_{on}$. [c]Association and dissociation rate constants of [^{3}H]-**7** in a classical radioligand kinetic binding assay at 28°C using SPA. [d]Association and dissociation rate constants of **7** measured in a competition association assay using SPA at 28°C.

Table 2. Functional activity (pEC_{50}), affinity (pK_i and K_D) and kinetic parameters (k_{on}, k_{off}, RT) for reference $mGlu_2$ PAMs 2-5

	pEC_{50}	pK_i[b]	k_{on} (M^{-1} min^{-1})[c]	k_{off} (min^{-1})[d]	RT (min)[e]	K_D (nM)[f]
2	7.03 ± 0.14[a]	7.22 ± 0.15	(4.6 ± 2.3) x 10^6	0.086 ± 0.022	11.6 ± 2.9	190 ± 100
3	6.97 ± 0.08[a]	7.10 ± 0.04	(1.2 ± 0.38) x 10^6	0.120 ± 0.020	8.4 ± 1.4	100 ± 36
4	7.1 ± 0.1[a]	7.58 ± 0.08	(1.7 ± 0.70) x 10^6	0.090 ± 0.015	11.1 ± 1.9	51 ± 22
5	6.25 ± 0.06	6.43 ± 0.03	(2.1 ± 0.65) x 10^5	0.128 ± 0.040	7.8 ± 2.4	600 ± 260

As previously described in [a] Farinha *et al.* (2015)[42], [b] **Chapter 2**[39]. [c,d,e,f]Values represent the mean ± SEM of at least three individual experiments. [e]RT = $1/k_{off}$. [f]Kinetic K_D values, defined by $K_D = k_{off} / k_{on}$.

The analysis of the triazolopyridines containing a substituted pyridine (Table 3) began with elaboration of the R^1 substitution. Compound **8** was taken as the starting point. Substitution of chlorine at the R^1 position by trifluoromethyl (**9**) resulted in an increase in potency, while affinity remained the same. Introduction of methyl (**10**) or iso-propyl (**11**) led to an approx. 10-fold decrease in affinity and potency. Interestingly both k_{on} and RT values were similar for **8**, **10** and **11** but 2-fold (k_{on}) and approx. 3-fold (RT) higher for **9**. Substitution of fluorine by chlorine at the R^2 position resulted in increased potency and affinity for **12**, **13** and **14**. In both cases, the PAMs with CF_3 at R^1 (**9** and **13**) showed modestly longer RTs of 30 and 23 minutes, respectively, along with highest potency and affinity.

Exploration of the pyridine R^3 revealed the importance of the position of the nitrogen. Compound **15** showed decreased potency and affinity compared to **8.** A similar trend was seen for **16** that showed values comparable to those reported previously which revealed decreased potency and affinity compared to **9**.[42] Values for k_{on} followed this trend whereas RTs remained the same for **15**, but decreased from 30 to 11 minutes for **16**. Subsequently the alkyl substituents on the pyridine ring were evaluated. Substitution of methyl in **15** by ethyl in **17**, led to an increased potency and affinity. Addition of a methyl group on the 5-position of **16**, did not change affinity or potency in **18**, nor were large changes seen in kinetic parameters. Introduction of the bulky and lipophilic iso-propyl in **19** and **20** increased potency, affinity and k_{on} slightly. Interestingly, the RT of **20** was reduced to only 5 minutes.

Substitution of the cyclopropylmethyl substituent at the R^4 position by 2,2,2-trifluoroethyl (**21**) resulted in a slight decrease in affinity, similar values for potency and RT, and a 5-fold increase in k_{on} compared to **8**. Next, the ethoxymethyl substituent was evaluated at R^4 (**22**), which yielded a slight decrease in potency, a 10-fold decrease in k_{on} and similar values for affinity and RT compared to **21**. Substitution of F in **22** by CF_3 at R^1 did not yield a drastic increase in affinity and potency (**23**). Together, **21**-**23** showed that a cyclopropyl methyl substituent at R^4 is preferred, as in all three cases the analogue bearing cyclopropyl methyl at R^4 showed a higher affinity (**8** or **9**).

The structure of substituted pyridine of **8** was changed to the short aliphatic iso- or cyclopropyl substituent, yielding **24**-**30** (Table 4). Potency and affinity of **24** were relatively low (pEC_{50} 6.65; pK_i 7.21). Changing the R^1 substituent to CF_3 (**25**) increased affinity and potency again (pEC_{50} 7.03; pK_i 8.05). Substitution of the fluorine on R^2 to chlorine (**26**) resulted in a ◎3-fold increase in affinity and potency.

Substitution of i-Pr at the R^3 position by a c-Pr induced an increase in affinity and potency in all cases (**27**-**29**). As observed in Table 3, replacing F at R^2 in **27** by Cl in **30** led to an increased affinity and potency and a concomitant increase in k_{on}. The data in Table 4 show that k_{on} values followed affinity, whereas RT values were all within a narrow range (8.2 – 11.9 min).

Table 3. Functional activity (pEC_{50}), affinity (pK_i and K_D) and kinetic parameters (k_{on}, k_{off}, RT) for $mGlu_2$ PAMs 8-23

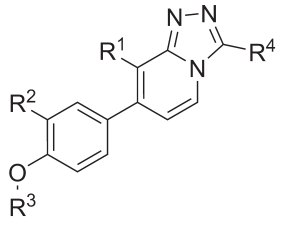

	R^1	R^2	R^3	R^4	pEC_{50}[a]	pK_i[b]	k_{on} (M^{-1} min^{-1})[c]	k_{off} (min^{-1})[d]	RT (min)[e]	K_D (nM)[f]
8	Cl	F		CH_2-(c-Pr)	7.39 (7.35;7.43)	8.71 ± 0.12	(6.3 ± 1.5) x 10^6	0.097 ± 0.024	10.3 ± 2.5	15.3 ± 5.3
9	CF3	F		CH_2-(c-Pr)	8.06 ± 0.14	8.59 ± 0.10	(1.3 ± 0.49) x 10^7	0.033 ± 0.009	30.1 ± 8.2	2.5 ± 1.2
10	Me	F		CH_2-(c-Pr)	7.11 (7.02; 7.19)	7.66 ± 0.33	(8.6 ± 3.3) x 10^6	0.086 ± 0.013	11.6 ± 1.8	10.0 ± 4.1
11	i-Pr	F		CH_2-(c-Pr)	7.55 (7.55; 7.54)	7.60 ± 0.24	(6.5 ± 1.4) x 10^6	0.070 ± 0.017	14.2 ± 3.5	10.7 ± 3.5
12	Cl	Cl		CH_2-(c-Pr)	7.91 (7.71; 8.11)	8.22 ± 0.13	(6.2 ± 2.4) x 10^7	0.061 ± 0.009	16.3 ± 2.4	1.0 ± 0.40
13	CF3	Cl		CH_2-(c-Pr)	8.54 (8.31; 8.78)	8.82 ± 0.22	(6.1 ± 2.4) x 10^6	0.044 ± 0.006	22.7 ± 2.9	7.3 ± 3.0

14	Me	Cl	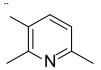	CH_2-(c-Pr)	7.76 ±0.26	7.83 ± 0.25	(5.5 ± 1.7) x 10^6	0.096 ± 0.021	10.5 ± 2.3	17.4 ± 6.5
15	Cl	F	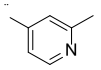	CH_2-(c-Pr)	6.60 (6.64; 6.55)	7.20 ± 0.14	(2.6 ± 0.72) x 10^6	0.096 ± 0.031	10.4 ± 3.4	37.6 ± 16
16	CF_3	F	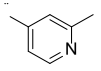	CH_2-(c-Pr)	7.25 ± 0.32	8.15 ± 0.05	(9.8 ± 5.2) x 10^6	0.090 ± 0.015	11.1 ± 1.8	9.2 ± 5.1
17	Cl	F	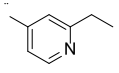	CH_2-(c-Pr)	7.00 ± 0.10	7.73 ± 0.08	(3.0 ± 0.97) x 10^6	0.069 ± 0.011	14.4 ± 2.3	23.3 ± 8.4
18	CF_3	F		CH_2-(c-Pr)	7.19 ± 0.10	8.00 ± 0.16	(8.3 ± 0.60) x 10^6	0.095 ± 0.020	10.5 ± 2.2	11.5 ± 2.5
19	Cl	F	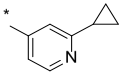	CH_2-(c-Pr)	7.06 ± 0.07	7.27 ± 0.20	(1.7 ± 0.82) x 10^6	0.073 ± 0.004	13.7 ± 0.8	42.7 ± 21
20	CF_3	F	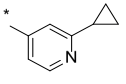	CH_2-(c-Pr)	7.73 ± 0.14	8.44 ± 0.07	(2.2 ± 0.42) x 10^7	0.189 ± 0.082	5.3 ± 2.3	8.6 ± 4.1
21	Cl	F		CH_2-CF_3	7.53 ± 0.11	8.10 ± 0.24	(2.9 ± 0.49) x 10^7	0.096 ± 0.013	10.5 ± 1.5	3.3 ± 0.7
22	Cl	F		CH_2-OEt	7.13 (7.27; 6.99)	8.19 ± 0.10	(3.0 ± 0.11) x 10^6	0.076 ± 0.004	13.2 ± 0.7	25.2 ± 1.6
23	CF_3	F		CH_2-OEt	7.53 ± 0.19	7.93 ± 0.26	(3.6 ± 2.1) x 10^7	0.075 ± 0.006	13.4 ± 1.0	2.1 ± 1.2

[a] Values represent the mean followed by individual values in parentheses when of two experiments and the mean ± SEM when of three or more experiments. [b,c,d,e,f] Values represent the mean ± SEM of at least three individual experiments, all performed in duplicate. [e] RT = $1/k_{off}$. [f] Kinetic K_D values, defined by $K_D = k_{off} / k_{on}$.

Table 4. Functional activity (pEC_{50}), affinity (pK_i and K_D) and kinetic parameters (k_{on}, k_{off}, RT) for $mGlu_2$ PAMs 24-30

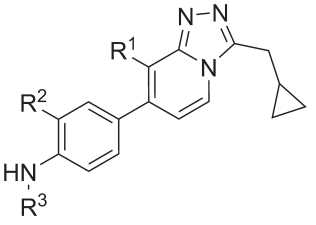

	R^1	R^2	R^3	pEC_{50} [a]	pK_i [b]	k_{on} (M^{-1} min^{-1}) [c]	k_{off} (min^{-1}) [d]	RT (min) [e]	K_D (nM) [f]
24	Cl	F	i-Pr	6.65 (6.43; 6.88)	7.21 ± 0.07	(5.0 ± 1.2) x 10^6	0.101 ± 0.009	9.9 ± 0.9	20.3 ± 5.4
25	CF_3	F	i-Pr	7.03 (7.44; 6.62)	8.05 ± 0.10	(4.6 ± 1.1) x 10^7	0.100 ± 0.029	10.0 ± 2.9	2.2 ± 0.8
26	CF_3	Cl	i-Pr	7.76 (7.55; 7.96)	8.41 ± 0.07	(3.6 ± 1.3) x 10^7	0.121 ± 0.035	8.2 ± 2.4	3.4 ± 1.6
27	Cl	F	c-Pr	7.20 (7.19; 7.21)	7.99 ± 0.05	(4.8 ± 1.5) x 10^6	0.061 ± 0.006	16.4 ± 1.7	12.7 ± 4.1
28	CF_3	F	c-Pr	7.52 (7.60; 7.43)	8.44 ± 0.07	(7.7 ± 4.8) x 10^7	0.086 ± 0.018	11.9 ± 2.3	1.1 ± 0.7
29	CF_3	Cl	c-Pr	8.11 (8.04; 8.18)	8.65 ± 0.11	(7.7 ± 3.8) x 10^7	0.088 ± 0.007	11.3 ± 0.9	1.2 ± 0.6
30	Cl	Cl	c-Pr	7.53 (7.54; 7.51)	8.17 ± 0.03	(1.4 ± 0.35) x 10^7	0.084 ± 0.016	11.9 ± 2.3	6.1 ± 1.9

[a] Values represent the mean followed by individual values in parentheses. [b,c,d,e,f] Values represent the mean ± SEM of at least three individual experiments. [e] $RT = 1/k_{off}$. [f] Kinetic K_D values, defined by $K_D = k_{off} / k_{on}$.

In addition to the results obtained with the first sub-series of triazolopyridines **8**-**23**, a 4-methoxy-3-pyridine moiety connected by a methylene spacer was introduced, leading to compounds **31-35** (Table 5). These molecules share a moderate to good potency and affinity (pEC_{50} 6.8 – 7.8; pK_i 7.9 – 8.7). Removal of the fluorine at the R^2 position (**32**) did not significantly change affinity, potency or kinetic parameters when compared to **31**. Changing the ether linker in **31** and **32** to an amine in **33** and **34** resulted in an approx. 3-fold increase in affinity and potency. A moderate increase in k_{on} was observed and interestingly a 4- and 2-fold increase in RT for **33** and **34**, respectively. This may be explained by the increased flexibility given by the methylene bridge between the triazolopyridine core and the pyridine substituent. As seen in many examples, substitution of CF_3 in **34** to Cl in **35** led to a decrease in affinity, potency and kinetic parameter values.

Reducing aromaticity and introducing more aliphatic and sp3 character can sometimes be beneficial for physicochemical properties and drug-likeness.[44] In order to evaluate the effects of aromaticity, the 4-methoxy-3-pyridyl substituent was replaced with a 4-tetrahydropyranyl ring (**36**, Table 6). This change resulted in a (pK_i) and potency (pEC_{50}) of 6.65 and 7.64, respectively, which were increased in **37** by the introduction of CF_3 in the R^1 position. Compound **37** has a high affinity (pK_i 8.28) and increased k_{on} (2.0×10^7 $M^{-1}min^{-1}$), however, contrary to the high affinity, its RT (4.1 min) was the shortest found throughout this study. As seen in the first series of ligands (Table 2), affinity and potency did not change by altering the linker atom from ether to amine (**38**, **39**). Increasing the linker length by a single methylene unit resulted in an approx. 10-fold loss in affinity, (**40**; pK_i 7.21). Values for k_{on} followed affinity, but RT values were all in the same range.

The tetrahydropyran moiety was then replaced by a cyclohexanol ring, leading to **41**-**48**. Again, compounds bearing CF_3 at R^1 (**42**, **46**) showed better affinity and potency than their chlorine analogues (**41**, **45**). Molecule **42** not only showed a high potency (pEC_{50} 8.03), affinity (pK_i 8.66) and k_{on} (1.1×10^7 $M^{-1}min^{-1}$), but also a longer RT of 31 minutes. Its cis-diastereomer **43** showed a 3-fold reduction in potency (pEC_{50} 7.38) and affinity (pK_i 8.03), a 2-fold reduction in k_{on} (5.7×10^6 $M^{-1}min^{-1}$) and a small reduction in RT (17 min). Introduction of a c-Pr substituent at R^3 (**44**) led to an increase in potency (pEC_{50} 8.95), affinity (pK_i 9.05) and k_{on} (1.4×10^7 $M^{-1}min^{-1}$), and also to a prolonged RT of 50 minutes, which was the highest value observed in this study. It may be that the cyclopropyl at R^3 directs the hydrophilic hydroxyl into a better position for interaction with the receptor. Changing R^4 from c-Pr to CF_3 (**45**) did not change any parameter compared to **41**. Changing the linker group from amine in **43** to ether in **46** did not affect affinity and potency. However, RT seemed to be somewhat increased. Differences between diastereomers were seen again in **47** and **48**. Whereas the potencies were similar, affinity was decreased 3-fold and k_{on} remained similar, while RT was prolonged by 2-fold when moving from a *trans* to *cis* configuration.

Table 5. Functional activity (pEC_{50}), affinity (pK_i and K_D) and kinetic parameters (k_{on}, k_{off}, RT) for $mGlu_2$ PAMs 31-35

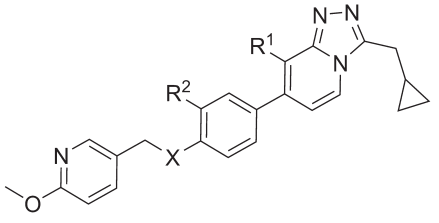

	R^1	R^2	X	pEC_{50} [a]	pK_i [b]	k_{on} (M^{-1} min^{-1}) [c]	k_{off} (min^{-1}) [d]	RT (min) [e]	K_D (nM) [f]
31	CF_3	F	O	7.39 (7.40; 7.37)	7.93 ± 0.14	(1.1 ± 0.40) x 10^7	0.173 ± 0.007	5.8 ± 0.2	16.0 ± 5.9
32	CF_3	H	O	7.24 ± 0.07	8.06 ± 0.16	(1.4 ± 0.86) x 10^7	0.125 ± 0.013	8.0 ± 0.8	8.7 ± 5.4
33	CF_3	F	NH	8.23 (8.13; 8.33)	8.69 ± 0.16	(1.5 ± 0.94) x 10^7	0.044 ± 0.005	22.7 ± 2.8	2.9 ± 1.9
34	CF_3	H	NH	7.82 ± 0.05	8.50 ± 0.09	(3.4 ± 1.3) x 10^7	0.069 ± 0.012	14.6 ± 2.6	2.0 ± 0.8
35	Cl	H	NH	6.82 (6.94; 6.71)	8.13 ± 0.08	(6.2 ± 1.6) x 10^6	0.097 ± 0.022	10.3 ± 2.3	15.6 ± 5.3

[a] Values represent the mean followed by individual values in parentheses when of two experiments and the mean ± SEM when of three or more experiments. [b,c,d,e,f] Values represent the mean ± SEM of at least three individual experiments, all performed in duplicate. [e] RT = $1/k_{off}$. [f] Kinetic K_D values, defined by $K_D = k_{off} / k_{on}$.

Table 6. Functional activity (pEC_{50}), affinity (pK_i and K_D) and kinetic parameters (k_{on}, k_{off}, RT) for $mGlu_2$ PAMs 36-48

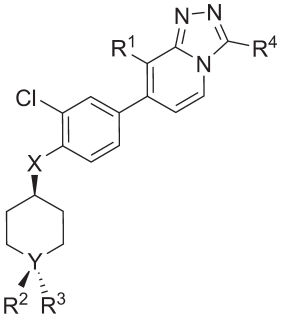

	R^1	R^2	R^3	R^4	X	Y	pEC_{50}[a]	pK_i[b]	k_{on} (M^{-1} min^{-1})[c]	k_{off} (min^{-1})[d]	RT (min)[e]	K_D (nM)[f]
36	Cl	-	-	CH_2-(c-Pr)	O	O	6.65 (6.54; 6.77)	7.64 ± 0.01	(3.3 ± 1.4) x 10^6	0.092 ± 0.014	10.9 ± 1.7	28.1 ± 13
37	CF_3	-	-	CH_2-(c-Pr)	O	O	7.42 (7.40; 7.45)	8.28 ± 0.18	(2.0 ± 0.61) x 10^7	0.241 ± 0.063	4.1 ± 1.1	12.3 ± 5.0
38	Cl	-	-	CH_2-(c-Pr)	NH	O	6.83 (6.77; 6.89)	7.41 ± 0.21	(7.0 ± 2.4) x 10^6	0.136 ± 0.023	7.3 ± 1.2	19.5 ± 7.5
39	CF_3	-	-	CH_2-(c-Pr)	NH	O	7.73 (7.77; 7.68)	8.30 ± 0.06	(1.8 ± 0.61) x 10^7	0.067 ± 0.008	15.0 ± 1.8	3.8 ± 1.4
40	CF_3	-	-	CH_2-(c-Pr)	CH_2-NH	O	6.20 (6.23; 6.18)	7.21 ± 0.06	(1.7 ± 0.18) x 10^6	0.091 ± 0.018	11.0 ± 2.1	54 ± 12
41	Cl	H	OH	CH_2-(c-Pr)	NH	C	7.48 ± 0.22	8.52 ± 0.08	(6.7 ± 1.3) x 10^6	0.084 ± 0.011	11.8 ± 1.6	12.7 ± 3.0
42	CF_3	H	OH	CH_2-(c-Pr)	NH	C	8.03 ± 0.12	8.66 ± 0.01	(1.1 ± 0.09) x 10^7	0.033 ± 0.002	30.8 ± 1.7	3.0 ± 0.3
43	CF_3	OH	H	CH_2-(c-Pr)	NH	C	7.38 ± 0.08	8.03 ± 0.17	(5.7 ± 1.3) x 10^6	0.058 ± 0.014	17.1 ± 4.0	10.3 ± 3.4
44	CF_3	OH	c-Pr	CH_2-(c-Pr)	NH	C	8.95 (9.00; 8.90)	9.05 ± 0.10	(1.4 ± 0.16) x 10^7	0.020 ± 0.005	49.5 ± 12.4	1.5 ± 0.4
45	Cl	H	OH	CH_2-CF_3	NH	C	7.38 (7.41; 7.34)	8.22 ± 0.20	(6.7 ± 1.3) x 10^6	0.074 ± 0.015	13.6 ± 2.8	10.8 ± 3.1
46	CF_3	OH	H	CH_2-(c-Pr)	O	C	7.60 (7.64; 7.57)	8.72 ± 0.15	(1.2 ± 0.31) x 10^7	0.036 ± 0.001	28.1 ± 0.7	3.0 ± 0.8
47	Cl	H	OH	CH_2-CF_3	O	C	6.80 (6.73; 6.88)	7.94 ± 0.04	(8.3 ± 3.6) x 10^6	0.137 ± 0.049	7.3 ± 1.2	16.6 ± 9.3
48	Cl	OH	H	CH_2-CF_3	O	C	7.01 (7.03; 6.99)	7.49 ± 0.21	(6.9 ± 1.5) x 10^6	0.056 ± 0.001	17.7 ± 0.2	8.1 ± 1.7

[a] Values represent the mean followed by individual values in parentheses when of two experiments and the mean ± SEM when of three or more experiments. [b,c,d,e,f] Values represent the mean ± SEM of at least three individual experiments, all performed in duplicate. [e] RT = $1/k_{off}$. [f] Kinetic K_D values, defined by $K_D = k_{off} / k_{on}$.

In general, CF_3 was shown to be the preferred substituent at R^1. Compounds bearing this substituent typically had a higher potency and affinity. Interestingly, all PAMs with a RT longer than 20 minutes bear this moiety, including **44** with the longest RT seen in this study (50 min). On the other hand, molecule **37** had the shortest RT (4.1 min) and also contains the CF_3 group, indicating that CF_3 in itself is not the driver for long RT. At the R^2 position chlorine was shown to be the best substituent for high potency and affinity. PAMs bearing a substituted pyridine revealed the importance of its substitutions in combination with the position of the nitrogen in the ring for potency, affinity and kinetic parameters.

The rather small differences in RT induced by substitutions at the R^1 and R^2 position at the central triazolopyridine core indicated that this region does not induce large differences in RT. On the other hand, small differences in the distal tail of the compounds induced large differences in RT. As shown in **chapter 2**, this triazolopyridine series binds with the scaffold and R^4 substituent in the deepest part of the receptor, whilst the distal tail points to the extracellular side.[39] These differences in RT may be explained by the tight receptor-ligand interactions of the triazolopyridine core compared to looser interactions on the extracellular side. Certain molecules may trap the more flexible ECL2 (or the tops of TMs 3 and 5) in conformations leading to longer RT. Such induced fit modulation of RT can involve ordering of loops to partially block the binding pocket and prevent ligand escape. This mechanism has been seen for multiple targets from different classes, amongst which the 5-HT_{2B} receptor as reported in the recently published LSD-bound crystal structure.[24,45] Selectivity of this series of $mGlu_2$ PAMs for other members of the mGlu family was good. Representatives (**12**, **27**, **37** and **45**) showed no activity at mGlu1, 3, 4, 5, 6, 7 or 8, see table S1.

In order to compare the kinetic parameters and affinity, a kinetic map was generated (Fig. 2). In this map k_{on} (x-axis), k_{off} (y-axis) and K_D (diagonal lines) were plotted. Whereas k_{off} values were all within a small range of about one order of magnitude between 0.020 min^{-1} (**44**) and 0.241 min^{-1} (**37**), k_{on} values were more diverse and were spread over almost two orders of magnitude between 1.7 x 10^6 $M^{-1}min^{-1}$ (**40**) to 7.7 x 10^7 $M^{-1}min^{-1}$ (**28** and **29**). The molecules were plotted per subgroup, as presented in the different tables. This revealed that **8**-**23** and **24**-**30** were mostly diverse in on-rates (**8**-**23**: 0.17 – 6.2 x 10^7 $M^{-1}min^{-1}$; **24**-**30**: 0.48 – 7.7 x 10^7 $M^{-1}min^{-1}$), whereas **31**-**35** and **36**-**48** were more diverse in off-rates (**31**-**35**: 0.044 – 0.17 min^{-1}; **36**-**48**: 0.020 – 0.24 min^{-1}), indicating that an increased affinity between close analogues may be achieved by optimizing one kinetic parameter at a time. Interestingly, the five reference $mGlu_2$ PAMs **2**-**5** and **7**, which are very diverse in structure and affinity, differed mostly in terms of on-rate (0.21 – 4.6 x 10^6 $M^{-1}min^{-1}$), whereas off-rates were very close (0.086 – 0.13 min^{-1}). As expected, the compounds with the highest affinity either have a long RT (**44**) or a fast k_{on} (**28**-**29**). Ideally, these optimized parameters may be combined leading to an $mGlu_2$ PAM with even more increased affinity, which would be represented in the top right corner of the kinetic map.

For further comparison, the compounds were arbitrarily divided in short RT (RT < 10 min), medium RT (10 – 20 min) and long RT (> 20 min) (Fig. 2).

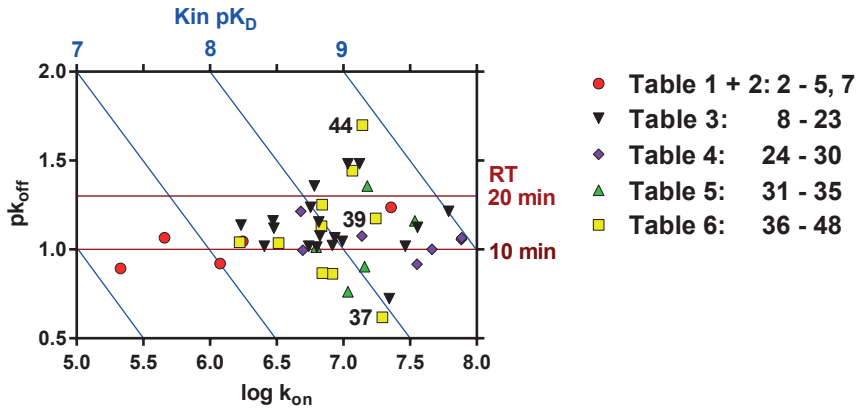

Figure 2. Kinetic map of all tested compounds. The dissociation rate (pk_{off}, k_{off}: min^{-1}) is plotted on the *y*-axis; the association rate (log k_{on}, k_{on}: $M^{-1}min^{-1}$) on the *x*-axis. Identical affinity (pK_D) values may result from a different combination of k_{on} and k_{off} ($K_D = k_{off} / k_{on}$, diagonal blue lines). Horizontal lines indicating a RT of 10 and 20 minutes divide the compounds in short, medium and long RT.

To gain more insight in the relationships between the different parameters studied, correlation plots were made (Fig. 3). First, the affinity (pK_i) and potency (pEC_{50}) were shown to be linearly correlated (Fig. 3A). Secondly, the affinity obtained from the classical radioligand displacement assay (pK_i) and affinity obtained from kinetic parameters (pK_D), were shown to be correlated (Fig. 3B). This further supported the use of the kinetic SPA radioligand binding assay. Long RT PAMs were shown to share a high affinity and potency, but by itself a high potency or affinity does not predict a long RT (Fig. 3A, 3B, S1). Then, the dissociation rate constants (pk_{off}) were plotted against the kinetic affinity data (pK_D) (Fig. 3C), which did not show correlation. Interestingly, the association rate constants (log k_{on}) were strongly correlated to affinity (pK_D) (Fig 3D). These parameters were both within a similar range of roughly two orders of magnitude for the compounds of our series. Interestingly, although having different structures and in some cases lower affinities and k_{on} values, the reference $mGlu_2$ PAMs (**2**-**5**) also fitted well in this correlation (Fig. 3D). This indicated that this correlation has likely revealed a general trend for PAMs and how they bind at the $mGlu_2$ receptor.

Correlations between kinetic parameters and affinity have been made before. Most of these studies found a correlation between k_{off} values and affinity or efficacy, for instance on the M_3 and A_{2A} receptors.[46–48] However, a correlation between association rate constants and affinity, as was shown here for $mGlu_2$ PAMs, has also been observed before. Exemplary GPCRs are the OX_2 receptor and β_2-adrenoreceptors,[49,50] and other targets such as the hERG channel.[51,52]

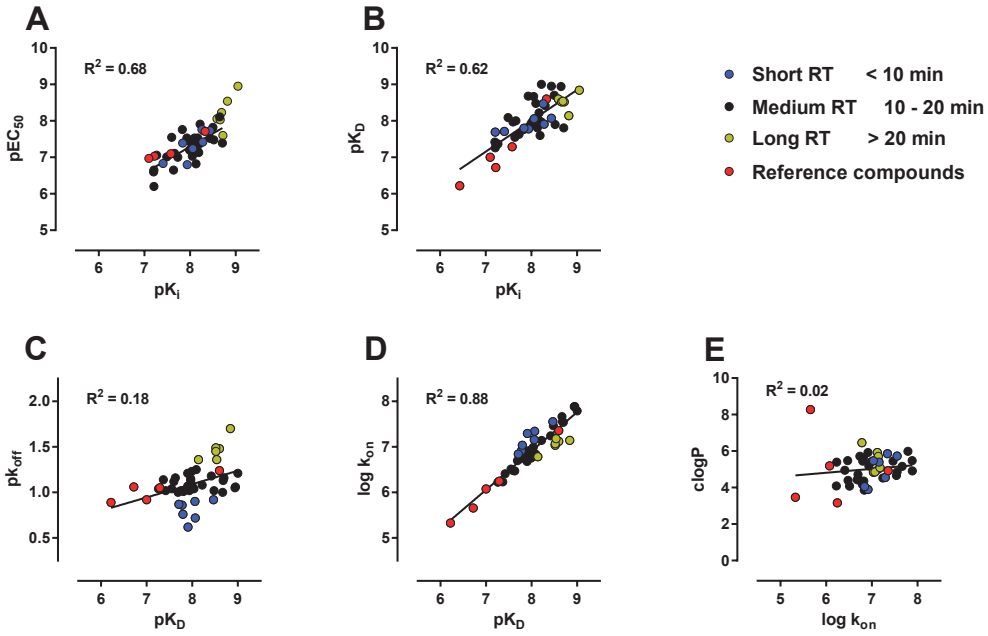

Figure 3. Correlation between affinity (pK_i) and potency (pEC_{50}) (A); affinity determined from [^{3}H]-**7** displacement assays (pK_i) and affinity determined based on kinetic parameters k_{on} and k_{off} obtained from [^{3}H]-**7** competition association experiments (pK_D) (B); affinity (pK_D) and dissociation rate (pk_{off}) (C); affinity (pK_D) and association rate (log k_{on}) (D); association rate (log k_{on}) and partition coefficient (clogP) (E).

These correlations are receptor-specific and may therefore be caused by differences in receptor structure, dynamics, or local environment of the receptor.

Recent simulation studies have stipulated the importance of fast association rates for receptor occupancy and drug dosing.[33,53] One of the mechanisms which may be responsible for these effects is receptor rebinding, which is described as the binding of freshly dissociated ligands from the local environment of the receptor.[54] These high local concentrations may lead to a prolonged activity of the drug, even when concentrations within the effect compartment have fallen below therapeutic levels.[55] For the $mGlu_2$ receptor, rebinding may play a role. The physiological synaptic environment of the receptor may permit more rebinding as its interstitial location will result in less diffusion and therefore higher local ligand concentrations.[56,57] Another reason for receptor rebinding would be binding of compound to or in the cell membrane close to the receptor which may then act as a repository and facilitate the approach of the compound to the receptor.[56] This would, however, require a correlation between lipophilicity and association rate constants, as lipophilic compounds are more likely to bind to the cell membrane. Since the plot in figure 3E shows no such correlation for the studied $mGlu_2$ PAMs, membrane binding is not likely to be involved for these compounds.

xCELLigence

We used a label-free, impedance-based technology (xCELLigence) to evaluate whether a long receptor binding RT leads to a prolonged functional activity. This method is based on the measurement of cellular impedance, expressed as Cell Index, and enables real-time recordings.[58] Responses induced by compound addition can thus be measured and quantified. Earlier studies have shown that results obtained were comparable to more classical endpoint assays.[59] As the assay is performed on whole cells at 37°C it is considered a valuable translational step towards *in vivo* experiments.[60] Endogenous glutamate levels at time of experiments were around 90 μM. Compound-induced responses therefore represent the PAM effects. As a control, reference compound **7** was used to check the response on CHO-K1 WT cells compared to CHO-K1_hmGlu$_2$ cells (Fig. S2). No response was found on the WT cells, indicating that the responses were mGlu$_2$ receptor-mediated. For further experiments we selected compounds with diversity in RT (measured at 28°C): **37** (4.1 min), its close analogue **39** with 3-4 -fold longer RT (15 min) and **44** with again a 3-fold longer RT compared to **39** (50 min; Fig. 4A-D). We determined their potency in the label-free assay using CHO-K1_hmGlu$_2$ cells and found pEC$_{50}$ values of 7.05 ± 0.04, 7.73 ± 0.23 and 7.95 ± 0.12, respectively. Then we performed a wash-out assay, in order to evaluate differences in compound-induced responses after washing. This enabled us to trace the remaining response exerted by only receptor-bound compound. To this end we first determined the EC$_{80}$ concentrations of short RT **37**, medium RT **39** and long RT **44**, which were 600, 200 and 60 nM, respectively. Then, cells were stimulated with this EC$_{80}$ concentration and just before maximal response was reached, after 5 minutes, cells were washed and fresh medium was added (Fig. 4E-G). By comparing these traces with control traces of unwashed wells, we evaluated the differences in responses between **37**, **39** and **44** as the ratio between the AUC of washed and unwashed wells (Fig. 4H). The functional effect of **37** and **39** were partially lost in this experimental set-up, while the effect of **44** remained almost unchanged. The wash-out assay showed a significant difference between short RT **37** and long RT **44**. The value for **39** was in between those of **37** and **44**, in agreement with its RT. Together, these data showed that a longer RT also leads to an increased functional effect under non-equilibrium conditions and that these parameters are positively correlated. Since equilibrium conditions are not always present in physiological conditions, these findings may be considered a translational step from *in vitro* towards *in vivo* experiments.

In vivo sleep-wake effects

Glutamate neurotransmission plays a key role in sleep-wake mechanisms and these processes have translational value for central activity and target engagement. Previous *in vivo* studies have repeatedly shown that positive allosteric modulation of the mGlu$_2$ receptor results in distinct changes in rodent sleep-wake organization, more specifically in a dose-dependent reduction in so-called Rapid Eye Movement Sleep or REM sleep.[61,62] Changes in sleep-wake

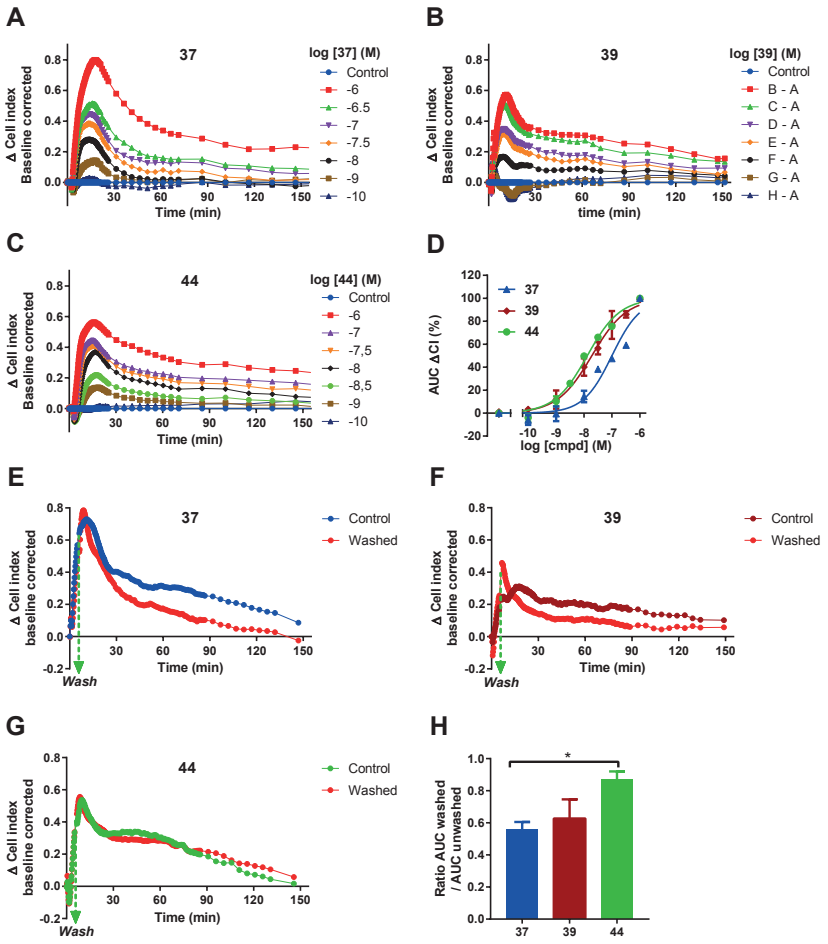

Figure 4. Concentration-dependent effects of **37** (A), **39** (B) and **44** (C) on CHO-K1 cells stably expressing the human $mGlu_2$ receptor. A representative example is shown of a baseline-corrected response, which was repeated three times in duplicate. (D) Concentration-effect curve of **37**, **39** and **44**, derived from the AUC up to 150 minutes. Data are from three individual experiments performed in duplicate and are expressed as percentage of maximum AUC. Responses in a label-free, impedance-based assay induced by an EC_{80} equivalent concentration of **37** (600 nM) (E), **39** (200 nM) (F) and **44** (60 nM) (G) with and without washing-step induced 5 minutes after stimulation. A representative example is shown of a baseline-corrected response, which was repeated three times in duplicate. (H) Ligand-induced response that is left after washing step. Data are expressed as the ratio between the AUC of the trace of the washed and unwashed wells. Data are from three individual experiments performed in duplicate and are expressed as the mean ± SEM. * $p < 0.05$.

states in the rat are of a dynamic nature, i.e. with more frequent transitions between sleep-wake states as compared to humans: therefore the effects of $mGlu_2$ PAM compounds on REM sleep are expressed as averages over for example 2 hour or 4 hours periods after compound administration. In order to investigate whether the different RT values are reflected in the sleep-wake related pharmacodynamic read-out, sleep-wake analysis of **9** and **20** (selected as

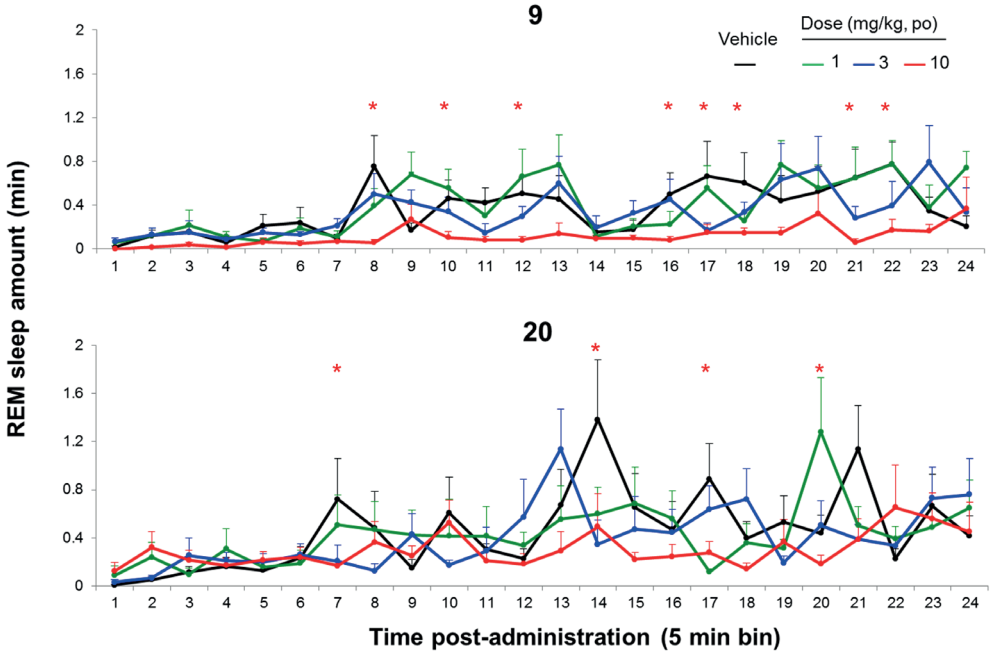

Figure 5. Average amount of REM sleep in minutes for 24 consecutive 5-min period during the first 2 hours of the recording session after oral administration of **9** (top panel) and **20** (bottom panel), each at 1, 3, 10 mg/kg, p.o. to Sprague-Dawley rats (n=8 for each condition). Black lines indicate control vehicle condition (20% CD), while the green, blue, and red lines indicate doses 1, 3, 10 mg/kg, respectively. Error flags indicate SEM values: please note that the higher time resolution of 5 minute bins also causes REM sleep changes to be expressed more dynamically and less 'consistent' as compared to reduction score averaged over the whole 2 hour post-administration period. * indicate $p < 0.05$ vehicle compared to 10 mg/kg, Mixed Model ANOVA.

examples with long versus short *in vitro* RT, respectively, yet having appropriate and similar pharmacokinetic behavior) was even done on a 5 minute basis to optimally capture sleep changes in function of time. All methods, (circadian) timings and analyses otherwise were similar to those reported earlier by Ahnaou et al. (2016).[62]

Figure 5 shows the effects of **9** and **20** on REM sleep reduction in rats for 24 consecutive 5-min periods after a single oral administration of 1, 3, and10 mg/kg and 20% CD vehicle control. The first 6 consecutive 5-minute periods can be discarded due to the confounding arousing effect of the oral administration procedure per se, the animal returning to undisturbed REM sleep baseline values after about 30 minutes. Molecule **9** showed a longer *in vitro* RT of 30 minutes whilst for **20** it was 5 minutes. Correspondingly, at the higher dose of 10 mg/kg, the effect of **9** on REM reduction seemed more immediate and constant compared to **20**. For both compounds no effects on total sleep were seen.

Compound **9** and **20** showed similar *in vitro* binding affinities with pK_i values of 8.59 and 8.44, respectively. At 10 mg/kg, estimated free levels in brain 1 hour post-administration are 5 and 3.5 ng/g for **9** and **20**, respectively. Hence the two molecules show similar affinity and roughly similar range of free concentrations in brain. While the underlying mechanism causing this different *in vivo* effect is still to be elucidated, this finding provides a first hint that different RT's may impact the *in vivo* effect. The interplay of RT with elimination/clearance from brain is important for the resulting *in vivo* effect, but with similar levels of **9** and **20** after 1 hour, it seems that RT may play a role in this case. To strengthen these observations, future experiments could include the synthesis of PET ligands with different residence times and further *in vivo* studies with a different endpoint such as cognition.

While potent GPCR antagonists can act via a long RT with expected improved clinical efficacy there is limited published data assessing the relationship between agonist/PAM RT and *in vivo* efficacy. Agonist responses are usually regulated by receptor desensitization and internalization, which can act to limit the effect and duration of receptor signaling. PAMs do not activate receptors in the absence of agonist, and hence allosteric modulators with prolonged action may not be negated by internalization and loss of function due to longer RT of the PAM-receptor complex.

CONCLUSIONS

In this study we described a series of 7-aryl-1,2,4-triazolo[4,3-a]pyridines with potent $mGlu_2$ PAM activity and a high affinity. An SPA radioligand binding assay was developed to study the kinetic parameters of these compounds. We showed that association rate constants range within three orders of magnitude, whereas RT values are more confined, from 4.1 minutes (**37**) up to 50 minutes (**44**). Correlation plots between affinity and kinetic parameters revealed a strong correlation between affinity and association rate constants, whereas no such correlation was found between RT and affinity.

Structure-kinetics relationships were explored in addition to the more traditional structure-activity/affinity relationships analysis. We learned that a CF_3 substituent at R^1 increased potency and affinity and was also important for RT, but did not lead to a long RT *per se* as shown by its presence in **37** ('short' RT) and **44** ('long' RT). Chlorine was the preferred substituent for R^2, it increased potency and affinity but not RT. Differences in the distal tail of the molecules, such as small changes in the pyridine moiety or single substitutions to the cyclohexanol, induced the biggest differences in RT. This was exemplified by the introduction of c-Pr in **44**, leading to a 3-fold increase in RT compared to **43**.

To evaluate whether a long RT also leads to a prolonged functional effect, **37**, **39** and **44** were evaluated in a wash-out assay using the label-free impedance based xCELLigence technique. The response of **44** on whole cells at physiological temperature remained more sustained after washing than that of **37** and **39.** These data suggested that an increased lifetime of the receptor-ligand complex (RT) is correlated to an increased functional effect under non-equilibrium conditions.

Together, these results show for the first time for a class C GPCR that optimization of ligand binding kinetics in addition to potency and affinity is possible. Given that pure PAMs do not exert an effect in the absence of glutamate and are thus less likely to induce on-target toxicity, a long RT seems a promising strategy for these ligands. As rebinding may be involved in $mGlu_2$ receptor occupancy, a RT for **44** in our system of 50 minutes may be prolonged in the interstitial synaptic environment. Without any on-target toxicity occurring, the design of $mGlu_2$ PAMs with even longer RTs may be a logical next step. Lastly, a first attempt was made to relate the compound's RT to its *in vivo* pharmacodynamic effect. Ultimately, this study may contribute to the development of compounds with a high affinity and efficacy *in vitro* and *in vivo*, not only for the $mGlu_2$ receptor but also for other GPCRs.

EXPERIMENTAL SECTION

Chemistry

Unless otherwise noted, all reagents and solvents were obtained from commercial suppliers and used without further purification. Thin layer chromatography (TLC) was carried out on silica gel 60 F254 plates (Merck). Flash column chromatography was performed on silica gel, particle size 60 Å, mesh of 230–400 (Merck) under standard techniques. Microwave assisted reactions were performed in a single-mode reactor, Biotage Initiator Sixty microwave reactor (Biotage), or in a multimode reactor, MicroSYNTH Labstation (Milestone, Inc.). Nuclear magnetic resonance (NMR) spectra were recorded with either a Bruker DPX-400 or a Bruker AV-500 spectrometer (Bruker AG) with standard pulse sequences, operating at 400 and 500 MHz, respectively, using $CDCl_3$ and DMSO-d_6 as solvents. Chemical shifts (δ) are reported in parts per million (ppm) downfield from tetramethylsilane (δ = 0). Coupling constants are reported in hertz. Splitting patterns are defined by s (singlet), d (doublet), dd (double doublet), t (triplet), q (quartet), quin (quintet), sex (sextet), sep (septet), or m (multiplet). Liquid chromatography combined with mass spectrometry (LCMS) was performed on either a HP 1100 HPLC system (Agilent Technologies) or Advanced Chromatography Technologies system composed of a quaternary or binary pump with degasser, an autosampler, a column oven, a diode array detector (DAD), and a column as specified in the respective methods below. Flow

from the column was split to a MS spectrometer. The MS detector was configured with either an electrospray ionization source or an ESCI dual ionization source (electrospray combined with atmospheric pressure chemical ionization). Nitrogen was used as the nebulizer gas. Data acquisition was performed with MassLynx-Openlynx software or with Chemsation-Agilent data browser software. Melting point values are peak values and were obtained with experimental uncertainties that are commonly associated with this analytical method. Melting points were determined in open capillary tubes on a Mettler FP62 apparatus with a temperature gradient of 10 °C/min. Maximum temperature was 300 °C.

Purities of all new compounds were determined by analytical RP HPLC using the area percentage method on the UV trace recorded at a wavelength of 254 nm, and compounds were found to have ≥95% purity unless otherwise specified.

8-Chloro-3-cyclopropylmethyl-7-{4-[(2,6-dimethylpyridin-3-yl)oxy]-3-fluorophenyl}[1,2,4]triazolo[4,3-a]-pyridine (8). To a stirred suspension of **50a** (1.7 g, 5.09 mmol) and **52a** (2.1 g, 6.12 mmol) in a saturated aqueous solution of $NaHCO_3$ (18 mL) and 1,4-dioxane (36 mL) was added $Pd(PPh_3)_4$ (0.589 g, 0.51 mmol). The mixture was heated at 150 °C for 10 min under microwave irradiation. The mixture was cooled to room temperature and filtered through a Celite pad. The filtrate was diluted with water (20 mL) and extracted with EtOAc (2 × 15 mL). The organic layer was washed with brine (15 mL), dried over anhydrous Na_2SO_4, and concentrated in vacuo. The crude was purified by flash column chromatography (silica gel, EtOAc in DCM, 0/100 to 20/80) to give the desired product **8** as a white solid (1.3 g, 60%). Mp 207.2 °C. ^{1}H NMR (500 MHz, $CDCl_3$) δ ppm 0.32-0.42 (m, 2H), 0.61-0.69 (m, 2H), 1.17-1.28 (m, 1H), 2.54 (s, 3H), 2.55 (s, 3H), 3.13 (d, *J* = 6.9 Hz, 2H), 6.87 (d, *J* = 6.9 Hz, 1H), 6.92 (t, *J* = 8.4 Hz, 1H), 7.02 (d, *J* = 8.4 Hz, 1H), 7.16 (d, *J* = 8.4 Hz, 1H), 7.25 (d, *J* = 9.2 Hz, 1H), 7.41 (dd, *J* = 11.3, 1.7 Hz, 1H), 7.98 (d, *J* = 6.9 Hz, 1H). LC–MS *m/z* 423 $[M + H]^+$, t_R = 2.86 min.

8-Trifluoromethyl-3-cyclopropylmethyl-7-{4-[(2,6-dimethylpyridin-3-yl)oxy]-3-fluorophenyl}[1,2,4]triazolo[4,3-a]-pyridine (9). Starting from **49a** (0.150 g, 0.54 mmol) and **52a** (0.242 g, 0.707 mmol) and following the procedure described for **8**, compound **9** was obtained as a white solid (0.139 g, 56%). ^{1}H NMR (400 MHz, $CDCl_3$) δ ppm 0.31-0.43 (m, 2H), 0.61-0.70 (m, 2H), 1.16-1.30 (m, 1H), 2.53 (s, 3H), 2.55 (s, 3H), 3.15 (d, *J* = 6.7 Hz, 2H), 6.79 (d, *J* = 7.2 Hz, 1H), 6.89 (t, *J* = 8.3 Hz, 1H), 7.01 (d, *J* = 8.3 Hz, 1H), 7.05 (br d, J = 8.6 Hz, 1H), 7.14 (d, *J* = 8.3 Hz, 1H), 7.22 (dd, *J* = 10.9, 2.1 Hz, 1H), 8.11 (d, *J* = 7.2 Hz, 1H). LC–MS *m/z* 457 $[M + H]^+$, t_R = 3.03 min.

8-Methyl-3-cyclopropylmethyl-7-{4-[(2,6-dimethylpyridin-3-yl)oxy]-3-fluorophenyl}[1,2,4]triazolo[4,3-a]-pyridine (10). Starting from **51a** (0.250 g, 1.127 mmol) and **52a** (0.464 g, 1.35 mmol) and following the procedure described for **8**, compound **10** was obtained as a white solid (0.103 g, 23%). Mp 147.4 °C. ^{1}H NMR (500 MHz, $CDCl_3$) δ ppm 0.32 - 0.39 (m, 2H), 0.60 - 0.67 (m, 2H), 1.16 - 1.29 (m, 1H), 2.55 (s, 6H), 2.65 (s, 3H) 3.11 (d, *J* = 6.65 Hz, 2H), 6.78 (d, *J* = 7.22 Hz, 1H), 6.93 (t, *J* = 8.38 Hz, 1H), 7.00 (d, *J* = 8.38 Hz, 1H), 7.07 (d, *J* = 8.38 Hz, 1H), 7.13 (d, *J* = 8.09 Hz, 1H), 7.23 (dd, *J* = 11.27, 2.02 Hz, 1H), 7.89 (d, *J* = 6.94 Hz, 1H). LC–MS *m/z* 403 $[M + H]^+$, t_R = 2.07 min.

8-Cyclopropyl-3-cyclopropylmethyl-7-{4-[(2,6-dimethylpyridin-3-yl)oxy]-3-fluorophenyl}[1,2,4]triazolo[4,3-a]-pyridine (11). Starting from **51b** (0.230 g, 0.93 mmol) and **52a** (0.382 g, 1.11 mmol) and following the procedure described for **8**, compound **11** was obtained as a white solid (0.269 g, 68%). Mp 166.4 °C. ^{1}H NMR (400 MHz, $CDCl_3$) δ ppm 0.29 - 0.38 (m, 2H), 0.58 - 0.67 (m, 2H), 0.90 - 1.00 (m, 2H), 1.14 - 1.31 (m, 1H), 1.55 - 1.70 (m, 2H) 2.10 (tt, *J*=8.64, 5.46 Hz, 1H), 2.54 (s, 3H), 2.55 (s, 3H), 3.06 (d, *J*=6.70 Hz, 2H), 6.73 (d, *J*=7.17 Hz, 1H), 6.93 (t, *J*=8.44 Hz, 1H), 7.00 (d, *J*=8.32 Hz, 1H), 7.13 (d, *J*=8.32 Hz, 1H), 7.15 - 7.20 (m, 1H), 7.32 (dd, *J* = 11.21, 1.97 Hz, 1H), 7.80 (d, *J* = 7.17 Hz, 1H). LC–MS *m/z* 429 $[M + H]^+$, t_R = 2.24 min.

8-Chloro-3-cyclopropylmethyl-7-{4-[(2,6-dimethylpyridin-3-yl)oxy]-3-chlorophenyl}[1,2,4]triazolo[4,3-a]-pyridine (12). Starting from **50a** (0.250 g, 0.75 mmol) and **52b** (0.385 g, 0.75 mmol) and following the procedure described for **8**, compound **12** was obtained as a white solid (0.100 g, 70%). Mp 182.7 °C. ^{1}H NMR (400 MHz, $CDCl_3$) δ ppm 0.31 - 0.41 (m, 2H), 0.57 - 0.70 (m, 2H), 1.21 - 1.33 (m, 1H), 2.51 (s, 3H), 2.56 (s, 3H), 3.13 (d, *J* = 6.94 Hz, 2H), 6.82 (d, *J* = 8.55 Hz, 1H), 6.87 (d, *J* = 6.94 Hz, 1H), 7.03 (d,

J = 8.32 Hz, 1H), 7.16 (d, *J* = 8.09 Hz, 1H), 7.37 (dd, *J* = 8.55, 2.31 Hz, 1H), 7.66 (d, *J* = 2.31 Hz, 1H), 7.97 (d, *J* = 7.17 Hz, 1H). LC–MS *m/z* 439 $[M + H]^+$, t_R = 3.08 min.

8-Trifluoromethyl-3-cyclopropylmethyl-7-{4-[(2,6-dimethylpyridin-3-yl)oxy]-3-chlorophenyl}[1,2,4]triazolo[4,3-a]-pyridine (13). Starting from **49a** (0.2 g, 0.73 mmol) and **52b** (0.26 g, 0.72 mmol) and following the procedure described for **8**, compound **13** was obtained as a white solid (0.217 g, 61%). Mp > 300ºC. ^{1}H NMR (400 MHz, $CDCl_3$) δ ppm 0.34 - 0.41 (m, 2H), 0.62 - 0.70 (m, 2H), 1.16 - 1.30 (m, 1H), 2.50 (s, 3H), 2.56 (s, 3H), 3.15 (d, *J* = 6.70 Hz, 2H), 6.79 (d, *J* = 8.09 Hz, 2H), 7.03 (d, *J* = 8.09 Hz, 1H), 7.11 - 7.19 (m, 2H), 7.49 (d, *J* = 2.31 Hz, 1H), 8.10 (d, *J* = 7.17 Hz, 1H). LC–MS *m/z* 473 $[M + H]^+$, t_R = 3.22 min.

8-Methyl-3-cyclopropylmethyl-7-{4-[(2,6-dimethylpyridin-3-yl)oxy]-3-chlorophenyl}[1,2,4]triazolo[4,3-a]-pyridine (14). Starting from **60a** (0.250 g, 0.127 mmol) and **52b** (0.464 g, 1.35 mmol) and following the procedure described for **8**, compound **14** was obtained as a white solid (0.107 g, 22%). Mp 121 °C. ^{1}H NMR (500 MHz, $CDCl_3$) δ ppm 0.36 (q, *J* = 5.01 Hz, 2H), 0.58 - 0.67 (m, 2H), 1.17 - 1.30 (m, 1H), 2.52 (s, 3H), 2.56 (s, 3H), 2.64 (s, 3H), 3.11 (d, *J* = 6.65 Hz, 2H), 6.78 (d, *J* = 6.94 Hz, 1H), 6.83 (d, *J* = 8.67 Hz, 1H), 7.02 (d, *J* = 8.38 Hz, 1H), 7.13 (d, *J* = 8.09 Hz, 1H), 7.18 (dd, *J* = 8.38, 2.02 Hz, 1H), 7.49 (d, *J* = 2.31 Hz, 1H), 7.89 (d, *J* = 6.94 Hz, 1H). LC–MS *m/z* 419 $[M + H]^+$, t_R = 2.23 min.

8-Chloro-3-cyclopropylmethyl-7-{4-[(2-methylpyridin-4-yl)oxy]-3-fluorophenyl}[1,2,4]triazolo[4,3-a]-pyridine (15). Starting from **50a** (1.71 g, 5.13 mmol) and **52c** (1.4 g, 5.67 mmol) and following the procedure described for **8**, compound **15** was obtained as a white solid (0.100 g, 70%). Mp > 300ºC. ^{1}H NMR (500 MHz, $CDCl_3$) δ ppm 0.34 - 0.41 (m, 2H), 0.63 - 0.70 (m, 2H), 1.18 - 1.28 (m, 1H), 2.55 (s, 3H), 3.14 (d, *J* = 6.65 Hz, 2H), 6.73 (dd, *J* = 5.78, 2.31 Hz, 1H), 6.78 (d, *J* = 2.31 Hz, 1H), 6.91 (d, *J* = 7.22 Hz, 1H), 7.27 - 7.34 (m, 1H), 7.36 - 7.41 (m, 1H), 7.45 (dd, *J* = 10.69, 2.02 Hz, 1H), 8.01 (d, *J* = 6.94 Hz, 1H), 8.41 (d, *J* = 5.78 Hz, 1H). LC–MS *m/z* 409 $[M + H]^+$, t_R = 2.57 min.

8-Trifluoromethyl-3-cyclopropylmethyl-7-{4-[(2-methylpyridin-4-yl)oxy]-3-fluorophenyl}[1,2,4]triazolo[4,3-a]-pyridine (16). Starting from **49a** (1.4 g, 5.08 mmol) and **52c** (1.84 g, 5.59 mmol) and following the procedure described for **8**, compound **16** was obtained as a white solid (0.233 g, 10%). Mp 194.6ºC. ^{1}H NMR (500 MHz, $CDCl_3$) δ ppm 0.34 - 0.44 (m, 2 H), 0.61 - 0.73 (m, 2H), 1.18 - 1.29 (m, 1H), 2.55 (s, 3H), 3.17 (d, *J* = 6.66 Hz, 2H), 6.70 (dd, *J* = 5.8, 2.6 Hz, 1H), 6.76 (d, *J* = 2.3 Hz, 1H), 6.83 (d, *J* = 7.2 Hz, 1H), 8.20 (br d, J = 8.4 Hz, 1H), 7.23 - 7.31 (m, 2H), 8.14 (d, *J* = 7.2 Hz, 1H), 8.41 (d, *J* = 5.8 Hz, 1H). LC–MS *m/z* 443 $[M + H]^+$, t_R = 2.70 min.

8-Chloro-3-cyclopropylmethyl-7-{4-[(2-ethylpyridin-4-yl)oxy]-3-fluorophenyl}[1,2,4]triazolo[4,3-a]-pyridine (17). Starting from **50a** (0.26 g, 0.78 mmol) and **52d** (0.293 g, 0.857 mmol) and following the procedure described for **8**, compound **17** was obtained as a white solid (0.316 g, 96%). Mp > 300ºC. ^{1}H NMR (500 MHz, $CDCl_3$) δ ppm 0.31 - 0.43 (m, 2H), 0.60 - 0.72 (m, 2H), 1.15 - 1.29 (m, 1H), 1.31 (t, J = 7.7 Hz, 3H), 2.82 (q, J = 7.6 Hz, 2H), 3.14 (d, J = 6.6 Hz, 2H), 6.72 (dd, *J* = 5.8, 2.3 Hz, 1H), 6.81 (d, *J* = 2.3 Hz, 1H), 6.91 (d, *J* = 6.9 Hz, 1H), 7.31 (t, J = 8.2 Hz, 1H), 7.35 - 7.42 (m, 1H), 7.45 (dd, *J* = 10.7, 2.0 Hz, 1H), 8.01 (d, *J* = 6.9 Hz, 1H), 8.44 (d, *J* = 5.8 Hz, 1H). LC–MS *m/z* 423 $[M + H]^+$, t_R = 2.04 min.

8-Trifluoromethyl-3-cyclopropylmethyl-7-{4-[(2,6-dimethylpyridin-4-yl)oxy]-3-fluorophenyl}[1,2,4]triazolo[4,3-a]-pyridine (18). Starting from **49a** (0.185 g, 0.67 mmol) and **52e** (0.3 g, 0.874 mmol) and following the procedure described for **8**, compound **18** was obtained as a white solid (0.100 g, 33%). Mp 232.5ºC. ^{1}H NMR (500 MHz, $CDCl_3$) δ ppm 0.24 - 0.50 (m, 2H) 0.55 - 0.79 (m, 2H) 1.05 - 1.39 (m, 1H) 2.50 (s, 6H) 3.17 (d, *J*=6.70 Hz, 2H) 6.56 (s, 2H) 6.84 (d, *J*=7.17 Hz, 1H) 7.16 - 7.21 (m, 1H) 7.22 - 7.29 (m, 2H) 8.14 (d, *J*=7.17 Hz, 1 H). LC–MS *m/z* 457 $[M + H]^+$, t_R = 2.94 min.

8-Chloro-3-cyclopropylmethyl-7-{4-[(2-cyclopropylpyridin-4-yl)oxy]-3-fluorophenyl}[1,2,4]triazolo[4,3-a]-pyridine (19). Starting from **50a** (0.103 g, 0.310 mmol) and **52f** (0.22 g, 0.310 mmol) and following the procedure described for **8**, compound **19** was obtained as a white solid (0.06 g, 45%). Mp > 300ºC. ^{1}H NMR (500 MHz, $CDCl_3$) δ ppm 0.38 (q, *J* = 5.11 Hz, 2H), 0.62 - 0.71 (m, 2H), 0.95 - 1.09 (m, 4H), 1.16 - 1.29 (m, 1H), 1.94 - 2.03 (m, 1H), 3.14 (d, *J* = 6.65 Hz, 2H), 6.66 (dd, *J* = 5.64, 2.46 Hz, 1H), 6.78 (d, *J* = 2.31 Hz, 1H), 6.90 (d, *J* = 6.94 Hz, 1H), 7.28 - 7.33 (m, 1H), 7.34 - 7.40 (m, 1H), 7.44 (dd, *J* = 10.69, 2.02 Hz, 1H), 8.00 (d, *J* = 6.94 Hz, 1H), 8.35 (d, *J* = 5.78 Hz, 1H). LC–MS *m/z* 435 $[M + H]^+$, t_R = 4.51 min.

8-Trifluoromethyl-3-cyclopropylmethyl-7-{4-[(2-cyclopropylpyridin-4-yl)oxy]-3-fluorophenyl}[1,2,4]triazolo[4,3-a]-pyridine (20). Starting from **49a** (0.2 g, 0.725 mmol) and **52f** (0.283 g, 0.798 mmol) and following the procedure described for **8**, compound **20** was obtained as a white solid (0.058 g, 17%). Mp 211.1ºC. ^{1}H NMR (500 MHz, $CDCl_3$) δ ppm 0.32-0.45 (m, 2H), 0.53 - 0.75 (m, 2H), 0.96 - 1.03 (m, 2H), 1.02 - 1.08 (m, 2H), 1.16 - 1.30 (m, 1H), 1.91 - 2.03 (m, 1H), 3.16 (d, *J* = 6.7 Hz, 2H), 6.63 (dd, *J* = 5.8, 2.3 Hz, 1H), 6.75 (d, *J* = 2.3 Hz, 1H), 6.83 (d, *J* = 7.2 Hz, 1H), 7.15-7.22 (m, 1H), 7.22 - 7.31 (m, 2H), 8.15 (d, *J* = 6.9 Hz, 1H), 8.35 (d, *J* = 5.5 Hz, 1H). LC–MS *m/z* 469 $[M + H]^+$, t_R = 3.31 min.

8-Chloro-3-(2,2,2-trifluoroethyl-7-{4-[(2,6-dimethylpyridin-3-yl)oxy]-3-fluorophenyl}[1,2,4]triazolo[4,3-a]-pyridine (21). Starting from **56c** (0.2 g, 0.55 mmol) and **52a** (0.228 g, 0.664 mmol) and following the procedure described for **8**, compound **21** was obtained as a white solid (0.032 g, 13%). Mp 164.5ºC. ^{1}H NMR (500 MHz, $CDCl_3$) δ ppm 2.53 (s, 3H), 2.55 (s, 3H), 4.11 (q, J = 9.9 Hz, 2H), 6.93 (t, *J* = 8.3 Hz, 1H), 6.98 (d, *J* = 7.2 Hz, 1H), 7.02 (d, *J* = 8.3 Hz, 1H), 7.16 (d, J = 8.3 Hz, 1H), 7.23 - 7.28 (m, 1H), 7.42 (dd, J = 11.1, 2.1 Hz, 1H), 8.01 (d, *J* = 7.2 Hz, 1H). LC–MS *m/z* 451 $[M + H]^+$, t_R = 3.24 min.

8-Chloro-3-(ethoxymethyl-7-{4-[(2,6-dimethylpyridin-3-yl)oxy]-3-fluorophenyl}[1,2,4]triazolo[4,3-a]-pyridine (22). Starting from **50b** (0.4 g, 1.19 mmol) and **52a** (0.488 g, 1.42 mmol) and following the procedure described for **8**, compound **22** was obtained as a white solid (0.310 g, 61%). Mp 180.3ºC. ^{1}H NMR (500 MHz, $CDCl_3$) δ ppm 1.23 (t, *J* = 6.94 Hz, 3H), 2.54 (s, 3 H), 2.55 (s, 3H), 3.58 (q, *J* = 6.94 Hz, 2H), 5.10 (s, 2H), 6.87 - 6.95 (m, 2H), 7.02 (d, *J* = 8.09 Hz, 1H), 7.16 (d, *J* = 8.09 Hz, 1H), 7.22 - 7.26 (m, 1H), 7.42 (dd, *J* = 11.27, 2.31 Hz, 1H), 8.25 (d, *J*=7.22 Hz, 1H). LC–MS *m/z* 427 $[M + H]^+$, t_R = 2.77 min.

8-Trifluoromethyl-3-(ethoxymethyl-7-{4-[(2,6-dimethylpyridin-3-yl)oxy]-3-fluorophenyl}[1,2,4] triazolo[4,3-a]-pyridine (23). Starting from **49b** (0.150 g, 0.536 mmol) and **52a** (0.239 g, 0.697 mmol) and following the procedure described for **8**, compound **23** was obtained as a white solid (0.150 g, 61%). Mp 142.2ºC. ^{1}H NMR (500 MHz, $CDCl_3$) δ ppm 1.23 (t, *J*=7.08 Hz, 3H), 2.53 (s, 3H), 2.54 (s, 3H), 3.59 (q, *J* = 7.13 Hz, 2H), 5.12 (s, 2H), 6.82 (d, *J* = 7.22 Hz, 1H), 6.90 (t, *J* = 8.24 Hz, 1H), 7.01 (d, *J* = 8.38 Hz, 1H), 7.06 (d, *J* = 8.09 Hz, 1H), 7.14 (d, *J* = 8.38 Hz, 1H), 7.23 (dd, *J* = 10.69, 2.02 Hz, 1H), 8.40 (d, *J* = 6.94 Hz, 1H). LC–MS *m/z* 461 $[M + H]^+$, t_R = 2.89 min.

8-Chloro-3-cyclopropylmethyl-7-[3-fluoro-4-(isopropylamino)-phenyl][1,2,4]triazolo[4,3-a]-pyridine (24). Starting from **50a** (0.350 g, 1.049 mmol) and **52g** (0.381 g, 1.36 mmol) and following the procedure described for **8**, compound **24** was obtained as a white solid (0.097 g, 26%). Mp 196.4ºC. ^{1}H NMR (500 MHz, $CDCl_3$) δ ppm 0.35 (q, *J* = 5.20 Hz, 2H), 0.60 - 0.67 (m, 2H), 1.15 - 1.26 (m, 1H), 1.29 (d, *J* = 6.36 Hz, 6H), 3.10 (d, *J* = 6.65 Hz, H), 3.72 (dq, *J* = 13.19, 6.49 Hz, 1H), 3.98 (br d, *J* = 5.20 Hz, 1H), 6.70 - 6.81 (m, 1H), 6.87 (d, *J* = 6.94 Hz, 1H), 7.17 - 7.31 (m, 2H) 7.91 (d, *J* = 7.22 Hz, 1H). LC–MS *m/z* 359 $[M + H]^+$, t_R = 3.11 min.

8-Trifluoromethyl-3-cyclopropylmethyl-7-[3-fluoro-4-(isopropylamino)-phenyl][1,2,4]triazolo[4,3-a]-pyridine (25). Starting from **49a** (0.350 g, 1.27 mmol) and **52g** (0.461 g, 1.65 mmol) and following the procedure described for **8**, compound **25** was obtained as a white solid (0.250 g, 50%). Mp 196.9ºC. ^{1}H NMR (500 MHz, $CDCl_3$) δ ppm 0.28-0.42 (m, 2H), 0.57 - 0.71 (m, 2H), 1.12 - 1.26 (m, 1H), 1.29 (d, *J* = 6.4 Hz, 6H), 3.12 (d, *J* = 6.6 Hz, 2H), 3.64-3.77 (m, 1H), 3.96 (d, *J* = 4.9 Hz, 1H), 6.74 (t, *J* = 8.4 Hz, 1H), 6.80 (d, *J* = 7.2 Hz, 1H), 7.02 (d, *J* = 10.1 Hz, 2H), 8.04 (d, *J* = 6.9 Hz, 1H). LC–MS *m/z* 393 $[M + H]^+$, t_R = 3.33 min.

8-Trifluoromethyl-3-cyclopropylmethyl-7-[3-chloro-4-(isopropylamino)-phenyl][1,2,4]triazolo[4,3-a]-pyridine (26). Starting from **49a** (0.350 g, 1.27 mmol) and **52h** (0.488 g, 1.65 mmol) and following the procedure described for **8**, compound **26** was obtained as a white solid (0.250 g, 50%). Mp 230ºC. ^{1}H NMR (500 MHz, $CDCl_3$) δ ppm 0.29 - 0.42 (m, 2H), 0.55 - 0.71 (m, 2H), 1.11 - 1.27 (m, 1H), 1.31 (d, *J* = 6.36 Hz, 6H), 3.13 (d, *J* = 6.65 Hz, 2H), 3.73 (dq, *J* = 13.11, 6.51 Hz, 1H), 4.38 (br d, *J* = 7.51 Hz, 1H), 6.71 (d, *J* = 8.67 Hz, 1H), 6.79 (d, *J* = 7.22 Hz, 1H), 7.16 (dd, *J* = 8.38, 1.44 Hz, 1H), 7.30 (d, *J* = 2.02 Hz, 1H), 8.03 (d, *J* = 6.94 Hz, 1H). LC–MS *m/z* 409 $[M + H]^+$, t_R = 3.71 min.

8-Chloro-3-cyclopropylmethyl-7-[3-fluoro-4-(cyclopropylamino)-phenyl][1,2,4]triazolo[4,3-a]-pyridine (27). Starting from **50a** (0.30 g, 0.9 mmol) and **52i** (0.3 g, 1.08 mmol) and following the procedure described for **8**, compound **27** was obtained as a white solid (0.147 g, 46%). ^{1}H NMR (500 MHz, $CDCl_3$) δ ppm 0.28 - 0.40 (m, 2H), 0.57 - 0.69 (m, 4H), 0.78 - 0.87 (m, 2H), 1.15 - 1.28 (m, 1H), 2.45 - 2.56 (m, 1H), 3.11 (d, *J* = 6.65 Hz, 2H), 4.60 (br s, 1H), 6.88 (d, *J* = 7.22 Hz, 1H), 7.13 - 7.20 (m, 1H), 7.21 - 7.31 (m, 2H), 7.92 (d, *J* = 6.94 Hz, 1H). LC–MS *m/z* 357 $[M + H]^+$, t_R = 3.30 min.

8-Trifluoromethyl-3-cyclopropylmethyl-7-[3-fluoro-4-(cyclopropylamino)-phenyl][1,2,4]triazolo[4,3-a]-pyridine (28). Starting from **49a** (0.20 g, 0.73 mmol) and **52i** (0.221 g, 0.8 mmol) and following the procedure described for **8**, compound **28** was obtained as a white solid (0.169 g, 60%). Mp. > 300ºC. ^{1}H NMR (400 MHz, $CDCl_3$) δ ppm 0.28 - 0.43 (m, 2H), 0.51 - 0.72 (m, 4H), 0.75 - 0.91 (m, 2H), 1.12 - 1.31 (m, 1H), 2.50 (tt, *J* = 6.56, 3.27 Hz, 1H), 3.13 (d, *J* = 6.70 Hz, 2H), 4.58 (br s, 1H), 6.80 (d, *J* = 6.94 Hz, 1H), 6.98 - 7.09 (m, 2H), 7.10 - 7.18 (m, 1H), 8.05 (d, *J* = 7.17 Hz, 1H). LC–MS *m/z* 391 $[M + H]^+$, t_R = 3.18 min.

8-Trifluoromethyl-3-cyclopropylmethyl-7-[3-chloro-4-(cyclopropylamino)-phenyl][1,2,4]triazolo[4,3-a]-pyridine (29). Starting from **49a** (0.20 g, 0.73 mmol) and **52j** (0.34 g, 0.8 mmol) and following the procedure described for **8**, compound **29** was obtained as a white solid (0.109 g, 37%). ^{1}H NMR (400 MHz, $CDCl_3$) δ ppm 0.31 - 0.40 (m, 2H), 0.59 - 0.69 (m, 4H), 0.81 - 0.89 (m, 2H), 1.15 - 1.27 (m, 1H), 2.46 - 2.56 (m, 1H), 3.13 (d, *J* = 6.70 Hz, 2H), 4.93 (s, 1H), 6.80 (d, *J* = 7.17 Hz, 1H), 7.11 - 7.16 (m, 1H), 7.17 - 7.23 (m, 1H), 7.28 (d, *J* = 1.85 Hz, 1H), 8.05 (d, *J* = 7.17 Hz, 1H). LC–MS *m/z* 407 $[M + H]^+$, t_R = 3.48 min.

8-Chloro-3-cyclopropylmethyl-7-[3-chloro-4-(cyclopropylamino)-phenyl][1,2,4]triazolo[4,3-a]-pyridine (30). Starting from **50a** (0.30 g, 0.9 mmol) and **52j** (0.32 g, 1.08 mmol) and following the procedure described for **8**, compound **30** was obtained as a white solid (0.147 g, 46%). Mp > 300ºC. ^{1}H NMR (500 MHz, $CDCl_3$) δ ppm 0.29 - 0.42 (m, 2H), 0.57 - 0.70 (m, 4H), 0.78 - 0.92 (m, 2H), 1.15 - 1.27 (m, 1H), 2.49 - 2.56 (m, 1H), 3.11 (d, *J* = 6.7 Hz, 2H), 4.60 (br s, 1H), 6.87 (d, *J* = 6.9 Hz, 1H), 7.18 (d, *J* = 8.3 Hz, 1H), 7.42 dd, *J* = 8.3, 2.1 Hz, 1H), 7.47 (d, *J* = 1.8 Hz, 1H), 7.92 (d, *J* = 7.2 Hz, 1H). LC–MS *m/z* 373 $[M + H]^+$, t_R = 3.83 min.

8-Trifluoromethyl-3-cyclopropylmethyl-7-{4-[(2-methoxypyridin-5-yl)methoxy]-3-fluorophenyl} [1,2,4] triazolo[4,3-a]-pyridine (31). Starting from **49a** (0.3 g, 1.088 mmol) and **52k** (0.721 g, 1.306 mmol) and following the procedure described for **8**, compound **31** was obtained as a white solid (0.198 g, 38%). Mp 148.5ºC. ^{1}H NMR (400 MHz, $CDCl_3$) δ ppm 0.37 (q, *J* = 5.09 Hz, 2H), 0.56 - 0.74 (m, 2H), 1.09 - 1.32 (m, 1H), 3.14 (d, *J* = 6.70 Hz, 2H), 3.96 (s, 3H), 5.12 (s, 2H), 6.79 (dd, *J* = 13.87, 7.63 Hz, 2H), 7.00 - 7.19 (m, 3H), 7.71 (dd, *J* = 8.55, 2.54 Hz, 1H) 8.09 (d, *J* = 7.17 Hz, 1H), 8.24 (d, *J* = 2.31 Hz, 1H). LC–MS *m/z* 473 $[M + H]^+$, t_R = 2.79 min.

8-Trifluoromethyl-3-cyclopropylmethyl-7-{4-[(2-methoxypyridin-5-yl)methoxy]- phenyl }[1,2,4] triazolo[4,3-a]-pyridine (32). Starting from **49a** (0.315 g, 1.15 mmol) and **52l** (0.430 g, 1.26 mmol) and following the procedure described for **8**, compound **32** was obtained as a white solid (0.286 g, 60%). Mp 159.1ºC. ^{1}H NMR (400 MHz, $CDCl_3$) δ ppm 0.29 - 0.45 (m, 2H), 0.55 - 0.72 (m, 2H), 1.10 - 1.33 (m, 1H), 3.14 (d, *J* = 6.70 Hz, 2H), 3.96 (s, 3H), 5.04 (s, 2H), 6.67 - 6.87 (m, 2H), 7.00 - 7.12 (m, 2H), 7.32 (d, *J* = 8.55 Hz, 2H), 7.70 (dd, *J* = 8.55, 2.31 Hz, 1H), 8.08 (d, *J* = 7.17 Hz, 1H), 8.25 (d, *J* = 2.31 Hz, 1H). LC–MS *m/z* 455 $[M + H]^+$, t_R = 3.73 min.

8-Trifluoromethyl-3-cyclopropylmethyl-7-{4-[(2-methoxypyridin-5-yl)methylamino]-3-fluorophenyl} [1,2,4]triazolo[4,3-a]-pyridine (33). Starting from **49a** (0.530 g, 1.92 mmol) and **52m** (0.758 g, 2.11 mmol) and following the procedure described for **8**, compound **33** was obtained as a white solid (0.460 g, 51%). Mp 160.4ºC. ^{1}H NMR (400 MHz, $CDCl_3$) δ ppm 0.30 - 0.42 (m, 2H), 0.59 - 0.71 (m, 2H), 1.15 - 1.27 (m, 1H), 3.13 (d, *J* = 6.70 Hz, 2H), 3.95 (s, 3H), 4.36 (d, *J* = 4.86 Hz, 2H), 4.44 (br s, 1H), 6.69 - 6.83 (m, 3H), 6.95 - 7.12 (m, 2H), 7.62 (dd, *J* = 8.44, 2.43 Hz, 1H), 8.05 (d, *J* = 7.17 Hz, 1H), 8.19 (d, *J* = 2.54 Hz, 1H). LC–MS *m/z* 472 $[M + H]^+$, t_R = 2.67 min.

8-Trifluoromethyl-3-cyclopropylmethyl-7-{4-[(2-methoxypyridin-5-yl)methylamino]-3-phenyl}[1,2,4] triazolo[4,3-a]-pyridine (34). Starting from **49a** (0.150 g, 0.544 mmol) and **52n** (0.204 g, 0.6 mmol) and following the procedure described for **8**, compound **34** was obtained as a white solid (0.115 g, 46%). Mp 127.5ºC. ^{1}H NMR (500 MHz, $CDCl_3$) δ ppm 0.29 - 0.42 (m, 2H), 0.60 - 0.68 (m, 2H), 1.17 - 1.24 (m, 1H), 3.12 (d, *J* = 6.94 Hz, 2H), 3.95 (s, 3H), 4.20 (br s, 1H), 4.32 (d, *J* = 4.91 Hz, 2H), 6.70 (d, *J* = 8.38 Hz, 2H), 6.76 (d, *J* = 8.38 Hz, 1H), 6.80 (d, *J* = 6.94 Hz, 1H), 7.21 (d, *J* = 8.67 Hz, 2H), 7.61 (dd, *J* = 8.53, 2.46 Hz, 1H), 8.03 (d, *J* = 7.22 Hz, 1H), 8.18 (d, *J* = 2.31 Hz, 1H). LC–MS *m/z* 454 $[M + H]^+$, t_R = 2.05 min.

8-Chloro-3-cyclopropylmethyl-7-{4-[(2-methoxypyridin-5-yl)methylamino]-3-phenyl} [1,2,4] triazolo[4,3-a]-pyridine (35). Starting from **50a** (0.150 g, 0.45 mmol) and **52n** (0.168 g, 0.494 mmol) and following the procedure described for **8**, compound **35** was obtained as a white solid (0.098 g, 51%). Mp 158.1ºC. ^{1}H NMR (400 MHz, $CDCl_3$) δ ppm 0.30 - 0.40 (m, 2H), 0.57 - 0.70 (m, 2H), 1.13 - 1.39 (m, 1H), 3.10 (d, *J* = 6.70 Hz, 2H), 3.95 (s, 3H), 4.33 (s, 3H), 6.69 - 6.79 (m, 3H), 6.89 (d, *J* = 7.17 Hz, 1H), 7.38 - 7.46 (m, 2H), 7.62 (dd, *J* = 8.55, 2.54 Hz, 1H), 7.91 (d, *J* = 7.17 Hz, 1H), 8.19 (d, *J* = 2.08 Hz, 1H). LC–MS *m/z* 420 $[M + H]^+$, t_R = 1.93 min.

8-Chloro-3-cyclopropylmethyl-7-[3-chloro-4-(tetrahydro-pyran-4-yloxy)-phenyl][1,2,4]triazolo[4,3-a]-pyridine (36). Starting from **50a** (0.20 g, 0.6 mmol) and **52o** (0.243 g, 0.72 mmol) and following the procedure described for **8**, compound **36** was obtained as a white solid (0.160 g, 64%). Mp. 189.1ºC. ^{1}H NMR (400 MHz, $CDCl_3$) δ ppm 0.30 - 0.43 (m, 2H), 0.56 - 0.73 (m, 2H), 1.15 - 1.30 (m, 1H), 1.92 (ddt, *J* = 17.05, 7.28, 3.55, 3.55 Hz, 2H), 2.02 - 2.17 (m, 2H), 3.12 (d, *J* = 6.70 Hz, 2H), 3.65 (ddd, *J* = 11.44, 7.40, 3.58 Hz, 2H), 4.05 (ddd, *J* = 11.44, 7.40, 3.58 Hz, 2H), 4.66 (tt, *J* = 7.11, 3.64 Hz, 1H), 6.86 (d, *J* = 6.94 Hz, 1H), 7.06 (d, *J* = 8.55 Hz, 1H), 7.43 (dd, *J* = 8.55, 2.31 Hz, 1H), 7.58 (d, *J* = 2.31 Hz, 1H), 7.96 (d, *J* =7.17 Hz, 1H). LC–MS *m/z* 418 $[M + H]^+$, t_R = 3.25 min.

8-Trifluoromethyl-3-cyclopropylmethyl-7-[3-chloro-4-(tetrahydro-pyran-4-yloxy)-phenyl][1,2,4] triazolo[4,3-a]-pyridine (37). Starting from **49a** (0.09 g, 0.33 mmol) and **52o** (0.138 g, 0.41 mmol) and following the procedure described for **8**, compound **37** was obtained as a white solid (0.083 g, 56%). Mp. 176.9ºC. ^{1}H NMR (400 MHz, $CDCl_3$) δ ppm 0.30 - 0.43 (m, 2H), 0.58 - 0.73 (m, 2H), 1.16 - 1.28 (m, 1H), 1.86-1.97 (m, 2H), 2.02 - 2.12 (m, 2H), 3.14 (d, *J* = 6.70 Hz, H), 3.59-3.69 (m, 2H), 4-4.09 (m, 2H), 4.61-4.68 (m, 2H), 6.78 (d, *J* = 7.2 Hz, 1H), 7.02 (d, *J* = 8.6 Hz, 1H), 7.20 (dd, *J* = 8.6, 2.1 Hz, 1H), 7.41 (d, *J* = 2.1 Hz, 1H), 8.09 (d, *J* =7.2 Hz, 1H). LC–MS *m/z* 452 $[M + H]^+$, t_R = 3.33 min.

8-Chloro-3-cyclopropylmethyl-7-[3-chloro-4-(tetrahydro-pyran-4-ylamino)-phenyl][1,2,4]triazolo[4,3-a]-pyridine (38). Starting from **50a** (0.20 g, 0.6 mmol) and **52p** (0.242 g, 0.72 mmol) and following the procedure described for **8**, compound **38** was obtained as a white solid (0.160 g, 64%). Mp. 221.3ºC. ^{1}H NMR (500 MHz, $CDCl_3$) δ ppm 0.28 - 0.41 (m, 2H), 0.56 - 0.71 (m, 2H), 1.13 - 1.29 (m, 1H), 1.45 - 1.71 (m, 2H), 2.10 (br d, *J* = 13.29 Hz, 2H), 3.11 (d, *J* = 6.65 Hz, 2H), 3.52 - 3.60 (m, 2H), 3.62 (br dd, *J* = 6.94, 3.18 Hz, 1H), 4.05 (dt, *J* = 11.78, 3.65 Hz, 2H), 4.49 (br d, *J* = 7.80 Hz, 1H), 6.78 (d, *J* = 8.38 Hz, 1H), 6.86 (d, *J* = 7.22 Hz, 1H), 7.39 (dd, J = 8.53, 2.17 Hz, 1H), 7.51 (d, *J* = 2.31 Hz, 1H), 7.92 (d, *J* = 7.22 Hz, 1H). LC–MS *m/z* 417 $[M + H]^+$, t_R = 4.08 min.

8-Trifluoromethyl-3-cyclopropylmethyl-7-[3-chloro-4-(tetrahydro-pyran-4-ylamino)-phenyl][1,2,4]triazolo[4,3-a]-pyridine (39). Starting from **49a** (0.07 g, 0.25 mmol) and **52p** (0.107 g, 0.32 mmol) and following the procedure described for **8**, compound **39** was obtained as a white solid (0.045 g, 39%). Mp. 198.4ºC. ^{1}H NMR (400 MHz, $CDCl_3$) δ ppm 0.31 - 0.42 (m, 2H), 0.58 - 0.71 (m, 2H), 1.16 - 1.27 (m, 1H), 1.55 - 1.68 (m, 2H), 2.09 (br d, *J* = 12.7 Hz, 2H), 3.13 (d, *J* = 6.7 Hz, 2H), 3.56 (td, J = 11.8, 2.3 Hz, 1H), 3.56-3.67 (m, 1H), 4.05 (dt, *J* = 11.7, 3.7 Hz, 2H), 4.47 (d, *J* = 7.6 Hz, 1H), 6.74 (d, *J* = 8.6 Hz, 1H), 6.78 (d, *J* = 7.2 Hz, 1H), 7.16 (dd, J = 8.3, 1.8 Hz, 1H), 7.32 (d, *J* = 2.1 Hz, 1H), 8.05 (d, *J* = 7.2 Hz, 1H). LC–MS *m/z* 451 $[M + H]^+$, t_R = 3.29 min.

8-Trifluoromethyl-3-cyclopropylmethyl-7-[3-chloro-4-(tetrahydro-pyran-4-ylaminomethyl)-phenyl][1,2,4]triazolo[4,3-a]-pyridine (40). Starting from **49a** (0.2 g, 0.73 mmol) and **52q** (0.306 g, 0.87 mmol) and following the procedure described for **8**, compound **40** was obtained as a white solid (0.060 g, 18%). ^{1}H NMR (400 MHz, $CDCl_3$) δ ppm 0.37 (q, *J* = 5.09 Hz, 2H), 0.59 - 0.74 (m, 2H), 1.10 - 1.32 (m, 2H), 1.41 - 1.73 (m, 2H), 1.92 (br dd, *J* = 12.60, 1.73 Hz, 2H), 2.69 - 2.86 (m, 1H), 3.15 (d, *J* = 6.70 Hz, 2H), 3.34 - 3.49 (m, 2H), 3.97 - 4.01 (m, 3H), 4.01 - 4.04 (m, 1H), 6.76 (d, *J* = 7.17 Hz, 1H), 7.22 - 7.28 (m, 1H), 7.37 (d, *J* = 1.62 Hz, 1H), 7.56 (d, *J* = 7.86 Hz, 1H), 8.10 (d, *J* = 7.17 Hz, 1H). LC–MS *m/z* 465 $[M + H]^+$, t_R = 2.09 min.

Trans-**8-Chloro-3-cyclopropylmethyl-7-[3-chloro-4-(4-hydroxy-cyclohexylamino)-phenyl][1,2,4]triazolo[4,3-a]-pyridine (41)**. Starting from **50a** (0.13 g, 0.388 mmol) and **52r** (0.15 g, 0.43 mmol) and following the procedure described for **8**, compound **41** was obtained as a white solid (0.087 g, 52%). Mp 270.9ºC. ^{1}H NMR (400 MHz, $CDCl_3$) δ ppm 0.29 - 0.42 (m, 2H), 0.56 - 0.71 (m, 2H), 1.17 - 1.25 (m, 1H), 1.47 (br s, 1H), 1.73 - 1.8 (m, 4H), 1.80-1.91 (m, 4H), 3.11 (d, J=6.7 Hz, 2H), 3.46 - 3.57 (m, 1H), 3.98 (br s, 1H), 4.60 (br d, J=7.6 Hz, 1H), 6.76 (d, J=8.8 Hz, 1H), 6.87 (d, J=7.2 Hz, 1H), 7.39 (dd, J=8.3, 2.3 Hz, 1H), 7.49 (d, J=2.1 Hz, 1H), 7.91 (d, J=7.2 Hz, 1H). LC–MS *m/z* 431 $[M + H]^+$, t_R = 3.49 min.

Trans-**8-Trifluoromethyl-3-cyclopropylmethyl-7-[3-chloro-4-(4-hydroxy-cyclohexylamino)-phenyl][1,2,4]triazolo[4,3-a]-pyridine (42)**. Starting from **49a** (0.3 g, 1.088 mmol) and **52r** (0.459 g, 1.306 mmol) and following the procedure described for **8**, compound **42** was obtained as a white solid (0.209 g, 41%). Mp. 290.7ºC. ^{1}H NMR (400 MHz, $CDCl_3$) δ ppm 0.3 - 0.43 (m, 2H), 0.58 - 0.71 (m, 2H), 1.16 - 1.25 (m, 1H), 1.29-1.42 (m, 2H), 1.42 - 1.53 (m, 3H), 2.03-2.12 (m, 2H), 2.20 (br d, *J* = 12.0 Hz, 2H), 3.13 (d, *J*=6.7 Hz, 2H), 3.32 - 3.43 (m, 1H), 3.70-3.80 (m, 1H), 4.39 (d, *J* = 7.6 Hz, 1H), 6.72 (d, *J* = 8.6 Hz, 1H), 6.79 (d, *J* = 7.2 Hz, 1H), 7.16 (dd, *J* = 8.6, 2.1 Hz, 1H), 7.30 (d, *J* = 2.1 Hz, 1H), 8.04 (d, *J* = 7.2 Hz, 1H). LC–MS *m/z* 465 $[M + H]^+$, t_R = 2.50 min.

Cis-**8-Chloro-3-cyclopropylmethyl-7-[3-chloro-4-(4-hydroxy-cyclohexylamino)-phenyl][1,2,4]triazolo[4,3-a]-pyridine (43)**. Starting from **50a** (0.13 g, 0.388 mmol) and **52s** (0.15 g, 0.43 mmol) and following the procedure described for **8**, compound **43** was obtained as a white solid (0.060 g, 36%). Mp. 273.7ºC. ^{1}H NMR (400 MHz, $CDCl_3$) δ ppm 0.27 - 0.43 (m, 2H) 0.57 - 0.70 (m, 2H), 1.02 - 1.32 (m, 2H), 1.68 - 1.98 (m, 8H), 3.11 (d, *J* = 6.70 Hz, 2H), 3.44 - 3.62 (m, 1H), 3.98 (br s, 1H), 4.60 (br d, *J* = 7.63 Hz, 1H), 6.76 (d, *J* = 8.79 Hz, 1H), 6.87 (d, *J* = 7.17 Hz, 1H), 7.39 (dd, *J* = 8.44, 2.20 Hz, 1H), 7.49 (d, *J* = 2.08 Hz, 1H), 7.91 (d, *J* = 7.17 Hz, 1H). LC–MS *m/z* 431 $[M + H]^+$, t_R = 3.08 min.

Cis-**8-Trifluoromethyl-3-cyclopropylmethyl-7-[3-chloro-4-(4-hydroxy-4-cyclopropyl-cyclohexylamino)-phenyl][1,2,4]triazolo[4,3-a]-pyridine (44)**. Starting from **49a** (0.143 g, 0.52 mmol) and **52t** (0.235 g, 0.6 mmol) and following the procedure described for **8**, compound **44** was obtained as a white solid (0.047 g, 18%). Mp > 300ºC. ^{1}H NMR (500 MHz, $CDCl_3$) δ ppm 0.04 - 0.16 (m, 2H), 0.18 - 0.33 (m, 5H), 0.34 - 0.43 (m, 2H), 0.60 (tt, *J* = 8.31, 5.56 Hz, 1H), 0.80 - 1.00 (m, 1H), 1.11 - 1.25 (m, 2H), 1.31 - 1.56 (m, 4H), 1.63 - 1.79 (m, 2H), 2.49 (d, *J* = 6.65 Hz, 2H), 2.97 (tdt, *J* = 11.13, 11.13, 7.37, 3.97, 3.97 Hz, 1H), 4.45 (d, *J* = 7.51 Hz, 1H), 5.95 (d, *J* = 7.22 Hz, 1H), 6.53 (d, *J* = 8.67 Hz, 1H), 6.73 (d, *J* = 7.22 Hz, 1H), 7.16 (s, 1H) 7.28 (d, *J* = 2.02 Hz, 1H). LC–MS *m/z* 465 $[M + H]^+$, t_R = 3.49 min.

Trans-**8-Chloro-3-(2,2,2-trifluoroethyl)-7-[3-chloro-4-(4-hydroxy-cyclohexylamino)-phenyl][1,2,4]triazolo[4,3-a]-pyridine (45)**. Starting from **56c** (0.11 g, 0.304 mmol) and **52r** (0.128 g, 0.365 mmol) and following the procedure described for **8**, compound **45** was obtained as a white solid (0.054 g, 39%). Mp > 300ºC. ^{1}H NMR (400 MHz, $CDCl_3$) δ ppm 1.28 - 1.52 (m, 5H), 2.08 (br d, *J* = 10.63 Hz, 2H), 2.20 (br d, *J* = 12.02 Hz, 2H), 3.26 - 3.46 (m, 1H), 3.62 - 3.85 (m, 1H), 4.08 (q, *J* = 9.71 Hz, 2H), 4.44 (d, *J* =

7.63 Hz, 1H), 6.77 (d, *J* = 8.55 Hz, 1H), 6.97 (d, *J* = 7.17 Hz, 1H), 7.39 (dd, *J* = 8.55, 2.08 Hz, 1H), 7.50 (d, *J* = 2.08 Hz, 1H), 7.94 (d, *J* = 7.17 Hz, 1H). LC–MS *m/z* 459 $[M + H]^+$, t_R = 3.23 min.

Trans-**8-Trifluoromethyl-3-cyclopropylmethyl-7-[3-chloro-4-(4-hydroxy-cyclohexyloxy)-phenyl][1,2,4] triazolo[4,3-a]-pyridine (46)**. Starting from **49a** (0.119 g, 0.432 mmol) and **52u** (0.183g, 0.518 mmol) and following the procedure described for **8**, compound **46** was obtained as a white solid (0.022 g, 27%). ^{1}H NMR (400 MHz, $CDCl_3$) δ ppm 0.31 - 0.41 (m, 2H), 0.61 - 0.71 (m, 2H), 1.09 - 1.32 (m, 2H), 1.42 - 1.56 (m, 2H), 1.67 - 1.80 (m, 2H), 2.05 - 2.23 (m, 4H), 3.14 (d, *J* = 6.70 Hz, 2H), 3.83 - 3.96 (m, 1H), 4.36 - 4.49 (m, 1H), 6.78 (d, *J* = 7.17 Hz, 1H), 7.02 (d, *J* = 8.79 Hz, 1H), 7.20 (dd, *J* = 8.44, 2.20 Hz, 1H), 7.39 (d, *J* = 2.31 Hz, 1H), 8.09 (d, *J* = 7.17 Hz, 1H). LC–MS *m/z* 466 $[M + H]^+$, t_R = 2.96 min.

Trans-**8-Chloro-3-(2,2,2-trifluoroethyl)-7-[3-chloro-4-(4-hydroxy-cyclohexyloxy)-phenyl][1,2,4] triazolo[4,3-a]-pyridine (47)**. Starting from **56c** (0.190 g, 0.526 mmol) and **52u** (0.222 g, 0.631 mmol) and following the procedure described for **8**, compound **47** was obtained as a white solid (0.065 g, 27%). Mp >300ºC. ^{1}H NMR (500 MHz, $CDCl_3$) δ ppm 1.42 (d, *J* = 3.76 Hz, 1H), 1.46 - 1.55 (m, 2H), 1.68 - 1.79 (m, 2H), 2.10 (td, *J* = 7.73, 3.61 Hz, 2H), 2.18 (td, *J* = 7.66, 3.47 Hz, 2H), 3.91 (td, *J* = 8.09, 4.05 Hz, 1H), 4.10 (q, *J* = 9.73 Hz, 2H), 4.46 (tt, *J* = 8.06, 3.79 Hz, 1H), 6.97 (d, *J* = 7.22 Hz, 1H), 7.08 (d, *J* = 8.38 Hz, 1H), 7.42 (dd, *J* = 8.53, 2.17 Hz, 1H), 7.57 (d, *J* = 2.31 Hz, 1H), 7.98 (d, *J*=7.22 Hz, 1H). LC–MS *m/z* 460 $[M + H]^+$, t_R = 3.23 min.

Cis-**8-Chloro-3-(2,2,2-trifluoroethyl)-7-[3-chloro-4-(4-hydroxy-cyclohexyloxy)-phenyl][1,2,4] triazolo[4,3-a]-pyridine (48)**. Starting from **56c** (0.150 g, 0.415 mmol) and **52v** (0.176g, 0.498 mmol) and following the procedure described for **8**, compound **48** was obtained as a white solid (0.044 g, 23%). Mp 196.7ºC. ^{1}H NMR (400 MHz, $CDCl_3$) δ ppm 1.39 - 1.48 (m, 1H), 1.66 - 1.93 (m, 6H), 2.06 - 2.21 (m, 2H), 3.81 (tq, *J* = 8.44, 4.24 Hz, 1H), 4.10 (q, *J* = 9.71 Hz, 2H), 4.56 (tt, *J* = 5.20, 2.77 Hz, 1H), 6.98 (d, *J* = 7.17 Hz, 1H), 7.06 (d, *J* = 8.55 Hz, 1H), 7.43 (dd, *J* = 8.55, 2.31 Hz, 1H), 7.57 (d, *J* = 2.31 Hz, 1H), 7.99 (d, *J* = 7.17 Hz, 1H). LC–MS *m/z* 460 $[M + H]^+$, t_R = 3.14 min.

8-Trifluoromethyl-3-(ethoxymethyl)-7-[3-chloro-1,2,4-triazolo[4,3-a]-pyridine (49b). Mp 104ºC. ^{1}H NMR (400 MHz, $CDCl_3$) δ ppm ^{1}H NMR (500 MHz, CHLOROFORM-d) δ ppm 1.22 (t, J=6.94 Hz, 3 H) 3.57 (q, J=6.94 Hz, 2 H) 5.08 (s, 2 H) 6.95 (d, J=7.22 Hz, 1 H) 8.35 (d, J=7.51 Hz, 1 H). LC–MS *m/z* 280 $[M + H]^+$, t_R = 1.32 min.

Biology

Membrane preparation

CHO-K1 cells stably expressing the wildtype $hmGlu_2$ receptor (CHO-K1_$hmGlu_2$) were grown in DMEM medium supplemented with 10% (v/v) fetal calf serum, 200 IU/mL penicillin, 200 μg/mL streptomycin, 30.5 μg/mL L proline and 400 μg/mL G418 at 37°C and 5% CO_2. Sodium butyrate (final concentration 5 mM) was added to the plates when cells growth reached 70% confluency.[63] 24 hours later, cells were detached from the plates by scraping into 5 ml of PBS and centrifuged for 5 min at 1500 rpm. Pellets were resuspended into ice-cold Tris buffer (50 mM Tris-HCl pH 7.4) and homogenized using an Ultra Turrax homogenizer (IKA Werke GmbH & Co.KG, Staufen, Germany). An Optima LE 80 K ultracentrifuge (Beckman Coulter, Fullerton, CA) at 31,000 rpm was used for separation of membranes and the cytosolic fraction at 4°C for 20 min. Pellets were resuspended in 10 ml Tris buffer and the centrifugation and homogenization steps were repeated. Remaining pellets were suspended into assay buffer (50 mM Tris-HCl pH 7.4, 2 mM $CaCl_2$, 10 mM $MgCl_2$) and the homogenization step was repeated. Aliquots were stored at -80°C. BCA protein determination was used to determine the membrane protein concentrations.

[^{35}S]GTPγS Binding Assay

[^{35}S]GTPγS binding experiments were performed as previously described.[12]

Radioligand Binding Assays

After thawing, membranes were homogenized by an Ultra Turrax homogenizer. **4** (10μM) was used to determine nonspecific binding. DMSO concentrations were ≤0.25%. For all experiments, radioligand concentrations were such that <10% of the amount added was receptor-bound to avoid ligand depletion.

For displacement assays, membrane protein aliquots (30 μg) were incubated with 6 nM [^{3}H]-**7** and 10 concentrations of competing ligand diluted by an HP D300 digital dispenser (Tecan, Giessen, The Netherlands) in assay buffer to a total volume of 100 μl. After 60 minutes at 15°C, incubation was terminated by rapid filtration over GF/C filterplates (PerkinElmer, Groningen, The Netherlands) on a PerkinElmer filtermate harvester. Filterplates were washed 10 times with ice-cold wash buffer (50 mM Tris-HCl pH 7.4) and filter-bound radioactivity was determined in a Microbeta 2450^{2} microplate counter (PerkinElmer).

For association, dissociation and competition association experiments a scintillation proximity assay (SPA) was developed and used. Membrane protein (20 μg) and pre-wetted wheat-germ agglutinin coated SPA beads (0.2 mg; RPNQ0001, PerkinElmer) were pre-coupled in assay buffer while gently shaking at room temperature for 30 minutes. Then, this membrane bead mixture was added to an Isoplate-96 (PerkinElmer) together with 6 nM [^{3}H]-**7** and competing ligand in case of competition association. After addition, the plate was rapidly placed in a Microbeta 2450^{2} microplate counter. Plates were recorded for 120 minutes measuring every 30 seconds at ambient temperature of 28°C. Binding values were determined in corrected counts per minute (CCPM). For dissociation assays, radioligand dissociation was initiated after 60 minutes of incubation by addition of 5 μl **4** (final concentration: 10 μM). Subsequently, plates were recorded for 120 minutes being measuring every 30 seconds.

Label-free whole-cell assays

Label-free whole-cell assays were performed using the xCELLigence real-time cell analyzer (RTCA DP) system as described previously [58,64]. Baseline impedance was measured using 45 μl culture medium (as described under membrane preparation) per well in 16 well E-plates (Westburg, Leusden, The Netherlands). 40,000 cells per well were added in a volume of 50 μl. After resting for 30 minutes at room temperature, E-plates were placed in the recording station within a humidified 37°C, 5% CO_2 incubator. Impedance (represented in the arbitrary unit Cell Index) was measured every 15 minutes overnight. After 18 hours, cells were stimulated with the indicated concentration of compound. Impedance was measured every 15 seconds for 20 minutes, then 5 minute intervals were used for the next 40 minutes, followed by 15 minute intervals thereafter. For washing experiments, cells were stimulated with an EC_{80} equivalent concentration of compound in a volume of 5 μl. Wells were washed after 5 minutes

by aspiration of the medium, addition of 100 µl fresh medium, which was subsequently aspirated and replaced by another 100 µl fresh medium. This washing step was chosen such that it was just before the maximum Cell Index level. In control wells, medium was pipetted up and down in order to induce similar mechanical cell stress.

Data Analysis

Data analyses were performed using Prism 6.04 (GraphPad software, San Diego, CA, USA). pIC_{50} values were acquired using non-linear regression curve fitting into a sigmoidal concentration-response curve using the equation: Y=Bottom + (Top-Bottom)/(1+$10^{(X\text{-}LogIC50)}$). pK_i values were acquired from pIC_{50} values using the Cheng-Prusoff equation.[65] Dissociation rate constants k_{off} were determined using an exponential decay analysis of radioligand binding. Association rate constants k_{on} were determined using the equation $k_{on} = (k_{obs} - k_{off})/[L]$, in which L is the concentration of radioligand used for association experiments and k_{obs} was determined using exponential association analysis.

Association and dissociation rate constants for unlabelled $mGlu_2$ PAMs were determined by nonlinear regression analysis of competition association data as described by Motulsky and Mahan.[40]

$$K_A = k_1[L]\cdot 10^{-9} + k_2$$
$$K_B = k_3[I]\cdot 10^{-9} + k_4$$
$$S = \sqrt{(K_A - K_B)^2 + 4\cdot k_1\cdot k_3\cdot L\cdot I\cdot 10^{-18}}$$
$$K_F = 0.5(K_A + K_B + S)$$
$$K_S = 0.5(K_A + K_B - S)$$
$$Q = \frac{B_{\max}\cdot k_1\cdot L\cdot 10^{-9}}{K_F - K_S}$$
$$Y = Q\cdot\left(\frac{k_4\cdot(K_F - K_S)}{K_F\cdot K_S} + \frac{k_4 - K_F}{K_F}e^{(-K_F\cdot X)} - \frac{k_4 - K_S}{K_S}e^{(-K_S\cdot X)}\right)$$

Experimental data are reported as k_{on} and k_{off} and the corresponding conversion of k_{off} to residence time (RT) is performed to be consistent with current state of the art.[24]

Data shown are the mean ± SEM of at least three individual experiments performed in duplicate unless stated otherwise. Statistical analysis was performed if indicated, using a two-tailed unpaired Student's t-test. Observed differences with p-values <0.05 were considered statistically significant. clogP values were calculated using ChemDraw Professional v15.0.0.106 (PerkinElmer).

REFERENCES

1. Kew JNC, Kemp JA. *Psychopharmacology (Berl)*. **2005**; 179: 4–29.

2. Niswender CM, Conn PJ. *Annu Rev Pharmacol Toxicol*. **2010**; 50: 295–322.

3. Muto T, Tsuchiya D, Morikawa K, Jingami H. *Proc Natl Acad Sci U S A*. **2007**; 104: 3759–64.

4. Nicoletti F, Bockaert J, Collingridge GL, Conn PJ, Ferraguti F, Schoepp DD, Wroblewski JT, Pin JP. *Neuropharmacology*. **2011**; 60: 1017–41.

5. Dunayevich E, Erickson J, Levine L, Landbloom R, Schoepp DD, Tollefson GD. *Neuropsychopharmacology*. **2008**; 33: 1603–10.

6. Patil ST, Zhang L, Martenyi F, Lowe SL, Jackson KA, Andreev B V, Avedisova AS, Bardenstein LM, Gurovich IY, Morozova MA, Mosolov SN, Neznanov NG, Reznik AM, Smulevich AB, Tochilov VA, Johnson BG, Monn JA, Schoepp DD. *Nat Med*. **2007**; 13: 1102–7.

7. Keov P, Sexton PM, Christopoulos A. *Neuropharmacology*. **2011**; 60: 24–35.

8. Trabanco AA, Cid JM. *Expert Opin Ther Pat*. **2013**; 23: 629–47.

9. Johnson MP, Baez M, Jagdmann GE, Britton TC, Large TH, Callagaro DO, Tizzano JP, Monn JA, Schoepp DD. *J Med Chem*. **2003**; 46: 3189–92.

10. Galici R, Jones CK, Hemstapat K, Nong Y, Echemendia NG, Williams LC, de Paulis T, Conn PJ. *J Pharmacol Exp Ther*. **2006**; 318: 173–85.

11. Fell MJ, Witkin JM, Falcone JF, Katner JS, Perry KW, Hart J, Rorick-Kehn L, Overshiner CD, Rasmussen K, Chaney SF, Benvenga MJ, Li X, Marlow DL, Thompson LK, Luecke SK, Wafford KA, Seidel WF, Edgar DM, Quets AT, Felder CC, Wang X, Heinz BA, Nikolayev A, Kuo M-S, Mayhugh D, Khilevich A, Zhang D, Ebert PJ, Eckstein JA, Ackermann BL, Swanson SP, Catlow JT, Dean RA, Jackson K, Tauscher-Wisniewski S, Marek GJ, Schkeryantz JM, Svensson KA. *J Pharmacol Exp Ther*. **2011**; 336: 165–177.

12. Lavreysen H, Langlois X, Ahnaou A, Drinkenburg W, te Riele P, Biesmans I, Van der Linden I, Peeters L, Megens A, Wintmolders C, Cid JM, Trabanco AA, Andrés JI, Dautzenberg FM, Lütjens R, Macdonald G, Atack JR. *J Pharmacol Exp Ther*. **2013**; 346: 514–27.

13. Cook D, Brown D, Alexander R, March R, Morgan P, Satterthwaite G, Pangalos MN. *Nat Rev Drug Discov*. **2014**; 13: 419–31.

14. Homepage: http://clinicaltrials.gov. The Effects AZD8529 on Cognition and Negative Symptoms in Schizophrenics: https://clinicaltrials.gov/show/NCT00986531 (accessed May 1, 2018).

15. Homepage: http://clinicaltrials.gov. The Study of AZD8529 for Smoking Cessation in Female Smokers: https://www.clinicaltrials.gov/ct2/show/NCT02401022?term=AZD8529&rank=1 (accessed May 1, 2018).

16. Cid JM, Tresadern G, Duvey G, Lütjens R, Finn T, Rocher J, Poli S, Vega JA, de Lucas AI, Matesanz E, Linares ML, Andrés JI, Alcazar J, Alonso JM, Macdonald GJ, Oehlrich D, Lavreysen H, Ahnaou A, Drinkenburg W, Mackie C, Pype S, Gallacher D, Trabanco AA. *J Med Chem*. **2014**; 57: 6495–512.

17. Lavreysen H, Ahnaou A, Drinkenburg W, Langlois X, Mackie C, Pype S, Lütjens R, Le Poul E, Trabanco AA, Nuñez JMC. *Pharmacol Res Perspect*. **2015**; 3: e00096.

18. Lavreysen H, Langlois X, Ver Donck L, Cid Nuñez JM, Pype S, Lütjens R, Megens A. *Pharmacol Res Perspect*. **2015**; 3: e00097.

19. Salih H, Anghelescu I, Kezic I, Sinha V, Hoeben E, Van Nueten L, De Smedt H, De Boer P. *J Psychopharmacol*. **2015**; 29: 414–425.

20. Kent JM, Daly E, Kezic I, Lane R, Lim P, De Smedt H, De Boer P, Van Nueten L, Drevets

WC, Ceusters M. *Prog Neuro-Psychopharmacology Biol Psychiatry*. **2016**; 67: 66–73.

21. http://www.addextherapeutics.com/investors/press-releases/news-details/article/addex-reports-top-linedata-from-a-successful-phase-2a-clinical-study-with-adx71149-inschizophrenia/ (accessed July 28, 2016).

22. http:// clinicaltrials.gov/show/NCT01582815 (accessed May 1, 2018).

23. Swinney DC. *Curr Opin Drug Discov Devel*. **2009**; 12: 31–9.

24. Copeland RA. *Nat Rev Drug Discov*. **2016**; 15: 87–95.

25. Guo D, Heitman LH, IJzerman AP. *ChemMedChem*. **2015**; 10: 1793–1796.

26. Swinney DC, Haubrich BA, Liefde I Van, Vauquelin G. *Curr Top Med Chem*. **2015**; 15: 2504–22.

27. Guo D, Heitman LH, IJzerman AP. *Chem Rev*. **2016**; 117: DOI: 10.1021/acs.chemrev.6b00025.

28. Guo D, Hillger JM, IJzerman AP, Heitman LH. *Med Res Rev*. **2014**; 34: 856–92.

29. Dowling MR, Charlton SJ. *Br J Pharmacol*. **2006**; 148: 927–37.

30. Tresadern G, Bartolome JM, Macdonald GJ, Langlois X. *Bioorg Med Chem*. **2011**; 19: 2231–41.

31. Kapur S, Seeman P. *Am J Psychiatry*. **2001**; 158: 360–369.

32. Yin N, Pei J, Lai L. *Mol Biosyst*. **2013**; 9: 1381–9.

33. Vauquelin G. *Br J Pharmacol*. **2016**; 173: 2319–2334.

34. Schoop A, Dey F. *Drug Discov Today Technol*. **2015**; 17: 9–15.

35. Cid JM, Tresadern G, Vega JA, de Lucas AI, Matesanz E, Iturrino L, Linares ML, Garcia A, Andrés JI, Macdonald GJ, Oehlrich D, Lavreysen H, Megens A, Ahnaou A, Drinkenburg W, Mackie C, Pype S, Gallacher D, Trabanco AA. *J Med Chem*. **2012**; 55: 8770–89.

36. Tresadern G, Cid J-MM, Trabanco AA. *J Mol Graph Model*. **2014**; 53: 82–91.

37. Cid-Nuñez, J. M., De Lucas Olivares, A. I., Trabanco-Suarez, A. A., MacDonald, G. J. **2010**.

38. Cid JM, Duvey G, Tresadern G, Nhem V, Furnari R, Cluzeau P, Vega JA, de Lucas AI, Matesanz E, Alonso JM, Linares ML, Andrés JI, Poli SM, Lutjens R, Himogai H, Rocher J, Macdonald GJ, Oehlrich D, Lavreysen H, Ahnaou A, Drinkenburg W, Mackie C, Trabanco AA. *J Med Chem*. **2012**; 55: 2388–2405.

39. Doornbos MLJ, Pérez-Benito L, Tresadern G, Mulder-Krieger T, Biesmans I, Trabanco AA, Cid JM, Lavreysen H, IJzerman AP, Heitman LH. *Br J Pharmacol*. **2016**; 173: 588–600.

40. Motulsky HJ, Mahan LC. *Mol Pharmacol*. **1984**; 25: 1–9.

41. Xia L, de Vries H, IJzerman AP, Heitman LH. *Purinergic Signal*. **2016**; 12: 115–126.

42. Farinha A, Lavreysen H, Peeters L, Russo B, Masure S, Trabanco AA, Cid J, Tresadern G. *Br J Pharmacol*. **2015**; 172: 2383–96.

43. Pérez-Benito L, Doornbos MLJ, Cordomí A, Peeters L, Lavreysen H, Pardo L, Tresadern G. *Structure*. **2017**; 25: 1–10.

44. Lovering F, Bikker J, Humblet C. *J Med Chem*. **2009**; 52: 6752–6756.

45. Wacker D, Wang S, McCorvy JD, Betz RM, Venkatakrishnan AJ, Levit A, Lansu K, Schools ZL, Che T, Nichols DE, Shoichet BK, Dror RO, Roth BL. *Cell*. **2017**; 168: 377–389.e12.

46. Sykes DA, Dowling MR, Charlton SJ. *Mol Pharmacol*. **2009**; 76: 543–51.

47. Guo D, Mulder-Krieger T, IJzerman AP, Heitman LH. *Br J Pharmacol*. **2012**; 166: 1846–1859.

48. Deyrup MD, Nowicki ST, Richards NGJ, Otero DH, Harrison JK, Baker SP. *Naunyn*

Schmiedebergs Arch Pharmacol. **1999**; 359: 168–77.

49. Mould R, Brown J, Marshall FH, Langmead CJ. *Br J Pharmacol*. **2014**; 171: 351–63.

50. Sykes D a, Charlton SJ. *Br J Pharmacol*. **2012**; 165: 2672–83.

51. Yu Z, Van Veldhoven JPD, Louvel J, 'T Hart IME, Rook MB, Van Der Heyden MAG, Heitman LH, IJzerman AP. *J Med Chem*. **2015**; 58: 5916–5929.

52. Yu Z, IJzerman AP, Heitman LH. *Br J Pharmacol*. **2015**; 172: 940–955.

53. de Witte WEA, Danhof M, van der Graaf PH, de Lange ECM. *Trends Pharmacol Sci*. **2016**; 37: 831–842.

54. Vauquelin G, Charlton SJ. *Br J Pharmacol*. **2010**; 161: 488–508.

55. Vauquelin G. *Expert Opin Drug Discov*. **2015**; 10: 1085–1098.

56. Vauquelin G. *Br J Clin Pharmacol*. **2016**; 82: 673–682.

57. Perry DC, Mullis KB, Øie S, Sadée W. *Brain Res*. **1980**; 199: 49–61.

58. Yu N, Atienza JM, Bernard J, Blanc S, Zhu J, Wang X, Xu X, Abassi Y. *Anal Chem*. **2006**; 78: 35–43.

59. Hillger JM, Diehl C, van Spronsen E, Boomsma DI, Slagboom PE, Heitman LH, IJzerman AP. *Biochem Pharmacol*. **2016**; 115: 114–122.

60. Xi B, Yu N, Wang X, Xu X, Abassi YA. *Biotechnol J*. **2008**; 3: 484–495.

61. Ahnaou A, Dautzenberg FM, Geys H, Imogai H, Gibelin A, Moechars D, Steckler T, Drinkenburg WHIM. *Eur J Pharmacol*. **2009**; 603: 62–72.

62. Ahnaou A, De Boer P, Lavreysen H, Huysmans H, Sinha V, Raeymaekers L, Van De Casteele T, Cid JM, Van Nueten L, MacDonald GJ, Kemp JA, Drinkenburg WHIM. *Neuropharmacology*. **2016**; 103: 290–305.

63. Cuisset L, Tichonicky L, Jaffray P, Delpech M. *J Biol Chem*. **1997**; 272: 24148–24153.

64. Hillger JM, Schoop J, Boomsma DI, Eline Slagboom P, IJzerman AP, Heitman LH. *Biosens Bioelectron*. **2015**; 74: 233–242.

65. Cheng Y, Prusoff WH. *Biochem Pharmacol*. **1973**; 22: 3099–108.

SUPPORTING FIGURES AND TABLE

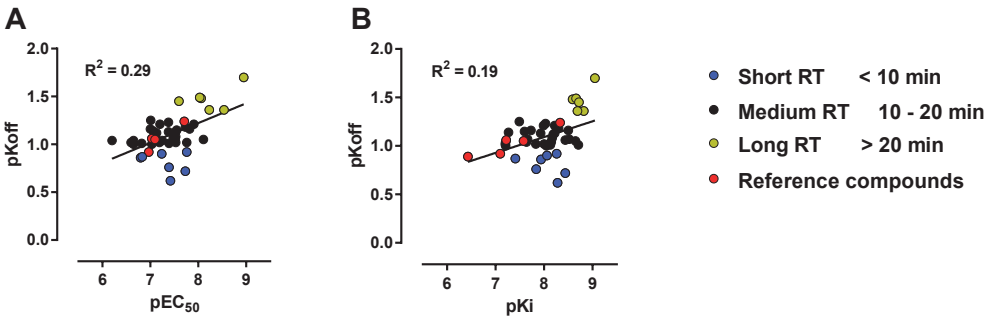

Figure S1. Correlation between potency (pEC_{50}) and dissociation rate (pk_{off}) (A); affinity (pK_i) and dissociation rate (pk_{off}) (B).

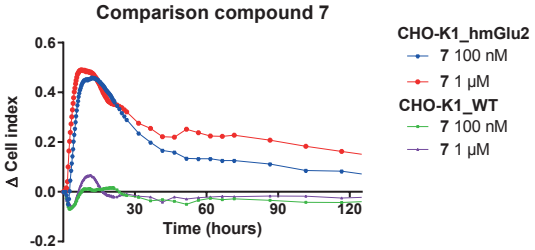

Figure S2. Comparison of PAM responses between CHO-K1 WT and CHO-K1_hmGlu$_2$ cells. Compound **7**-induced responses: 100 nM (green) and 1 µM (purple) on CHO-K1 WT cells (ATCC) and 100 nM (blue) and 1 µM (red) on CHO-K1_hmGlu2 cells. 40,000 cells per well were added in a volume of 50 µl. After resting for 30 minutes at room temperature, E-plates were placed in the recording station within a humidified 37°C, 5% CO2 incubator. Impedance was measured every 15 minutes overnight. After 18 hours, cells were stimulated with indicated concentration of compound. Impedance was measured every 15 seconds for 20 minutes, then 5 minute intervals were used for 40 minutes, followed by 15 minute intervals. A representative example is shown of a baseline-corrected response, which was repeated three times in duplicate.

Table S1. Selectivity data for representative $mGlu_2$ PAMs at $mGlu_{1,3,4,5,6,7,8}$.

Compound	$hmGlu_1$-agCa-pEC_{50}	$hmGlu_1$-anCa-pIC_{50}	$hmGlu_3$-agCa-pEC_{50}	$hmGlu_3$-anCa-pIC_{50}	$hmGlu_4$-agGT-pEC_{50}	$hmGlu_4$-anGT-pIC_{50}	$hmGlu_5$-pamCa_pEC_{50}	$hmGlu_5$-agCa-pEC_{50}	$hmGlu_5$-anCa-pIC_{50}	$rmGlu_6$-agGT-pEC_{50}	$rmGlu_6$-anGT-pIC_{50}	$hmGlu_7$-agCa-pEC_{50}	$hmGlu_7$-anCa-pIC_{50}	$hmGlu_8$-agCa-pEC_{50}	$hmGlu_8$-anCa-pIC_{50}
12	<4.52	<4.52	<4.52	<4.52	<4.52	<4.52	<4.52	<4.52	<4.52	<4.52	<4.52	<4.6	<4.6	<4.6	<4.6
27	<4.52	<4.52	<4.52	<4.52	<4.52	<4.52	<4.52	<4.52	<4.52	<4.52	<4.52	<4.6	<4.6	<4.6	<4.6
37	<4.52	<4.52	<4.52	<4.52	<4.52	<4.52	<4.52	<4.52	<5	<4.52	<4.52	<4.6	<4.6	<4.6	<4.6
45	<4.52	<4.52	<4.52	<4.52	<4.52	<4.52	<4.52	<4.52	<4.52	<4.52	<4.52	<4.6	<4.6	<5	<5

Ag, agonism; Ant, antagonism; PAM, positive allosteric modulation; Ca, data from calcium response in Ca^{2+}-based FDSS assay; GT, data from GTPγS assay. All assays used human receptor except $mGlu_6$ which used rat. Further details of methods can be found in Pérez-Benito *et al.* (2017).[43]

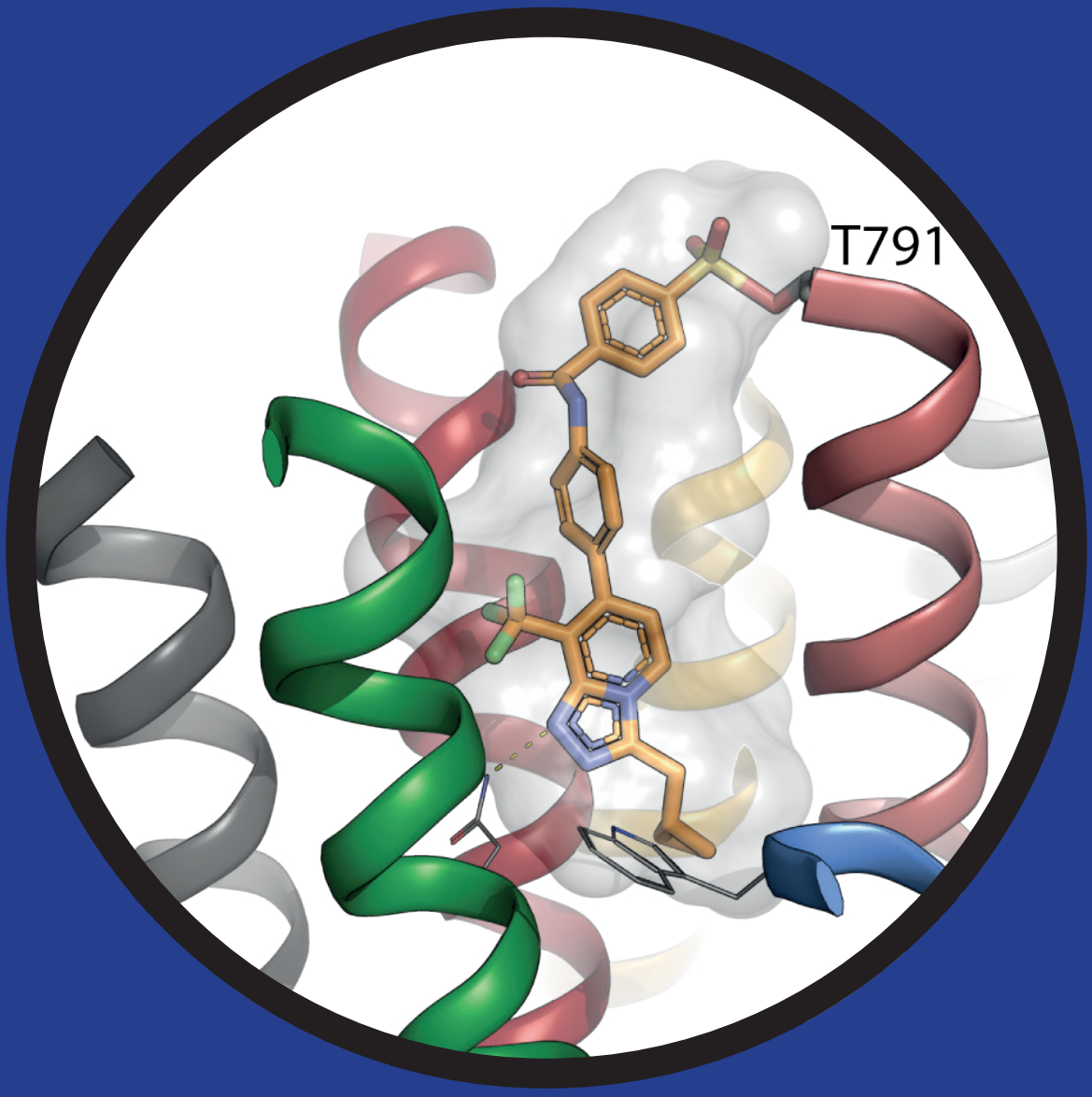
T791

CHAPTER 5

A covalent allosteric probe for the metabotropic glutamate receptor 2: Design, synthesis and pharmacological characterization

Maarten L J Doornbos, Xuesong Wang, Sophie C Vermond, Luc Peeters, Laura Pérez-Benito, Andrés A Trabanco, Hilde Lavreysen, José María Cid, Laura H Heitman, Gary Tresadern & Adriaan P IJzerman

Journal of Medicinal Chemistry.
Publication Date (Web) March 1, 2018.
doi:10.1021/acs.jmedchem.8b00051.

5

ABSTRACT

Covalent labelling of G protein-coupled receptors (GPCRs) by small molecules is a powerful approach to understand binding modes, mechanism of action, pharmacology and even facilitate structure elucidation. We report the first covalent positive allosteric modulator (PAM) for a class C GPCR, the $mGlu_2$ receptor. Three putatively covalent $mGlu_2$ PAMs were designed and synthesized. Pharmacological characterization identified **2** to bind the receptor covalently. Computational modelling combined with receptor mutagenesis revealed $T791^{7.29x30}$ as the likely position of covalent interaction. We show how this covalent ligand can be used to characterize the PAM binding mode and that it is a valuable tool compound in studying receptor function and binding kinetics. Our findings advance the understanding of the $mGlu_2$ PAM interaction and suggest **2** is a valuable probe for further structural and chemical biology approaches.

INTRODUCTION

Over the last years covalent ligands for G protein-coupled receptors (GPCRs) have re-emerged as valuable tool compounds to characterize the structure, expression pattern and function of these proteins.[1] A major obstacle in GPCR structure elucidation using crystallization is the dynamic behavior of their seven-transmembrane (7TM) domain, especially when in the active state.[2] Covalent ligands can stabilize the 7TM domain of the receptor without the likelihood of dissociation from the binding site. The use of covalent ligands for structure elucidation has been taken as an approach to facilitate receptor crystallization, as was shown recently for the crystal structures of the adenosine A_1 and multiple beta 2 adrenergic receptors amongst others.[3,4] Beyond structural considerations, covalent molecules are valuable pharmacological tools useful for further understanding of binding modes, and other chemical biology and proteomics applications.

The metabotropic glutamate (mGlu) receptors belong to the class C GPCRs and are activated by glutamate, the most abundant neurotransmitter.[5] The mGlu receptors are obligatory dimers and are characterized by their large extracellular Venus flytrap (VFT) domain - binding endogenous glutamate - which is connected to the 7TM domain via a cysteine rich domain.[6] For mGlu receptors, allosteric modulators that bind in the 7TM domain are pursued widely for drug discovery as they are typically more subtype-selective than orthosteric ligands and only function in the presence of endogenous agonist.[7] Positive allosteric modulation of the $mGlu_2$ receptor has been shown to be a potential strategy for the treatment of neurological disorders such as schizophrenia and anxiety.[8] Although the structure of the extracellular domain of the $mGlu_2$ receptor is known,[9] the current understanding of the structure of the 7TM domain is based on the crystal structures of the $mGlu_1$ and $mGlu_5$ 7TM domains, which were crystallized in an inactive state with a negative allosteric modulator (NAM) bound in the allosteric binding pocket.[10–12]

We have had a long-standing interest in $mGlu_2$ receptor PAMs leading to characterization of multiple medicinal chemistry series[13,14] that were also studied with site-directed mutagenesis.[15,16] We have further characterized the binding kinetics and pharmacology of selected leads in **chapters 2 and 4**.[17,18] Robust *in vivo* pharmacodynamic effects were observed in several animal models with some molecules such as 1-Butyl-3-chloro-4-(4-phenyl-1-piperidinyl)-(1*H*)-pyridone (JNJ-40411813/ADX71149) advancing to human clinical trials.[19–22] Despite this, further and more rigorous approaches to understand $mGlu_2$ PAM binding and receptor pharmacology are needed. In this study we have designed and synthesized three novel putatively covalent $mGlu_2$ PAMs based on computational approaches and previous understanding of the PAM binding mode. These compounds were fully characterized *in vitro*, resulting in the

identification of 4-[[4-[3-(Cyclopropylmethyl)-8-(trifluoromethyl)-[1,2,4]triazolo[4,3-a]pyridin-7-yl]phenyl]carbamoyl]benzenesulfonyl fluoride (**2**) as a covalently binding $mGlu_2$ PAM. The binding mode was studied using computational docking, which identified several amino acid residues that potentially formed the covalent interaction. Using site-directed mutagenesis $T791^{7.29x30}$ was confirmed as the residue responsible for the covalent interaction.

RESULTS AND DISCUSSION

CHEMISTRY

Based on a series of analogues of 3-(cyclopropylmethyl)-7-[(4-phenyl-1-piperidinyl) methyl]-8-(trifluoromethyl)-1,2,4-triazolo[4,3-a]pyridine (**1**, JNJ-46281222)[23] we recently developed a novel series of $mGlu_2$ PAMs bearing the 7-aryl-1,2,4-triazolo[4,3-a]pyridine as the core structure, also including the molecules described in **chapter 4**.[13,17] This scaffold was used to design three novel putative covalent $mGlu_2$ PAMs for which the fluorosulfonyl moiety was chosen as a reactive warhead. A 4-fluorosulfonyl-phenyl ring was connected to the 7-phenyl-1,2,4-triazolo[4,3-a]pyridine-core via an amide linker to the phenyl ring at the 4-position (**2**), the 3-position (**3**) or the 4-position with a methylene spacer in between to increase flexibility (**4**), as depicted in figure 1. The synthesis of target compounds **2–4** is shown in Scheme 1. They were prepared via Suzuki coupling of the 7-chlorotriazolopyridine **5**[24] with the corresponding commercially available boronic acids (**6a-c**) and subsequent amide formation of **7a-c** with the commercially available chemoreactive group. This electrophilic fluorosulfonyl moiety was chosen as a warhead to achieve a covalent interaction with a nucleophilic amino acid at the allosteric binding pocket of the $mGlu_2$ receptor. This moiety has been widely used and was chosen for its wide reactivity to various nucleophilic residues: serine, threonine, tyrosine, lysine, cysteine and histidine.[25]

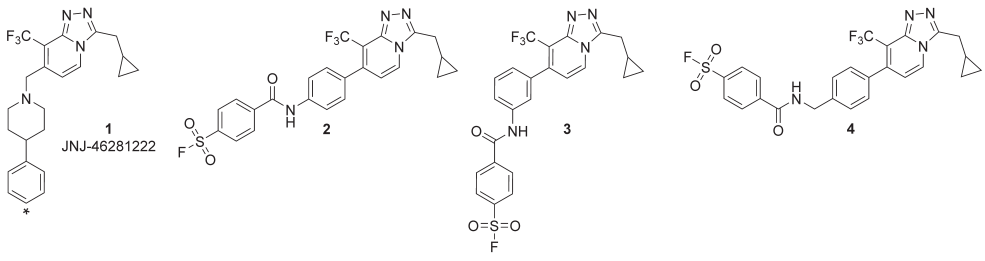

Figure 1. Structure of **1** and novel $mGlu_2$ PAMs **2-4**. The position of the tritium label of [^{3}H]-**1** is denoted by *.

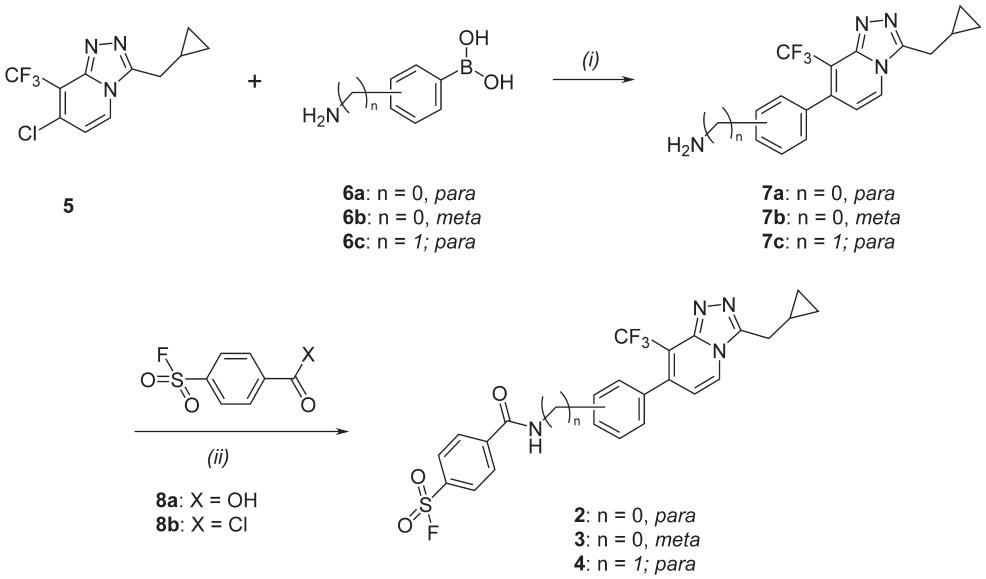

Scheme 1. Synthesis of compounds **2–4.** *Reagents and conditions:* (i) $Pd(PPh_3)_4$, $NaHCO_3$, H_2O/1,4-dioxane, 150 °C, 10-15 min, microwave, 61-68% for **7a-c**. (ii) a) **8a**, HATU, DIPEA, DMF, rt, 3h, 68-75% for **2** and **3** b) **8b**, 1,4-dioxane, 90°C, 30 min, 33% for **4**.

BIOLOGY AND STRUCTURE-REACTIVITY CONSIDERATIONS

Firstly, the potency of the compounds to enhance the effect of glutamate at its EC_{20} was determined using a [^{35}S]GTPγS assay. Reference PAM **1**, showed a high potency (Table 1; pEC_{50} 7.74 ± 0.03). Compounds **2**-**4** were all able to increase the response of the EC_{20} glutamate concentration to a similar level as **1** and thus behaved as functional $mGlu_2$ PAMs with potencies of around 100 nM for **2** and **3** (pEC_{50} values of 6.80 ± 0.06 and 6.80 ± 0.04, respectively). The highest potency was found for **4**, with a pEC_{50} value of 7.82 ± 0.06.

Subsequently, the apparent affinities of the compounds were determined in a [^{3}H]JNJ-46281222 displacement assay (Table 1). The pK_i value of 8.12 ± 0.19 for **1** was close to its pEC_{50} value. Also, **2** and **3** had pK_i values close to their pEC_{50} values, 7.21 ± 0.11 and 6.95 ± 0.11, respectively. Compound **4** had the highest affinity with a pK_i value of 8.24 ± 0.08.

The pEC_{50} and pK_i values (7.74 ± 0.03 and 8.12 ± 0.13, respectively) of **1** were similar to those reported in **chapter 2**.[18] The potency and affinity parameters of **2**-**4** compared favorably with the well-studied **1**, which was one of the most potent compounds identified from the same triazolopyridine scaffold and was used as a control throughout the study. Even though the fluorosulfonyl moiety at the distal tail in **2**-**4** was more bulky and hydrophilic than the unsubstituted phenyl of **1** and the other compounds studied previously and in **chapter 4**,[17,23] the affinity and potency values were only reduced approximately 10-fold for **2** and **3** compared to **1** and not at all for **4**. The shift of the 4-fluorosulfonyl-phenyl ring from the 4-position in **2** to the 3-position in **3** did not change the potency and affinity, whereas the greater flexibility of the methylene spacer in **4** most likely resulted in its increased potency and affinity compared

to **2**. Selectivity of this series of $mGlu_2$ PAMs was good. Representative **3** showed no activity at $mGlu_{1,3,5,8}$ (Table S1).

Table 1. Functional activity (pEC_{50}), affinity (pK_i) and kinetic parameters (k_{on}, k_{off}, RT) for $mGlu_2$ PAMs **1-4**

	pEC_{50}[a]	pK_i[a]	pK_i (3 hr pre-incubation)[a]	k_{on} (M^{-1} s^{-1})[a]	k_{off} (s^{-1})[a]	RT (min)[a, b]
1	7.74 ± 0.03	8.12 ± 0.13	8.12 ± 0.19	(1.2 ± 0.072) x 10^{6}, [c]	0.0013 ± 0.0002[c]	12 ± 2.3[c]
2	6.80 ± 0.06	7.21 ± 0.11	8.21 ± 0.14*	'(3.2 ± 1.2) x 10^{3}'	'(3.2 ± 3.1) x 10^{-13}'	'((5.2 ± 4.9) x 10^{10})'
3	6.80 ± 0.04	6.95 ± 0.11	6.78 ± 0.09	(2.1 ± 0.77) x 10^{4}	0.00091 ± 0.00033	18 ± 6.7
4	7.82 ± 0.06	8.24 ± 0.08	8.38 ± 0.10	(2.2 ± 0.17) x 10^{5}	0.00057 ± 0.00016	29 ± 8.3

[a] Values represent the mean ± SEM of at least three individual experiments, performed in duplicate. [b] RT (min) = $1/(60*k_{off})$. [c] As described in **chapter 4**.[17] * <0.01, unpaired student's t-test compared to co-incubation.

Since a covalent interaction would induce insurmountable binding to the allosteric binding site, we set up a radioligand displacement assay using a 3 hour pre-incubation of CHO-K1_ $hmGlu_2$ membranes with increasing concentrations of the four PAMs. This pre-incubation was followed by addition of [^{3}H]JNJ-46281222 and a subsequent incubation for 1 hour. Data were compared to the control experiments with no pre-incubation, i.e. co-incubation of the radioligand and the compounds studied.

Compound **1** showed no difference in affinity between the co-incubation and the pre-incubation assays (Table 1; pK_i 8.12 in both cases), indicating that **1** does not bind insurmountably to the allosteric binding pocket. On the contrary, the addition of a pre-incubation step resulted in a 10-fold increase in affinity for **2** (Table 1; Fig. 2A), indicating that this compound binds the receptor insurmountably as no re-equilibration of **2** occurred after addition of [^{3}H] JNJ-46281222. Both **3** and **4** did not reveal a significant shift in receptor affinity when tested in the two-step binding assay, indicating they do not bind the receptor insurmountably. The observation of a shift in affinity of **2** after pre-incubation is in agreement with previously described covalent ligands for the histamine H_4 and adenosine A_{2A} receptors.[26,27]

Competition binding experiments are generally not the preferred method for evaluation of covalent interactions with GPCRs.[28,29] Therefore, the kinetic parameters k_{on} and k_{off} of **1**-**4** were determined (Table 1). The kinetic parameters for **1** were determined in classical [^{3}H] JNJ-46281222 association and dissociation experiments, yielding the association rate constant k_{on} (k_1 = 1.2 x 10^6 $M^{-1}s^{-1}$) and dissociation rate constant k_{off} (k_2 = 0.0013 s^{-1}), leading to a residence time (RT) of 12 minutes. Using these values we determined the kinetic k_{on} (k_3) and k_{off} (k_4) values for **2-4** using a competition association assay based on the Motulsky and Mahan model.[30] In contrast to **1**, **2** showed a much slower on-rate (3.2 x10^3 $M^{-1}s^{-1}$) and a negligible off-rate (3.2 x 10^{-13} s^{-1}), leading to an infinite RT, indicative for irreversible binding.

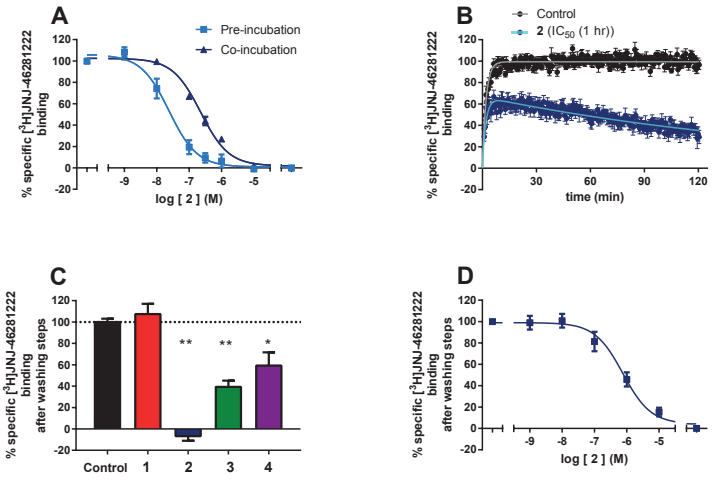

Figure 2. A.) Displacement of [^{3}H]JNJ-46281222 by **2** with and without a pre-incubation of 3 hours. B.) Competition association assay of **2** at its IC_{50} concentration determined in the co-incubation assay. C.) [^{3}H]JNJ-46281222 binding after pre-incubation with a 10x IC_{50} concentration of $mGlu_2$ PAM followed by 4 extensive washing cycles. D.) [^{3}H]JNJ-46281222 binding after pre-incubation with increasing concentrations of **2** followed by 4 extensive washing cycles. Data represent the mean ± SEM of at least three individual experiments performed in duplicate. * p<0.01; ** p<0.0001, one-way ANOVA with Dunnett's post-test compared to control.

The competition association curve of **2** shows an overshoot followed by a declining curve that did not reach equilibrium (Fig. 2B). Compound **3** showed an on-rate of 2.1 x 10^4 $M^{-1}s^{-1}$ and an off-rate of 0.00091 s^{-1}, leading to a RT of 18 minutes, which is comparable to **1**. The on-rate of **4** was 10-fold faster (2.2 x 10^5 $M^{-1}s^{-1}$) and off-rate slower than **3** (0.00057 s^{-1}), leading to a RT of 29 minutes. The values for **3** and **4** indicate reversible binding behavior which is in line with the displacement experiments. The shape of the competition association curve of **2** (Fig. 2B) is typical for an irreversible interaction, similar to that seen recently with the irreversibly binding FSCPX at the adenosine A_1 receptor.[31] As the values determined for k_{on} and k_{off} of **2** are far from the kinetic parameters of the radioligand and beyond the duration of the experiments, they should be considered approximate values. Still, this does not change the conclusion of an infinite RT. Furthermore, **2** can be used as a tool compound for studying binding kinetics of allosteric modulators at the $mGlu_2$ receptor, a strategy that was followed before for the adenosine A_1 receptor.[32]

To distinguish between irreversible and pseudo-irreversible interactions of **2-4** we performed radioligand binding assays followed by extensive washing steps. A washout assay was developed in which 1 hour pre-incubation with a 10 x IC_{50} concentration of compound was followed by at least three extensive wash and centrifugation cycles. After the subsequent incubation with [^{3}H]JNJ-46281222, radioligand displacement was assessed and compared to the control condition without any competitor (100% radioligand binding). For **1** (unlabeled

JNJ-46281222), no radioligand displacement was found, indicating that **1** was completely washed away (Fig. 2C). For compound **3** and **4**, [^{3}H]JNJ-46281222 was displaced partially, indicating that a portion of the receptor population was still bound but no persistent covalent interactions occurred. This partial recovery of **3** and **4** was likely caused by their slower binding kinetics compared to **1**. Pre-incubation with compound **2** completely abolished [^{3}H] JNJ-46281222 binding after the washing cycles, indicating its irreversible binding to the $mGlu_2$ receptor (Fig. 2C). This was further confirmed by pre-incubation with increasing concentrations of **2**, followed by four extensive washing cycles. For this effect a concentration-response curve was established, with an apparent pK_i value for **2** of 6.63 ± 0.14 which is another qualitative assessment of the irreversible interaction.

To evaluate the effect of irreversible binding of **2** on the functional PAM response, the following [^{35}S]GTPγS set up was used. Increasing concentrations of **2** and a glutamate concentration equivalent to its EC_{20} value were pre-incubated with membranes for three hours, followed by a 1 hour incubation with [^{35}S]GTPγS, resulting in a potency of 6.75 ± 0.13, which was 7-fold higher than when co-incubation only was performed (pEC_{50} 5.90 ± 0.08) (Fig 3A). The pEC_{50} value determined after 3 hour pre-incubation followed by 1 hour co-incubation with [^{35}S]GTPγS (6.75 ± 0.13) was similar to the potency assessed in the standard [^{35}S]GTPγS protocol (6.80 ± 0.06), which also included a pre-incubation step.

The ability of bound **2** to behave as a PAM was studied by repeating the washout assay but with a [^{35}S]GTPγS binding assay subsequent to the washing cycles (Fig. 3B). Compound **2** was still able to induce [^{35}S]GTPγS binding in the presence of an EC_{20} concentration of glutamate after the washing steps. The level was comparable to the control situation in which the compound was added after the washing steps. As a further control, the assay was also performed using **1**, which did not induce [^{35}S]GTPγS binding as it was washed away (Fig. 2C), in contrast to the situation in which **1** was added after washing (Fig. 3B).

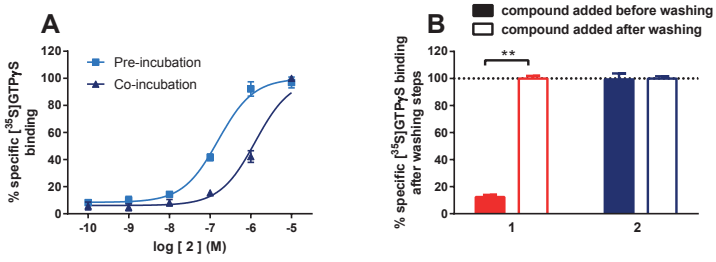

Figure 3. A.) Compound-induced [^{35}S]GTPγS binding after 60 min of incubation with [^{35}S]GTPγS with or without a 3 hour pre-incubation in the presence of a glutamate concentration equivalent to its EC_{20} value. B.) [^{35}S]GTPγS binding after stimulation with a 10x IC_{50} concentration of $mGlu_2$ PAM which was added either before or after 4 extensive washing cycles. All experiments were performed in the presence of a glutamate concentration equivalent to its EC_{20} value. Data represent the mean ± SEM of at least three individual experiments performed in duplicate. ** p<0.0001, unpaired student's t-test.

COMPUTATIONAL MODELLING

It is well understood that allosteric modulators of mGlu receptors bind in the 7TM domain in a similar conserved site as class A GPCRs.[7] Crystallography has shown variation in the exact location of allosteric ligands in this site.[33] Our previous experimental and computational studies have helped to pinpoint the binding mode of $mGlu_2$ receptor PAMs of several chemical series.[15,16] This work greatly helped the design of molecules **2** to **4**. With a strong certainty that the triazolopyridine core binds deepest in the receptor as described in **chapter 2** and by Pérez-Benito *et al.* (2017)[16] we designed and docked multiple different candidate fluorosulfonyl-phenyl molecules. Idea molecules were docked into a homology model of the $mGlu_2$ receptor allosteric binding site using a model and approach as described previously.[16,23] Due to flexibility and sequence differences there is increased uncertainty of the amino acid position and conformation in the extracellular side of the receptor model. From the docking, **2** to **4** allowed the fluorosulfonyl to explore different vectors and depths of the extracellular side of the binding site. Our approach relying upon a model of the ligand receptor binding mode, and not a crystal structure, was more high risk. Therefore, we chose the fluorosulfonyl-phenyl as the warhead because it can react with various nucleophilic amino acids as to increase the chance to find a covalent ligand.

The docking results for molecule **2** showed the triazolopyridine core overlapped with that of **1** (Fig. 4), which was included in earlier reports. As mentioned, this positioning and orientation of the scaffold is consistent with previous SAR and mutagenesis work.[34] The flexible distal tail of **2** containing the fluorosulfonyl moiety was pointing towards the top of transmembrane helices 3 or 7 and extracellular loop (ECL) 2. As suggested by the $mGlu_1$ structure, ECL2 forms a lid on top of the 7TM pocket in all class C GPCRs, which is likely happening to $mGlu_2$ as well.[10,35] Whilst the scaffold consistently adopted the shown binding orientation, two different binding modes were possible for the distal part of the molecule (Fig. 4). In the first binding mode, the distal phenyl relaxes into the 7TM of the receptor. This is analogous to the binding mode and behavior of **1** reported in the computational studies described in **chapter 2**, as shown comparing pale blue and dark orange molecules in figure 4. The fluorosulfonyl moiety is presented close to $T791^{7.29x30}$ located in our model at the top of TM-7. If the ligand maintains a more linear orientation, it will present a second possible binding mode as shown in pale orange in figure 4, where the fluorosulfonyl group points towards two alternative arginines: $R635^{3.32x32}$ and R720 (ECL2).

RECEPTOR MUTAGENESIS

Based on the two potential binding modes of **2**, multiple nucleophilic amino acid residues were within a radius of 4 Å to the fluorosulfonyl warhead and hence were potential candidates to form the covalent bond with the fluorosulfonyl. Although arginines are not widely reported to behave as nucleophiles the proximity of several in the extracellular region may permit some to be less protonated and we therefore did not want to overlook this possi-

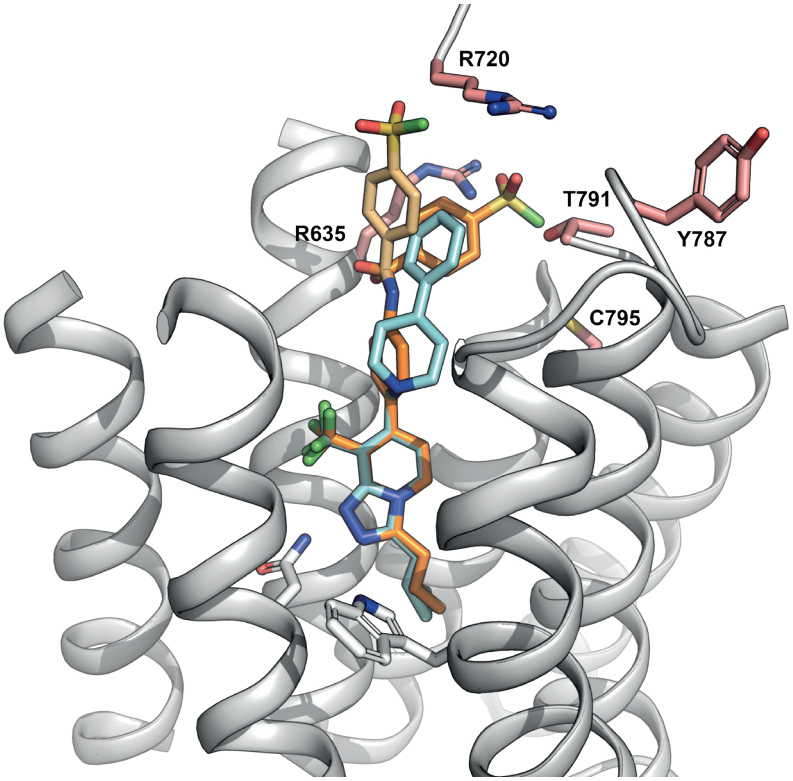

Figure 4. Proposed binding mode of $mGlu_2$ PAMs **1** (pale blue) and **2** (dark and pale orange). The two possible binding modes for **2** are distinguished using dark and pale orange coloring. The five amino acids chosen as possible candidates for the covalent interaction are highlighted in salmon color and labelled.

bility. The amino acids included R635$^{3.32x32}$ and R720 (ECL2), and T791$^{7.29x30}$. Meanwhile, Y787 (ECL3) and C795$^{7.33x34}$ were further away but given the flexibility of the extracellular region of the receptor they were still considered as possible candidates for interaction with the ligand warhead.

For all these five residues alanine substitutions were made. These $mGlu_2$ receptor mutants were transiently transfected into CHO-K1 cells and membrane preparations were made.

Control experiments confirmed the integrity and function of the mutant receptors, as shown in the supporting information (Fig. S1; Table S2). [^{3}H]LY341495 binding experiments were performed to assess the expression of transiently transfected WT and mutant $mGlu_2$ receptors, revealing a similar affinity of glutamate for the WT and all mutants, which confirmed the integrity of the orthosteric binding pocket. All mutants were still able to induce [^{35}S]GTPγS binding upon stimulation by glutamate with similar potencies, which confirmed the function of the receptor was maintained. Furthermore, all mutants were still able to bind [^{3}H]

JNJ-46281222, which was displaced by unlabeled **1** with similar affinities, which confirmed the integrity of the allosteric binding site (Fig. S1; Table S2).

To evaluate which of the amino acid residues was responsible for covalent binding of **2**, the washout assay was repeated (Fig 5A). Compound **1** was used as a control and showed around maximal [^{3}H]JNJ-46281222 binding after washing in all cases, confirming that **1** was washed away during the washing cycles. The transiently transfected WT $mGlu_2$ showed a similar effect of **2** after washing compared to the stable CHO-K1_$hmGlu_2$ cell line, i.e. complete inhibition of [^{3}H]JNJ-46281222 binding. Mutants R635$^{3.32x32}$A, R720A, Y787A and C795$^{7.33x34}$A showed a similar negligible level of [^{3}H]JNJ-46281222 binding, indicating that **2** was still binding covalently. However, T791$^{7.29x30}$A showed [^{3}H]JNJ-46281222 binding to all available binding sites, and thus a loss of covalent binding.

A full curve [^{3}H]JNJ-46281222 displacement assay using the T791$^{7.29x30}$A mutant revealed a pK_i for **2** of 6.45 ± 0.03 (Fig. 5C), which was similar to the transiently transfected WT $mGlu_2$ receptor (Fig. 5B; 6.76 ± 0.04), but lower than the pK_i found at the CHO-K1_$hmGlu_2$ membranes (Table 3). This discrepancy is likely caused by the difference in technique used, a filtration binding assay in contrast to an SPA assay.

The loss of irreversible interaction for the T791$^{7.29x30}$A mutant was further confirmed in the displacement assay, as the [^{3}H]JNJ-46281222 displacement curves of **2** with and without pre-incubation step lost the large shift shown on the WT receptor (Fig. 5C) and were almost overlapping for this mutant (Fig. 5B), indicating a loss of insurmountable binding behavior. Together, these experiments indicated that T791$^{7.29x30}$ was the residue responsible for making the covalent bond between the receptor and **2**. A similar approach was used recently for the adenosine A_{2A} and neurotensin NTS1 receptors where a lysine and cysteine residue were found to be responsible for the covalent interaction, respectively.[27,36] The position of the covalent bond was used to predict the binding mode of **2**, which further increased the understanding of the binding of PAMs to the binding pocket in addition to our recent mutagenesis and computational work described in **chapter 2** and elsewhere.[15,16,18]

Compound **2** can be a useful structural biology tool as it would be expected to stabilize the 7TM domain in its active state, thereby potentially facilitating crystallization of the active state receptor. This could be highly valuable for structure elucidation of an active state of a Class C GPCR which up to now remains unreported. Furthermore, there is no crystal structure of the 7TM domain of the $mGlu_2$ receptor. Thus far the crystal structures of class C 7TM domains were the NAM bound structures of $mGlu_1$ and $mGlu_5$.[10–12] A PAM bound structure would greatly enhance our understanding of the activation mechanism of class C GPCRs. Recently Gregory *et al.* (2016) published the first clickable covalent photo-affinity ligands for the $mGlu_5$ receptor.[37] These ligands are NAMs for the receptor and bind the receptor covalently upon

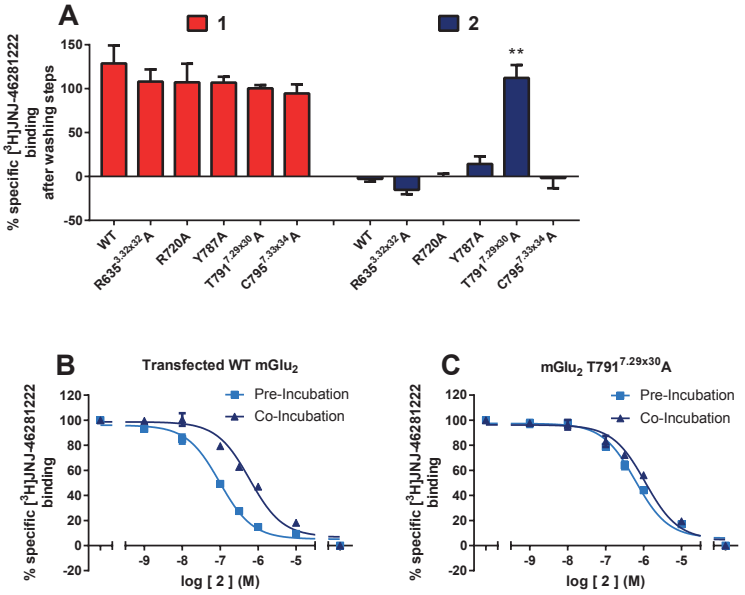

Figure 5. A.) [^{3}H]JNJ-46281222 binding to transiently transfected mGlu$_2$ mutants after pre-incubation with **1** or **2** at a 10x IC$_{50}$ concentration followed by 4 extensive washing cycles. B, C.) Displacement of specific [^{3}H]JNJ-46281222 binding from transiently transfected WT (B) and T791$^{7.29x30}$A (C) mGlu$_2$ receptor by **2** with and without a pre-incubation of 3 hours. Experiments were performed in the presence of a glutamate concentration equivalent to its EC$_{20}$ value. Data represent the mean ± SEM of at least three individual experiments performed in duplicate. ** p<0.0001, one-way ANOVA with Dunnett's post-test compared to WT.

photo-activation. The ligands contain an alkyne click handle that can be used for conjugation of clickable dyes. These probes can then be used for various purposes such as imaging in native tissues.[37] Such a strategy is also of interest for the mGlu$_2$ receptor and **2** may be used as a starting point for further chemical optimization.

Covalent ligands have proved to be successful medicines for various indications, but due to safety concerns they are mostly neglected in drug discovery.[38] This is especially the case for neuroscience indications that often require chronic treatment thus exacerbating such fears. Nevertheless, the introduction of covalent warheads into ligands that were optimized for non-covalent affinity may overcome some of the expected difficulties of off-target-activities. Such highly targeted, selective covalent inhibitors represent the current state of the art.[39] Furthermore, covalent allosteric modulators are even more likely to be used as therapeutics compared to orthosteric ligands since they lack intrinsic efficacy, thereby avoiding problems due to on-target toxicity.[40]

CONCLUSION

In conclusion, this study reports the design, synthesis and pharmacological characterization of the first covalent PAM for a class C GPCR. In addition, a combined computational and mutagenesis approach enabled the identification of T791$^{7.29x30}$ as the position of the covalent interaction. Due to its favorable allosteric properties, this compound may be considered a tool compound to further evaluate the use of covalent ligands as potential GPCR therapeutics. Furthermore, it enhances the understanding of the binding mode of PAMs, may be considered a starting point of further development of a functionalized PAM probe, and could be a valuable tool compound for structure elucidation of the $mGlu_2$ receptor.

EXPERIMENTAL SECTION

Chemistry

Unless otherwise noted, all reagents and solvents were obtained from commercial suppliers and used without further purification. Thin layer chromatography (TLC) was carried out on silica gel 60 F254 plates (Merck). Flash column chromatography was performed on silica gel, particle size 60 Å, mesh = 230–400 (Merck), under standard techniques. Microwave assisted reactions were performed in a single-mode reactor, Biotage Initiator Sixty microwave reactor (Biotage), or in a multimode reactor, MicroSYNTH Labstation (Milestone, Inc.). Nuclear magnetic resonance (NMR) spectra were recorded with either a Bruker DPX-400 or a Bruker AV-500 spectrometer (Bruker AG) with standard pulse sequences NMR data operating at 400 and 500 MHz, respectively, using $CDCl_3$ and DMSO-d_6 as solvents. Chemical shifts (δ) are reported in parts per million (ppm) downfield from tetramethylsilane (δ = 0). Coupling constants are reported in hertz. Splitting patterns are defined by s (singlet), d (doublet), dd (double doublet), t (triplet), q (quartet), quin (quintet), sex (sextet), sep (septet), or m (multiplet). Liquid chromatography combined with mass spectrometry (LC–MS) was performed either on a HP 1100 HPLC system (Agilent Technologies) or Advanced Chromatography Technologies system composed of a quaternary or binary pump with degasser, an autosampler, a column oven, a diode array detector (DAD), and a column as specified in the respective methods. Flow from the column was split to a MS spectrometer. The MS detector was configured with either an electrospray ionization source or an ES-CI dual ionization source (electrospray combined with atmospheric pressure chemical ionization). Nitrogen was used as the nebulizer gas. Data acquisition was performed with MassLynx- Openlynx software or with Chemstation-Agilent Data Browser software.

Compounds are described by their experimental retention times (Rt) and ions. The reported molecular ion corresponds to the [M+H]+ (protonated molecule) and/or [M-H]- (deprotonated molecule). Purities of all new compounds were determined by analytical RP-HPLC using the area percentage method on the UV trace recorded at a wavelength of 254 nm, and compounds were found to have ≥95% purity unless otherwise specified. For (LC)MS-characterization of the compounds of the present manuscript, the following method was used.

General procedure

The High Performance Liquid Chromatography (HPLC) measurement was performed using an LC pump, a diode-array (DAD) or a UV detector and a column as specified in the respective methods. If necessary, additional detectors were included (see table of methods below). Flow from the column was brought to the Mass Spectrometer (MS) which was configured with an atmospheric pressure ion source. It is within the knowledge of the skilled person to set the tune parameters (e.g. scanning range, dwell time…) in order to obtain ions allowing the identification of the compound's nominal monoisotopic molecular weight (MW) and/or exact mass monoisotopic molecular weight. Data acquisition was performed with appropriate software. Compounds are described by their experimental retention times (R_t) and ions. If not specified differently in the table of data, the reported molecular ion corresponds to the $[M+H]^+$ (protonated molecule) and/or $[M-H]^-$ (deprotonated molecule). In case the compound was not directly ionizable the type of adduct is specified (i.e. $[M+NH_4]^+$, $[M+HCOO]^-$, etc…). For molecules with multiple isotopic patterns (Br, Cl..), the reported value is the one obtained for the lowest isotope mass. All results were obtained with experimental uncertainties that are commonly associated with the method used. Hereinafter, "DAD" means Diode Array Detector, "SQD" Single Quadrupole Detector, "CSH", Charged Surface Hybrid.

Method 1

In addition to the general procedure: Reversed phase HPLC was carried out on an Eclipse Plus-C18 column (3.5 µm, 2.1 x 30 mm) from Agilent, with a flow rate of 1.0 ml/min, at 60ºC without split to the MS detector. The gradient conditions used are: 95 % A (0.5 g/l ammonium acetate solution + 5 % acetonitrile), 5 % B (mixture of acetonitrile / methanol, 1/1), kept 0.2 minutes, to 100 % B at 1.0 minute, kept till 1.15 minutes and equilibrated to initial conditions at 1.3 minutes, kept until 3.0 minutes. Injection volume 2 µl. Low-resolution mass spectra (single quadrupole, SQD detector) were acquired by scanning from 100 to 1000 in 0.1 seconds using an inter-channel delay of 0.08 second. The capillary needle voltage was 3 kV. The cone voltage was 20 V for positive ionization mode and 30 V for negative ionization mode. This method was used for compounds **7a-c**.

Method 2

In addition to the general procedure: Reversed phase UPLC was carried out on an CSH -C18 column (1.7 µm, 2.1 x 50 mm) from Waters, with a flow rate of 1.0 ml/min, at 50ºC without split to the MS detector. The gradient conditions used are: 95 % A (0.5 g/l ammonium acetate solution + 5 % acetonitrile), 5 % B (acetonitrile), to 95 % B at 4.6 minutes, kept until

5.0 minutes. Injection volume 2 µl. Low-resolution mass spectra (single quadrupole, SQD detector) were acquired by scanning from 100 to 1000 in 0.1 seconds using an inter-channel delay of 0.08 second. The capillary needle voltage was 3 kV. The cone voltage was 25 V for positive ionization mode and 30 V for negative ionization mode. This method was used for compounds **2-4.**

4-[[4-[3-(Cyclopropylmethyl)-8-(trifluoromethyl)-[1,2,4]triazolo[4,3-a]pyridin-7-yl]phenyl]carbamoyl] benzenesulfonyl fluoride (2). DIPEA (0.079 mL, 0.4514 mmol) was added to a stirred solution of **7a** (0.1 g, 0.301 mmol), **8a** (0.074 mg, 0.3611 mmol) and HATU (0.195 mg, 0.512 mmol) in DMF (2 mL). The mixture was stirred at room temperature for 3 hours. The mixture was diluted with CH_2Cl_2 and washed with sat. NH_4Cl and $NaHCO_3$ aqueous saturated solution. The organic layer was separated, dried (Na_2SO_4), filtered and the solvents evaporated in vacuo. The crude product was purified by flash column chromatography (silica; CH_2Cl_2 in MeOH 100/0 to 94/6). The desired fractions were collected and the solvents evaporated in vacuo to yield **2** (0.116 g, 75%). ^{1}H NMR (500 MHz, DMSO-d_6) δ 10.84 (s, 1H), 8.75 (d, *J*=7.22 Hz, 1H), 8.22-8.41 (m, 4H), 7.93 (d, *J*=8.38 Hz, 2H), 7.47 (d, *J*=8.67 Hz, 2H), 6.97 (d, *J*=6.94 Hz, 1H), 3.15 (d, *J*=6.94 Hz, 2H), 1.19-1.31 (m, 1H), 0.46-0.66 (m, 2H), 0.23-0.41 (m, 2H). LC-MS: m/z 519 $[M + H]^+$, *t*R = 2.24 min.

4-[[3-[3-(Cyclopropylmethyl)-8-(trifluoromethyl)-[1,2,4]triazolo[4,3-a]pyridin-7-yl]phenyl]carbamoyl] benzenesulfonyl fluoride (3). Starting from **7b** (0.260 g, 0.7824 mmol) and **8b** (0.192 mg, 0.9388 mmol) and following the procedure described for **2**, compound **3** was obtained (0.274 g, 68%). ^{1}H NMR (500 MHz, DMSO-d_6) δ 10.83 (s, 1H), 8.76 (d, *J*=7.22 Hz, 1H), 8.22-8.42 (m, 4H), 7.81-7.99 (m, 2H), 7.54 (t, *J*=7.80 Hz, 1H), 7.21 (d, *J*=7.80 Hz, 1H), 6.96 (d, *J*=7.22 Hz, 1H), 3.15 (d, *J*=6.65 Hz, 2H), 1.12-1.37 (m, 1H), 0.46-0.66 (m, 2H), 0.23-0.42 (m, 2H). LC-MS: m/z 519 $[M + H]^+$, *t*R = 2.24 min.

4-[[4-[3-(Cyclopropylmethyl)-8-(trifluoromethyl)-[1,2,4]triazolo[4,3-a]pyridin-7-yl]phenyl]methylcarbamoyl] benzenesulfonyl fluoride (4). 7c (0.050g, 0.144 mmol) in 1,4-dioxane (0.5 mL) was added to **8b** (0.038 g, 0.173 mmol). The resulting suspension was heated at 90ºC for 30 min. After cooling, the suspension was filtered, washed with Et_2O and dried under vacuum. The crude product was purified by flash column chromatography (silica; CH_2Cl_2 in MeOH 100/0 to 94/6) to give **4** as a white solid. (0.025 g, 33%). ^{1}H NMR (400 MHz, DMSO-d_6) δ 9.55 (t, *J*=5.90 Hz, 1H), 8.73 (d, *J*=6.94 Hz, 1H), 8.13-8.39 (m, 4H), 7.31-7.55 (m, 1H), 6.92 (d, *J*=7.40 Hz, 1H), 4.62 (d, *J*=6.01 Hz, 2H), 3.13 (d, *J*=6.70 Hz, 2H), 1.14-1.31 (m, 2H), 0.45-0.62 (m, 2H), 0.20-0.40 (m, 2H). LC-MS: m/z 533 $[M + H]^+$, *t*R = 2.13 min.

4-[3-(Cyclopropylmethyl)-8-(trifluoromethyl)-[1,2,4]triazolo[4,3-a]pyridin-7-yl]aniline (7a). $Pd(PPh_3)_4$ (0.075 g, 0.065 mmol) was added to a stirred suspension of **5** (0.300 g, 1.0883 mmol) and **6a** (0.164 g, 1.197 mmol) in a saturated aqueous solution of $NaHCO_3$ (2 mL) and 1,4-dioxane (5 mL). The mixture was heated at 150 °C for 15 min under microwave irradiation, then cooled to room temperature and filtered through a Celite pad. The filtrate was diluted with water (20 mL) and extracted with EtOAc (2 × 15 mL). The organic layer was washed with brine (15 mL), dried over anhydrous Na_2SO_4, and concentrated in vacuo. The crude was purified by flash column chromatography (silica gel, MeOH–NH_3 in CH_2Cl_2, 0/100 to 5/95) to give the desired product **7a** as a pale yellow solid (0.227 g, 61%). LC-MS: m/z 333 $[M + H]^+$, *t*R = 1.62 min.

3-[3-(Cyclopropylmethyl)-8-(trifluoromethyl)-[1,2,4]triazolo[4,3-a]pyridin-7-yl]aniline (7b). Starting from **5** (0.300 g, 1.0883 mmol) and **6b** (0.208 g, 1.197 mmol) and following the procedure described for **7a**, compound **7b** was obtained as a pale yellow solid (0.265 g, 68%). LC-MS: m/z 333 $[M + H]^+$, *t*R = 1.64 min.

[4-[3-(Cyclopropylmethyl)-8-(trifluoromethyl)-[1,2,4]triazolo[4,3-a]pyridin-7-yl]phenyl]methanamine (7c). Starting from **5** (0.300 g, 1.0883 mmol) and **6c** (0.279 g, 1.197 mmol) and following the procedure described for **7a**, compound **7c** was obtained as a pale yellow solid (0.245 g, 65%). LC-MS: m/z 347 [M + H]+, tR = 1.5 min.

Biology

Cell Culture

CHO-K1 cells (CCL-61; ATCC, Rockville, MD, USA) were grown in Dulbecco's modified Eagle's medium/Nutrient F-12 Ham (DMEM/F12) supplemented with 10% (v/v) fetal calf serum, 100 IU·mL^{-1} penicillin, 100 µg·mL^{-1} streptomycin and 100 mM pyruvate. CHO-K1 cells

stably expressing the wildtype (WT) hmGlu$_2$ receptor (CHO-K1_hmGlu$_2$; Janssen Research and Development) were grown in Dulbecco's modified Eagle's medium (DMEM) supplemented with 10% (v/v) fetal calf serum, 200 IU·mL^{-1} penicillin, 200 μg·mL^{-1} streptomycin, 30.5 μg·mL^{-1} L-proline and 400 μg·mL^{-1} G418. All cells were grown at 37°C and 5% CO_2 and were subcultured at a ratio of 1:10 twice every week.

Plasmids and Transient Transfection

cDNA encoding human mutated and non-mutated mGlu$_2$ receptors was synthesized by GeneArt® (Life Technologies, Carlsbad, CA, USA), subcloned to the pcDNA3.1(+) expression vector (Life Technologies) and amplified by *E. Coli* transformation. 24 hours before transfection, cells were seeded in 15 cm Ø culture plates at high density (20,000 cells/cm^2). Transient transfections in CHO-K1 cells were performed using the cationic lipid transfection reagent LTX lipofectamine reagent (Life Technologies).

Cell Membrane Preparation

CHO-K1_hmGlu$_2$ cells in DMEM without G418 were plated into 15 cm Ø plates. Upon growth to 70% confluency sodium butyrate (final concentration 5 mM) was added to the plates [41]. After 24 hours, cells were detached by scraping into 5 ml of PBS and subsequently centrifuged at 1500 rpm for 5 min. Pellets were resuspended in ice-cold Tris buffer (50 mM Tris-HCl pH 7.4) and homogenized using an Ultra Turrax homogenizer at 24,000 rpm (IKA-Werke GmbH & Co.KG, Staufen, Germany). Membranes and the cytosolic fraction were separated by centrifugation at 31,000 rpm at 4°C for 20 min in an Optima LE-80 K ultracentrifuge (Beckman Coulter, Fullerton, CA). After resuspension of pellets in 10 ml Tris buffer, the centrifugation and homogenization steps were repeated. The remaining pellets were suspended into assay buffer (50 mM Tris-HCl pH 7.4, 2 mM $CaCl_2$, 10 mM $MgCl_2$) which was followed by homogenization. Aliquots were stored at -80°C.

[^{3}H]JNJ-46281222 binding assays using CHO-K1_hmGlu$_2$ membranes

Membrane homogenates (15 μg) and pre-wetted wheat-germ agglutinin coated SPA beads (0.2 mg; RPNQ0001, PerkinElmer, Groningen, The Netherlands) were pre-coupled in assay buffer while gently shaking at room temperature for 30 minutes. Then, this membrane bead mixture was added to an Isoplate-96 (PerkinElmer) together with 6 nM [^{3}H]JNJ-46281222 and increasing concentrations of competing ligand. Nonspecific binding was determined using 10 μM JNJ-40068782 (**9**)[42]. In case of pre-incubation experiments, [^{3}H]JNJ-46281222 was added after a 3 hour pre-incubation of the samples containing membrane and competitor. Plates were counted in a Microbeta 2450^2 Trilux scintillation microplate counter (PerkinElmer) after a 1 hour incubation at 25°C.

For competition association experiments, the plate was rapidly placed in the microplate counter after addition of the membrane homogenates. Plates were recorded for 120 minutes

measuring every 30 seconds at ambient temperature. The assay buffer in these experiments contained 1 mM glutamate, as this was shown to induce monophasic association and dissociation. This enabled straightforward determination of kinetic parameters and resembles a condition at which PAMs likely exert their effect under physiological conditions.[18]

[^{3}H]JNJ-46281222 binding assays using transiently transfected CHO-K1 hmGlu$_2$ membranes

Membrane homogenates (30 or 60 μg) were diluted in ice-cold assay buffer (50 mM Tris-HCl pH 7.4, 2 mM $CaCl_2$, 10 mM $MgCl_2$) to a total reaction volume of 100 μl containing increasing concentrations of competing ligand and 6 nM [^{3}H]JNJ-46281222. Nonspecific binding was determined using 10 μM **9**. After 1 hour at 15°C, incubation was terminated by rapid filtration over GF/C filters through a Brandel harvester 24 (Brandel, Gaithersburg, MD, USA) Filters were subsequently washed at least three times using ice-cold wash buffer (50 mM TRIS-HCl pH 7.4). Filter-bound radioactivity was determined using liquid scintillation spectrometry on a TRI-Carb 2810 TR counter (PerkinElmer).

Irreversible binding of [^{3}H]JNJ-46281222 to CHO-K1_hmGlu$_2$ and transiently transfected hmGlu$_2$ membranes.

Membrane homogenates (30, 60 or 120 μg) were chosen such that specific binding was close to 10% to allow for good resolution and avoid ligand depletion. Samples were incubated with mGlu$_2$ PAMs **1**-**4** at a 10x IC_{50} concentration in a total volume of 400 μl (CHO-K1_hmGlu$_2$ membranes) assay buffer containing 1 mM glutamate in Eppendorf tubes. 0.25% DMSO was taken as a control for total binding and non-specific binding.

After incubation for 1 hour at 25°C while gently shaking, the samples were centrifuged at 16,100x*g* at 4°C for 5 minutes. Unbound ligands were removed by aspiration of supernatant. 1 ml of assay buffer was added, pellets were resuspended and samples were incubated for 20 min. at 25°C. This centrifugation and washing cycle was repeated 4 times. After that, supernatant was removed and the membranes were resuspended in a total volume of 400 μl (CHO-K1_hmGlu$_2$) or 100 μl (transiently transfected hmGlu$_2$ mutants) containing 6 nM [^{3}H] JNJ-46281222 and 1 mM glutamate in tubes. Non-specific binding was determined using 10 μM **9**. After 1 hour incubation at 25°C, incubations were terminated and samples obtained and analyzed as described under '*[^{3}H]JNJ-46281222 Binding*'.

[^{35}S]GTPγS Binding Assays

Membrane homogenates (5 or 10 μg) were diluted in ice-cold assay buffer (50 mM Tris-HCl pH 7.4, 100 mM NaCl, 3 mM $MgCl_2$) supplemented with 10 μM GDP (Sigma-Aldrich, St. Louis, MO, USA) and 5 μg saponin to a total reaction volume of 80 μl containing increasing concentrations of ligand of interest and a glutamate concentration equivalent to its EC_{20} value (4 μM) in case of a PAM dose-response curve. Basal receptor stimulation was determined using assay buffer, maximum receptor stimulation was determined using 1 mM glutamate.

Samples were pre-incubated for 30 minutes at 25 °C. Subsequently, 20 µl [^{35}S]GTPγS (final concentration 0.3 nM; PerkinElmer) was added. The reaction was stopped after a 90 minute incubation at 25 °C by rapid filtration through a 96-well GF/B filterplate (PerkinElmer) on a PerkinElmer filtermate harvester. Plates were washed with ice-cold wash buffer (50 mM Tris-HCl pH 7.4, 5 mM $MgCl_2$). Filter-bound radioactivity was determined by scintillation spectrometry using the Microbeta^2 counter.

Irreversible binding to CHO-K1_hmGlu$_2$ membranes in a functional [^{35}S]GTPγS binding assay.

Experiments were performed as described under '*Irreversible binding of [^{3}H]JNJ-46281222 to CHO-K1_hmGlu$_2$ and transiently transfected mutant hmGlu$_2$ membranes'*, with assay buffer as described under '*[^{35}S]GTPγS Binding'*. PAMs were diluted in assay buffer containing a glutamate concentration equivalent to its EC_{20} value (4 µM). After the washing steps, membrane suspensions were transferred to tubes in a volume of 360 µl assay buffer containing saponin (10 µg) and GDP (10 µM). PAM samples contained an EC_{20} glutamate concentration, total binding was determined using 1 mM glutamate and basal [^{35}S]GTPγS binding was determined using assay buffer only. Samples were pre-incubated for 30 minutes at 25 °C. Subsequently, 40 µl [^{35}S]GTPγS (final concentration 0.3 nM) was added. The reaction was stopped after a 30 minute incubation at 25 °C by rapid filtration over GF/B filters through a Brandel harvester 24 (Brandel, Gaithersburg, MD, USA). Filters were subsequently washed at least three times using ice-cold wash buffer (50 mM Tris-HCl pH 7.4, 5 mM $MgCl_2$). Samples were analyzed as described under '*[^{3}H]JNJ-46281222 Binding*'.

[^{3}H]LY341495 Binding Assays

Membrane homogenates (5 µg) were diluted in assay buffer (50 mM Tris-HCl pH 7.4, 2 mM $CaCl_2$, 10 mM $MgCl_2$) to a total reaction volume of 100 µl containing increasing concentrations of glutamate (100 nM to 1 mM) and 3 nM [^{3}H]LY341495 (ARC, St. Louis, MO, USA). Non-specific binding was determined using 1 mM glutamate. After incubation for 1 hour at 25°C, samples were rapidly filtered through a 96-well GF/B filterplate (PerkinElmer) on a PerkinElmer filtermate harvester and washed three times with ice-cold wash buffer (50 mM Tris-HCl pH 7.4). Samples were analyzed as described under '*[^{3}H]JNJ-46281222 Binding*'.

For all radioligand binding experiments DMSO concentrations were ≤0.25% and radioligand concentrations were chosen such that <10% of the amount added was receptor-bound to avoid ligand depletion.

Data analysis

Data analyses were performed using Prism 7.00 (GraphPad software, San Diego, CA, USA). pIC_{50} values were obtained using non-linear regression curve fitting into a sigmoidal concentration-response curve using the equation: Y=Bottom + (Top-Bottom)/(1+10^(X-LogIC$_{50}$)). pK_i values were obtained from pIC_{50} values using the Cheng-Prusoff equation [43]. pEC_{50} values were

determined using non-linear regression curve fitting into a sigmoidal concentration-response curve with variable slope using the equation: Y=Bottom + (Top-Bottom)/(1+10$^{((LogEC50-X)*Hillslope)}$). Association and dissociation rate constants for unlabeled mGlu$_2$ PAMs were determined by nonlinear regression analysis of competition association data as described by Motulsky and Mahan.[30] In these equations k_1 and k_2 represent the k_{on} and k_{off} of [^{3}H]JNJ-46281222, which are described in table 1.

$$K_A = k_1[L]\cdot 10^{-9} + k_2$$
$$K_B = k_3[I]\cdot 10^{-9} + k_4$$
$$S = \sqrt{(K_A - K_B)^2 + 4\cdot k_1 \cdot k_3 \cdot L \cdot I \cdot 10^{-18}}$$
$$K_F = 0.5(K_A + K_B + S)$$
$$K_S = 0.5(K_A + K_B - S)$$
$$Q = \frac{B_{max}\cdot k_1 \cdot L \cdot 10^{-9}}{K_F - K_S}$$
$$Y = Q\cdot\left(\frac{k_4\cdot(K_F - K_S)}{K_F \cdot K_S} + \frac{k_4 - K_F}{K_F}e^{(-K_F\cdot X)} - \frac{k_4 - K_S}{K_S}e^{(-K_S\cdot X)}\right)$$

Data shown represent the mean ± SEM of at least three individual experiments performed in duplicate. Statistical analysis was performed if indicated, using a one-way ANOVA with Dunnett's post-test or an unpaired student's t-test. Observed differences were considered statistically significant if p-values were below 0.05.

Computational efforts

The mGlu$_2$ receptor homology model: Method is as described in **chapter 2**. An active state model of the 7TM domain of human mGlu$_2$ receptor (Uniprot code Q14416) bound to G protein was built using a combination of structural templates. The crystal structure of the human mGlu$_5$ (PDB 4OO9, [11]) was used to model all 7TM helices except TM6. ECL2 is not refined in the mGlu$_5$ X-ray structure therefore this important loop was modelled based on the mGlu$_1$ receptor crystal structure (PDB 4OR2, [10]). Finally, the β_2AR (PDB ID 3SN6, [44]) active structure was used to model both TM6 in its distinct open conformation as well as the corresponding G protein. The sequence identity between mGlu$_2$ and mGlu$_5$ 7TM's is 51%. The initial model was constructed in MOE v2014.9 (Chemical computing group Inc., Montreal, QC, Canada) and then Maestro (Schrodinger LLC, New York, NY, USA) was used for structure preparation. The Protein Preparation tool was used to fix any missing sidechains/atoms, PROPKA assigned protonation states, the hydrogen bonding network was optimized, and brief minimization until no further change of RMSD to within 0.5 Å removed any structural clashes.

Docking of 2: The ligand was prepared for docking using Maestro. Conformational sampling was performed with ConfGen and multiple conformers were docked into the mGlu$_2$ active state model using Glide XP. As there is no ligand in the mGlu$_2$ model, the docking grid was centered on the ligand position in the mGlu$_1$ receptor structure, based on superposition

of $mGlu_1$ and $mGlu_2$. Sampling was increased in the Glide docking by turning on expanded sampling and passing 100 initial poses to post-docking minimization. All other docking parameters were set to the defaults.

REFERENCES

1. Weichert D, Gmeiner P. *ACS Chem Biol*. **2015**; 10: 1376–1386.

2. Nygaard R, Zou Y, Dror RO, Mildorf TJ, Arlow DH, Manglik A, Pan AC, Liu CW, Fung JJ, Bokoch MP, Thian FS, Kobilka TS, Shaw DE, Mueller L, Prosser RS, Kobilka BK. *Cell*. **2013**; 152: 532–42.

3. Glukhova A, Thal DM, Nguyen AT, Vecchio EA, Jörg M, Scammells PJ, May LT, Sexton PM, Christopoulos A. *Cell*. **2017**; 168: 867–877.e13.

4. Weichert D, Kruse AC, Manglik A, Hiller C, Zhang C, Hubner H, Kobilka BK, Gmeiner P. *Proc Natl Acad Sci*. **2014**; 111: 10744–10748.

5. Niswender CM, Conn PJ. *Annu Rev Pharmacol Toxicol*. **2010**; 50: 295–322.

6. Pin J-P, Bettler B. *Nature*. **2016**; 540: 60–68.

7. Lindsley CW, Emmitte KA, Hopkins CR, Bridges TM, Gregory KJ, Niswender CM, Conn PJ. *Chem Rev*. **2016**; 116: 6707–6741.

8. Nicoletti F, Bockaert J, Collingridge GL, Conn PJ, Ferraguti F, Schoepp DD, Wroblewski JT, Pin JP. *Neuropharmacology*. **2011**; 60: 1017–41.

9. Monn JA, Prieto L, Taboada L, Pedregal C, Hao J, Reinhard MR, Henry SS, Goldsmith PJ, Beadle CD, Walton L, Man T, Rudyk H, Clark B, Tupper D, Baker SR, Lamas C, Montero C, Marcos A, Blanco J, Bures M, Clawson DK, Atwell S, Lu F, Wang J, Russell M, Heinz BA, Wang X, Carter JH, Xiang C, Catlow JT, Swanson S, Sanger H, Broad LM, Johnson MP, Knopp KL, Simmons RM a, Johnson BG, Shaw DB, McKinzie DL. *J Med Chem*. **2015**; 58: 1776–1794.

10. Wu H, Wang C, Gregory KJ, Han GW, Cho HP, Xia Y, Niswender CM, Katritch V, Meiler J, Cherezov V, Conn PJ, Stevens RC. *Science*. **2014**; 344: 58–64.

11. Doré AS, Okrasa K, Patel JC, Serrano-Vega M, Bennett K, Cooke RM, Errey JC, Jazayeri A, Khan S, Tehan B, Weir M, Wiggin GR, Marshall FH. *Nature*. **2014**; 511: 557–62.

12. Christopher JA, Aves SJ, Bennett KA, Doré AS, Errey JC, Jazayeri A, Marshall FH, Okrasa K, Serrano-Vega MJ, Tehan BG, Wiggin GR, Congreve M. *J Med Chem*. **2015**; 58: 6653–6664.

13. Cid JM, Tresadern G, Vega JA, de Lucas AI, Matesanz E, Iturrino L, Linares ML, Garcia A, Andrés JI, Macdonald GJ, Oehlrich D, Lavreysen H, Megens A, Ahnaou A, Drinkenburg W, Mackie C, Pype S, Gallacher D, Trabanco AA. *J Med Chem*. **2012**; 55: 8770–89.

14. Cid JM, Duvey G, Tresadern G, Nhem V, Furnari R, Cluzeau P, Vega JA, de Lucas AI, Matesanz E, Alonso JM, Linares ML, Andrés JI, Poli SM, Lutjens R, Himogai H, Rocher J, Macdonald GJ, Oehlrich D, Lavreysen H, Ahnaou A, Drinkenburg W, Mackie C, Trabanco AA. *J Med Chem*. **2012**; 55: 2388–2405.

15. Farinha A, Lavreysen H, Peeters L, Russo B, Masure S, Trabanco AA, Cid J, Tresadern G. *Br J Pharmacol*. **2015**; 172: 2383–96.

16. Pérez-Benito L, Doornbos MLJ, Cordomí A, Peeters L, Lavreysen H, Pardo L, Tresadern G. *Structure*. **2017**; 25: 1–10.

17. Doornbos MLJ, Cid JM, Haubrich J, Nunes A, van de Sande JW, Vermond SC, Mulder-Krieger T, Trabanco AA, Ahnaou A, Drinkenburg WH, Lavreysen H, Heitman LH, IJzerman AP, Tresadern G. *J Med Chem*. **2017**; 60: 6704–6720.

18. Doornbos MLJ, Pérez-Benito L, Tresadern G, Mulder-Krieger T, Biesmans I, Trabanco AA, Cid JM, Lavreysen H, IJzerman AP, Heitman LH. *Br J Pharmacol*. **2016**; 173: 588–600.

19. Lavreysen H, Langlois X, Ver Donck L, Cid Nuñez JM, Pype S, Lütjens R, Megens A. *Pharmacol Res Perspect*. **2015**; 3: e00097.

20. Salih H, Anghelescu I, Kezic I, Sinha V, Hoeben E, Van Nueten L, De Smedt H, De Boer P. *J Psychopharmacol*. **2015**; 29: 414–425.

21. Kent JM, Daly E, Kezic I, Lane R, Lim P, De Smedt H, De Boer P, Van Nueten L, Drevets WC, Ceusters M. *Prog Neuro-Psychopharmacology Biol Psychiatry*. **2016**; 67: 66–73.

22. Cid JM, Tresadern G, Duvey G, Lütjens R, Finn T, Rocher J, Poli S, Vega JA, de Lucas AI, Matesanz E, Linares ML, Andrés JI, Alcazar J, Alonso JM, Macdonald GJ, Oehlrich D, Lavreysen H, Ahnaou A, Drinkenburg W, Mackie C, Pype S, Gallacher D, Trabanco AA. *J Med Chem*. **2014**; 57: 6495–512.

23. Cid JM, Tresadern G, Vega JA, De Lucas AI, Del Cerro A, Matesanz E, Linares ML, García A, Iturrino L, Pérez-Benito L, Macdonald GJ, Oehlrich D, Lavreysen H, Peeters L, Ceusters M, Ahnaou A, Drinkenburg W, Mackie C, Somers M, Trabanco AA. *J Med Chem*. **2016**; 59: 8495–8507.

24. Cid-Nuñez, J. M., De Lucas Olivares, A. I., Trabanco-Suarez, A. A., MacDonald, G. J. **2010**.

25. Narayanan A, Jones LH. *Chem Sci*. **2015**; 6: 2650–2659.

26. Nijmeijer S, Engelhardt H, Schultes S, van de Stolpe AC, Lusink V, de Graaf C, Wijtmans M, Haaksma EEJ, de Esch IJP, Stachurski K, Vischer HF, Leurs R. *Br J Pharmacol*. **2013**; 170: 89–100.

27. Yang X, Dong G, Michiels TJM, Lenselink EB, Heitman L, Louvel J, IJzerman AP. *Purinergic Signal*. **2017**; 13: 191–201.

28. Kenakin T, Jenkinson S, Watson C. *J Pharmacol Exp Ther*. **2006**; 319: 710–723.

29. Strelow JM. *SLAS Discov Adv Life Sci R&D*. **2017**; 22: 3–20.

30. Motulsky HJ, Mahan LC. *Mol Pharmacol*. **1984**; 25: 1–9.

31. Xia L, de Vries H, IJzerman AP, Heitman LH. *Purinergic Signal*. **2016**; 12: 115–126.

32. Guo D, van Dorp EJH, Mulder-Krieger T, van Veldhoven JPD, Brussee J, IJzerman AP, Heitman LH. *J Biomol Screen*. **2013**; 18: 309–20.

33. Congreve M, Oswald C, Marshall FH. *Trends Pharmacol Sci*. **2017**; xx: 1–11.

34. Tresadern G, Cid J-MM, Trabanco AA. *J Mol Graph Model*. **2014**; 53: 82–91.

35. Harpsøe K, Boesgaard MW, Munk C, Bräuner-Osborne H, Gloriam DE. *Bioinformatics*. **2017**; 33: 1116–1120.

36. Kling RC, Plomer M, Lang C, Banerjee A, Hübner H, Gmeiner P. *ACS Chem Biol*. **2016**; 11: 869–875.

37. Gregory KJ, Velagaleti R, Thal DM, Brady RM, Christopoulos A, Conn PJ, Lapinsky DJ. *ACS Chem Biol*. **2016**; 11: 1870–1879.

38. Singh J, Petter RC, Baillie TA, Whitty A. *Nat Rev Drug Discov*. **2011**; 10: 307–317.

39. Baillie TA. *Angew Chemie - Int Ed*. **2016**; 55: 13408–13421.

40. Lu S, Zhang J. *Drug Discov Today*. **2017**; 22: 447–453.

41. Cuisset L, Tichonicky L, Jaffray P, Delpech M. *J Biol Chem*. **1997**; 272: 24148–24153.

42. Lavreysen H, Langlois X, Ahnaou A, Drinkenburg W, te Riele P, Biesmans I, Van der Linden I, Peeters L, Megens A, Wintmolders C, Cid JM, Trabanco AA, Andrés JI, Dautzenberg FM, Lütjens R, Macdonald G, Atack JR. *J Pharmacol Exp Ther*. **2013**; 346: 514–27.

43. Cheng Y, Prusoff WH. *Biochem Pharmacol*. **1973**; 22: 3099–108.

44. Rasmussen SGF, DeVree BT, Zou Y, Kruse AC, Chung KY, Kobilka TS, Thian FS, Chae PS, Pardon E, Calinski D, Mathiesen JM, Shah ST a, Lyons J a, Caffrey M, Gellman SH, Steyaert J, Skiniotis G, Weis WI, Sunahara RK, Kobilka BK. *Nature*. **2011**; 477: 549–55.

SUPPORTING FIGURE AND TABLES

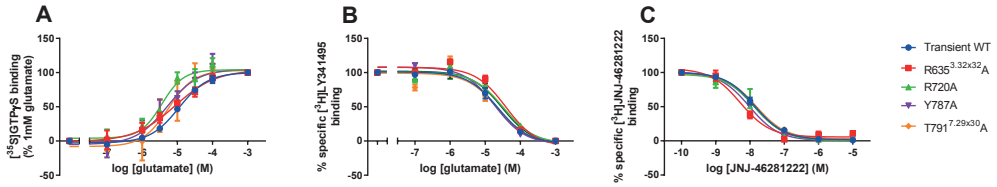

Figure S1. Effect of transiently transfected $mGlu_2$ receptor mutants on [^{35}S]GTPγS binding (A) and displacement of [^{3}H]LY341495 (B) and [^{3}H]JNJ-46281222 (C). Data represent the mean ± SEM of at least three individual experiments performed in duplicate.

Table S1. Selectivity data for representative $mGlu_2$ PAM **3** at $mGlu_{1,3,5,8}$.

Compound	$hmGlu_1$-Ago-Ca-pEC_{50}	$hmGlu_1$-Anta-Ca-pIC_{50}	$hmGlu_1$-PAM-Ca-pEC_{50}	$hmGlu_3$-Ago-Ca-pEC_{50}	$hmGlu_3$-Anta-Ca-pIC_{50}	$hmGlu_3$-PAM-Ca-pEC_{50}	$hmGlu_5$-Ago-Ca-pEC_{50}	$hmGlu_5$-Anta-Ca-pIC_{50}	$hmGlu_5$-PAM-Ca-pEC_{50}	$hmGlu_8$-Ago-Ca-pEC_{50}	$hmGlu_8$-Anta-Ca-pIC_{50}
3	<4.3	<4.3	<4.3	<4.3	<4.3	<4.3	<4.3	~4.69	<4.3	<4.3	<4.3

Ago, agonism; Anta, antagonism; PAM, positive allosteric modulation; Ca, data from calcium response in Ca^{2+}-based FDSS assay; All assays used the human receptor. Further details of methods can be found in Pérez-Benito *et al.* (2017).[16]

Table S2. Effect of transiently transfected $mGlu_2$ receptor mutants on [^{35}S]GTPγS binding and displacement of [^{3}H]LY341495 and [^{3}H]JNJ-46281222. Data represent the mean ± SEM of at least three individual experiments performed in duplicate.

	[^{35}S]GTPγS binding	[^{3}H]LY341495 displacement	[^{3}H]JNJ-46281222 displacement
Mutant	**Glutamate pEC_{50}**	**Glutamate pIC_{50}**	**JNJ-46281222 pK_i**
Transient WT	4.95 ± 0.04	5.07 ± 0.12	8.38 ± 0.13
R635$^{3.32x32}$A	4.9 ± 0.22[a]	4.84 ± 0.04	8.76 ± 0.10
R720A	5.08 ± 0.11	4.91 ± 0.03	8.51 ± 0.18
Y787A	5.43 ± 0.05	5.07 ± 0.09	8.55 ± 0.04
T791$^{7.29x30}$A	5.31 ± 0.21	5.13 ± 0.05	8.36 ± 0.07
C795$^{7.33x34}$A	5.30 ± 0.25	4.94 ± 0.06	8.42 ± 0.07

Values represent the mean ± SEM of at least three individual experiments, performed in duplicate. [a] As previously described by Farinha *et al.* (2015).[15]

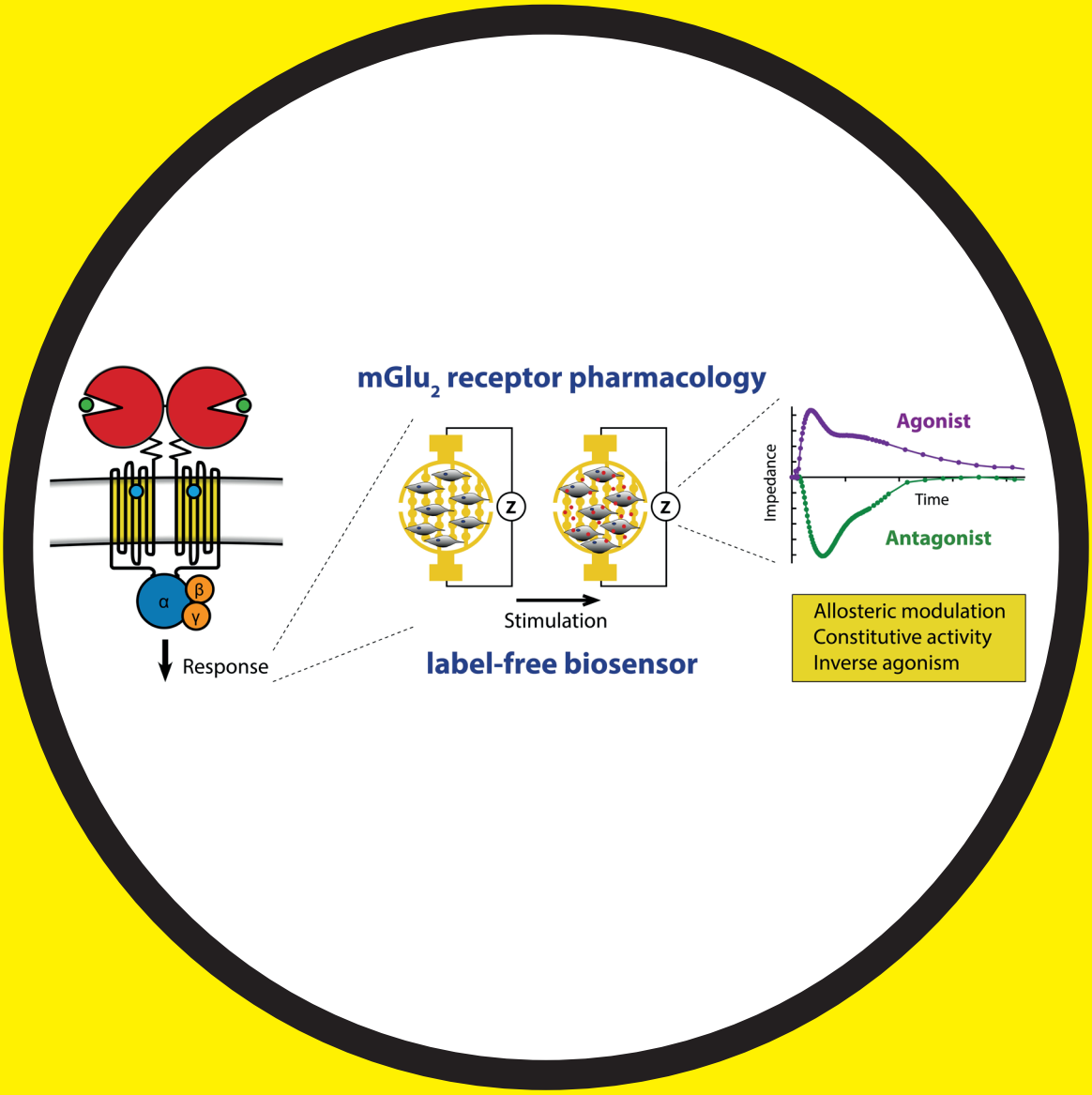
mGlu2 receptor pharmacology
α
β
γ
Response
Z
Z
Stimulation
label-free biosensor
Impedance
Time
Agonist
Antagonist
Allosteric modulation
Constitutive activity
Inverse agonism

CHAPTER 6

Constitutive activity of the metabotropic glutamate receptor 2 explored with a whole-cell label-free biosensor

Maarten L J Doornbos, Ilse Van der Linden, Liesbeth Vereyken, Gary Tresadern, Adriaan P IJzerman, Hilde Lavreysen & Laura H Heitman

Biochemical Pharmacology 152 (2018) 201–210. doi:10.1016/j.bcp.2018.03.026.

6

ABSTRACT

Label-free cellular assays using a biosensor provide new opportunities for studying G protein-coupled receptor (GPCR) signaling. As opposed to conventional *in vitro* assays, integrated receptor-mediated cellular responses are determined in real-time rather than a single downstream signaling pathway. In this study, we examined the potential of a label-free whole cell impedance-based biosensor system (i.e. xCELLigence) to study the pharmacology of one GPCR in particular, the $mGlu_2$ receptor. This receptor is a target for the treatment of several psychiatric diseases such as schizophrenia and depression.

After optimization of assay conditions to prevent interference of endogenous glutamate in the culture medium, detailed pharmacological assessments were performed. Concentration-response curves showed a concentration-dependent increase in impedance for agonists and positive allosteric modulators, whereas receptor inhibition by an antagonist or negative allosteric modulator resulted in a concentration-dependent decrease in cellular impedance. Interestingly, constitutive receptor activity was observed that was decreased by LY341495, which therefore behaved as an inverse agonist here, a property that was heretofore unappreciated. This was confirmed by concentration-dependent modulation of LY341495 potency and efficacy by a allosteric modulators.

In summary, the use of the xCELLigence system to study $mGlu_2$ receptor pharmacology was validated. This is the first class C GPCR to be characterized extensively by such method, opening new avenues to study receptor pharmacology including inverse agonism and demonstrating its value for future drug discovery efforts of mGlu receptors as well as other GPCRs.

INTRODUCTION

Traditionally, drug discovery at G protein-coupled receptors (GPCRs) has been based on screening drug candidates using functional *in vitro* endpoint-based assays in which the ability of a compound to activate or inhibit a certain pathway is determined. Over the last decade on the other hand the use of label-free cellular assays has greatly increased.[1,2] These assays, typically using a biosensor, measure cellular responses upon ligand stimulation, which result in morphological changes of the whole cell.[3] Thereby some of the caveats of traditional endpoint assays are circumvented: no labels (e.g. radioactive, fluorescent) or reporter genes are required and measurements can be performed continuously.[4] Cell types used include recombinant cell lines, cell lines endogenously expressing the target of interest and even patient-derived cells.[5] Label-free assays used to study GPCR responses are mostly based on measurement of changes in cell morphology either optically, such as EPIC (Corning Inc.) or by changes in impedance, such as xCELLigence (ACEA Biosciences).[1,6] These systems have proven valuable in studying GPCR pharmacology in different cell lines.[7–9]

Being a presynaptic regulator of glutamate release, the $mGlu_2$ receptor has been of great interest in drug discovery over the last decade. This receptor, a class C GPCR, has emerged as therapeutic target for various psychiatric diseases amongst which schizophrenia, depression and anxiety, which are characterized by glutamatergic dysfunction.[10,11] A variety of glutamate-like agonists that can dampen glutamate hyperfunction was developed, of which LY2140023 of Eli Lilly, a prodrug of LY404039 showed improvement in positive and negative symptoms in schizophrenic patients, which could not be confirmed in later clinical studies.[12,13] Inhibition of the $mGlu_2$ receptor can be beneficial for glutamate hypofunction in depression, and when considering the orthosteric binding site antagonist LY341495 has been the most studied for this purpose.[14,15] Since the orthosteric site is highly conserved among the mGlu receptor subtypes and medicinal chemistry of orthosteric ligands is constrained to hydrophilic glutamate derivatives, drug development efforts later shifted to allosteric modulators for the $mGlu_2$ receptor, which have been shown to bind in a less evolutionary conserved binding site within the transmembrane domain.[16–18] This allosteric binding site is more hydrophobic and allows more chemical diversity.[19] Therefore, subtype selectivity is obtained relatively easier and allosteric modulators are more prone to cross the blood brain barrier due their increased lipophilicity. Allosteric modulators enhance or inhibit the affinity and/or efficacy of the endogenous agonist glutamate and some positive allosteric modulators (PAMs) also show intrinsic efficacy, referred to as PAM agonism.[20] Reference PAMs in the field include JNJ-40068782,[21] BINA[22] and JNJ-46281222.[23] Two PAMs entered clinical trials, AZD8529 of AstraZeneca and JNJ-40411813 (also known as ADX71149) from Janssen/Addex.[24–29] A number of $mGlu_2$ negative allosteric modulators (NAMs) have been characterized *in vivo*, including a recent series

of NAMs from Janssen and RO4491533 and decoglurant from Roche, of which the latter also advanced into clinical trials.[30–32] Taken together, discovery efforts have resulted in a great diversity of selective and high affinity $mGlu_2$ ligands, but no compounds have successfully passed clinical evaluation.

To increase the understanding on ligand-induced $mGlu_2$ responses, we evaluated in this study the use of the label-free impedance-based xCELLigence system to study the pharmacology of the $mGlu_2$ receptor *in vitro*. A benefit of this biosensor is that experiments are performed under more relevant conditions than most traditional assays (i.e. living cells at 37°C in culture medium). After optimization of pre-treatment conditions to reduce the concentration of endogenous glutamate in the assay medium, responses of an agonist, antagonist, PAM and NAM were studied. Furthermore, we evaluated constitutive receptor activity by using antagonist/inverse agonist and NAM pre-treatment experiments. Finally, the effects of a PAM or NAM on agonist efficacy were studied. Taken together, biosensor-based label-free systems are helpful in studying (novel) $mGlu_2$ pharmacology in a more physiologically relevant environment. Our studies may be equally relevant for other class C GPCRs.

MATERIALS AND METHODS

Materials

LY354740, RO4491533 and JNJ-46281222 were synthesized at Janssen Research and Development (Toledo, Spain). LY341495 was obtained from Tocris BioScience (Bristol, UK). Benzoylchloride, Dulbecco's modified Eagle's medium (DMEM), glutamate, glutamine, glutamate-d5 standards, glutamate-pyruvate transaminase (GPT), pertussis toxin (PTX) and sodium pyruvate were from Sigma-Aldrich (St. Louis, MO, USA). Penicillin, streptomycin, L-Proline and G418 were obtained from Duchefa Biochemie (Haarlem, The Netherlands). Fetal calf serum (FCS) was from Biowest (Nuaillé, France). PET E-plates 16 and 96 for the xCELLigence DP and SP system (ACEA Biosciences, San Diego, CA, USA) were obtained from Bioké (Leiden, the Netherlands). Chinese hamster ovary cells (CHO-K1, CCL-61) were from ATCC (Rockville, MD, USA). CHO-K1 cells stably expressing the $hmGlu_2$ receptor (CHO-K1_$hmGlu_2$) were from Janssen Research and Development (Beerse, Belgium). Acetonitrile ULC/MS-grade was purchased from Biosolve (Valkenswaard, The Netherlands). Formic acid 98-100% and disodium tetraborate decahydrate were obtained from Merck (Darmstadt, Germany). High purity water was obtained with a Milli-Q Reference Ultrapure Water Purification System (Merck Millipore, Billerica, MA, USA). Other chemicals were of analytical grade and from standard commercial sources.

Cell culture

CHO-K1_hmGlu2 cells were grown in DMEM supplemented with 10% (v/v) FCS, 200 IU·mL^{-1} penicillin, 200 µg·mL^{-1} streptomycin, 30.5 µg·mL^{-1} L-proline and 400 µg·mL^{-1} G418 at 37°C and 5% CO_2. CHO-K1 WT cells were cultured in the same medium without G418.

Analysis of glutamate concentration

Preparation of stock solutions and curves

As glutamate is present in the culture medium as an endogenous entity, a calibration curve had to be prepared in an artificial matrix, for which demineralised water was used. Therefore, a quality check was performed to validate quantification of the samples with a standard addition step (a known amount of glutamate is spiked to a sample). The calibration curve was prepared in a range of 0.010 — 50 µg/ml, starting from a stock solution of 100 µg/ml glutamate in water. Glutamate-d5 was used as a stable isotope labelled internal standard (STIL).

Sample preparation

Glutamate was quantified after derivatization with benzoylchloride. 20µL medium was transferred to a sample tube, subsequently 20µL of the calibration curve in water was added followed by 20µL of STIL Glu-d5 and 20µL of NaBorate solution (100mM, pH 8). For derivatization, 40µl benzoylchloride (3% v/v in acetonitrile) was transferred to the sample tubes, after which samples were incubated for 15 min at 50°C and subsequently cooled to room temperature for 10 min. Finally, 200µL 0.1% formic acid was added. Samples were vortexed and centrifuged for 3min at 6000g, after which the supernatant was analyzed.

Liquid chromatography – mass spectrometry

Chromatographic separation was performed with an Acquity UPLC system (Waters, Millford, Boston, USA). Injections of 2 µL were made on an Acquity UPLC BEH C18 2.1 x 50 mm (1.7 µm particles) column held at 55°C at a flow rate of 0.400 ml/min. Chromatographic elution started isocratically at 2% solvent B (acetonitrile) and 98% solvent A (0.1% formic acid) for 0.2 min. A subsequent linear gradient to 30% B in 1.8 min, followed by a wash step (0.2 min at 98% solvent B) and 0.8 min equilibration time at 2%B resulted in a total run time of 3 min/injection.

Instrument parameters were optimized by injecting a glutamate standard solution (2 ng/ml in 0.1% formic acid/acetonitrile,v/v; 80/20) at a flow rate of 10 µl/min. The following source parameters were used: source temperature 150°C, desolvation temperature 450°C, capillary 2.9kV, sampling cone 30V, source offset 50V, cone gas 150 L/h, desolvation gas 900 L/h, collision gas flow 0.18 ml/min and nebulizer gas 6 ml/min. Glutamate was analyzed in the positive ion mode with electrospray ionization and detected by multiple reaction monitoring (MRM) (collision energy 20 eV and dwell time 75 ms) on a triple quad Xevo TQ-s system (Waters, Manchester, UK), monitoring the channels of *m*/*z* 252.1 -> 105.1 (quantifier) and *m*/*z* 252.1->130.1 (qualifier), respectively. The MRM transition monitored for the STIL Glu-d5 is *m*/*z* 257.1 -> 105.1. During method optimization, special consideration was given to the chroma-

tographic separation of glutamate and glutamine. The incubation medium has an excessive amount of glutamine present and it is known that glutamine, with a MW 1 Da lower than glutamate, gives crosstalk in the MRM channel of glutamate. Therefore, glutamine was also monitored, at *m/z* 251.1 -> 105.1 as a qualifier. Quantitative values were obtained by relating chromatographic peak areas to those derived from separately run calibration standards as described above. Calibration curves were plotted using a non-weighted log-log linear regression.

Label-free whole-cell assays

Label-free whole-cell assays were performed using the xCELLigence real-time cell analyzer (RTCA) system[3,33] as previously described.[7] The system measures whole-cell responses based on changes in electrical impedance generated by adherence of cells to gold-coated electrodes at the bottom of microelectronic E-plates. Relative changes in impedance (Z) are recorded continuously and displayed in the dimensionless parameter Cell Index (CI), which is defined as $(Z_i - Z_0)\ \Omega / 15\Omega$. Z_i is the impedance at a given time and Z_0 is the baseline impedance measured at the start of the experiment in the absence of cells.

Z_0 was measured after adding 45 µl, or in the case of pre-incubation experiments 40 µl, culture medium per well in 16 or 96 well E-plates. 50 µl of cell suspension was added to the plate containing 40,000 cells per well. After resting at room temperature for 30 minutes, E-plates were mounted in the recording station within a humidified 37°C, 5% CO_2 incubator. Subsequently, impedance was measured overnight every 15 minutes. To remove endogenous glutamate, refreshment of culture medium by culture medium or serum-free culture medium with GPT (3 U/ml) and additional pyruvate (3 mM) was performed 3 hours before stimulation unless stated otherwise. For evaluation of constitutive receptor activity, pre-incubation with antagonist LY341495 or NAM RO4491533 was performed 1 hour before stimulation. After 19 hours, cells were stimulated with increasing concentrations of ligand (i.e. agonist, antagonist, PAM or NAM). Final well volumes after addition of compounds were 100 µl in all cases. DMSO concentrations were constant between wells and were ≤ 0.1%. For inhibition of $G\alpha_i$ signaling, cells were seeded in culture medium containing PTX (300 ng/ml) when indicated. PTX concentrations were kept constant also after medium refreshment.

Data analysis

RTCA software 2.0 (ACEA Biosciences) was used to obtain the experimental data. All analyses were performed using Prism 7.00 (GraphPad software, San Diego, CA, USA). Ligand responses were normalized to Δ cell index (ΔCI) after subtracting baseline (vehicle control) to correct for ligand-independent effects. Maximum or minimum peak responses were considered as the highest or lowest level of ΔCI within 60 min after compound stimulation and were used for bar graphs and concentration-response curves. pEC_{50} and pIC_{50} values were obtained using non-linear regression curve fitting into a sigmoidal dose-response curve with variable

slope. Data shown are the mean ± SEM of at least three individual experiments performed in duplicate. Statistical analyses were performed as indicated. If p-values were below 0.05, observed differences were considered statistically significant.

RESULTS AND DISCUSSION

Serum-free assay medium with GPT resulted in lowest levels of endogenous glutamate

One of the benefits of the xCELLigence biosensor is that experiments can be performed under more relevant conditions than most traditional assays (i.e. living cells at 37°C in culture medium). However, endogenous glutamate is often found in culture medium and is also continuously produced by cells.[34] As high levels of glutamate will interfere with functional responses by other $mGlu_2$ receptor agonists, we first determined the concentration of endogenous glutamate in culture medium using HPLC analysis, which was found to be 78 ± 2.0 μM (Table 1). Since the potency of glutamate to activate the $mGlu_2$ receptor is around 10 μM, this concentration is capable to activate the $mGlu_2$ receptor to a high level as shown in **chapter 2 and 6** and earlier by Pin *et al.* (1999).[35] Hence, we aimed to reduce the concentration of endogenous glutamate in the culture medium. For this purpose, glutamate-pyruvate transaminase (GPT; 3 U/ml) was added in the presence of additional pyruvate (3 mM), a procedure commonly used in the field of mGlu receptors, e.g. [36,37]. This treatment led to an almost 4-fold lower concentration of glutamate in the culture medium: 23 ± 0.09 μM. At this concentration, glutamate is still able to activate the receptor over 50% and will thus significantly interfere with the functional readout. Next, we switched to serum-free medium, which we determined to contain only 0.22 ± 0.005 μM endogenous glutamate, indicating that the fetal calf serum (FCS) present in the culture medium was the main source of glutamate.

Importantly, when seeded in serum-free medium, cells did not attach to the bottom of the wells, did not proliferate and therefore did not show any remarkable level of impedance (data not shown). This clearly indicated that cells required FCS for growth and proliferation. Therefore, serum-free medium was added to the wells by medium refreshment three hours before stimulation only. Of note, during these first three hours of the serum-free medium being on the cells, the concentration of glutamate increased to 13 ± 0.47 μM at the time of stimulation (Table 1). Therefore, GPT and pyruvate were added to this serum-free assay medium, resulting in a stable concentration of endogenous glutamate during the signaling read-out of 1 hour (i.e. from 1.6 ± 0.09 μM at the moment of stimulation to 2.3 ± 0.62 μM two hours after stimulation, Table 1). This residual level of endogenous glutamate only slightly activates the receptor to a maximum level of approximately 10%, leaving a large experimental window for further (exogenous) agonist-induced receptor signaling studies.

Table 1. Glutamate concentrations (μM) in culture medium or serum-free medium with and without addition of GPT (3U / ml) and pyruvate (3 mM). Medium was added to the cells at the time of medium refreshment (-3 hrs).

Time of:	Time from stimulation (hrs)	Culture medium		Serum-free medium	
		- GPT	*+ GPT*	*- GPT*	*+ GPT*
medium refreshment	-3	78 ± 2.0	23 ± 0.09	0.22 ± 0.005	0.098 ± 0.004
	-2.5	83 ± 1.6	23 ± 0.58	3.7 ± 0.20	1.2 ± 0.09
pre-treatment	-1	88 ± 1.3	25 ± 0.90	9.8 ± 0.09	1.2 ± 0.10
stimulation	0	100 ± 3.0	28 ± 1.1	13 ± 0.47	1.6 ± 0.09
	2	100 ± 9.4	33 ± 1.9	17 ± 2.1	2.3 ± 0.62

Data are shown as mean ± SEM of at least three individual experiments performed in duplicate.

Endogenous glutamate reduced agonist yet enhanced antagonist responses

The $mGlu_2$ receptor-mediated signaling was monitored on the xCELLigence RTCA system. In the field of class C GPCRs, this technique was never characterized extensively, yet it was used as a tool in two studies: Scandroglio *et al.* (2010)[38] presented a small proof of concept study on the $mGlu_1$ receptor and we reported on the $mGlu_2$ receptor using the xCELLigence as a tool to assess the effect of binding kinetics on functional efficacy of $mGlu_2$ PAMs in **chapter 3 and 4**. Here, CHO-K1_$hmGlu_2$ cells stably expressing the $hmGlu_2$ receptor were used. 40,000 cells/well were seeded in culture medium 19 hours prior to stimulation (Fig. 1A). The cells adhered well to the bottom of the wells on the gold-coated electrodes, which is essential for sufficient measurements of impedance.[39] Therefore no additional well coatings had to be used. Overnight proliferation generally led to cell indices (CI) between 3 and 5 (Fig. 1B for two representative traces), dependent on cell passage number and confluency.

As discussed above, the concentration of endogenous glutamate varied between different pre-treatment conditions (Table 1). To assess how this affected the response of an $mGlu_2$ receptor agonist or antagonist, responses of a single 1 μM concentration of LY354740 and LY341495 were obtained, respectively. This concentration was chosen such that it is well above the respective potencies of the two ligands. The traces of the agonist LY354740 at 1 μM were always "positive", inducing an increase in Cell Index and thus impedance (Fig. 1C,D). The responses after different pre-treatment conditions varied greatly. When using normal culture medium containing a high concentration of endogenous glutamate at the time of stimulation (100 ± 3.0 μM), a small LY354740 response was observed, with peaks at an average maximum ΔCI level of 0.098 ± 0.012 (Fig. 1D). In the presence of GPT and pyruvate the glutamate concen-

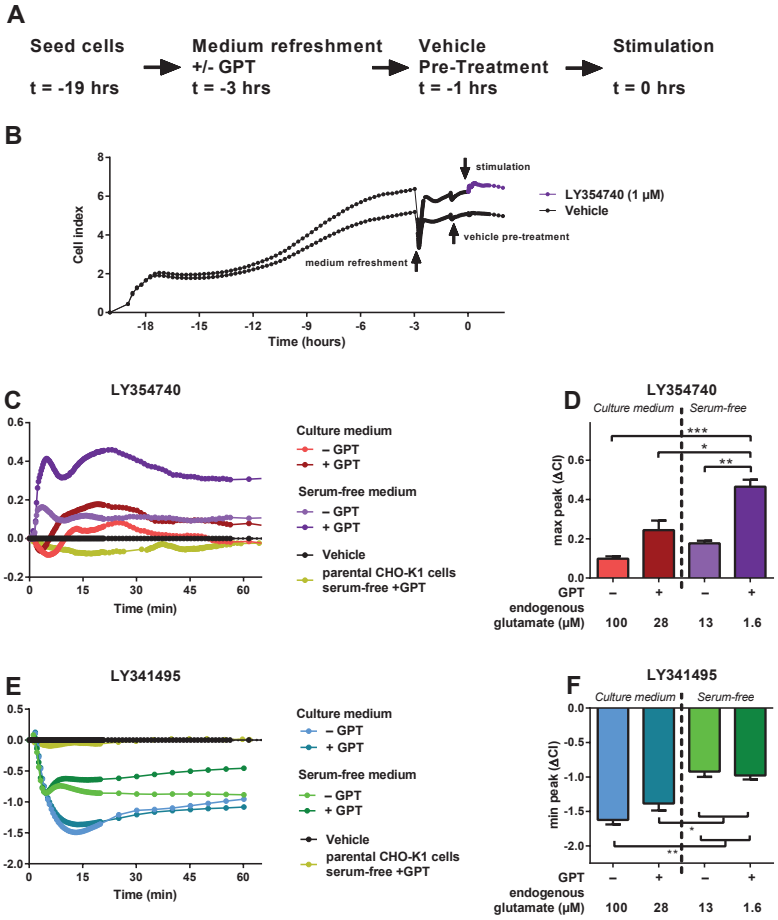

Figure 1. Agonist LY354740 and antagonist LY341495-induced responses in the presence of different concentrations of endogenous glutamate. A) Set-up of experiments. B) Typical growth curve of CHO-K1 cells stably expressing the $mGlu_2$ receptor (40,000 cells/well). 3 hours prior to stimulation culture medium was replaced by serum-free medium containing GPT (3 U/ml) and additional pyruvate (3 mM). Cells were stimulated with LY354740 (1 µM). Serum-free medium with 0.025% DMSO was used as vehicle control. C) Responses induced by 1 µM LY354740 after different pre-treatment conditions and the response of 1 µM LY354740 on CHO-K1 WT cells three hours after replacement of culture medium by serum-free medium containing GPT. D) Maximum peak values induced by 1 µM LY354740 in the presence of different concentrations of endogenous glutamate as presented in table 1. E) Responses induced by 1 µM LY341495 after different pre-treatment conditions and the response of 1 µM LY341495 on CHO-K1 WT cells three hours after replacement of culture medium by serum-free medium containing GPT. F) Maximum peak values induced by 1 µM LY341495 in the presence of different concentrations of endogenous glutamate as presented in table 1. All xCELLigence traces are from representative experiments performed in duplicate. Bar graphs represent mean ± SEM of at least three individual experiments performed in duplicate. Statistical analyses were performed using one-way ANOVA with Tukey's post-test. * $p < 0.05$, ** $p < 0.01$, *** $p < 0.001$.

tration was reduced to 28 ± 1.1 μM at stimulation, resulting in an increased LY354740 response with maximum peaks of 0.24 ± 0.05 ΔCI. This response reached a similar maximum level as when culture medium was replaced by serum-free medium, although the LY354740 response was more prompt in that case (Fig. 1C). The highest and significantly increased LY354740 response was obtained using medium refreshment with serum-free medium containing GPT and pyruvate, which contained 1.6 ± 0.09 μM endogenous glutamate at the time of stimulation, leading to significantly increased maximum peaks of 0.47 ± 0.04 ΔCI. Even in the presence of a high concentration of endogenous glutamate, LY354740 was still able to induce responses (Fig. 1C,D), which exemplified the sensitivity of the xCELLigence system, registering very small ligand-induced responses.

In contrast to the positive LY354740 responses, 1 μM antagonist LY341495 induced opposite negative responses in Cell Index (Fig. 1E). As for the agonist LY354740, the peak level (i.e. minimum peak in case of LY341495) was dependent on the medium refreshment conditions, although in reversed order. When using normal culture medium the peak of LY341495 was the largest, -1.62 ± 0.06 ΔCI (Fig. 1F). Treatment of culture medium with GPT already reduced the peak slightly, but when medium was refreshed by serum-free medium peaks were significantly reduced to minimum levels of -0.92 ± 0.08 ΔCI. Moreover, addition of GPT did not further increase the minimum peak of LY341495 (-0.98 ± 0.06 ΔCI, Fig. 1F), indicating a relatively large response of the compound on its own. Interestingly, in serum-free medium with GPT, the trace returned to baseline more readily after the peak (Fig. 1E), indicating that the difference in glutamate levels still slightly altered the shape of the trace. Importantly, no compound-induced responses were observed for both LY354740 and LY341495 at 1 μM in parental wild-type CHO-K1 cells (Fig. 1C,E), confirming that all responses were $mGlu_2$ receptor-mediated. This was in line with our previous observation that PAM JNJ-46281222 did not induce significant responses on parental CHO-K1 cells as shown in **chapter 4**.

Taken together, the lowest level of endogenous glutamate was reached by medium refreshment with serum-free medium supplemented with GPT, which was used for all further experiments. Of note, the presence of the glutamate degrading enzyme GPT excluded further experimentation with exogenous glutamate, since such experiments would not result in meaningful parameters for potency and/or efficacy. The responses of LY354740 and LY341495 were affected by the different endogenous glutamate concentrations from the culture medium. LY354740 peaks increased upon reduction of endogenous glutamate levels. On the contrary, LY341495 peaks were reduced when endogenous glutamate levels were lowered. Both observations indicate competition of the two molecules for the orthosteric glutamate binding site, which has been shown in radioligand binding experiments with [^{3}H]LY354740 and [^{3}H]LY341495 as the radioligands.[40,41]

Agonist LY354740 and antagonist LY341495 induced concentration-dependent responses at low levels of endogenous glutamate

Once the assay conditions were optimized, the potency of agonist LY354740 and antagonist LY341495 were determined. For LY354740 the impedance increased concentration-dependently with a "positive" peak (i.e. positive ΔCI values) around 10 minutes, then gradually decreasing with a second 'shoulder' peak around 20 minutes (Fig. 2A). A concentration-response curve obtained from the maximum peak levels within the first 60 minutes after stimulation revealed a pEC_{50} value of 6.70 ± 0.24 (Table 2; Fig. 2B). This potency was lower than observed in other assay types such as Ca^{2+} mobilization (pEC_{50} 7.4)[42] and similar to the potency obtained in electrophysiology experiments on hippocampal slices (pEC50 6.9).[43]

Table 2 Potency (pEC_{50} or pIC_{50}) of ligands at the $mGlu_2$ receptor in CHO-K1_$hmGlu_2$ cells after refreshment of medium by serum-free medium containing GPT (3 U/ml) and pyruvate (3 mM).

Compound		pEC_{50}	pIC_{50}
LY354740	*Agonist*	6.70 ± 0.24	-
LY341495	*Antagonist*	-	8.15 ± 0.09
JNJ-46281222	*PAM*	7.17 ± 0.24	-
RO4491533	*NAM*	-	7.34 ± 0.19

pEC_{50}/IC_{50} data are shown as mean ± SEM from at least three individual experiments performed in duplicate.

Stimulation with increasing concentrations of the antagonist LY341495 resulted in concentration-dependent negative peaks with a minimum around 15 minutes (Fig. 2A). For low concentrations it took around 30 minutes to return to baseline, while at 0.1 and 1 μM LY341495 the trace returned to baseline after 120 or 180 minutes, respectively (data not shown). A pIC_{50} value of 8.15 ± 0.09 was obtained from the minimum peak levels (Fig. 2B; Table 2), which was in agreement with potencies reported before using cAMP, Ca^{2+}-mobilization and [^{35}S]GTPγS assays.[14,31] The concentration-response curve of LY354740 had a pseudo-Hill coefficient of around unity (n_H 0.92) compared to the curve of LY341495 that was much steeper (n_H -1.81). As mentioned before, LY341495 showed negative responses in Cell Index, indicating that it exhibits an opposite pharmacological effect compared to the agonist LY354740, resulting in an opposite impedance measured. Similar observations have been seen using other label-free systems (i.e. the CellKey and EPIC system), in which agonists induced an increase in response, while inverse agonists caused a decrease in response.[1,44] However, these studies do not present a mechanistic understanding as they were performed on two non-disclosed GPCRs. Given that in these studies inverse agonists induced negative responses, LY341495 may also be an inverse agonist at the $mGlu_2$ receptor, especially since the concentration of endogenous glutamate was reduced to a level only slightly able to activate the receptor.

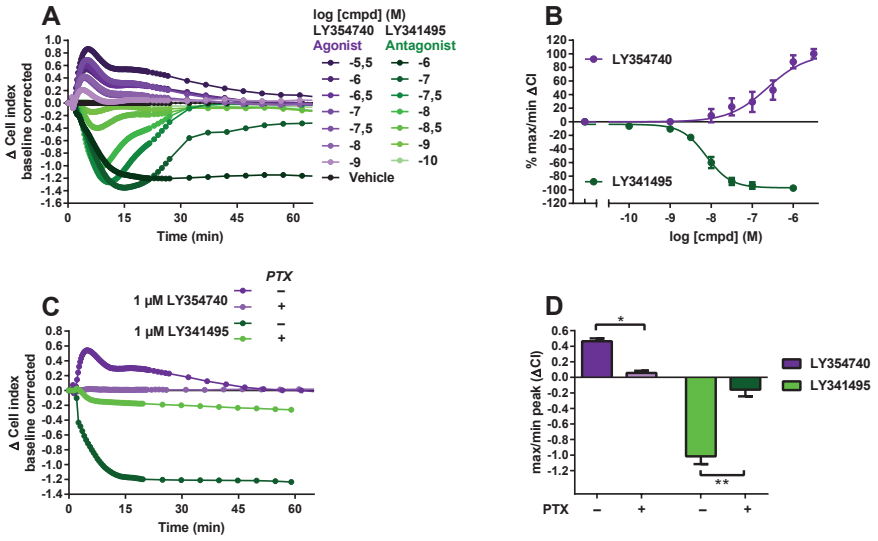

Figure 2. Agonist LY354740 and antagonist LY341495-induced concentration-effect responses at low concentration of endogenous glutamate (1.6 ± 0.09 μM). A) Cells were stimulated by increasing concentrations of agonist LY354740 or antagonist LY341495. B) Concentration-response curves were obtained from maximum (LY354740) or minimum (LY341495) ΔCI values and normalized from vehicle-induced ΔCI (0%) to maximum or minimum ΔCI (100% or -100% respectively). C) Responses of 1 μM LY354740 and 1 μM LY341495 in the absence or presence of PTX (300 ng/ml). D) Comparison of maximum peak values induced by 1 μM LY354740 and minimum peak values induced by 1 μM LY341495 in the absence or presence of PTX (300 ng/ml). All xCELLigence traces are from representative experiments performed in duplicate. Concentration-response curves (panel B) represent mean ± SEM of at least three individual experiments performed in duplicate. Bar graphs represent mean ± SEM of at least three individual experiments performed in duplicate. Statistical analysis was performed using a two-tailed unpaired Student's t-test. * $p < 0.01$, ** $p < 0.001$.

Finally, the selective G$\alpha_{i/o}$ inhibitor PTX was used to evaluate whether the effects induced by the agonist LY354740 and antagonist LY341495 were mediated via G$\alpha_{i/o}$ protein-dependent signaling. Responses of LY354740 and LY341495 were almost completely lost in the presence of PTX, which indicated that the opposite compound-induced cellular responses were both resulting from signaling via G$\alpha_{i/o}$ (Fig. 2C,D). The residual responses in the presence of PTX most likely represent incomplete inhibition of the G$\alpha_{i/o}$-mediated signaling.

Agonist efficacy was increased by PAM and decreased by NAM treatment

Before measuring the effect of allosteric modulators on agonist efficacy, responses of a PAM and a NAM in the absence of exogenous agonist were determined. Both allosteric modulators showed responses on their own without added agonist, which were likely caused by the low level of endogenous glutamate (1.6 ± 0.09 μM) still present in the serum-free culture medium with GPT (Table 1). Stimulation with the PAM JNJ-46281222 resulted in positive dose-dependent responses, leading to a pEC$_{50}$ of 7.17 ± 0.24 for this compound (Table 2; Fig. 3A,B).

The potency of the PAM was lower than in a [^{35}S]GTPγS assay as shown in **chapter 2** (pEC_{50} of 7.71).[23] This may be caused by the concentration of endogenous glutamate that is lower than the typical EC_{20} glutamate concentrations used in standard [^{35}S]GTPγS assays used to determine the potency of allosteric modulators or by the differences in assay types.[45,46] Treatment with the NAM RO4491533 induced negative peaks in Cell Index yielding a pIC_{50} value of 7.34 ± 0.19, which was lower than observed before in a [^{35}S]GTPγS assay (pIC_{50} 8.7).[45] In this case the difference may be due to the high EC_{80} glutamate concentration used in the [^{35}S]GTPγS assay or, again, due to the differences in assay type. The concentration-response curve of JNJ-46281222 was shallow with a pseudo-Hill coefficient of 0.59 compared to RO4491533's which was around unity (n_H -1.02). Of note, this is the first observation that Cell Indices go up in the presence of a PAM and down when using a NAM, like JNJ-46281222 and RO4491533, respectively. In that sense, the effects of allosteric modulators for the $mGlu_2$ receptor resemble orthosteric compound-induced responses as described above.

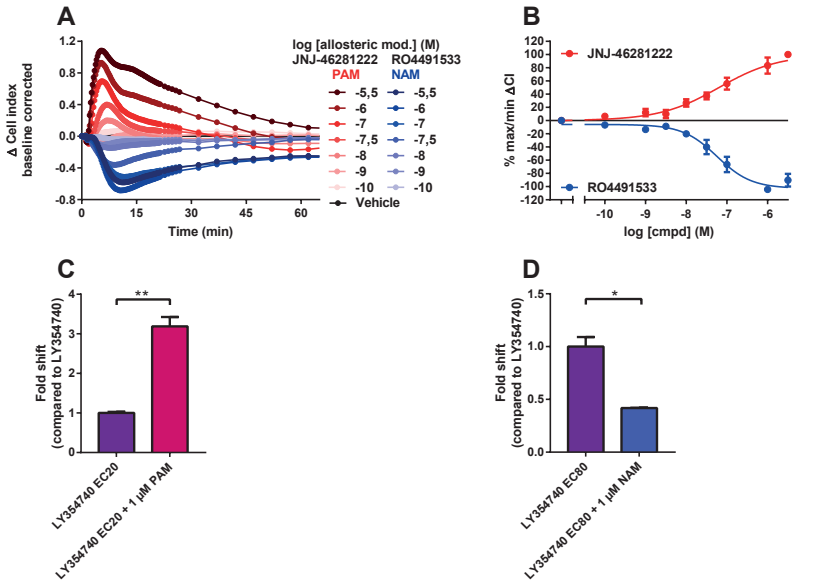

Figure 3. Positive allosteric modulator (PAM) JNJ-46281222 and negative allosteric modulator (NAM) RO4491533-induced responses at low concentration (1.6 ± 0.09 μM) of endogenous glutamate. A) Cells were stimulated by increasing concentrations of JNJ-46281222 or RO4491533. B) Concentration-response curves were obtained from maximum (JNJ-46281222) or minimum (RO4491533) ΔCI values and normalized from vehicle-induced ΔCI values (0%) to maximum (100%) or minimum (-100%) ΔCI values. C) Responses induced by an EC_{20} LY354740 concentration in the absence and presence of 1 μM JNJ-46281222. D) Responses induced by an EC_{80} LY354740 concentration in the absence and presence of 1 μM RO4491533. xCELLigence traces are from representative experiments performed in duplicate. Bar graphs represent mean ± SEM of at least three experiments performed in duplicate, where data was normalized to the response of PAM or NAM on itself (1.0). Statistical analysis was performed using a two-tailed unpaired Student's t-test. * $p < 0.01$, ** $p < 0.001$.

To study the effects of a PAM on agonist efficacy, cellular responses to an LY354740 concentration equivalent to its EC_{20} response (30 nM) were determined in the absence and presence of 1 μM JNJ-46281222. This resulted in a significant 3-fold increase in the LY354740 peak response, confirming that JNJ-46281222 behaves as a PAM for this agonist (Fig. 3C). The effect of 1 μM of the NAM RO4491533 was determined using an LY354740 concentration equivalent to its EC_{80} concentration (300 nM). This yielded a significant, more than twofold reduction in the response of LY354740 (Fig. 3D), which is a typical NAM effect. These experiments showed that xCELLigence is able to assess the effects of allosteric modulators on agonist efficacy, which is in line with work reported by Chen *et al.* (2015)[47] on allosteric modulation of the M_4 muscarinic acetylcholine receptor.

LY341495 pre-treatment revealed constitutive receptor activity

The maximum peak height of the agonist LY354740 was much lower compared to the negative peaks of the antagonist LY341495 (Fig. 2 A,C). In order to study the underlying mechanism, cells were pretreated with 1 μM LY341495 1 hour prior to stimulation (Fig. 4A). The response of subsequent stimulation by 1 μM LY354740 was increased significantly from an average max peak of 0.47 ± 0.04 ΔCI up to a level of 1.21 ± 0.16 (Fig. 4B,C). This was opposite to the expected loss of agonist response by the pre-treatment with a high concentration of a competitive antagonist that is still present at the time of stimulation with agonist. The effect of LY341495 pre-treatment on the LY354740 peak was concentration-dependent: pre-treatment with 10 nM LY341495 slightly increased LY354740 traces, whereas 100 nM and 1 μM LY341495 were able to further and significantly increase the peak height of 1 μM LY354740 stimulation (Fig. 4C). All traces reached baseline after 30-45 minutes. In contrast to the other traces, the trace of 1 μM LY354740 after pre-treatment with 1 μM LY341495 increased slightly after that point reaching a plateau around 0.4 ΔCI. Treatment with the selective $G\alpha_{i/o}$ inhibitor PTX revealed that the LY354740 response after pre-treatment with LY341495 was lost in the presence of PTX, indicating that this is also a mostly, if not fully, $G\alpha_{i/o}$-mediated response (Fig. 4B,C). In contrast to LY341495, pre-treatment with 1 μM of the NAM RO4491533 resulted in a typical reduced agonist response of LY354740 (Fig. 4D,E).

Together, these results show that LY341495 increased the window of agonist response by almost 3-fold. This is a larger increase than can be explained by the level of endogenous glutamate (1.6 μM at stimulation), which might enable approximately 10% receptor activation. Blockade of glutamate binding may thus increase the agonist-induced response by a similar level. Therefore, we believe that the increased agonist response after pre-treatment with LY341495 indicates that the receptor is constitutively active and that LY341495 is behaving as an inverse agonist. This was confirmed by the fact that, in contrast to pre-treatment with LY341495, pre-treatment by the NAM RO4491533 resulted in a decreased agonist response (Fig. 4D,E). Such a decreased agonist response is similar to the expected effect of pre-treatment with a neutral antagonist.

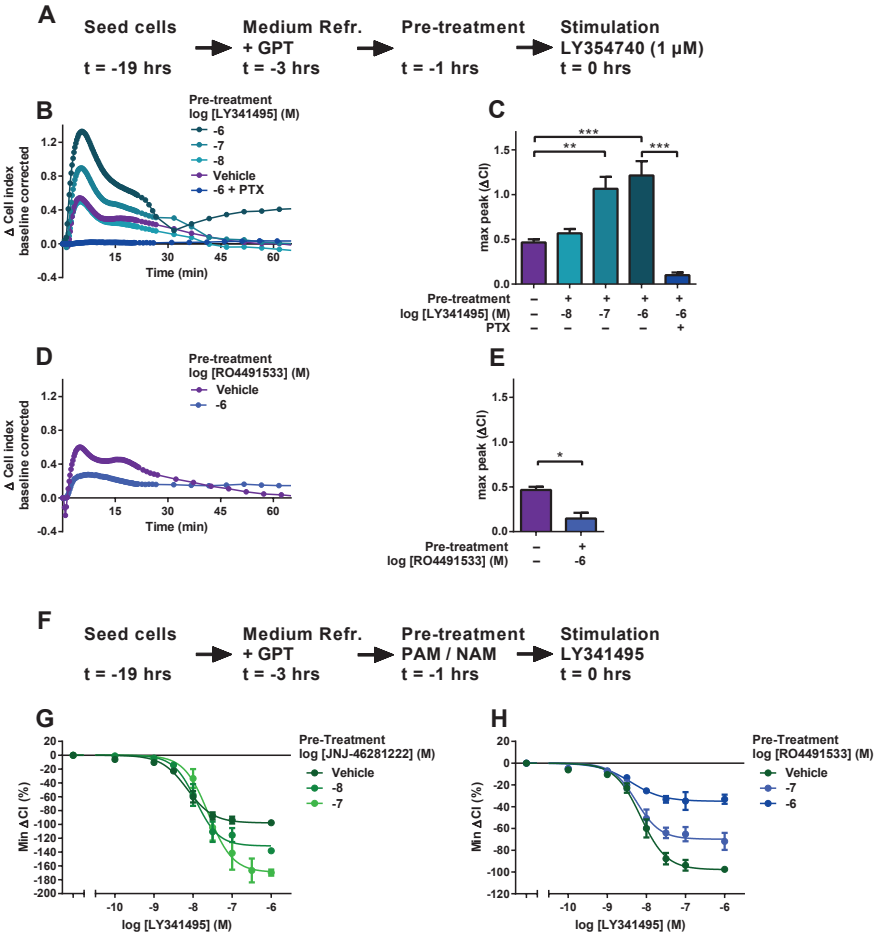

Figure 4. Evaluation of LY341495 inverse agonism. A) Set-up of experiments. B) Cells were stimulated with 1 µM LY354740 after pre-treatment with increasing concentrations of LY341495. Pre-treatment with 1 µM LY341495 was also performed in the presence of PTX (300 ng/ml). C) Comparison of maximum peak values induced by 1 µM LY354740 after pre-treatment with increasing concentrations of LY341495. Pre-treatment with 1 µM LY341495 was also performed in the presence of PTX (300 ng/ml). D) Cells were stimulated with 1 µM LY354740 after pre-treatment with 1 µM NAM RO4491533 or vehicle. E) Comparison of maximum peak values induced by 1 µM LY354740 after pre-treatment with 1 µM RO4491533 or vehicle. F) Set-up of experiments. G,H) Concentration-response curves were obtained from minimum ΔCI values and normalized from vehicle-induced ΔCI values (0%) to minimum (-100%) ΔCI values after vehicle pre-treatment. xCELLigence traces are from representative experiments performed in duplicate. Bar graphs represent mean ± SEM of at least three individual experiments performed in duplicate. Concentration-response curves represent mean ± SEM of at least three individual experiments performed in duplicate. Statistical analysis was performed using a one-way ANOVA with Dunnett's (C) post-test or using a two-tailed unpaired Student's t-test (E). * $p < 0.01$, ** $p < 0.001$, *** $p < 0.0001$.

To further assess the inverse agonism of LY341495, concentration-response curves were obtained after pre-treatment with increasing concentrations of the PAM JNJ-46281222 (Fig. 4F,G). The curves shifted from a pIC_{50} of 8.15 ± 0.09 without PAM pre-treatment to 7.89 ± 0.13 in the presence of 10 nM PAM, to 7.55 ± 0.13 in the presence of 100 nM PAM. Such a modulatory shift in potency in the presence of a PAM is typical for an inverse agonist and is not expected for a neutral antagonist.[48,49] Next to the shift in potency, increasing concentrations of PAM pre-treatment resulted in a larger window of LY341495 response. On the contrary, pre-treatment with NAM RO4491533 did not result in significant alteration in LY341495 potency (Fig. 4H), a pIC_{50} values of 8.22 ± 0.14 in the presence of 100 nM NAM and 8.35 ± 0.12 in the presence of 1 μM NAM were found. The efficacy window of LY341495 was reduced dose-dependently up to more than 60% at 1 μM NAM, showing that the NAM is not only able to strongly reduce agonist efficacy without changing potency,[31] but similarly affects the inverse agonist activity of LY341495.

A shift in LY341495 potency induced by the PAM could be the reason of increased potency of endogenous glutamate. However, the large shift in efficacy cannot be explained by presence of endogenous agonist, nor can the large reduction of efficacy after NAM pre-treatment. Together, inverse agonism by LY341495 was further confirmed by these PAM and NAM pre-treatment experiments in this system that measures phenotypic morphological responses of the whole cell, in this case via the $G\alpha_{i/o}$ signaling pathway. On a separate note, receptor desensitization induced by endogenous glutamate could be of concern here. However, the $mGlu_2$ receptor is known to be resistant to agonist-induced desensitization which was also seen in our hands in repeated stimulation experiments (data not shown).[50,51] Doumazane *et al.* (2013)[52] found a higher FRET signal after application of 1 μM LY341495, similar to the effect of LY341495 pre-treatment presented here. These authors reasoned that this effect was mediated by either constitutive activity or presence of endogenous glutamate, which was not elucidated any further. Inverse agonism by LY341495 has been reported before. For example, DiRaddo *et al.* (2014)[53] found that LY341495 was behaving as inverse agonist after pre-treatment with agonist, when using the Glo-sensor cAMP assay with CHO-K1 cells stably expressing the $mGlu_2$ receptor. Moreover, inverse agonism by LY341495 at the $mGlu_2$ receptor was also seen in studies investigating receptor cross-signaling in $mGlu_2$-$5HT_{2A}$ heterocomplexes.[54,55] Generally, LY341495 is considered a neutral antagonist for the $mGlu_2$ receptor[14,15] as most *in vitro* assays did not yield inverse agonism, which is likely due to differences in cell lines or assay systems used.

CONCLUSION

In conclusion, we have validated the use of the impedance-based biosensor xCELLigence system to study $mGlu_2$ pharmacology. High levels of endogenous glutamate reduced the agonist activation window and therefore efforts were made to reduce these. We characterized $mGlu_2$ signaling with an agonist, antagonist and both positive and negative allosteric modulators; the latter two modulated the response of both orthosteric agonist and antagonist. Remarkable and opposite effects on impedance were observed for compounds with opposite pharmacological effects. Both the agonist and PAM increased impedance whereas the antagonist and NAM decreased this read-out. Importantly, we show that constitutive $mGlu_2$ receptor activity could be inhibited by the antagonist LY341495 which therefore behaved as an inverse agonist in the system used. The present study provides an extended ensemble of the properties of $mGlu_2$ ligands in comparison to conventional *in vitro* assays. Together the results show that label-free biosensors, such as the xCELLigence, are valuable tools in drug discovery and pharmacological profiling at the $mGlu_2$ receptor as well as other GPCRs

REFERENCES

1. Scott CW, Peters MF. *Drug Discov Today*. **2010**; 15: 704–716.
2. Fang Y. *Expert Opin Drug Discov*. **2015**; 10: 331–343.
3. Yu N, Atienza JM, Bernard J, Blanc S, Zhu J, Wang X, Xu X, Abassi Y. *Anal Chem*. **2006**; 78: 35–43.
4. Halai R, Cooper M a. *Expert Opin Drug Discov*. **2012**; 7: 123–31.
5. Hillger JM, Lieuw W-L, Heitman LH, IJzerman AP. *Drug Discov Today*. **2017**; 0.
6. Lundstrom K. *Expert Opin Drug Discov*. **2017**; 12: 335–343.
7. Hillger JM, Schoop J, Boomsma DI, Eline Slagboom P, IJzerman AP, Heitman LH. *Biosens Bioelectron*. **2015**; 74: 233–242.
8. Nederpelt I, Vergroesen RD, IJzerman AP, Heitman LH. *Biosens Bioelectron*. **2016**; 79: 721–727.
9. Grundmann M, Tikhonova IG, Hudson BD, Milligan G, Kenakin T, Grundmann M, Tikhonova IG, Hudson BD, Smith NJ, Mohr K, Ulven T. *Cell Chem Biol*. **2016**; 23: 392–403.
10. Marek GJ. *Eur J Pharmacol*. **2010**; 639: 81–90.
11. Niswender CM, Conn PJ. *Annu Rev Pharmacol Toxicol*. **2010**; 50: 295–322.
12. Patil ST, Zhang L, Martenyi F, Lowe SL, Jackson KA, Andreev B V, Avedisova AS, Bardenstein LM, Gurovich IY, Morozova MA, Mosolov SN, Neznanov NG, Reznik AM, Smulevich AB, Tochilov VA, Johnson BG, Monn JA, Schoepp DD. *Nat Med*. **2007**; 13: 1102–7.

13. Adams DH, Kinon BJ, Baygani S, Millen BA, Velona I, Kollack-Walker S, Walling DP. *BMC Psychiatry*. **2013**; 13: 143.

14. Kingston A., Ornstein P., Wright R., Johnson B., Mayne N., Burnett J., Belagaje R, Wu S, Schoepp D. *Neuropharmacology*. **1998**; 37: 1–12.

15. Witkin JM, Mitchell S, Wafford K, Carter G, Gilmour G, Li J, Eastwood B, Overshiner C, Li X, Rorick-Kehn L, Rasmussen K, Anderson W, Nikolayev A, Tolstikov V, Kuo M-S, Catlow J, Li R, Smith S, Mitch C, Ornstein P, Swanson S, Monn J. *J Pharmacol Exp Ther*. **2017**: jpet.116.238121.

16. Conn PJ, Lindsley CW, Meiler J, Niswender CM. *Nat Rev Drug Discov*. **2014**; 13: 692–708.

17. Wu H, Wang C, Gregory KJ, Han GW, Cho HP, Xia Y, Niswender CM, Katritch V, Meiler J, Cherezov V, Conn PJ, Stevens RC. *Science*. **2014**; 344: 58–64.

18. Doré AS, Okrasa K, Patel JC, Serrano-Vega M, Bennett K, Cooke RM, Errey JC, Jazayeri A, Khan S, Tehan B, Weir M, Wiggin GR, Marshall FH. *Nature*. **2014**; 511: 557–62.

19. Gregory KJ, Dong EN, Meiler J, Conn PJ. *Neuropharmacology*. **2011**; 60: 66–81.

20. Christopoulos A, Changeux J-P, Catterall WA, Fabbro D, Burris TP, Cidlowski JA, Olsen RW, Peters JA, Neubig RR, Pin J-P, Sexton PM, Kenakin TP, Ehlert FJ, Spedding M, Langmead CJ. *Pharmacol Rev*. **2014**; 66: 918–947.

21. Lavreysen H, Langlois X, Ahnaou A, Drinkenburg W, te Riele P, Biesmans I, Van der Linden I, Peeters L, Megens A, Wintmolders C, Cid JM, Trabanco AA, Andrés JI, Dautzenberg FM, Lütjens R, Macdonald G, Atack JR. *J Pharmacol Exp Ther*. **2013**; 346: 514–27.

22. Galici R, Echemendia NG, Rodriguez AL, Conn PJ. *J Pharmacol Exp Ther*. **2005**; 315: 1181–7.

23. Doornbos MLJ, Pérez-Benito L, Tresadern G, Mulder-Krieger T, Biesmans I, Trabanco AA, Cid JM, Lavreysen H, IJzerman AP, Heitman LH. *Br J Pharmacol*. **2016**; 173: 588–600.

24. Cid JM, Tresadern G, Duvey G, Lütjens R, Finn T, Rocher J, Poli S, Vega JA, de Lucas AI, Matesanz E, Linares ML, Andrés JI, Alcazar J, Alonso JM, Macdonald GJ, Oehlrich D, Lavreysen H, Ahnaou A, Drinkenburg W, Mackie C, Pype S, Gallacher D, Trabanco AA. *J Med Chem*. **2014**; 57: 6495–512.

25. Lavreysen H, Ahnaou A, Drinkenburg W, Langlois X, Mackie C, Pype S, Lütjens R, Le Poul E, Trabanco AA, Nuñez JMC. *Pharmacol Res Perspect*. **2015**; 3: e00096.

26. Lavreysen H, Langlois X, Ver Donck L, Cid Nuñez JM, Pype S, Lütjens R, Megens A. *Pharmacol Res Perspect*. **2015**; 3: e00097.

27. Salih H, Anghelescu I, Kezic I, Sinha V, Hoeben E, Van Nueten L, De Smedt H, De Boer P. *J Psychopharmacol*. **2015**; 29: 414–425.

28. Kent JM, Daly E, Kezic I, Lane R, Lim P, De Smedt H, De Boer P, Van Nueten L, Drevets WC, Ceusters M. *Prog Neuro-Psychopharmacology Biol Psychiatry*. **2016**; 67: 66–73.

29. Cook D, Brown D, Alexander R, March R, Morgan P, Satterthwaite G, Pangalos MN. *Nat Rev Drug Discov*. **2014**; 13: 419–31.

30. Goeldner C, Ballard TM, Knoflach F, Wichmann J, Gatti S, Umbricht D. *Neuropharmacology*. **2013**; 64: 337–46.

31. Campo B, Kalinichev M, Lambeng N, El Yacoubi M, Royer-Urios I, Schneider M, Legrand C, Parron D, Girard F, Bessif A, Poli S, Vaugeois J-M, Le Poul E, Celanire S. *J Neurogenet*. **2011**; 25: 152–66.

32. Van Gool M, Alonso De Diego SA, Delgado O, Trabanco AA, Jourdan F, Macdonald GJ, Somers M, Ver Donck L. *ChemMedChem*. **2017**; 12: 905–912.

33. Xi B, Yu N, Wang X, Xu X, Abassi YA. *Biotechnol J*. **2008**; 3: 484–495.

34. Wahrheit J, Nicolae A, Heinzle E. *BMC Proc*. **2013**; 7: P44.

35. Pin JP, De Colle C, Bessis AS, Acher F. *Eur J Pharmacol*. **1999**; 375: 277–94.

36. Lavreysen H, Le Poul E, Van Gompel P, Dillen L, Leysen JE, Lesage ASJ. *Mol Pharmacol*. **2002**; 61: 1244–54.

37. Sengmany K, Singh J, Stewart GD, Conn PJ, Christopoulos A, Gregory KJ. *Neuropharmacology*. **2017**; 115: 60–72.

38. Scandroglio P, Brusa R, Lozza G, Mancini I, Petrò R, Reggiani A, Beltramo M. *J Biomol Screen*. **2010**; 15: 1238–47.

39. Lieb S, Michaelis S, Plank N, Bernhardt G, Buschauer A, Wegener J. *Pharmacol Res*. **2016**; 108: 65–74.

40. Johnson BG, Wright R a, Arnold MB, Wheeler WJ, Ornstein PL, Schoepp DD. *Neuropharmacology*. **1999**; 38: 1519–29.

41. Schaffhauser H, Richards JG, Cartmell J, Chaboz S, Kemp JA, Klingelschmidt A, Messer J, Stadler H, Woltering T, Mutel V. *Mol Pharmacol*. **1998**; 53: 228–33.

42. Monn JA, Prieto L, Taboada L, Pedregal C, Hao J, Reinhard MR, Henry SS, Goldsmith PJ, Beadle CD, Walton L, Man T, Rudyk H, Clark B, Tupper D, Baker SR, Lamas C, Montero C, Marcos A, Blanco J, Bures M, Clawson DK, Atwell S, Lu F, Wang J, Russell M, Heinz BA, Wang X, Carter JH, Xiang C, Catlow JT, Swanson S, Sanger H, Broad LM, Johnson MP, Knopp KL, Simmons RM a, Johnson BG, Shaw DB, McKinzie DL. *J Med Chem*. **2015**; 58: 1776–1794.

43. Kilbride J, Huang L, Rowan MJ, Anwyl R. *Eur J Pharmacol*. **1998**; 356: 149–157.

44. Lee PH, Gao A, van Staden C, Ly J, Salon J, Xu A, Fang Y, Verkleeren R. *Assay Drug Dev Technol*. **2008**; 6: 83–94.

45. Pérez-Benito L, Doornbos MLJ, Cordomí A, Peeters L, Lavreysen H, Pardo L, Tresadern G. *Structure*. **2017**; 25: 1–10.

46. Kenakin TP. A Pharmacology Primer - fourth edition, Academic Press: San Diego, **2014**.

47. Chen ANY, Malone DT, Pabreja K, Sexton PM, Christopoulos A, Canals M. *J Biomol Screen*. **2015**; 20: 646–654.

48. Lane JR, May LT, Parton RG, Sexton PM, Christopoulos A. *Nat Chem Biol*. **2017**; 13: 929–937.

49. Canals M, Lane JR, Wen A, Scammells PJ, Sexton PM, Christopoulos A. *J Biol Chem*. **2012**; 287: 650–659.

50. Iacovelli L, Molinaro G, Battaglia G, Motolese M, Di Menna L, Alfiero M, Blahos J, Matrisciano F, Corsi M, Corti C, Bruno V, De Blasi A, Nicoletti F. *Mol Pharmacol*. **2009**; 75: 991–1003.

51. Lennon SM, Rivero G, Matharu A, Howson P a, Jane DE, Roberts PJ, Kelly E. *Eur J Pharmacol*. **2010**; 649: 29–37.

52. Doumazane E, Scholler P, Fabre L, Zwier JM, Trinquet E, Pin J-P, Rondard P. *Proc Natl Acad Sci U S A*. **2013**; 110: E1416-25.

53. DiRaddo JO, Miller EJ, Hathaway H a, Grajkowska E, Wroblewska B, Wolfe BB, Liotta DC, Wroblewski JT. *J Pharmacol Exp Ther*. **2014**; 349: 373–82.

54. Fribourg M, Moreno JL, Holloway T, Provasi D, Baki L, Mahajan R, Park G, Adney SK, Hatcher C, Eltit JM, Ruta JD, Albizu L, Li Z, Umali A, Shim J, Fabiato A, MacKerell AD, Brezina V, Sealfon SC, Filizola M, González-Maeso J, Logothetis DE. *Cell*. **2011**; 147: 1011–23.

55. Baki L, Fribourg M, Younkin J, Eltit JM, Moreno JL, Park G, Vysotskaya Z, Narahari A, Sealfon SC, Gonzalez-Maeso J, Logothetis DE. *Pflügers Arch - Eur J Physiol*. **2016**; 468: 775–793.

CHAPTER 7

Conclusions and future perspectives

7

Over the last decades, the number of ligands for the metabotropic glutamate receptor 2 ($mGlu_2$) has vastly increased.[1] Initially the focus of discovery programs was on ligands targeting the orthosteric binding site, which later shifted to the allosteric site for which selectivity is more easily achieved.[2] Despite these tremendous efforts, no drug targeting the $mGlu_2$ receptor has reached the market so far. Therefore this thesis aimed to increase the understanding of the mechanism of action of the $mGlu_2$ receptor. To achieve this, a variety of pharmacological concepts are covered in this thesis, including allosteric modulation, binding kinetics, constitutive activity, inverse agonism and insurmountability. To study these concepts novel assays and tool compounds were developed. Ultimately, a better understanding of the *in vitro* parameters involved in *in vivo* efficacy contributes to the development of safe and efficacious drug therapies. This chapter combines the conclusions from this thesis, followed by the future perspectives that arise from these conclusions.

CONCLUSIONS

The concept of allosteric modulation has been widely evaluated in the field of G protein-coupled receptors (GPCRs).[2] Especially for class C GPCRs the allosteric binding site in the seven-transmembrane (7TM) domain is being explored thoroughly, as it provides better opportunities for selectivity compared to the orthosteric binding site located in the extracellular Venus Flytrap (VFT) domain.[1] Understanding of the architecture of the mGlu receptor allosteric binding site is based on crystal structures of the negative allosteric modulator (NAM)-bound 7TM domain of the $mGlu_1$ and $mGlu_5$ receptors.[3–6] The allosteric binding site of the $mGlu_2$ receptor has been elucidated using mutagenesis studies, which revealed overlapping binding sites for positive allosteric modulators (PAMs) and NAMs.[7–11] Moreover, these studies revealed a transmission switch (i.e. amino acid residues that relocate upon the conformational change from the inactive to active state of the 7TM domain or vice versa) that is located in the same receptor region as the agonist binding site in class A GPCRs.[12]

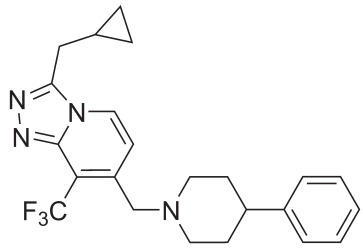

Figure 1. Structure of JNJ-46281222.

In **Chapter 2**, JNJ-46281222 (Fig. 1) was characterized as an $mGlu_2$-selective, highly potent PAM with nanomolar affinity. This ligand and its radiolabeled version were therefore used as tool compounds throughout this thesis. JNJ-46281222 increased the potency and affinity of agonists, which is typical for a PAM. Furthermore, it behaved as PAM agonist with a submaximal intrinsic activity, i.e. activity on its own. The maximum binding capacity of JNJ-46281222 was increased by the presence of the agonist glutamate without changing its affinity, which indicated a two-way mechanism of allosteric modulation (Fig. 2). On the other hand, JNJ-46281222's maximum binding and affinity were decreased by the presence of GTP (which initiates dissociation of the G protein), indicating its preference for a G protein bound state of the receptor. Using computational docking and molecular dynamics studies, the PAM binding mode was visualized. Subsequent binding experiments using mutant receptors confirmed this PAM's binding mode.[11,13]

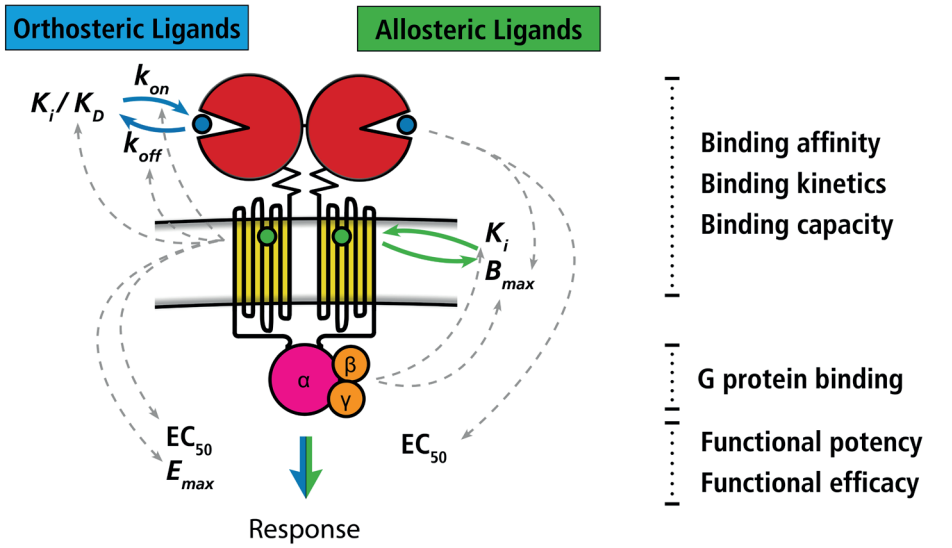

Figure 2. Summary of the findings obtained in **Chapters 2** and **3**. Allosteric modulators were shown to affect the potency, affinity and/or efficacy of orthosteric ligands (blue bar in figure): PAMs were shown to increase the affinity (K_i/K_D) and potency (EC_{50}) of orthosteric agonists, by reducing the dissociation rate constant k_{off}. Furthermore, they increase the efficacy (E_{max}) of orthosteric agonists. NAMs do not affect agonist affinity or potency, but decrease the efficacy drastically. Furthermore, NAMs may probe-dependently alter the kinetic parameters (k_{on}, k_{off}) of agonists leaving affinity and potency unchanged. Both PAMs and NAMs do not affect the affinity and potency of antagonists. Vice versa, orthosteric ligands were shown to affect the potency and maximum binding capacity (B_{max}) of allosteric ligands (green bar in figure). Agonists glutamate and LY354740 increase the maximum PAM binding capacity without changing the PAM affinity. Furthermore, the PAM potency is increased at increasing glutamate concentrations, whereas NAM potency is not affected by the presence of an agonist. GTP-initiated dissociation of the G protein (pink and orange) results in a decreased PAM binding affinity and binding capacity, indicating the importance of the G protein for PAM binding.

Chapter 3 describes the first kinetic study of orthosteric ligand binding at the $mGlu_2$ receptor from an allosteric modulation perspective. Kinetic radioligand binding assays were set up to determine the kinetic binding parameters for the endogenous $mGlu_2$ agonist glutamate for the first time. Its off-rate is fast, resulting in a residence time (RT) below 1 minute, whereas the on-rate is relatively high, resulting in an affinity ($K_D = k_{off} / k_{on}$) comparable to the K_i value obtained from equilibrium binding assays. Furthermore, the affinity and potency of the orthosteric ligands tested were strongly correlated to their association rate constants k_{on}, showing that on-rate is driving the affinity and thus target occupancy of orthosteric $mGlu_2$ ligands. The off-rates of the endogenous agonist glutamate and synthetic agonist LY354740 were decreased by the presence of a PAM, which resulted in increased affinities, whereas on-rates were unaffected. The NAM RO4491533 increased both on- and off-rates of glutamate without changing the affinity, but did not alter these kinetic parameters for agonist LY354740, indicating probe-dependency. Of note, the experiments had to be performed at 0°C to enable

recording of the association and dissociation of the radioligand used. Ideally, these should be done at 37°C, but this was practically unfeasible due to very fast binding events at that temperature.

The next step was to study the binding kinetics of a novel series of $mGlu_2$ PAMs. **Chapter 4** starts with classical determinations of *in vitro* affinity and potency of 41 novel 7−Aryl-1,2,4-triazolo[4,3−*a*]pyridines and 4 reference PAMs. All compounds behaved as functional and selective $mGlu_2$ PAMs with micromolar to subnanomolar affinity and potency. In addition to these classical parameters kinetic parameters k_{on} and k_{off} were determined and RTs were calculated subsequently. To do so, a kinetic radioligand binding assay using the scintillation proximity assay (SPA) was developed. In addition to typical structure-affinity/activity relationships (SAR), structure-kinetics relationships (SKR) of these novel allosteric modulators were obtained. The PAMs showed various kinetic profiles in which k_{on} values ranged over 3 orders of magnitude, whereas k_{off} and thus RT were within a small 10-fold range. As seen for orthosteric ligands in **chapter 3**, the affinity of all PAMs was k_{on}-driven, showing that this likely is a receptor-specific characteristic.

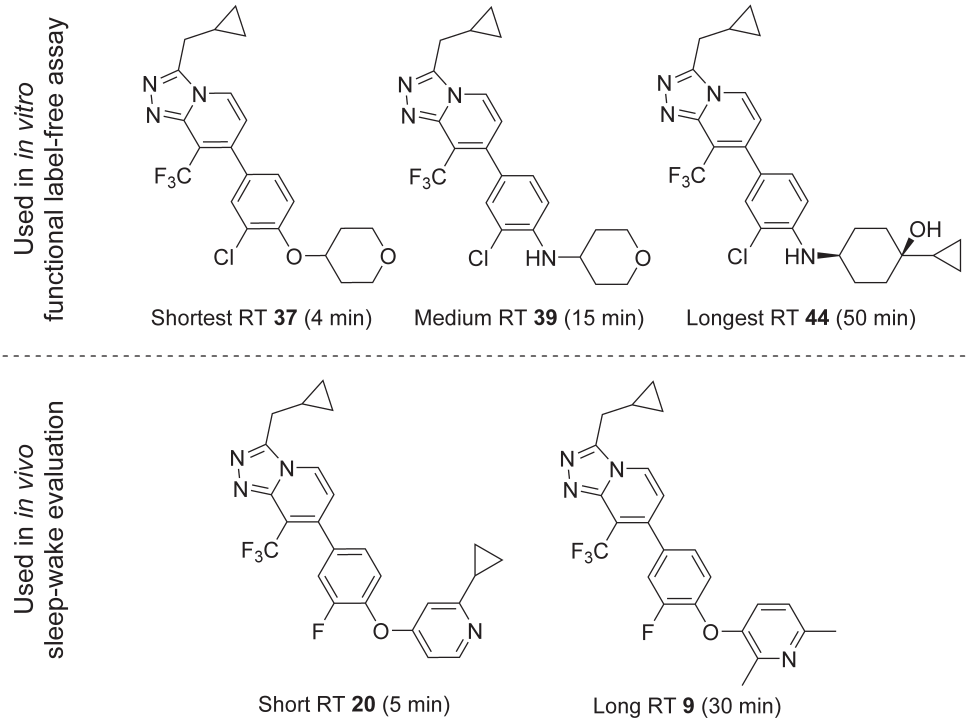

Figure 3. Structure of the shortest RT PAM (**37**), a medium RT PAM (**39**) and the longest RT PAM (**44**) used for evaluation in an *in vitro* functional label-free assay and the short RT PAM (**20**) and long RT PAM (**9**) used in *in vivo* sleep-wake evaluation, as described in **Chapter 4**.

Subsequently, the shortest RT PAM **37**, a medium RT PAM **39** and long RT PAM **41** (Fig. 3) were evaluated for their functional efficacy in the label-free xCELLigence assay detecting changes in cell morphology. The results obtained showed a correlation between RT and the duration of action of the PAM in this label-free assay. Ultimately, the translation from *in vitro* binding kinetics to *in vivo* efficacy was evaluated. Two PAMs with similar affinity, potency and pharmacokinetics (PK), but with divergent RTs were selected. Compared to short RT PAM **20**, the effects of the long RT PAM **9** on sleep-wake states were translated significantly better into sustained inhibition of rapid eye movement sleep, which is a well-established *in vivo* measure for $mGlu_2$ efficacy. This provides a first hint that *in vivo* $mGlu_2$ PAM efficacy benefits from a longer *in vitro* RT.

The association rate constant k_{on} is often believed to equal the diffusion rate limit. However, this thesis shows that for both orthosteric and allosteric ligands of the $mGlu_2$ receptor the k_{on} values are spread over multiple orders of magnitude whereas k_{off} values are within a small range. The diffusion rate limit is around 10^8 - 10^9 $M^{-1}s^{-1}$,[14] the k_{on} values obtained in this thesis range from 10^3 – 10^7 $M^{-1}s^{-1}$, which clearly shows that the k_{on} value is a ligand-specific characteristic that is not equal between ligands and is not equal to the diffusion rate limit either.

Together, these results showed the importance of understanding binding kinetics. Affinity-only driven selection will result in high affinity PAMs with a high k_{on} but not necessarily an optimized k_{off}, which is key for *in vivo* efficacy. Therefore, experiments that enable quantification of kinetic parameters k_{on}, k_{off} and RT will be a valuable addition to the experimental set-up used in drug discovery.

Covalent labeling of GPCRs by small molecules is a powerful approach to establish further understanding of receptor binding modes, mechanism of action, receptor expression patterns, receptor pharmacology and even to facilitate structure elucidation.[15,16] **Chapter 5** describes the first covalent PAM probe for a class C GPCR. Based on previous $mGlu_2$ medicinal chemistry efforts three novel putative covalent PAMs were designed, synthesized and pharmacologically characterized. All three compounds still behaved as selective $mGlu_2$ PAMs with good affinity and potency. Using an equilibrium-based affinity-shift assay and a kinetic competition association assay, compound **2** was identified as covalent PAM, which was confirmed in wash-out assays. The receptor binding mode of **2** was studied using computational modelling which also identified 5 nucleophilic amino acid residues potentially responsible for formation of the covalent bond with compound **2**. Receptor mutagenesis studies identified $T791^{7.29x30}$ as the likely position of covalent interaction.

Together, compound **2** was identified as a valuable tool compound to study the $mGlu_2$ PAM binding mode and binding kinetics. These findings advance the understanding of the $mGlu_2$ PAM interactions and suggest that compound **2** is useful for structure elucidation of the active state 7TM domain.

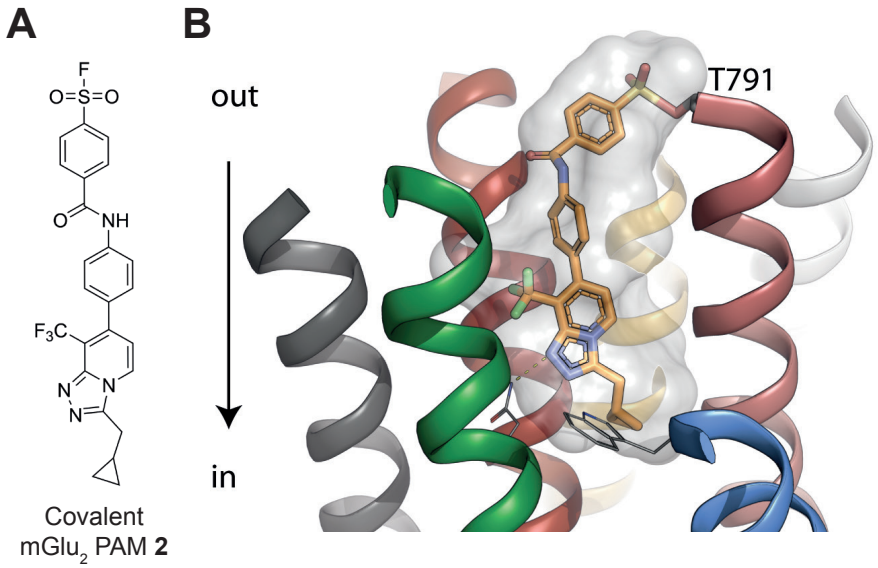

Figure 4. A) Structure of covalent $mGlu_2$ PAM **2**. B) After binding to the allosteric binding pocket, **2** forms a covalent interaction with residue $T791^{7.29x30}$, as described in **Chapter 5**.

Label-free assays using biosensors to study GPCRs have emerged over the last decade.[17,18] These assays provide new opportunities, as compared to conventional *in vitro* assays they determine integrated receptor-mediated responses on whole cells that are recorded in real time without the need for any labels. **Chapter 6** describes the set-up of such a label-free biosensor assay (i.e. xCELLigence) to study $mGlu_2$ receptor pharmacology and continues on the basic set-up that was established in **chapter 4**. The xCELLigence technology records cellular impedance that is generated by adhesion of cells to gold-coated electrodes.

Firstly, assay conditions had to be optimised as the culture medium contained a high level of endogenous glutamate which interferes with exogenous agonist signalling. Glutamate pyruvate transaminase (GPT) was used successfully to reduce these glutamate levels. Subsequently, detailed pharmacological assays were performed, yielding potencies for agonist LY354740, antagonist LY341495, PAM JNJ-46281222 and NAM RO4491533, which were comparable to literature values. Responses of the agonist and PAM showed a dose-dependent increase in impedance, whereas stimulation by the antagonist or NAM resulted in a dose-dependent decrease in impedance. This showed that opposite pharmacological responses also resulted in opposite responses on cell morphology and thus impedance measured. Interestingly, constitutive receptor activity was observed that could be inhibited by LY341495 which is commonly considered a classical antagonist for the $mGlu_2$ receptor but behaved as inverse agonist in this system. This was confirmed by concentration-dependent negative modulation of LY341495 potency by the PAM JNJ-46281222.

Thus, the label-free xCELLigence system was validated as a useful methodology to study $mGlu_2$ pharmacology. This is the first class C GPCR extensively characterized by a label-free biosensor assay, opening new avenues to study receptor pharmacology and novel concepts of receptor activation.

In conclusion, by a variety of techniques ranging from *in vitro* binding experiments to *in vivo* efficacy studies, we have shed light on the mechanism of action of the $mGlu_2$ receptor at a molecular level. The obtained insights are valuable for the design of ligands for the orthosteric binding site (**Chapter 3**) and particularly for the allosteric binding site (**Chapters 2, 4, 5**). The results were generated using novel tool compounds (**Chapters 2 and 5**) and novel assays to study binding kinetics and receptor pharmacology (**Chapters 4 and 6**). Together, these insights are valuable in future discovery projects for drugs targeting the $mGlu_2$ receptor as well as other GPCRs.

FUTURE PERSPECTIVES

Allosteric modulation and its potential for drug therapy

There is an urgent need for the development of new drug therapies for devastating neurological and neurodegenerative diseases such as schizophrenia and Alzheimer's disease, respectively. While the development of new medicines is effortful for all therapeutics areas, CNS drug discovery efforts have been particularly challenging resulting in high attrition rates during the various phases of the drug development process.[19] Many of the marketed CNS drugs exert their effect via a GPCR and currently multiple GPCRs are being evaluated as novel targets for treatment of CNS diseases with an unmet medical need, illustrating their vast and remaining potential for drug therapy.[20] Historically, drug discovery efforts have focused on the development of classical agonists and antagonists that target the orthosteric binding site of the receptor. However, targeting this orthosteric binding site of the mGlu receptor family presents challenges for subtype selectivity and drug-like properties that are essential for CNS drug candidates.[2] For these reasons most drug discovery efforts for mGlu receptors as well as other class C GPCRs have shifted towards the development of allosteric modulators. These are molecules that bind to a binding site that is topographically distinct and less conserved than the orthosteric glutamate binding site. Together this has resulted in promising subtype selective lead compounds that have been or are currently in clinical trials.[21]

Since allosteric modulators show little or no intrinsic activity by themselves and do not have to compete with the endogenous agonist, they provide an enhanced efficacy and safety

profile over typical orthosteric ligands. This has been widely acknowledged in the field resulting in vast discovery efforts and increasing numbers of allosteric modulators for GPCRs reaching clinical trials over the last decade.[20] Currently, two allosteric modulator drugs are on the market: the chemokine receptor CCR5 (CCR5; class A GPCR) NAM Maraviroc for treatment of HIV infection[22] and the calcium-sensing receptor (CaSR; class C GPCR) PAM Cinacalcet for treatment of chronic kidney disease involving hyperparathyroidism.[23] Current research efforts that increase the understanding of the mechanism of allosteric modulation will result in increasing numbers of candidate drugs which will ultimately yield an increased number of allosteric modulator drugs accessing the market in the next decade.

Allosteric modulation especially holds promise for class C GPCRs, as illustrated by the success of Cinacalcet. These receptors provide an allosteric binding site in their 7TM domain which is located in a similar location and uses a similar transmission switch mechanism compared to class A GPCR binding sites.[13] The allosteric binding sites are well explored, resulting in highly potent allosteric modulators for all major receptor families within this class – mGlu, $GABA_B$, sweet and umami taste and CaSR receptors. Multiple of these compounds have reached clinical development stages already.[19,28] Together, class C GPCRs provide promising drug targets for novel allosteric modulators and within the next decade novel allosteric modulator therapies may be provided in addition to Cinacalcet.

The potential of the $mGlu_2$ receptor for drug therapy

The $mGlu_2$ receptor is a potential drug target for various neurological disorders such as schizophrenia, anxiety, depression and cognition.[29–32] Therefore, many $mGlu_2$ PAMs and NAMs with *in vivo* efficacy have been developed, resulting in multiple clinical studies so far. In recent years $mGlu_2$ PAMs AZD8529 and JNJ-40411813 and the NAM Decoglurant have been in clinical studies, but unfortunately they were withdrawn due to a lack of efficacy. Despite the lack of clinical success so far, the use of allosteric modulators at the $mGlu_2$ receptor still provides promising opportunities for drug treatment. Together with current fundamental research efforts on the mechanism of action of the $mGlu_2$ receptor, the clinical results provide novel insights that will determine the next development steps towards an $mGlu_2$ allosteric modulator-based therapy. Such a next step may be the repurposing of the clinical compounds for specific patient populations or a different therapeutic indication, as suggested for JNJ-40411813, which demonstrated effect in a small population of schizophrenic patients with residual negative symptoms[33] and AZD8529, which was evaluated in a clinical trial for smoking cessation.[34] More importantly, novel $mGlu_2$ allosteric modulators will be designed and developed based on novel molecular strategies, including those that are discussed in this thesis. These future molecules will bear enhanced properties and therefore hold a strong promise for future allosteric drugs targeting the $mGlu_2$ receptor.

The promise of drug-target binding kinetics

The interest in drug-target binding kinetics has increased tremendously over the last decade.[35,36] The lack of technologies able to record binding kinetics has long been a limiting factor for the quantification of this parameter. Over the recent years many novel assays, such as a qualitative kinetic screening method using radioligand binding,[37] SPA assays,[38] FRET assays[39] and label-free binding assays[40] have been developed to determine kinetic binding and activation parameters.[41] Importantly, many of these assays are now ready to be implemented in larger scale drug discovery programs. The enhanced interest in binding kinetics of both academia and pharmaceutical industry is illustrated by the successful IMI project Kinetics for Drug Discovery (K4DD) that incorporated researchers from universities and different industrial partners.[41] Recently, the European Medicines Agency changed its requirements for first in human studies of new investigational products and now also demands information on the duration of *in vitro* action – and thus binding kinetics.[42] Given the increased number of techniques available to determine binding kinetics in high throughput and the awareness that is raised across the drug discovery community, the importance of assessing binding kinetics is anticipated to increase tremendously in the coming years. We will most likely enter an era in which medicinal chemists will design not only for affinity and potency, but also for kinetic parameters. This in itself will be a valuable and promising addition to the current discovery process. For the $mGlu_2$ receptor in particular we have shown that *in vitro* binding kinetics and specifically residence time is linked to *in vivo* efficacy of PAMs. This opens promising avenues for novel $mGlu_2$ PAMs whose chemical design is based on *in vitro* kinetic parameters in addition to classical affinity and potency parameters. Ultimately, this will increase the chance of desirable *in vivo* and in the end *in human* efficacy.

Covalent ligands as tool compounds for GPCRs

Covalent ligands for GPCRs have shown to be valuable tool compounds to study their mode of action.[16] The use of covalent ligands in structure elucidation of GPCRs has shown its potential and this will be used more and more in the near future. Together with other recent advances in the GPCR structure elucidation field - increased throughput of crystal structures using crystal soaking[43] and structure elucidation using cryo-electron microscopy[44,45] – the use of covalent ligands will contribute to increased understanding of GPCR structure and function. In the field of mGlu receptors an active state 7TM structure would be a valuable addition to the current NAM-bound inactive state structures of $mGlu_1$ and $mGlu_5$.[3–6] The covalent PAM **2** described in **chapter 5** could be a valuable tool to determine such active-state 7TM domain of the $mGlu_2$ receptor.

In addition, covalent ligands for GPCRs and other drug targets have been developed as promising useful probes for chemical biology applications, such as fluorescent labelling of receptors in native tissues.[46] Further research on the covalent $mGlu_2$ PAM **2** described in **chapter 5** could focus on the functionalization of the molecule for example by addition of a

'click-handle' that can be used to link the covalent molecule to a fluorescent dye in order to visualise the receptor in cells and tissues *in vivo* and ultimately even *in human*.

Covalent ligands as GPCR therapeutics

Application of a covalent mode of action is commonly avoided in the pharmaceutical industry to prevent off-target toxicity.[47] Specifically, reactive electrophilic moieties are avoided in drug design, as exemplified by the restraint use of moieties that are included in the so-called "pan-assay interference compounds" (PAINS).[48] On the other hand, drugs that bind their biological target covalently have a long history as illustrated by the 39 approved covalent drugs[49] including well-known and commonly used medicines such as aspirin (COX1,2-inhibitor),[50] omeprazole (H^+/K^+ ATPase-inhibitor)[51] and clopidogrel ($P2Y_{12}$ receptor antagonist).[52]

Current discovery efforts on covalent ligands focus on so-called "targeted covalent inhibitors".[15] Such molecules possess a high affinity for a specific target and avoid off-target toxicity by using a weakly reactive electrophilic warhead. This approach has been studied extensively in the field of kinase inhibitors for cancer therapy,[53] and is nowadays increasingly evaluated for drug targeting of GPCRs.[16] These molecules are receptor inhibitors, though when it comes to molecules that should activate GPCRs, PAMs provide a clear benefit over orthosteric agonists as they only activate the receptor whilst an agonist is bound and thus do not activate the target receptor permanently.[54] In a therapeutic context, covalent PAMs may result in less frequent drug dosing without a loss of efficacy. For these reasons, covalent PAMs targeted at mGlu receptors provide a promising therapeutic strategy. Successful development of covalent kinase drugs as safe and efficacious cancer therapies will support the efforts towards other targets such as GPCRs. Overall, if the selectivity and thus the safety of covalent molecules can be guaranteed these molecules provide valuable opportunities for future drug therapy where they will be added to the already marketed covalent drugs.

The application of label-free technologies for GPCR drug discovery

The number of biosensor-based label-free technologies in the drug discovery field has increased vastly over the last decade and is still increasing.[18,55] Since these assays measure integrated cellular responses of whole cells in real-time they can be used to study activation kinetics in addition to classical receptor pharmacology parameters. Further automation of label-free assays will enable implementation of these techniques in drug discovery programs. Another important advantage of biosensor-based label-free assays over most classical assays is that cells with low receptor expression can be used such as cell lines endogenously expressing the receptor of interest or even patient-derived cells like lymphoblastoid cell lines (LCLs).[56] By using these cells, the effects of interindividual genetic differences in receptor sequence on the drug efficacy can be studied, which is an important step towards precision medicine.[57] Currently, huge progress is being made in the use of stem cells to study responses of individual patients. These human induced pluripotent stem cells (iPSCs) are generated

from adult cells which are subsequently reprogrammed to the cell type of interest using the right cellular matrix.[58] This provides valuable progress in the use of patient-derived material, since in this way specific cell types, or even organ-like structures – so-called 'organoids' - can be used.[58] The number of different cell types that can be obtained from iPSCs is increasing tremendously at this moment. Of great importance for the field of $mGlu_2$ receptor research is the development of neuronal cultures based on iPSCs which can be used to study disease mechanisms of for example schizophrenia.[59] These cells provide a radical step forward for *in vitro* experimentation as only a very limited number of neuronal cell lines was available so far. Given the tremendous progress that is being made in the development of iPSC-derived cell types, powerful developments may be expected in the coming years when combining these cells with the advantages of label-free assays. As an example, such experimental set-up was applied to cardiomyocytes derived from iPSCs that were studied using the label-free xCELLigence assay.[60] Altogether, development of label-free assays based on cell types from patient-derived iPSCs will result in more focused insights in disease mechanisms and as such this experimental set-up holds great promise for the study of the $mGlu_2$ receptor as well as other GPCRs.

Final notes

Throughout this thesis the molecular mechanism of action of the $mGlu_2$ receptor has been studied to better understand the key *in vitro* parameters that drive *in vivo* efficacy. To obtain these insights, various pharmacological concepts were studied, including allosteric modulation and binding kinetics and to be able to do so multiple tool compounds and assays were developed. Together, the results obtained in this thesis contribute to the improved understanding of the molecular processes involved in GPCR drug action. This improved understanding will ultimately contribute to increasing the number and the quality of drug candidates that will hopefully become novel, safe and efficacious drug therapies for the $mGlu_2$ receptor as well as for other GPCRs in the near future.

REFERENCES

1. Niswender CM, Conn PJ. *Annu Rev Pharmacol Toxicol*. **2010**; 50: 295–322.

2. Conn PJ, Christopoulos A, Lindsley CW. *Nat Rev Drug Discov*. **2009**; 8: 41–54.

3. Doré AS, Okrasa K, Patel JC, Serrano-Vega M, Bennett K, Cooke RM, Errey JC, Jazayeri A, Khan S, Tehan B, Weir M, Wiggin GR, Marshall FH. *Nature*. **2014**; 511: 557–62.

4. Wu H, Wang C, Gregory KJ, Han GW, Cho HP, Xia Y, Niswender CM, Katritch V, Meiler J, Cherezov V, Conn PJ, Stevens RC. *Science*. **2014**; 344: 58–64.

5. Christopher JA, Aves SJ, Bennett KA, Doré AS, Errey JC, Jazayeri A, Marshall FH, Okrasa K, Serrano-Vega MJ, Tehan BG, Wiggin GR, Congreve M. *J Med Chem*. **2015**; 58: 6653–6664.

6. Christopher J, Orgován Z, Congreve M, Dore AS, Errey JC, Marshall FH, Mason JS, Okrasa K, Rucktooa P, Serrano-Vega MJ, Ferenczy GG, Keseru GM. *J Med Chem*. **2018**: acs.jmedchem.7b01722.

7. Schaffhauser H, Rowe BA, Morales S, Chavez-Noriega LE, Yin R, Jachec C, Rao SP, Bain G, Pinkerton AB, Vernier J, Bristow LJ, Varney MA, Daggett LP. *Mol Pharmacol*. **2003**; 64: 798–810.

8. Hemstapat K, Da Costa H, Nong Y, Brady AE, Luo Q, Niswender CM, Tamagnan GD, Conn PJ. *J Pharmacol Exp Ther*. **2007**; 322: 254–64.

9. Rowe BA, Schaffhauser H, Morales S, Lubbers LS, Bonnefous C, Kamenecka TM, McQuiston J, Daggett LP. *J Pharmacol Exp Ther*. **2008**; 326: 240–51.

10. Lundström L, Bissantz C, Beck J, Wettstein JG, Woltering TJ, Wichmann J, Gatti S. *Br J Pharmacol*. **2011**; 164: 521–37.

11. Farinha A, Lavreysen H, Peeters L, Russo B, Masure S, Trabanco AA, Cid J, Tresadern G. *Br J Pharmacol*. **2015**; 172: 2383–96.

12. Pérez-Benito L, Doornbos MLJ, Cordomí A, Peeters L, Lavreysen H, Pardo L, Tresadern G. *Structure*. **2017**; 25: 1–10.

13. Perez-Benito L, Doornbos MLJ, Cordomí A, Peeters L, Lavreysen H, Tresadern G, Pardo L. *Submitt to PNAS*. **2016**.

14. Smith GF. *Prog Med Chem*. **2009**; 48: 1–29.

15. Baillie TA. *Angew Chemie - Int Ed*. **2016**; 55: 13408–13421.

16. Weichert D, Gmeiner P. *ACS Chem Biol*. **2015**; 10: 1376–1386.

17. Fang Y. *Expert Opin Drug Discov*. **2015**; 10: 331–343.

18. Scott CW, Peters MF. *Drug Discov Today*. **2010**; 15: 704–716.

19. Nickols HH, Conn PJ. *Neurobiol Dis*. **2014**; 61: 55–71.

20. Hauser AS, Attwood MM, Rask-Andersen M, Schiöth HB, Gloriam DE. *Nat Rev Drug Discov*. **2017**; 16: 829–842.

21. Leach K, Gregory KJ. *Pharmacol Res*. **2017**; 116: 105–118.

22. Swinney DC, Beavis P, Chuang K-T, Zheng Y, Lee I, Gee P, Deval J, Rotstein DM, Dioszegi M, Ravendran P, Zhang J, Sankuratri S, Kondru R, Vauquelin G. *Br J Pharmacol*. **2014**; 171: 3364–75.

23. Davey AE, Leach K, Valant C, Conigrave AD, Sexton PM, Christopoulos A. *Endocrinology*. **2012**; 153: 1232–41.

24. Pin J-P, Galvez T, Prézeau L. *Pharmacol Ther*. **2003**; 98: 325–354.

25. Hlavackova V, Goudet C, Kniazeff J, Zikova A, Maurel D, Vol C, Trojanova J, Prézeau L, Pin J-P, Blahos J. *EMBO J*. **2005**; 24: 499–509.

26. El Moustaine D, Granier S, Doumazane E, Scholler P, Rahmeh R, Bron P, Mouillac B, Banères J-L, Rondard P, Pin J-P. *Proc Natl Acad Sci U S A*. **2012**; 109: 16342–7.

27. Kniazeff J, Bessis A-S, Maurel D, Ansanay H, Prézeau L, Pin J-P. *Nat Struct Mol Biol*. **2004**; 11: 706–13.

28. Urwyler S. *Pharmacol Rev*. **2011**; 63: 59–126.

29. Dunayevich E, Erickson J, Levine L, Landbloom R, Schoepp DD, Tollefson GD. *Neuropsychopharmacology*. **2008**; 33: 1603–10.

30. Patil ST, Zhang L, Martenyi F, Lowe SL, Jackson KA, Andreev B V, Avedisova AS, Bardenstein LM, Gurovich IY, Morozova MA, Mosolov SN, Neznanov NG, Reznik AM, Smulevich AB, Tochilov VA, Johnson BG, Monn JA, Schoepp DD. *Nat Med*. **2007**; 13: 1102–7.

31. Feyissa AM, Woolverton WL, Miguel-Hidalgo JJ, Wang Z, Kyle PB, Hasler G, Stockmeier CA, Iyo AH, Karolewicz B. *Prog Neuropsychopharmacol Biol Psychiatry*. **2010**; 34: 279–83.

32. Goeldner C, Ballard TM, Knoflach F, Wichmann J, Gatti S, Umbricht D. *Neuropharmacology*. **2013**; 64: 337–46.

33. Salih H, Anghelescu I, Kezic I, Sinha V, Hoeben E, Van Nueten L, De Smedt H, De Boer P. *J Psychopharmacol*. **2015**; 29: 414–425.

34. Cross AJ, Anthenelli R, Li X. *Biol Psychiatry*. **2017**: 1–8.

35. Guo D, Heitman LH, IJzerman AP. *Chem Rev*. **2017**; 117: 38–66.

36. Copeland RA. *Nat Rev Drug Discov*. **2016**; 15: 87–95.

37. Guo D, van Dorp EJH, Mulder-Krieger T, van Veldhoven JPD, Brussee J, IJzerman AP, Heitman LH. *J Biomol Screen*. **2013**; 18: 309–20.

38. Xia L, de Vries H, IJzerman AP, Heitman LH. *Purinergic Signal*. **2016**; 12: 115–126.

39. Nederpelt I, Georgi V, Schiele F, Nowak-Reppel K, Fernández-Montalván AE, Ijzerman AP, Heitman LH. *Br J Pharmacol*. **2016**; 173: 128–141.

40. Nederpelt I, Kuzikov M, de Witte WEA, Schnider P, Tuijt B, Gul S, IJzerman AP, de Lange ECM, Heitman LH. *Sci Rep*. **2017**; 7: 14169.

41. Schuetz DA, de Witte WEA, Wong YC, Knasmueller B, Richter L, Kokh DB, Sadiq SK, Bosma R, Nederpelt I, Heitman LH, Segala E, Amaral M, Guo D, Andres D, Georgi V, Stoddart LA, Hill S, Cooke RM, De Graaf C, Leurs R, Frech M, Wade RC, de Lange ECM, IJzerman AP, Müller-Fahrnow A, Ecker GF. *Drug Discov Today*. **2017**; 22: 896–911.

42. Guideline on strategies to identify and mitigate risks for first-in-human and early clinical trials with investigational medicinal products - http://www.ema.europa.eu/docs/en_GB/document_library/Scientific_guideline/2017/07/WC500232186.pdf, **2017**.

43. Rucktooa P, Cheng RKY, Segala E, Geng T, Errey JC, Brown GA, Cooke RM, Marshall FH, Doré AS. *Sci Rep*. **2018**; 8: 41.

44. Zhang Y, Sun B, Feng D, Hu H, Chu M, Qu Q, Tarrasch JT, Li S, Sun Kobilka T, Kobilka BK, Skiniotis G. *Nature*. **2017**; 546: 248–253.

45. Liang YL, Khoshouei M, Radjainia M, Zhang Y, Glukhova A, Tarrasch J, Thal DM, Furness SGB, Christopoulos G, Coudrat T, Danev R, Baumeister W, Miller LJ, Christopoulos A, Kobilka BK, Wootten D, Skiniotis G, Sexton PM. *Nature*. **2017**; 546: 118–123.

46. Soethoudt M, Stolze SC, Westphal M V., van Stralen L, Martella A, van Rooden EJ, Guba W, Varga Z V., Deng H, van Kasteren SI, Grether U, IJzerman AP, Pacher P, Carreira EM, Overkleeft HS, Ioan-Facsinay A, Heitman LH, van der Stelt M. *J Am Chem Soc*. **2018**: jacs.7b11281.

47. Bauer RA. *Drug Discov Today*. **2015**; 20: 1061–1073.

48. Baell JB, Holloway GA. *J Med Chem*. **2010**; 53: 2719–2740.

49. Singh J, Petter RC, Baillie TA, Whitty A. *Nat Rev Drug Discov*. **2011**; 10: 307–317.

50. Funk CD, Funk LB, Kennedy ME, Pong AS, Fitzgerald GA. *FASEB J*. **1991**; 5: 2304–2312.

51. Wallmark B. *Scand J Gastroenterol*. **1986**; 21: 11–16.

52. Savi P, Pereillo JM, Uzabiaga MF, Combalbert J, Picard C, Maffrand JP, Pascal M,

Herbert JM. *Thromb Haemost*. **2000**; 84: 891–6.

53. Ward RA, Anderton MJ, Ashton S, Bethel PA, Box M, Butterworth S, Colclough N, Chorley CG, Chuaqui C, Cross DAE, Dakin LA, Debreczeni JÉ, Eberlein C, Finlay MR V., Hill GB, Grist M, Klinowska TCM, Lane C, Martin S, Orme JP, Smith P, Wang F, Waring MJ. *J Med Chem*. **2013**; 56: 7025–7048.

54. Lu S, Zhang J. *Drug Discov Today*. **2017**; 22: 447–453.

55. Fang Y. *Front Pharmacol*. **2014**; 5 MAR: 1–8.

56. Hillger JM, Schoop J, Boomsma DI, Eline Slagboom P, IJzerman AP, Heitman LH. *Biosens Bioelectron*. **2015**; 74: 233–242.

57. Hillger JM, le Roy B, Wang Z, Mulder-Krieger T, Boomsma DI, Slagboom PE, Danen EHJ, IJzerman AP, Heitman LH. *Biochem Pharmacol*. **2017**.

58. Muguruma K. *Cerebellum*. **2017**: 1–5.

59. Prytkova I, Brennand KJ. *Front Cell Neurosci*. **2017**; 11: 1–8.

60. Scott CW, Zhang X, Abi-Gerges N, Lamore SD, Abassi YA, Peters MF. *Toxicol Sci*. **2014**; 142: 331–338.

SUMMARY

During the course of drug discovery translational steps are made. The translation from *in vitro* to *in vivo* experiments is not as predictive as one would desire, resulting in selection of inefficacious compounds but also in overlooking of promising drug candidates. This is not different for the $mGlu_2$ receptor for which no drugs are available on the market so far despite enormous drug discovery efforts. Therefore, there is a need to improve the molecular understanding of key *in vitro* parameters that drive *in vivo* efficacy. Hence, this thesis focuses on the concepts of target binding kinetics and functional efficacy of both allosteric and orthosteric ligands of the $mGlu_2$ receptor. **Chapter 1** introduces these main concepts studied throughout the thesis. The chapter starts with an introduction to G protein-coupled receptors (GPCRs), with a focus on the $mGlu_2$ receptor. Subsequently, the concepts of allosteric modulation, binding kinetics and covalent receptor binding are described. In **Chapter 2**, JNJ-46281222 is introduced and characterized extensively. This highly potent positive allosteric modulator (PAM) is used throughout the different chapters as a prototypical tool compound. Furthermore, the mechanism of positive allosteric modulation of the $mGlu_2$ receptor is studied. JNJ-46281222 behaved as a typical PAM, increasing the affinity and potency of agonists. Next to that, JNJ-46281222 behaved as PAM agonist with submaximal efficacy at higher concentrations compared to the efficacy of the endogenous agonist glutamate. A two-way mechanism of allosteric modulation was postulated, as the maximum binding capacity of JNJ-46281222 was increased by the presence of the agonist glutamate, whereas glutamate left the affinity of JNJ-46281222 unchanged. On the other hand, the presence of GTP (which initiates dissociation of the G protein) decreased JNJ-46281222 binding indicating that the PAM prefers the G protein-bound state of the receptor. Computational docking and molecular dynamics studies were used to visualize and understand the PAM binding mode. These experiments were followed by receptor mutagenesis experiments which confirmed the binding mode of JNJ-46281222.

Chapter 3 describes the first kinetic study of orthosteric ligands at the $mGlu_2$ receptor. After the set-up of an assay enabling the quantification of target binding kinetics, kinetic parameters of the endogenous agonist glutamate were determined followed by those of other orthosteric ligands. To increase the understanding of the binding mechanism and effect of allosteric modulation on this process, experiments were repeated in the presence of a PAM and a NAM (negative allosteric modulator). We found that affinity is strongly correlated to the association rate constant k_{on}, showing that on-rate is driving affinity and thus target occupancy of orthosteric $mGlu_2$ ligands. In contrast to the wide range of on-rates, dissociation rate constants (k_{off}) were all within a small 6-fold range. Functional assays showed that the presence of a PAM not only increased the duration of (orthosteric) ligand binding, but also the duration of ligand efficacy.

In **chapter 4**, an extensive structure-kinetics relationships (SKR) study was performed using 41 novel $mGlu_2$ PAMs all bearing the 7−aryl-1,2,4-triazolo[4,3−*a*]pyridine-scaffold. In addition to classical parameters of affinity and potency, kinetic parameters were determined and residence times (RTs) were calculated. To this end, a kinetic radioligand binding assay, a so-called scintillation proximity assay (SPA) was developed. The novel PAMs showed various kinetic profiles in which k_{on} values ranged over three orders of magnitude, whereas k_{off} values were within a 10-fold range. Like in **chapter 3**, k_{on} was the driver for affinity, showing that this is likely receptor-specific. Even though RTs were within a small range, we showed in a functional assay that PAMs with divergent RTs showed different duration of action. Ultimately, a long and a short RT PAM were evaluated for their *in vivo* efficacy, which provided the first hint that *in vivo* efficacy of $mGlu_2$ PAMs benefits from a longer *in vitro* RT. Together, the results obtained in **chapters 3** and **4**, have shown the importance of target binding kinetics for drug design of novel $mGlu_2$ receptor ligands. Therefore, experiments that enable quantification of kinetic parameters k_{on}, k_{off} and RT will be a valuable addition to the experimental set-up used in drug discovery.

Covalent labelling of GPCRs is a powerful approach to gain further understanding of ligand binding, mechanism of action, receptor expression patterns, receptor pharmacology and it may ultimately facilitate structure elucidation. **Chapter 5** describes the design, synthesis and pharmacological characterization of the first covalent PAM probe for a class C GPCR. Furthermore, the compound was used to study its receptor binding mode using computational modelling that also identified the amino acid residue likely responsible for covalent binding, which was confirmed in receptor mutagenesis experiments.

Chapter 6 describes the set-up of a label-free biosensor assay that enables studying $mGlu_2$ receptor pharmacology without the need of any label. After optimization of assay conditions, typical agonist, antagonist, PAM and NAM responses were monitored. Interestingly, constitutive activity of the $mGlu_2$ receptor was found in this system and LY341495 behaved as inverse agonist, which had not been shown before as the compound is commonly considered

a classical (neutral) antagonist. The $mGlu_2$ receptor is thus the first class C GPCR extensively characterized by a label-free biosensor, opening new possibilities to study receptor pharmacology and novel concepts of receptor activation.

Finally, the general conclusions obtained throughout the different chapters of this thesis are discussed in **chapter 7**. Together, the results obtained in this thesis contribute to the understanding of the mechanism of action of the $mGlu_2$ receptor at a molecular level and have shown the importance of target binding kinetics for drug discovery. The novel insights that have been obtained throughout this thesis provide valuable information for future drug discovery projects targeting the $mGlu_2$ receptor as well as other GPCRs.

NEDERLANDSE SAMENVATTING

Bij het ontwikkelen van nieuwe geneesmiddelen worden op meerdere momenten in het proces vertaalslagen gemaakt. Resultaten uit *in vitro* experimenten zijn niet zo voorspellend voor de effectiviteit van stoffen in *in vivo* experimenten als we zouden willen. Dit resulteert in het selecteren van moleculen die later niet effectief blijken, maar ook in het missen van moleculen die juist wel veelbelovend zijn. Dit is niet anders voor de metabotrope glutamaat-receptor 2 ($mGlu_2$ receptor), waarvoor ondanks enorm veel onderzoek en ontwikkeling nog geen medicijnen op de markt zijn. Dit laat zien dat er behoefte is aan een beter begrip op moleculair niveau van de *in vitro* parameters die ten grondslag liggen aan *in vivo* effect van stoffen. Daarom richt dit proefschrift zich op de thema's van receptorbindingskinetiek en functionele effectiviteit van zowel allostere als orthostere liganden van de $mGlu_2$ receptor.

Hoofdstuk 1 introduceert de hoofdthema's die in dit proefschrift worden behandeld. Na een introductie van G-eiwitgekoppelde receptoren met een focus op de $mGlu_2$ receptor volgt een inleiding van de thema's allostere modulatie, receptorbindingskinetiek en covalente receptorbinding.

In **Hoofdstuk 2** is JNJ-462841222 geïntroduceerd en uitgebreid gekarakteriseerd. Deze zeer potente positieve allostere modulator (PAM) is in alle hoofdstukken van dit proefschrift gebruikt als model-PAM. Verder is in dit hoofdstuk het mechanisme van positieve allostere modulatie van de $mGlu_2$ receptor onderzocht. JNJ-46281222 liet karakteristieke PAM-eigenschappen zien door de affiniteit en potentie van de endogene agonist glutamaat te verhogen. Daarnaast gedroeg JNJ-46281222 zich als zogeheten PAM-agonist. Bij hogere concentraties is de stof in staat de receptor submaximaal te activeren ten opzichte van volledige activatie door glutamaat. Vervolgens is aangetoond dat het mechanisme van allostere modulatie in twee richtingen verloopt. In aanvulling op de effecten van de PAM op de affiniteit en potentie van agonisten is in dit hoofdstuk aangetoond dat het maximaal aantal bindingsplaatsen van JNJ-46281222 wordt verhoogd in aanwezigheid van glutamaat, terwijl de affiniteit van de PAM onder deze condities niet veranderde. Verder werd aangetoond dat het aantal PAM-bindingsplaatsen sterk afnam in aanwezigheid van GTP (dat zorgt voor dissociatie van het G eiwit), wat onderschrijft dat deze PAM liever bindt aan G-eiwitgekoppelde receptoren. Vervolgens zijn computationele en moleculair dynamische studies uitgevoerd om de bindingspose en

het mechanisme van binden van de PAM in de receptor te bestuderen en zodoende beter te begrijpen. De PAM-bindingslocatie die hieruit volgde is vervolgens bevestigd met receptor-mutagenese-experimenten.

Hoofdstuk 3 beschrijft de eerste kinetische studie van orthostere liganden van de $mGlu_2$ receptor. Na het opzetten van een experimentele methode voor het kwantificeren van bindingskinetiek zijn de kinetische parameters van de endogene agonist glutamaat bepaald. Vervolgens is dit ook gedaan voor andere orthostere liganden. Om het begrip van het mechanisme van receptorbinding en de invloed van allostere modulatoren hierop te vergroten zijn de experimenten herhaald in aan- en afwezigheid van een PAM of een NAM (negatieve allostere modulator). We lieten zien dat de affiniteit van orthostere liganden sterk is gecorreleerd aan de associatiesnelheidsconstante (k_{on}). Dit toont aan dat de k_{on} de bepalende factor is voor de affiniteit en ten gevolge daarvan ook voor de receptorbezetting van orthostere $mGlu_2$ liganden. In tegenstelling tot de grote variatie aan k_{on}-waarden (1000-voudig verschil), waren de waarden van de dissociatiesnelheidsconstanten (k_{off}) veel minder divers, maximaal zesvoudig verschillend. Met behulp van functionele experimenten werd vervolgens aangetoond dat de aanwezigheid van een PAM leidt tot een verlenging van de functionele respons van glutamaat in aanvulling op de verlenging van de ligandbinding.

In **hoofstuk 4** is een uitgebreide studie gedaan van structuur-kinetiekrelaties. Hiervoor zijn 41 nieuwe $mGlu_2$ PAMs bestudeerd die allemaal de 7−aryl-1,2,4-triazolo[4,3−*a*]pyridine-scaffold bevatten. Naast de klassieke bepalingen van affiniteit en potentie werden kinetische parameters (k_{on} en k_{off}) en verblijftijden (RTs) bepaald. Hiervoor werd allereerst een zogeheten scintillation proximity assay (SPA) opgezet en gevalideerd. Deze nieuwe PAMs vertoonden verschillende kinetische profielen, waarin de k_{on}-waarden tot wel duizend keer uit elkaar lagen, terwijl k_{off}-waarden allemaal binnen een tienvoud van elkaar lagen. Dit liet zien dat net zoals in **hoofdstuk 3** k_{on} de affiniteit bepaalt en dat dit daarom karakteristiek is voor deze receptor. Ondanks dat de verblijftijden maar weinig van elkaar verschilden, lieten we in een functioneel experiment zien dat de duur van het effect van PAMs gelieerd is aan de verblijftijd van deze moleculen op de receptor. Uiteindelijk zijn een PAM met een korte en een lange verblijftijd onderzocht in een diermodel. In deze experimenten liet de PAM met een lange verblijftijd een beter effect zien *in vivo* dan de PAM met een korte verblijftijd op de receptor. Dit is de eerste aanwijzing dat het *in vivo* effect van $mGlu_2$ PAMs verbetert door een langere *in vitro* verblijftijd. Samen laten de resultaten van **hoofdstuk 3** en **4** zien dat receptorbindingskinetiek belangrijk is voor het ontwikkelen van nieuwe geneesmiddelen. Daarom zouden experimenten die het mogelijk maken om kinetische parameters k_{on}, k_{off} en RT te bepalen een waardevolle toevoeging zijn aan de bestaande *in vitro* experimenten die in het proces van geneesmiddelenontwikkeling toegepast worden.

Het covalent labellen van GPCRs is een waardevolle methode om het begrip van receptorbinding, werkingsmechanisme, receptorexpressie en receptorfarmacologie te vergroten en zou daarnaast ook kunnen bijdragen aan het ophelderen van de structuur van receptoren.

Hoofdstuk 5 beschrijft het ontwerp, de synthese en de farmacologische karakterisatie van de eerste covalente PAM van een klasse C GPCR. Vervolgens is dit molecuul gebruikt om de receptorbinding te bestuderen met behulp van computationele modellen. Deze modellen werden ook gebruikt om een aantal aminozuurresiduen te identificeren die verantwoordelijk zouden kunnen zijn voor de covalente binding tussen PAM en receptor. In mutagenese experimenten is vervolgens het specifieke aminozuurresidu verantwoordelijk voor de covalente binding geïdentificeerd.

Hoofdstuk 6 beschrijft het opzetten van een experimentele methode voor het bestuderen van de $mGlu_2$ receptorfarmacologie waarvoor geen labels benodigd zijn, maar die is gebaseerd op het gebruik van een biosensor. Nadat de experimentele condities waren geoptimaliseerd konden typische agonist-, antagonist-, PAM- en NAM-responsen worden gemeten. Het was belangwekkend dat we met behulp van deze methode ook constitutieve activiteit van de $mGlu_2$ receptor konden waarnemen. LY341495 gedroeg zich als inverse agonist, terwijl deze stof algemeen bekend staat als klassieke (neutrale) antagonist. De $mGlu_2$ receptor is de eerste klasse C GPCR die uitgebreid is gekarakteriseerd met behulp van een biosensormethode. Dit biedt nieuwe mogelijkheden voor het bestuderen van receptorfarmacologie en nieuwe thema's op het gebied van receptoractivatie.

Tenslotte zijn de conclusies van de verschillende hoofdstukken besproken in **hoofdstuk 7**. De resultaten uit dit proefschrift dragen bij aan het begrip van het werkingsmechanisme van de $mGlu_2$ receptor op moleculair niveau en hebben het belang van receptorbindingkinetiek voor de ontwikkeling van nieuwe geneesmiddelen krachtig onderstreept. De nieuwe inzichten die in de verschillende hoofdstukken van dit proefschrift verkregen zijn bieden waardevolle informatie voor toekomstig onderzoek naar en ontwikkeling van nieuwe geneesmiddelen voor zowel de $mGlu_2$ receptor als voor andere GPCRs.

SAMENVATTING VOOR LEKEN

Iedereen maakt in zijn leven gebruik van geneesmiddelen. Door het grote aantal geneesmiddelen vandaag de dag, is het moeilijk voor te stellen dat er een tijd was waarin maar enkele medicijnen beschikbaar waren. Toch was het aantal geneesmiddelen honderd jaar geleden, in het begin van de twintigste eeuw, zeer beperkt en waren aandoeningen die tegenwoordig relatief eenvoudig met geneesmiddelen te genezen zijn toen moeilijker te behandelen en soms zelfs levensbedreigend. Sindsdien is het aantal beschikbare geneesmiddelen enorm toegenomen. Geneesmiddelenontwikkeling zoals we die vandaag de dag kennen komt voort uit de gigantische toename van kennis van de processen in het menselijk lichaam die betrokken zijn bij ziekten en daarnaast door de sterk toegenomen mogelijkheden om een grote diversiteit aan moleculen te synthetiseren. Deze samenvatting beschrijft eerst het proces van geneesmiddelenontwikkeling. Vervolgens wordt aangegeven waar in het proces van geneesmiddelenontwikkeling de resultaten uit dit proefschrift bijdragen aan de ontwikkeling van toekomstige medicijnen. Tenslotte wordt dit hoofdstuk afgesloten met een samenvatting van de resultaten uit dit proefschrift.

Het proces van geneesmiddelenontwikkeling kan worden onderverdeeld in verschillende fasen (Figuur 1). De ontwikkeling van een nieuw geneesmiddel start met de onderzoeksfase waarin allereerst het begrijpen van de ziekte waarvoor de therapie bedoeld is centraal staat. Wanneer de ziekte voldoende op moleculair niveau begrepen is en er een aangrijpingspunt voor een geneesmiddel is geïdentificeerd kan met het ontwerpen van een potentieel geneesmiddel begonnen worden. In deze fase wordt een groot aantal moleculen (kandidaat-geneesmiddelen) gesynthetiseerd. Dit aantal kan oplopen tot 10.000. Al deze moleculen worden vervolgens getest op hun werkzaamheid en affiniteit voor het aangrijpingspunt. Voor deze experimenten worden celkweekmodellen gebruikt, zogeheten *in vitro* experimenten. Op basis van de resultaten van deze experimenten wordt vervolgens een selectie gemaakt van moleculen die veelbelovend zijn en daarom doorgaan naar de volgende fase.

Het proces van geneesmiddelenontwikkeling

Figuur 1. Overzicht van de verschillende fasen van het proces van geneesmiddelenontwikkeling. De rode pijlen geven een vertaalstap weer, waarbij op basis van behaalde resultaten een selectie van veelbelovende kandidaat-geneesmiddelen wordt gemaakt die in de volgende fase verder getest wordt. Pictogrammen zijn van *thenounproject.com*. Het figuur is gebaseerd op *vib.be/nl/mens-en-gezondheid/Pages/De-ontwikkeling-van-een-geneesmiddel.Het proces van geneesmiddelenontwikkeling*

In deze preklinische ontwikkelingsfase wordt de werkzaamheid en de veiligheid van de kandidaat-geneesmiddelen verder getest met *in vitro* experimenten. Daarnaast wordt er getest in proefdiermodellen, de zogeheten *in vivo* experimenten. Aan de hand van de behaalde resultaten kan dan bepaald worden of de kandidaat-geneesmiddelen voldoende werkzaam en veilig zijn om geselecteerd te worden voor klinische experimenten.

De klinische experimenten zijn onderverdeeld in drie fasen. Er wordt begonnen met studies in gezonde vrijwilligers (fase 1), gevolgd door studies bij kleine groepen patiënten (fase 2) en een grote groep patiënten (fase 3). Hierbij zijn vooral de veiligheid en de werkzaamheid van het geneesmiddel van belang. Daarnaast wordt er gekeken hoe het geneesmiddel zich in het lichaam gedraagt (opname, verdeling, afbraak, uitscheiding).

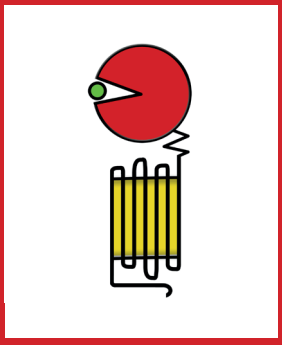

Box 1. G-eiwitgekoppelde receptoren

Een veelgebruikte groep van aangrijpingspunten van geneesmiddelen zijn G-eiwitgekoppelde receptoren (GPCRs). Dit zijn eiwitten die zich in de celwanden bevinden en overal in ons lichaam te vinden zijn. Deze receptoren zijn betrokken bij de signaaloverdracht in ons lichaam en zijn het aangrijpingspunt van meer dan 30% van de beschikbare medicijnen. Veel van deze medicijnen kennen we allemaal, bijvoorbeeld bètablokkers tegen een hoge bloeddruk en antihistaminica tegen hooikoorts. Moleculen die aan deze receptoren binden kunnen grofweg worden onderverdeeld in twee groepen. Agonisten die de receptor activeren (lichaamseigen zoals adrenaline, of geneesmiddelen zoals ventolin tegen astma) en antagonisten die de werking van lichaamseigen processen verminderen (bijvoorbeeld cafeïne, of geneesmiddelen zoals metoprolol en andere bèta-blokkers).

Op het moment dat al deze verschillende fasen succesvol doorlopen zijn kan er een uitgebreid dossier worden ingediend bij de autoriteiten om toestemming te krijgen om het nieuwe geneesmiddel op de markt te mogen brengen. Wanneer het medicijn op de markt is wordt het nog gevolgd: de bijwerkingen en eventuele andere interacties worden constant in de gaten gehouden.

Waar in het proces van geneesmiddelenontwikkeling dragen de resultaten in dit proefschrift bij?

Tijdens het proces van geneesmiddelenontwikkeling wordt op meerdere momenten een selectie gemaakt op basis van de beschikbare resultaten, zogeheten vertaalstappen (aangegeven met rode pijlen in figuur 1). Tijdens de onderzoeksfase worden alle 10.000 nieuw gemaakte stoffen getest in celkweekmodellen. Op basis van de beschikbare resultaten uit de celkweekmodellen wordt een selectie gemaakt van stoffen die worden getest in de preklinische fase, dit gaat vaak om ongeveer 100 stoffen, nog maar 1% van de 10.000 dus. Van deze 100 stoffen blijken er gemiddeld uiteindelijk maar ongeveer 10 veilig en werkzaam. 90 van de 100 stoffen worden dus wel getest, maar blijken niet goed genoeg te zijn. Dit laat zien dat de voorspellende waarde van de celkweekmodellen die in de onderzoeksfase gebruikt worden lang niet zo goed is als we zouden wensen, maar 10% van de geselecteerde stoffen blijkt veilig en werkzaam. Dit leidt tot het onnodig uitvoeren van heel veel experimenten, waaronder veel *in vivo* experimenten met proefdieren. De resultaten die in dit proefschrift beschreven worden dragen bij aan het beter begrijpen van wat er nodig is om een betere selectie te maken in de onderzoeksfase en zo het preklinisch onderzoek te verbeteren en het gebruik van proefdieren te verminderen. Hiervoor is gebruik gemaakt van een aangrijpingspunt voor potentiele nieuwe geneesmiddelen, de metabotrope glutamaat-receptor 2 ($mGlu_2$). Deze receptor (Box 1) is op moleculair niveau onderzocht en daarnaast zijn er extra experimenten ontwikkeld om de voorspellende waarde van *in vitro* experimenten te vergroten. Uiteindelijk wordt op deze manier een bijdrage geleverd aan het verbeteren van het proces van geneesmiddelenontwikkeling.

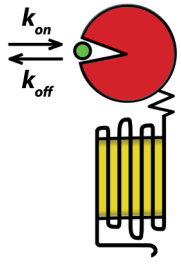

Box 2. Bindingskinetiek

Kinetiek of kinetica is de leer van bewegingskrachten en snelheden. In de farmacologie wordt kinetiek gebruikt om de snelheid van bepaalde processen te beschrijven. Wanneer we spreken over bindingskinetiek gaat het over de snelheid waarmee een molecuul bindt aan zijn aangrijpingspunt. In de context van het onderzoek beschreven in dit proefschrift gaat het dan over de snelheid waarmee een molecuul bindt aan de receptor (beschreven door de associatiesnelheidsconstante k_{on}) en de snelheid waarmee het molecuul loslaat van de receptor (beschreven door de dissociatiesnelheidsconstante k_{off}). Aan de hand van de k_{off} kan dan de verblijftijd (residence time (RT) in het Engels) van een molecuul bepaald worden. Deze verblijftijd geeft een indicatie voor de duur van de binding van het molecuul aan de receptor.

Samenvatting van het proefschrift

In het onderzoek zoals beschreven in dit proefschrift is gebruik gemaakt van de metabotrope glutamaat-receptor 2 ($mGlu_2$ receptor) als modelreceptor. Glutamaat is een signaalstof in onze hersenen en is de lichaamseigen activator (agonist) van deze receptor. Bij verschillende ziekten van het centrale zenuwstelsel zoals schizofrenie en depressie is de signalering van glutamaat verstoord. Omdat de $mGlu_2$ receptor de afgifte van glutamaat reguleert, wordt deze receptor gezien als aangrijpingspunt voor toekomstige medicijnen. Het doel van dit proefschrift is het werkingsmechanisme van de $mGlu_2$ receptor beter te begrijpen en om te evalueren of het toevoegen van kinetische *in vitro* experimenten (Box 2) zorgt voor een betere voorspelling van het uiteindelijke effect van potentiële medicijnen *in vivo*.

Hoofdstuk 1 geeft een introductie op de verschillende concepten die in dit proefschrift worden behandeld. De belangrijkste van deze concepten zijn hier beschreven in Box 1-3. In **hoofdstuk 2** is het mechanisme van allostere modulatie van de $mGlu_2$ receptor onderzocht. **Hoofdstuk 3** beschrijft het opzetten van de eerste methode om kinetiek (Box 2) van orthostere moleculen voor de $mGlu_2$ receptor te bepalen. Daarnaast werd bekeken hoe allostere modulatoren de kinetiek van orthostere moleculen beïnvloeden. In **hoofdstuk 4** is een grote groep van 41 nieuwe positieve allostere modulatoren voor de $mGlu_2$ receptor bestudeerd. Naast de klassieke parameters van affiniteit (hoe goed bindt een molecuul) en potentie (hoe werkzaam is het molecuul) werd hier ook gekeken naar de bindingskinetiek. Het bleek dat stoffen met een lange verblijftijd op de receptor een betere werkzaamheid lieten zien *in vivo*. Wanneer nu opnieuw een selectie gemaakt zou worden voor de *in vivo* te testen moleculen zou er mogelijk een andere en misschien betere selectie zijn gemaakt. **Hoofdstuk 5** beschrijft het ontwerp, synthese en karakterisering van een positieve allostere modulator die covalent aan de $mGlu_2$ receptor bindt. Dit wil zeggen dat dit molecuul vast 'klikt' aan de receptor en niet meer loslaat. Een dergelijk molecuul is waardevol bij het bestuderen van de receptor en in het bijzonder van de bindingsplaats in de receptor. In **hoofdstuk 6** wordt een nieuwe methode beschreven die gebruikt kan worden om de $mGlu_2$ receptor te bestuderen. De conclusies uit de verschillende hoofdstukken zijn beschreven in **hoofdstuk 7**.

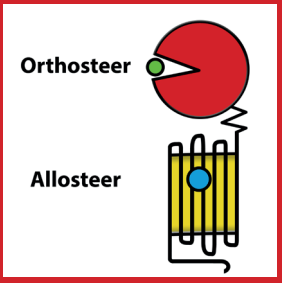

Box 3. Allostere modulatie

Moleculen binden op een vaste plaats op de receptor. Lichaamseigen moleculen binden op de zogeheten orthostere bindingsplaats. In de afgelopen decennia is gebleken dat veel receptoren daarnaast nog een tweede bindingsplaats hebben. Deze wordt omschreven als allostere bindingsplaats. Moleculen die op deze plaats aan de receptor binden worden allostere modulatoren genoemd. Deze moleculen hebben over het algemeen weinig effect op zichzelf (ze activeren of remmen de receptor niet of weinig in afwezigheid van een orthostere agonist), maar kunnen het effect van lichaamseigen moleculen versterken (positieve allostere modulatoren (PAMs)) of juist afremmen (negatieve allostere modulatoren (NAMs)).

LIST OF PUBLICATIONS

Part of this thesis:

Maarten L.J. Doornbos, Sophie C. Vermond, Hilde Lavreysen, Gary Tresadern, Adriaan P. IJzerman, Laura H. Heitman. *Impact of allosteric modulation: exploring the binding kinetics of glutamate and other orthosteric ligands of the metabotropic glutamate receptor 2.* Biochemical Pharmacology 155 (**2018**) 356–365. doi:10.1016/j.bcp.2018.07.014.

Maarten L J Doornbos, Ilse Van der Linden, Liesbeth Vereyken, Gary Tresadern, Adriaan P IJzerman, Hilde Lavreysen, Laura H Heitman. *Constitutive activity of the metabotropic glutamate receptor 2 explored with a whole-cell label-free biosensor.* Biochemical Pharmacology 152 (**2018**) 201–210. doi:10.1016/j.bcp.2018.03.026.

Maarten L. J. Doornbos, Xuesong Wang, Sophie C. Vermond, Luc Peeters, Laura Pérez-Benito, Andrés A. Trabanco, Hilde Lavreysen, José María Cid, Laura H. Heitman, Gary Tresadern, Adriaan P. IJzerman. *A covalent allosteric probe for the metabotropic glutamate receptor 2: Design, synthesis and pharmacological characterization.* Journal of Medicinal Chemistry. Publication Date (Web) March 1, **2018**. doi:10.1021/acs.jmedchem.8b00051.

Maarten L. J. Doornbos, José María Cid, Jordi Haubrich, Alexandro Nunes, Jasper W. van de Sande, Sophie C. Vermond, Thea Mulder-Krieger, Andrés A. Trabanco, Abdellah Ahnaou, Wilhelmus H Drinkenburg, Hilde Lavreysen, Laura H. Heitman, Adriaan P. IJzerman, Gary Tresadern. *Discovery and Kinetic Profiling of 7-Aryl-1,2,4-triazolo[4,3-a]pyridines: Positive Allosteric Modulators of the Metabotropic Glutamate Receptor 2.* Journal of Medicinal Chemistry 60 (**2017**) 6704–6720. doi:10.1021/acs.jmedchem.7b00669.

Maarten L J Doornbos, Laura Pérez-Benito, Gary Tresadern, Thea Mulder Krieger, Ilse Biesmans, Andrés A Trabanco, Jose María Cid, Hilde Lavreysen, Adriaan P IJzerman, Laura H Heitman. *Molecular mechanism of positive allosteric modulation of the metabotropic glutamate receptor 2 by JNJ-46281222.* British Journal of Pharmacology 173 (**2016**) 588–600. doi:10.1111/bph.13390.

Not part of this thesis:

Maarten L.J. Doornbos and Laura H. Heitman. *Protocol for a Label-free impedance-based whole cell assay to study GPCR pharmacology.* Manuscript submitted; invitation from Methods in Cell Biology.

Laura Pérez-Benito, Maarten L.J. Doornbos, Arnau Cordomí, Luc Peeters, Hilde Lavreysen, Leonardo Pardo, Gary Tresadern. *Molecular Switches of Allosteric Modulation of the Metabotropic Glutamate 2 Receptor*. Structure 25 (**2017**) 1–10. doi: 10.1016/j.str.2017.05.021.

João F.S. Carvalho, Julien Louvel, Maarten L.J. Doornbos, Elisabeth Klaasse,Zhiyi Yu, Johannes Brussee, Adriaan P. IJzerman. *Strategies to reduce HERG K+ channel blockade. Exploring heteroaromaticity and rigidity in novel pyridine analogues of dofetilide.* Journal of Medicinal Chemistry 56 (**2013**) 2828–40. doi: 10.1021/jm301564f.

Annelien J.M. Zweemer, Indira Nederpelt, Hilde Vrieling, Sarah Hafith, Maarten L.J. Doornbos, Henk de Vries, Jeffrey Abt, Raymond Gross, Dean Stamos, John Saunders, Martine J. Smit, Adriaan P. IJzerman, Laura H. Heitman. *Multiple binding sites for small-molecule antagonists at the CC chemokine receptor 2*. Molecular Pharmacology 84 (**2013**) 551–61. doi: 10.1124/mol.113.086850.

CURRICULUM VITAE

Maarten Doornbos was born in Leiden on the 10th of May in 1989. After graduating from pre-university education at the Stedelijk Gymnasium Leiden in 2007 he started studying Bio-Pharmaceutical Sciences at Leiden University. The bachelor was finished with a research internship at the division of Medicinal Chemistry under supervision of Dr. Annelien Zweemer. The project focused on the molecular pharmacology of diverse ligands of the CC chemokine receptor 2 (CCR2). In September 2011 Maarten started the master Bio-Pharmaceutical Sciences. He performed a 9-month research internship at the division of Medicinal Chemistry which comprised two projects that were supervised by Dr. João Carvalho and Dr. Julien Louvel. The first project focused on the synthesis of novel molecules to gain molecular understanding of hERG channel blockade. The project resulted in a publication in the Journal of Medicinal Chemistry. The second project was focused on the synthesis of novel antagonists for the Adenosine A_1 receptor. From February 2013 onwards Maarten performed a 6-month research internship at the division of Neuroscience Discovery at Janssen Research and Development in Beerse, Belgium under supervision of Luc Peeters and Dr. Hilde Lavreysen. There he worked on a project focused on the mapping of the allosteric binding pocket of the metabotropic glutamate receptor 2 ($mGlu_2$) using a receptor-mutagenesis approach. The results obtained in this project are part of a publication in Structure.

After obtaining his master degree in September 2013 he started as a PhD candidate at the division of Medicinal Chemistry under supervision of Dr. Laura Heitman and Prof. Dr. Ad IJzerman. The project was a joined effort with the division of Neuroscience Discovery at Janssen Research and Development and was funded by the Vlaams Agentschap Innoveren & Ondernemen. Throughout his PhD studies Maarten presented parts of the work described in this thesis at several national and international conferences. He was invited speaker at various occasions, including the FIGON Dutch Medicines Days 2016 and 2017.

From May to September 2017 he worked as interim assistant professor in the division of Medicinal Chemistry. Currently, Maarten works as project manager at Catalyze in Amsterdam.

Ad & Laura

Gary
Hilde
Ilse
Lieve
Luc
Ilse
Laura
José
Pim
Abdel
Andrès
Liesbeth

Julien
Miriam
Dong
Maris
Annelien
Zhiyi
Rongfang
Arnault
Bart
Indira
Julia
Gerard
Thea
Henk
Jaco
Daan
Elaine

Isaura
Lia
Lance
Andrea
Marjolein
Natalia
Anna
Xue
Xuesong
Tasia
Brandon
Huub
Lindsey
Shardul
Willem
Xuhan

Alexandro
Jordi
Xuesong
Sophie
Dorrit
Huub

Bruno
Emy
Jasper
Miranda
Just

ACKNOWLEDGEMENTS

The work presented in this thesis does not in any way describe the great experience that the last years have been. It especially lacks to show the input and support of so many others: students, colleagues, collaborators, supervisors, friends and family.

In the first place I want to thank my promotor and co-promotor **Ad** and **Laura**. You have shown me the way through this joyful adventure. The lessons that you have taught me will remain useful throughout my career and personal life. I am especially thankful for the confidence that you have given me while standing in for Laura during her maternity leave.

Over the last years I have had the opportunity to collaborate with great people from Neuroscience Discovery at Janssen. I want to especially thank the IWT-team **Hilde**, **Gary**, **Lieve** and **Ilse** for the very fine collegiality. It has always been a great pleasure to work with you.

A big thanks to all the colleagues that have provided support and great fun during the work in the labs, conferences, coffee breaks, lab outings, weekends, dinners, movie nights, borrels, and so many more events. Special thanks to my office mates **Indira**, **Julia**, **Zhiyi**, **Andrea**, **Lance** and **Natalia** for all work related conversations and non-work related fun. A special thanks to **Thea** and **Henk** for support, collaboration and good conversations.

I am thankful to all the students that have contributed to this work. Especially **Alexandro**, **Jordi**, **Xuesong** and **Sophie**. Your work has greatly contributed to various chapters of this thesis and during your master internships you have been of great inspiration while making me think about the project from different angles.

Anna and **Rongfang**, thanks for being my paranimphs. I am happy to have you on my side during this special day.

I finish with the most important person, **Manon**.